DEPARTAMENTO DE INGENIERÍA QUÍMICA

FACULTAD DE CIENCIAS Y TECNOLOGÍAS QUÍMICAS

UNIVERSIDAD DE CASTILLA-LA MANCHA

STUDY OF IMPROVED ELECTRODES FOR HIGH TEMPERATURE PEM FUEL CELLS BASED ON PBI MEMBRANES

PhD dissertation to obtain a doctorate degree from the University of Castilla- La Mancha

Hector Zamora Triguero

Advisors

Prof. Dr. Manuel Andrés Rodrigo Rodrigo

Prof. Dr. Justo Lobato Bajo

Ciudad Real, January 2017

DEPARTAMENTO DE INGENIERÍA QUÍMICA

FACULTAD DE CIENCIAS Y TECNOLOGÍAS QUÍMICAS

UNIVERSIDAD DE CASTILLA-LA MANCHA

ESTUDIO DE ELECTRODOS MEJORADOS PARA SU APLICACIÓN EN PILAS PEM DE ALTA TEMPERATURA BASADAS EN MEMBRANAS DE PBI

Memoria para optar al grado de Doctor (Doctorado internacional) por la Universidad de Castilla-La Mancha

Héctor Zamora Triguero

Directores

Prof. Dr. Manuel Andrés Rodrigo Rodrigo

Prof. Dr. Justo Lobato Bajo

Ciudad Real, Enero de 2017

D. Manuel Andrés Rodrigo Rodrigo, Catedrático de Ingeniería Química de la Universidad de Castilla-La Mancha, y

D. Justo Lobato Bajo, Profesor titular del Departamento de Ingeniería Química de la Universidad de Castilla-La Mancha,

CERTIFICAN

Que el presente trabajo de investigación titulado:

"ESTUDIO DE ELECTRODOS MEJORADOS PARA SU APLICACIÓN EN PILAS PEM DE ALTA TEMPERATURA BASADAS EN MEMBRANAS DE PBI", constituye la memoria que presenta **D. Héctor Zamora Triguero** para aspirar al grado de Doctor por la Universidad de Castilla-La Mancha en el programa de doctorado de Ingeniería Química y Ambiental, y que ha sido realizado en los laboratorios del Departamento de Ingeniería Química de la Universidad de Castilla-La Mancha bajo su dirección.

Y para que conste a los efectos oportunos, firman el presente certificado en Ciudad Real a 28 de Noviembre de 2016.

Dr. Justo Lobato Bajo Dr. Manuel Andrés Rodrigo Rodrigo

FINANCIAL SUPPORT

The author further thanks the European Commission as this work was partially supported by the Seventh Framework Program through the project CISTEM (FCH-JU Grant Agreement Number 325262). Financial support from MINECO (Spanish government) is also acknowledged (CTM2013-45612R) through project ELECTROTECH4PEST. Also, the author is gratefully with UCLM and Carl Von Ossietzky Universität for the financial support for the internship performed in NEXT ENERGY (Oldemburg, Germany) through the IPID4ALL program.

En estas líneas quiero expresar mi agradecimiento a todas y cada una de las personas que han tenido mayor o menor implicación en la realización de esta Tesis Doctoral ya que sin ellas, no habría sido posible la finalización de la misma.

En primer lugar quiero dar las gracias al Departamento de Ingeniería Química de la Universidad de Castilla La Mancha. A Pablo, por su excelente labor dirigiendo al grupo de Ingeniería Electroquímica, y especialmente a mis directores, Manuel A. Rodrigo y Justo Lobato, los cuales confiaron en mí para iniciar mis estudios de Doctorado y que han sabido guiarme durante todos estos años, ayudándome en todo momento, resolviendo mis dudas, animándome a continuar y dándome apoyo, enseñándome a mejorar como investigador y como persona.

A mis compañeros y amigos del Laboratorio, Salva, Inma, Yeray, Maria José, Jose Fernando, Martín, Sarita, y al resto de mis compañeros del Enrique Costa, por los buenos momentos pasados y toda la ayuda que me han dado durante estos años.

Especialmente, a mis revisoras estrella, Alexandra y María, por ayudarme con la carga de trabajo que esta tesis ha supuesto, ayudándome en momentos críticos en estos tres años, con esas reacciones interminables para preparar el PBI, los millones de datos de voltametrías….sin las cuales todo este trabajo no hubiera sido posible, además de ayudarme a dejar la tesis en un formato mucho más bonito. Y como no a Jorge, compañero de fatigas del proyecto europeo durante estos 3 años, ayudando a sobrellevar todo el trabajo y presión que ha supuesto, y con los muy buenos ratos que hemos pasado y quedan por pasar dentro y fuera del laboratorio.

Al personal de la división de pilas de combustible de la empresa NEXT ENERGY, por permitirme hacer la estancia en sus instalaciones y por todas las cosas que he aprendido

con ellos. Y gracias a Javi, por ayudarme tanto en la estancia como a hacer más llevaderos esos tres meses fuera de casa.

A mis amigos en general, tanto de la Universidad como de Cuenca, por apoyarme y distraerme en los momentos más duros de la tesis, cuando parecía que esto no acababa nunca.

A mi familia, por darme el apoyo desde el principio de la carrera para poder llegar a este punto, con todo el esfuerzo económico y personal que supone, ayudándome siempre en todo lo que han podido.

A Helena, por darme todo el cariño, apoyo y comprensión durante todos estos 3 años, animándome en todo momento, y aguantándome en los ratos malos, disfrutando todos los buenos.

A todos los que de una manera u otra han aportado su granito de arena para esta Tesis,

Gracias.

Index

CHAPTER 1. Summary /Resumen

Nowadays, it is assumed that the oil age has entered its final stretch, with a maximum horizon of 40 to 50 years. The growing energy demand, together with the negative environmental impact of non-renewable energy sources, make necessary to focus the research efforts on the development of energy sources and technologies that may reduce the dependence of our economy on oil, which in turn, will help to prevent the negative consequences of an abrupt cessation of the current energy supplies.

Fuel cells are devices that can be used to produce energy from hydrogen and other fuels with high efficiency. Attending to the components, electrolyte, reactants and operational conditions, fuel cells are divided into different types.

In this work, the study is focused on polymer electrolyte membrane (PEM) fuel cells, particularly in a variety of this type of fuel cells, the High Temperature Proton Exchange Membrane Fuel Cells (HT-PEMFCs), which have been an active field of research and development for more than two decades. This kind of fuel cells operates in a wide temperature range (from 100 to 200 ºC), relative higher to the traditional PEMFC technology, which typically operates at 80 ºC (also called Low Temperature PEMFC or LT-PEMFC). Although, it may be thought that the temperature range from 100 to 200 ºC is not very high respect to the 80 ºC of the LT-PEMFCs, a significant effort is indeed behind the development of high temperature polymer electrolyte membranes and their cells, from both, the materials science and the technological points of view. Thus, the high temperature operation range has a negative effect on the thermal, chemical, and mechanical stability of the membrane and electrodes that constitutes the MEA (membrane-electrode assembly), the central part of the fuel cell. In this point, many research activities have been focused on the enhancement of the PBI membranes, increasing their durability and physicochemical properties to increase the fuel cell performance, while the improvement of the electrodes have still two main critical points: the reduction in the cost associated to the catalytic layer, since precious metals such

as Pt or Pd are used as electrocatalysts, and the improvement of the electrochemical resistance and durability of the electrodes at the operating conditions of the fuel cell.

The improvement of the electrodes can be focused on the improvement of the gas diffusion layer or the catalytic layer. On one hand, the Gas Diffusion Layer (GDL) of the electrodes of HT-PEMFCs is situated between the catalyst layer and bipolar plate and it is subdivided into the Gas Diffusion Backing (GDB) and the Micro-Porous Layer (MPL). GDB is composed of carbon fibers, usually carbon cloths or papers substrates. Their main function is to promote an adequate diffusion of the gases through the entire electrode surface, and also to collect and transport the current to bipolar plates. On the other hand, the MPL, consisting of porous nano-sized carbon powders, improves the diffusion of reactant gases and liquids, minimizing electric contact resistance between the catalyst layer and bipolar plates, and managing the water balance during production, expulsion, supply and evaporation. The degradation of this layer carries out a significant decrease in the service lifetime and performance of the fuel cell. On the other hand, one of the main challenges of HT-PEMFC is to get high performance and durability with low-cost catalysts and this fact is becoming a bottleneck for the technology, because of the high price of platinum, which, unfortunately, is the key and almost the only catalyst available today for HT-PEMFC. One interesting topic of research deals with the reduction of the platinum content in the electrocatalyst. At this point, two main ways are usually studied to reduce the platinum content: the first way consists of increasing the platinum utilization in the catalyst layers, improving the bounding and active area of the metal particles by improving the synthesis method or the catalyst support, allowing the use of lower Pt amounts in the MEA manufacturing. The other way consists of reducing the platinum load by alloying Pt with inexpensive metals such as Co, Fe, etc. In supported electrocatalysts, platinum is typically dispersed into carbonaceous materials, being the preparation of this mixture carbon-platinum very important, because it may affect the performance of the whole HT-PEMFC. Surface area, porosity, electrical conductivity,

electrochemical stability and surface functional groups are the key characteristics to be optimized in order to get a good electrocatalyst support.

The conventionally used carbon support and raw materials to prepare the Pt catalyst and the MPL is the Vulcan Carbon XC72, due to their good physicochemical properties, easily commercial available and low cost, but unfortunately, Vulcan carbon undergoes high corrosion processes under typical operation conditions at both electrodes in the HT-PEMFCs, being more significant those happening on the cathode. This corrosion is caused by the hot acidic conditions provided by the PBI membrane doped with phosphoric acid, and the high voltages achieved by the MEA during the start-on and shut-down operations.

With this background, this PhD was focused on the improvement of the performance and durability of the cathodic electrode used in HT-PEMFC, trying to overcome the main limitations of the technology nowadays. Regarding to this goal, it is worth having in mind some points about two critical components of the electrodes, which have a strong influence on the durability of the fuel cell: the MPL, and the catalyst support, focused on the usage on the cathode side, because of the potential formation of powerful radical oxidants during the reduction of oxygen, which accelerates the oxidation and corrosion processes of the electrode elements. Taking into account this fact, in the present work, the main objective is the development of optimized MPLs and catalysts supports to be used in the cathode of HT-PEMFCs based on PBI membranes doped with phosphoric acid. The target is to improve its durability and performance with respect to the standard and well-known Vulcan carbon based electrodes. Based on the state of the art of the technology in the moment of the starting up this PhD, different carbonaceous (Carbon nanofibers platelet (CNFp), carbon nanospheres (CNSs), both manufactured in our facilities) and non-carbonaceous materials (Silicon carbide (SiC) and Silicon-titanium carbide (Si_xTi_yC) with different Si:Ti ratios, both commercially available) were proposed to substitute the Vulcan carbon black in both elements.

In the first part of this Thesis, all materials were physicochemically characterized. Critical parameters, such as surface area, porosity, hydrophobicity and electrical conductivity were studied. It was observed that non-carbonaceous materials (based on SiC materials) exhibited lower porosity, electrical conductivity and hydrophobic character than the carbonaceous one. It was also observed that the Si:Ti ratio of the binary carbide had a critical influence on these parameters, especially in terms of the electrical conductivity, which was increased with higher ratios of TiC on the binary carbide composition, and surface area and porosity, which decreased with the TiC content, but increasing the average pore size. Moreover, since the density of the non-carbonaceous materials is much higher than the carbonaceous one, the material loading to prepare the MPL was investigated, finding the optimum value in the range between 2 and 4 mg cm^{-2}.

Once fully characterized, all studied materials were evaluated as MPL. The stability of the materials under harsh conditions was evaluated firstly through ex-situ characterization. Thermal stability under hot acidic environment of different MPLs prepared with all studied materials was assesed placing the samples impregnated in 85% wt. phosphoric acid into an oven during 8 hours at 185 ºC. Results showed that non-carbonaceous and CNSs based MPLs exhibited an excellent stability under these conditions, while the Vulcan carbon and carbon nanofibers underwent high degradation on the material surface, determined by X-ray diffraction analysis. Then, electrochemical stability of the materials was investigated. Circular electrodes prepared with the different materials were subjected to cyclic voltammetries in 2M phosphoric acid solution. Similar results than those obtained in the thermal stability study were attained, being the CNSs and the binary carbide the most promising materials to be used as MPL.

Then, preliminary short-term tests of 100 hours were carried out into a 25 cm^2 fuel cell using MEAs with cathodes prepared with the new materials. Carbon nanofibers based MPL exhibited a bad performance due to the layer was compact and exhibited very low gas

permeability. Regarding to the non-carbonaceous materials, both showed same mass transfer problems due to the low porosity of the SiC based materials. In addition, SiC also exhibited very high ohmic resistance, traduced in low performance of the MEAs manufactured with these materials. Nevertheless, the CNSs based MEA showed an acceptable performance in terms of power density, and the stability was greatly improved as compared to that of a standard Vulcan carbon based MEA. It was also observed that the $Si_{0.7}Ti_{0.3}C$ material exhibited closely similar properties (in terms of electrical conductivity and porosity) than CNSs, so it was decided to consider both materials to be tested as MPL raw materials in a fully optimized cathode.

Once the development of the MPL was completed, the attention was focused on the catalysts. Thus, different 40% wt. Pt based catalysts where synthesized by the formic acid method using the different materials as catalysts supports. The manufactured catalysts were physicochemically analyzed by X-ray diffraction (XRD), SEM and TEM microscopy and temperature programmed reduction (TPR) analysis, in order to get more information about the dispersion of the Pt particles and the presence of Pt oxides on the final catalyst. Results showed that CNSs and $Si_{0.7}Ti_{0.3}C$ are not adequate to prepare Pt based catalyst, because their very low surface area avoids the correct deposition of the Pt particles. Opposite, the CNFp achieved excellent values in terms of Pt particle size and dispersion. Regarding to the rest of SiC based materials, the $Si_{0.9}Ti_{0.1}C$ achieved the best results, with higher Pt size than the value achieved using Vulcan carbon or CNFp, but still into an acceptable range to get good electrochemical active surface area (ECSA). As it is known, this parameter is directly related to the Pt size and dispersion, and the higher the values of these two parameters, the higher is the active surface area of the catalyst. In order to get more information about the activity and electrochemical stability of the synthesized catalyst, they were subjected to a voltammetry analysis. In first place, Rotating Disk Electrode (RDE) measurements were performed to evaluate the ECSA and the oxygen reduction reaction (ORR) of the catalysts, since they will

be used on the cathode side, achieving the best results using the $Si_{0.9}Ti_{0.1}C$ and the CNFp based catalyst, which showed values in terms of activity closer to the achieved by the commercial Pt/Vulcan XC72 catalyst. As it was expected, the highest ECSA values were also achieved by these catalysts, while the Pt/SiC and Pt/$Si_{0.7}Ti_{0.3}C$ based catalyst achieved lower ECSA values, due to the worse Pt dispersion on the catalyst support. Stability of the electrocatalysts was evaluated using 1.5 cm^2 circular carbonaceous electrodes with a catalyst layer of 0.3 mg Pt cm^{-2} prepared with the different catalysts. These electrodes were placed in a half cell system and were subjected to a cyclic voltammetry test in 2M phosphoric acid solution at 50 ºCin order to analyze the electrochemical degradation of the different catalyst layers by the decreasing of the ECSA value. Results showed that SiC, Si_xTi_yC (10 and 20% mol. content) and CNFp based catalyst underwent much lower degradation rate than the commercial Pt/Vulcan carbon catalyst.

Finally, preliminary short-term fuel cell operation tests with the new catalysts in the cathode of a 25 cm^2 MEA were carried out. In this case, the CNFp and $Si_{0.9}Ti_{0.1}C$ based MEAs exhibited very good values in terms of stability ($Si_{0.9}Ti_{0.1}C$) and performance (CNFp) as compared to the obtained by fuel cells equipped with standard Vulcan XC72 based cathodes.

In the last Chapter of the PhD, two optimized cathodes were manufactured using only the optimum materials selected in the previous studies: the first one using the optimum carbonaceous materials (CNSs in the MPL and 40%Pt/CNFp as catalyst) and the second one using the non-carbonaceous materials ($Si_{0.7}Ti_{0.3}C$ in the MPL and 40%Pt/ $Si_{0.9}Ti_{0.1}C$ as catalyst). Then, short life tests of around 300 hours were used to evaluate the behavior of these optimized electrodes in a 25 cm^2 HT-PEMFC system set up at 160 ºC. The obtained results were compared to those obtained by a fuel cell equipped with a standard Vulcan carbon cathode. In order to maximize the degradation of the MEA, pure oxygen was used as oxidant, and characterization protocols (polarization curves, EIS, cyclic voltammetries and linear sweep voltammetries) were performed every 48 hours during the tests. The optimized

nanocarbonaceous-based cathode exhibited excellent results in terms of stability and performance, improving these values with respect to the obtained by a standard Vulcan carbon-based cathode at the end of the test. No signs of degradation were observed during the life test, but an activation process, with a final voltage increasing rate of around +27 μV h^{-1}, while the standard MEA exhibited voltage drops around -47 μV h^{-1}. Regarding to the maximum power density values achieved, the optimized nanocarbonaceous based MEA showed final values around 350 mW cm^{-2}, while the fuel cell equipped with the standard cathode showed 300 mW cm^{-2}. This fact can be explained in terms of the enhancement of the stability of the catalytic layer, since no signs of active surface losses were noticed during the cyclic voltammetries performed along the different characterization tests.

On the other hand, the Si_xTi_yC based MEA did not show a good performance, probably due to the high ohmic resistance, with exerted cell voltages around 70 mV below the values obtained by the fuel cell equipped with the Vulcan carbon. Further studies must be performed with this material in order to optimize the usage of the novel binary carbide on HT-PEMFC technology, since it has been demonstrated than when $Si_{0.9}Ti_{0.1}C$ is used as catalyst support, an important increase in terms of the stability of the electrode is observed. Also, it could be possible to reduce the Pt loading using Pt/CNFp catalyst, since mass transfer problems were detected when air was used as oxidant, which means that the optimization of this parameter could increase the performance attained by this electrode which, in turn, will help to reduce the cost of the MEA manufacturing.

Actualmente, se asume que la era del petróleo ha entrado en su recta final, con un horizonte máximo previsible de uso de esta fuente de energía que estaría en el intervalo de 40 a 50 años. En este contexto, la demanda creciente de energía, junto con el negativo impacto ambiental derivado del empleo de las fuentes de energía no renovables, están haciendo necesario centrar los esfuerzos de investigación en el desarrollo de nuevas fuentes de energía y de nuevas tecnologías de conversión, que puedan reducir la dependencia de nuestra economía con respecto al petróleo. Esto, a su vez, ayudaría a prevenir las consecuencias negativas de una interrupción brusca del suministro de energía basado en petróleo.

Las celdas de combustible son dispositivos que pueden ser utilizados para producir energía a partir del hidrógeno y otros combustibles. Se clasifican en diferentes tipos atendiendo a los componentes, los electrolitos, los reactivos y las condiciones de funcionamiento. De entre ellos, este trabajo se ha centrado en las celdas de combustible de membrana polimérica, especialmente en las celdas de combustible de membrana de intercambio protónico de alta temperatura (HT-PEMFCs), que han sido un campo de investigación y desarrollo muy importante durante más de dos décadas. Este tipo de celdas opera en un amplio intervalo de temperatura (de 100 a 200 ºC), relativamente superior a las tradicionales celdas PEM de baja temperatura (LT-PEMFC), que normalmente operan a 80 ºC. Aunque se puede pensar que la diferencia entre las temperaturas de operación de ambas tecnologías no es muy grande, se ha tenido que realizar un importante esfuerzo en el desarrollo de la membrana polimérica que actúa como electrolito en este tipo de celdas, tanto desde el punto de vista de la ciencia de los materiales como de la operatividad. Así, es sobradamente conocido que el aumento del intervalo de temperatura de operación tiene un efecto negativo en la estabilidad de la membrana y de los electrodos que constituyen la MEA (siglas en lengua inglesa del ensamblaje membrana-electrodo), la parte central de la celda de combustible. En este punto, en Tesis anteriores la actividad de investigación de nuestro Grupo de investigación se centró en la mejora del polibenzimidazol (PBI), el polímero empleado en

la síntesis de estas membranas, aumentando su durabilidad y propiedades físico-químicas, lo que tuvo una repercusión positiva en el rendimiento de la celda. Actualmente, nuestra investigación está centrada en la mejora de los electrodos, cuya operatividad tiene todavía dos puntos críticos importantes: la reducción en el coste asociado a la capa catalítica, ya que se utilizan grandes cantidades de metales preciosos (como el Pt o Pd) como electrocatalizadores, y la mejora de la resistencia electroquímica y durabilidad de los electrodos en las condiciones de operación de la celda de combustible.

La mejora de los electrodos puede estar centrada en la capa de difusión de gases (cuyo acrónimo en inglés es GDL), o en el catalizador contenido en los mismos. La GDL de los electrodos de HT-PEMFCs está situada entre la capa catalítica y las placas bipolares, y se subdivide en las capas macroporosa (GDB) y microporosa (MPL). La GDB está compuesta por fibras de carbono, en forma de tela o papel. Su función principal es servir de soporte para el resto de las capas del electrodo y transportar la corriente eléctrica hasta las placas bipolares. Además, favorece una adecuada difusión de los gases a través de toda la superficie del electrodo. La MPL, normalmente de naturaleza carbonosa, mejora la difusión de los gases y líquidos, minimizando la resistencia eléctrica de contacto entre la capa catalítica y la GDB. También ayuda a mejorar la gestión del agua durante la operación de la celda. La degradación de esta capa produce una importante disminución en la vida útil y en el rendimiento de la celda de combustible.

En este contexto, uno de los principales retos de la tecnología de HT-PEMFCs es conseguir un alto rendimiento y durabilidad de las celdas, y un bajo coste. Este último punto se está convirtiendo en un factor limitante para la tecnología, debido al elevado precio del platino que, por desgracia, es el principal y casi el único catalizador eficiente disponible hoy en día. Por este motivo, las investigaciones que abordan la reducción del contenido de platino son de un gran interés en la actualidad. Las dos principales vías de actuación que se están siguiendo son: el incremento en la utilización de platino en la capa catalítica, mediante la

mejora de la dispersión del platino por la superficie del soporte catalítico, y la reducción en la carga de platino mediante su aleación con metales no nobles, tales como Co, Fe, etc.

El soporte catalítico tiene una gran repercusión en el rendimiento de la celda. El área superficial, la porosidad, la conductividad eléctrica, la estabilidad electroquímica y la existencia de grupos funcionales en la superficie del soporte son las características clave buscadas para un buen soporte catalítico. El negro de carbón es la familia de materiales más utilizados como soporte catalítico y como MPLs, siendo el carbón comercial Vulcan XC72 el material más común, debido a sus buenas propiedades físico-químicas, su amplia disponibilidad comercial y su bajo coste. Por desgracia, este material sufre procesos de corrosión severos bajo las condiciones de operación de las celdas de combustible de alta temperatura, siendo estos procesos más importantes en el cátodo. Esta corrosión está favorecida por el ácido fosfórico caliente que proviene de la membrana de PBI y por los altos valores de potencial alcanzados por la MEA durante el arranque y apagado de la celda.

Con estos antecedentes, la presente Tesis parte de la necesidad de mejorar el rendimiento y la durabilidad de los cátodos utilizados en HT-PEMFCs, tratando de superar las principales limitaciones que presenta la tecnología hoy en día. En relación a este objetivo, centra su interés en los dos componentes críticos de los cátodos, que tienen una fuerte influencia de la durabilidad de la celda de combustible: la MPL, y el soporte catalítico. Así, el objetivo principal se concreta en la optimización de MPLs y soportes catalíticos de los cátodos de HT-PEMFCs basadas en membranas de PBI dopadas con ácido fosfórico, mejorando su rendimiento y durabilidad con respecto a los electrodos basados en el tradicional Vulcan XC72. Teniendo en cuenta el estado del arte de la tecnología en el momento de la puesta en marcha de esta Tesis, se han estudiado diferentes materiales carbonosos (nanofibras de Carbono Platelet (CNFp) y nanoesferas de carbono (CNSs), fabricados en nuestras instalaciones) y no carbonosos (carburo de Silicio (SiC) y carburo de Silicio-Titanio (Si_xTi_yC), para sustituir el carbón Vulcan en ambos elementos.

En la primera parte de esta Tesis, todos los materiales fueron caracterizados fisicoquímicamente. Se estudiaron parámetros importantes tales como el área superficial, la porosidad, la hidrofobicidad y la conductividad eléctrica. Se observó que los materiales no carbonosos tenían unas menores porosidades, conductividades eléctricas y carácter hidrofóbico respecto a los materiales carbonosos. También se observó que la proporción de Si:Ti en el carburo binario influía de forma notable sobre estos parámetros, especialmente en la conductividad eléctrica (que se incrementaba con la mayor proporción de TiC en el carburo binario) y en el área superficial y la porosidad (que disminuían con el contenido en TiC). Por otra parte, ya que la densidad de los materiales no carbonosos es mucho mayor que la de los carbonosos, se estudió la influencia de la carga del material al preparar la MPL, encontrando que el valor óptimo para estos materiales novedosos está en un intervalo de entre 2 y 4 mg cm^{-2}, frente a los 2 mg cm^{-2} usados en las MPLs preparadas con carbón Vulcan.

Una vez caracterizados, todos los materiales estudiados fueron evaluados como componente para la MPL. En primer lugar, se evaluó la estabilidad de los materiales, mediante la colocación de muestras impregnadas en disoluciones al 85% en peso en ácido fosfórico en un horno, durante 8 horas a 185 ºC. Los resultados mostraron que las MPLs preparadas con CNSs y materiales no carbonosos tienen una excelente estabilidad térmica en estas condiciones, mientras que las preparadas con el carbón Vulcan y las nanofibras sufren una elevada degradación. Posteriormente se evaluó la estabilidad electroquímica de los materiales, para lo que se sometió a electrodos preparados con los diferentes materiales a una serie de voltametrías cíclicas en una disolución 2M de ácido fosfórico. Se alcanzaron conclusiones similares a las obtenidas en la evaluación de la estabilidad térmica, siendo las CNSs y los carburos binarios los materiales más prometedores para ser utilizado como MPL.

Una vez finalizados estos estudios se llevaron a cabo ensayos de operación de 100 horas(también denominados ensayos de vida) en una celda de combustible de 25 cm^2, utilizando MEAs en las que las MPL de los cátodos estaban preparadas con los nuevos

materiales. La MEA basada en CNFp exhibió un mal funcionamiento debido a que era muy compacta y, como consecuencia, presentaba una muy baja permeabilidad a los gases. Con respecto a las MEAs preparadas con los dos materiales no carbonosos, también mostraron problemas de transporte debido a la baja porosidad de los materiales basados en SiC. Además, en el caso de la MEA preparada con SiC se obtuvo una elevada resistencia óhmica, que generó un bajo rendimiento. Por el contrario, la MEA basada en CNSs exhibió un rendimiento aceptable en términos de densidad de potencia y una gran mejora en términos de estabilidad cuando se la comparaba con una MEA estándar basada en carbón Vulcan. También se observó que el $Si_{0.7}Ti_{0.3}C$ mostraba propiedades muy similares (en términos de conductividad eléctrica y de la porosidad) que las CNSs.

Finalizado el estudio de caracterización de la MPL, la atención se centró en la evaluación de la influencia de los nuevos materiales en la capa catalítica. Para ello, diferentes catalizadores con un contenido en Pt del 40% en peso fueron sintetizados por el método del ácido fórmico, empleando los diferentes materiales estudiados como soportes catalíticos. Estos catalizadores fueron analizados por difracción de rayos X (DRX), microscopía electrónica SEM y TEM, y análisis de reducción a temperatura programada (TPR), con el fin de obtener más información acerca de la dispersión de las partículas de Pt y la presencia de especies oxidadas. Los resultados obtenidos mostraron que las CNSs y $Si_{0.7}Ti_{0.3}C$ no son adecuados para preparar catalizadores basados en Pt, debido a que su baja área superficial evita la correcta deposición de las partículas de Pt. Por el contrario, las CNFp consiguieron excelentes resultados en términos de tamaño de partícula y de dispersión de Pt. En cuanto al resto de materiales no carbonosos, el $Si_{0.9}Ti_{0.1}C$ alcanzó los mejores resultados, aunque con mayor tamaño medio de partícula de Pt que el valor alcanzado usando Vulcan o CNFp. No obstante, el tamaño estaba en un intervalo todavía aceptable para obtener una adecuada área electroquímicamente activa (ECSA), parámetro que, como es bien sabido, está directamente relacionado con el tamaño de Pt y la dispersión de las partículas metálicas. Para obtener más

información acerca de la actividad y estabilidad electroquímica de los catalizadores, los electrodos fueron sometidos a un análisis voltamperométrico en el que mediante un Electrodo de Disco Rotatorio (RDE) se determinó el ECSA y la actividad hacia la reacción catódica de reducción de oxígeno (ORR), obteniendo mejores resultados los catalizadores soportados sobre $Si_{0.9}Ti_{0.1}C$ y CNFp, que mostraron valores en términos de actividad en el mismo intervalo que un catalizador comercial de Pt/Vulcan XC72. Como era de esperar, estos catalizadores también obtuvieron los mayores valores de ECSA, mientras que los catalizadores de Pt/SiC y Pt/ $Si_{0.7}Ti_{0.3}C$ obtuvieron peores resultados, debido a la peor dispersión de Pt en el soporte. La estabilidad electroquímica de los catalizadores fue evaluada usando electrodos circulares de 1.5 cm^2 con una capa catalítica de 0.3 mg Pt cm^{-2} preparada con los diferentes soportes. Estos electrodos fueron colocados en una semicelda utilizando una disolución de ácido fosfórico caliente 2M, con el fin de aumentar la velocidad de degradación de las diferentes muestras. Los resultados mostraron que los catalizadores basados en SiC, Si_xTi_yC (10 y 20% mol. TiC) y CNFp sufrieron una menor velocidad de degradación que el catalizador comercial que contenía carbón Vulcan. También se realizaron estudios de vida de 100 horas para comprobar el funcionamiento de los nuevos catalizadores en un celda de combustible de alta temperatura. En este caso, las MEAs preparadas usando los catalizadores basados en CNFp y $Si_{0.9}Ti_{0.1}C$ mostraron una muy buena estabilidad ($Si_{0.9}Ti_{0.1}C$) y rendimiento (CNFp) en comparación con los resultados obtenidos por la MEA estándar preparada con los componentes estándar.

En la última parte del trabajo de investigación que conforma esta Tesis, se prepararon dos cátodos en los que para fabricar la MPL y capa catalítica se utilizaron exclusivamente los materiales que mejores características demostraron en los estudios previos. Así, en el primero de los cátodos se usaron materiales carbonosos (CNSs en la MPL y 40% Pt/CNFp como catalizador) y en el segundo, materiales no carbonosos ($Si_{0.7}Ti_{0.3}C$ en la MPL y 40% Pt/ $Si_{0.9}Ti_{0.1}C$ como catalizador). Estos cátodos fueron evaluados en ensayos de vida más largos

que los utilizados en los estudios anteriores (300 horas utilizando oxígeno puro como oxidante) y se compararon los resultados con los obtenidos por una MEA estándar. Con el fin de maximizar la degradación de la MEA, se realizaron pruebas de caracterización (curvas de polarización, EIS, voltametrías cíclicas y de barrido lineal) cada 48 horas. La MEA preparada con nanomateriales de carbono mostró excelentes resultados en términos de estabilidad y rendimiento, mejorando estos valores con respecto a los obtenidos por la MEA estándar. Así, mientras que en la MEA estándar se observaba un proceso de degradación con una pérdida de voltaje de -47 $\mu V\ h^{-1}$ aproximada, la MEA preparada con los nuevos materiales carbonosos mostró un proceso de activación en vez de degradación durante todo el ensayo, con un aumento del voltaje promedio de aproximadamente 27 $\mu V\ h^{-1}$. Con respecto a la densidad de potencia máxima, la MEA preparada con los materiales carbonosos novedosos mostró valores finales de alrededor de 350 $mW\ cm^{-2}$, mientras que la MEA estándar alcanzó solamente 300 $mW\ cm^{-2}$. Este hecho fue explicado en términos de la mejora de la estabilidad de la capa catalítica, ya que no había signos de pérdidas importantes de área activa a lo largo de las diferentes pruebas de caracterización, situación opuesta a la MEA estándar, donde sí se observaron pérdidas apreciables de este parámetro. Por último, la MEA basada en Si_xTi_yC no mostró un buen rendimiento, probablemente debido a su elevada resistencia óhmica, con valores de voltaje que estaban aproximadamente 70 mV por debajo de los valores obtenidos por MEA estándar. A pesar de estos peores resultados, se deberían hacer estudios adicionales con este material, con el fin de optimizar el uso de este carburo binario en la tecnología de HT-PEMFC, ya que cuando se utiliza $Si_{0.9}Ti_{0.1}C$ como soporte catalítico se observa un aumento importante en términos de la estabilidad del electrodo. También, podría ser interesante reducir la carga de Pt en los catalizadores de Pt/CNFp, lo que ayudaría a reducir los problemas de transporte detectados al usar este catalizador, o combinar los materiales carbonosos y no carbonosos más prometedores entre ellos (MPL preparada con CNSs y $Pt/Si_{0.9}Ti_{0.1}C$ como catalizador, por ejemplo).

CHAPTER 2. Introduction

2.1. Hydrogen as energy vector

Nowadays, it is assumed that the oil age has entered its final stretch, with a maximum horizon of 40 to 50 years. Then, it is expected that world production of conventional oil starts to decline, while its demand remains increasing, especially due to emerging countries like China and India. This growing demand, together with the negative environmental impact of non-renewable energy sources, makes necessary to focus the research efforts on the development of energy sources and technologies that may reduce the dependence of our economy on cheap oil, which in turn, will help to prevent the negative consequences of an abrupt cessation of the current energy supplies.

In this context, the development of renewable energy has emerged as an important challenge for Society that will help to increase energy self-sufficiency levels, while allowing a more environmental-friendly model. In the last years, it has been demonstrated that hydrogen can be used as a possible renewable and sustainable alternative [1]. In this sense, it must be pointed out that hydrogen is not a pure energy source, but an energy vector, since hydrogen is not found isolated in nature, being necessary another compound such as petroleum or water to obtain it. This fact has been one of the hottest topics of debate in recent years [2-4], although the production of hydrogen with electrolysis processes powered with green energies has been found to be one of the most environmentally-friendly alternatives. Moreover, the final products when hydrogen is used as fuel, either in fuel cells or in combustion engines, are water, energy and heat, making this fuel of the most environmentally-sustainable fuels nowadays [5,6]. These reasons make the hydrogen technology a better alternative than other energy sources/technologies, such as nuclear energy.

The critical point in the exploitation of the hydrogen is related with its transport, storage and distribution, due to the particular physicochemical properties of this element.

However, the so-called “hydrogen economy” exhibits some benefits, such as the high energy efficiency of the hydrogen in fuel cells, not limited ty the Carnot efficiency, because in fuel cells the chemical energy contained in hydrogen is transformed directly into electricity and heat [7]. In addition, this kind of technology can be suited to portable applications, replacing the batteries with hydrogen cartridges (which can be used also with methanol).

2.2. Fuel cells

As it was pointed out elsewhere [5-7], fuel cells are devices that can be used to produce energy from hydrogen. Attending to the components, electrolyte, reactants and operational conditions, fuel cells are divided into different types. However, all of them show the same operational system, shown schematically in Figure 2.1.

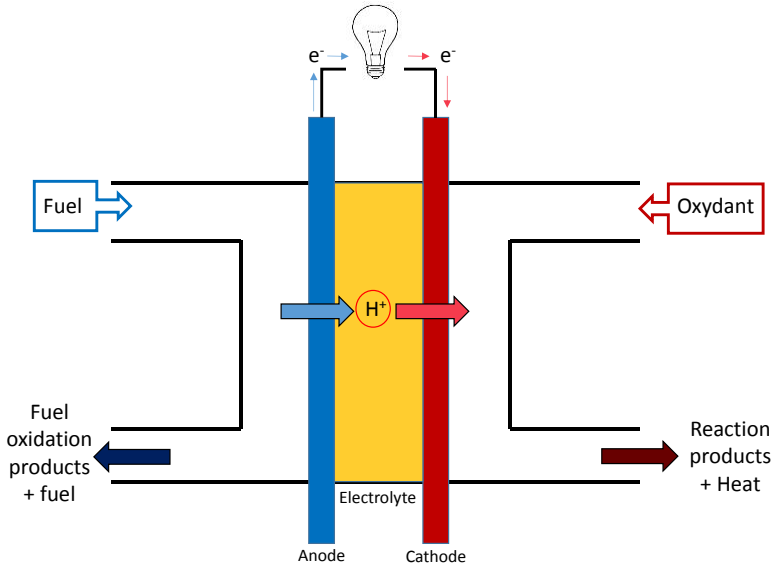

Figure 2.1. Schematic operation of a fuel cell

Firstly, fuel is introduced into the anodic section of the fuel cell, in which is oxidized, generating protons and electrons. Electrons are conducted by an external electrical circuit, producing the energy, and ionic species cross through the electrolyte to the cathodic section, closing the ionic circuit and reacting with the oxidant, generating the reduced oxidant products (usually water) and heat.

Fuel cells directly convert the free energy (ΔG) of a reaction into electricity. Thermodynamic allows relating the chemical energy to electrical energy using Equation 2.1 [8], wherein *n* is the number of exchanged electrons, *F* is the Faraday constant, and E_0 is the cell voltage at thermodynamic equilibrium. For the system most commonly used in fuel cells (hydrogen and oxygen gas as fuel and oxidant, respectively) the ΔG value is -237 kJ mol^{-1}, which corresponds to a standard equilibrium potential of 1.23 V. This fact allows to the fuel cells to achieve higher efficiency values than thermal machines, which are known to be limited by the Carnot's cycle [8].

$$\Delta G = n.F.E_o \qquad (2.1)$$

In addition to this fact, fuel cells exhibit some advantages respect to the traditional energy sources, such as [7, 9]:

- Environmental benefits. Fuel cells are very interesting from the environmental point of view, because of their zero emissions when fed with hydrogen, which could help to reduce the carbon dioxide emissions and the emission of other air pollutants derived from the usage of conventional non-renewable fuels.
- The absence of moving parts, which greatly simplifies maintenance of the fuel cell.
- Easy to be located at any location, key point for distributed power generation.
- Possibility to operate with different fuels: hydrogen, alcohols, natural gas…
- Reasonable availability and proven reliability and durability of the systems operating at low temperature.
- High flexibility and modularity of facilities, allowing a perfect match to the load demand.
- Possibility of remote operation of the cell, which reduces the costs of operation and maintenance.
- Fast response to changes in energy demand.

All this reasons make fuel cells a very attractive alternative energy device, but this technology also presents disadvantages:

- Difficult entry into the energy market, due to the currently high cost of these systems.
- The durability and reliability of the units operating at high temperatures (T> 800 ° C) has not been fully demonstrated.
- The full development of the value chain of this technology is not adequate yet, being necessary to develop systems for the efficient distribution and storage of hydrogen, etc.

2.3. High temperature PEM fuel cells

As it is pointed out elsewhere [5, 7], attending to the operational temperature, electrolyte, fuel, electrodes and catalysts, fuel cells can be divided into different groups. In this work, the study is focused on polymer electrolyte membrane (PEM) fuel cells, particularly in a sub type of this type of fuel cells, the High Temperature Proton Exchange Membrane Fuel Cells (HT-PEMFCs), which have been an active field of research and development for more than two decades.

This type of fuel cells operates in a wide temperature range (from 100 to 200 ºC), relative higher to the traditional PEMFC technology, which typically operates at 80 ºC (also called Low Temperature PEMFC or LT-PEMFC). It should be stressed that fuel cells working at temperatures up to 200 ºC still are classified as low temperature fuel cells, in contrast to the "real" high temperature fuel cells, which are molten carbonate fuel cells (MCFC) and solid oxide fuel cells (SOFC), all working at temperature above 600 ºC [9]. Although, it may think that the temperature range from 100 to 200 ºC is not very high respect to the 80 ºC of the LT-PEMFCs, a significant effort is indeed behind the development of high temperature polymer electrolyte membranes and their cells, from both the materials science and the technological points of view. Thus, the high temperature range has a negative effect on the

thermal, chemical, and mechanical stability of polymer materials of which the membrane is made of. Likewise, because water is not in liquid phase within this temperature range, conductivity of membranes becomes a handicap and other ionic transport mechanisms need to be promoted. In this context, the use of phosphoric acid with PBI membranes in HT-PEMFCs was a real milestone for the technology [9].

2.3.1 HT-PEMFCs components

The most important components constituting a PEMFC are the end plates, the electrodes and the ion exchange membrane. All of them are represented in Figure 2.2 [8]. Moreover, in addition to these components, different gaskets are located between the membrane-electrode assembly (MEA) and bipolar plates, and also into the feeding channels, to prevent leakage of gases fed to the cell.

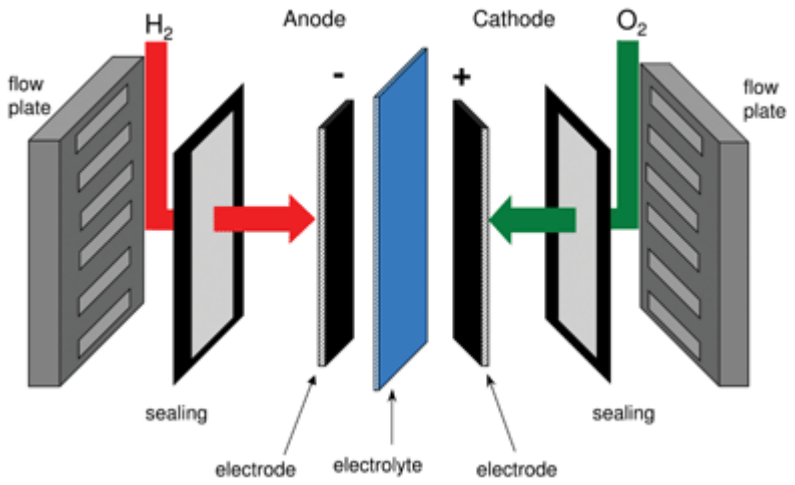

Figure 2.2. Schematic representation of the HT-PEMFC typical components

Because this work is going to be focused on the development of one of the components, it is worth describing their most important features.

Bipolar and final plates: The final and bipolar plates have the function of acting as a support for all elements of the cell, allowing the electron transit through the external circuit and providing a primary gas distribution through the electrodes. In laboratory plants, the

traditional building material of the bipolar plates is graphite, because of its chemical stability and high electrical and thermal conductivity [10]. However, for full-scale use, the choice of graphite turns out to be relatively unfeasible due to its fragility and difficulty to be mechanized. Alternatively, it has been proposed the use of metals, such as stainless steel or titanium, but alone, these materials show corrosion problems, leading to the formation of oxide layers which increase the resistance of the system [10, 11]. In order to face these problems, a layer of a noble metal (platinum, gold or silver) [11, 12] can be deposited covering their surface. This coating avoids corrosion problems, although it increases significantly the manufacturing cost.

Electrodes, which are divided into two different layers:

- Gas diffusion layer, essential for the operation of fuel cells and meets three functions: To facilitate the diffusion of gas to the electrodes; mechanically support the whole MEA; and provide a way out of the anode and the cathode inlet electrons [13]. The diffusion layer is located between the plates and the catalyst layer, and its porous nature ensures the effective distribution of each reactive gas to the catalyst. Gas diffusion layer has a double layer structure: First, a macroporous layer, consisting of a fiber cloth or paper carbon, which serves as a current collector and as a physical support for electrode. It is often called gas diffusion backing (GDB). To manufacture this material, carbon fibers are carbonized at 1000 ºC and then they undergo a process of "graphitization" at a temperature between 1750-2700 ° C. The operational conditions of the fuel cell in which the electrodes will be used define the graphitization conditions, being higher in HT-PEMFCs, because the working environment is much more corrosive than in LT-PEMFCs. In a final step, PTFE is added the GDB to increase its hydrophobicity character [14].

The other component of the GDL is a thinner layer, the MPL, which is usually composed of carbon black powder and a hydrophobic agent (PTFE or FEP) in a percentage between 5 and 30%. To manufacture this layer, an ink containing the carbonaceous powder, the hydrophobic agent and a solvent is prepared. Then, the microporous ink is deposited on the GDB using airbrushing or other similar methods, resulting in MPL itself. Finally, the complete GDL it sintered at a temperature that varies with the hydrophobic agent used (280 ° C to 360 ° C for FEP and PTFE, respectively). It has been demonstrated that the addition of the MPL increases the effective utilization of the catalyst and improve the overall performance of fuel cells. In addition, the use of MPL carries out some other advantages [15, 16]:

- It allows a more homogeneous distribution of the current density, because of a more intimate contact between the microporous layer (gas diffusion layer) and the catalytic layer.
- It avoids the migration of the catalyst particles over the catalytic layer, increasing the durability of the fuel cell and stabilizing the catalytic activity for longer periods.
- In LT-PEMFC, the microporous layer helps to solve the flooding problems related to the liquid water generation in the cell. In HT-PEMFCs, due to the absence of liquid water, this parameter is not as critical as for the case of LT-PEMFCs [16]. However, its pore size and distribution improve the diffusion of the reactants through the electrode surface, improving the overall performance of the fuel cell.

The most critical parameter is the gas permeability (especially, the permeability of oxygen when air is used as oxidizing agent). An inadequate gas distribution through the electrode surface may cause a serious decrease in the fuel cell performance. MPL provides a high pore volume with small average pore size, which improves the gas

diffusion [26]. A suitable pore size distribution improves the fuel cell performance, achieving higher values if the porosity is graded and inhomogeneous. In addition, it has been demonstrated in LT-PEMFC that the usage of graded porosity MPL enhances the water removal and the cell performance at high current densities [17, 18]. At this point, it is worth saying that the type of carbon used in the synthesis of the MPL directly influences the pore size and porosity of the system. [15].

- Catalytic layer, where the electrochemical reactions of the fuel cell take place. Its location is between the polymer electrolyte membrane and the gas diffusion layer, and should be in close contact with both elements [19]. This layer generally consists of a supported noble metal catalyst deposited on a porous carbon support. In general, platinum is the most active of all noble metals to catalyze the reactions that occur in the PEMFC cells (both the anode and the cathode). However, the price of the material, and especially their limited availability for possible main stream application in fuel cells, has been encouraged in recent years the development of other catalytic materials such as platinum alloys with other transition metals (Pt-Ru, Pt-Sn, Pt-Cr, etc.). It has also been faced the direct substitution of the platinum by non-noble metal alloys (Fe-Co, Fe-Ni, etc), but all of them are still well below than the platinum catalysts in terms of performance [20]. Alloys of platinum with other noble metals are found to not only achieve the objective of reducing the required amount of platinum in the catalytic layer, but also they also increase tolerance of platinum to poisons, such as carbon monoxide [21]. The second element of the catalytic layer is the support, whose function is to act as electronic conductor. It also improves the dispersion of the catalyst, increasing therefore its active area and performance. To manufacture the catalytic layer, usually inks containing the Pt supported catalysts and the polymer electrolyte are used. This allows to generate a three dimensional grid (Three Phase Boundary, TPB) in the catalytic layer, in which platinum particles are in contact with

carbon particles (that allow the electrons transport) and also with the polymer (ionomer), allowing the movement of ionic charges in the catalytic layer [22, 23]. In Figure 2.3, a representation of the triple layer structure of the electrode is shown.

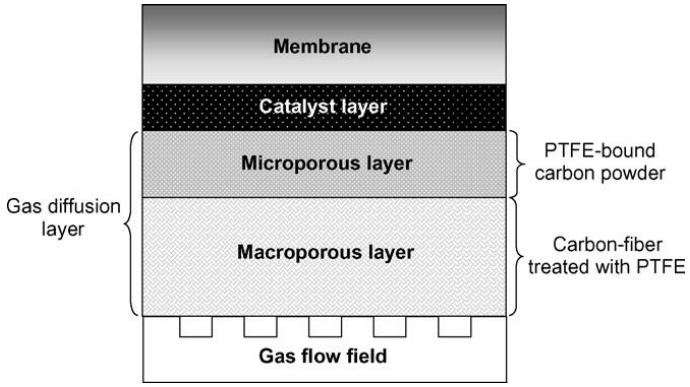

Figure 2.3. Schematic representation of the different electrode components.

Ion exchange membrane. The function of the ion exchange membranes (usually proton exchange membranes) is to permit the transport of ionic charges, closing the ionic circuit of the electrochemical cell. Simultaneously, this membrane acts as a barrier to prevent crossing of gases through it. Hence, this barrier prevents the direct combustion of fuel and, consequently, avoids a decrease in the efficiency [24]. These membranes must have high mechanical and chemical stability, since they are in contact with relatively extreme oxidizing and reducing gases in an acid environment [25], and they also need to exhibit a high ionic conductivity to avoid significant ohmic drops. They must have high durability and reliability, because they are the most sensitive part of the system. The technological development of the PEMFC cells has been always linked to advances in polymeric materials used as the electrolyte. At the present moment, the perfluorosulfonated polymers, such as Nafion, are the preferred choice to be used in the casting of proton exchange membranes for LT-PEMFC [26].

An important limiting factor is that these membranes must be hydrated, in order to allow the transit of ionic charges [27], which unable the membranes prepared with these materials to work above 100 ° C. Other problems related with the use of

perfluorosulfonated membranes are related to the high cost of the material, low tolerance to CO, some environmental problems related to the management membranes after application, and high methanol permeability, which significantly limits its application in PEM fuel cells fed with methanol (DMFC) [28]. In HT-PEMFCs, this material does not work properly and it has been substituted by other polymers, such as the polybenzimidazole (PBI), which performs in a way that help to overcome the problems related with the hydration of the Nafion membranes at temperatures over 100 ºC. Thus, this material exhibits excellent mechanical, thermal and chemical properties within the operational temperature range of HT-PEMFC, and it also has an excellent proton conductivity when doped with phosphoric acid. In addition, this type of membranes has received an intensive research activity, in order to improve the mechanical and service lifetime properties of this material to enhance the HT-PEMFC performance. Thus, modifications such as heat treatments, or the developing of composite PBI membranes have been studied, with promising results [29-31] making the PBI membranes the best option nowadays to be used in HT-PEMFC technology. Unfortunately, the acid doping requirements of these PBI membranes also increases the degradation of the other components of the fuel cell, as it will be explained below.

2.4. Electrode degradation in HT-PEMFCs

As it has been said, the temperature range used by the PBI based HT-PEMFC, in addition to the acidic environment created by the phosphoric acid of the membrane and the working potential, have a negative impact in terms of durability on the components of the fuel cell. Especially, carbonaceous components are strongly affected by these degradation effects. In the case of the electrodes, composed by the macroporous, microporous and catalytic layer, this degradation produces an important impact in terms of performance and lifetime of the fuel cell.

2.4.1. GDL degradation

As it was discussed in the previous section, the GDL is a key element in the performance of the fuel cell, and its durability has a strong effect on the service lifetime of the PEMFC. Durability of this layer strongly depends of the stability of the MPL. The degradation of this layer has the following negative effects: [14]:

- **Hydrophobicity losses.** The GDB and MPL combine a hydrophobic/hydrophilic structure, since the surface sections covered by fluoropolymer are hydrophobic, while carbon exposed areas are hydrophilic. Fresh GDL has a generally higher hydrophobic character, which is deteriorated during the operation of the fuel cell. The operating conditions of the PEMFC cause degradation of the MEA, and this degradation is higher in the case of HT-PEMFC because PBI membranes undergo higher degradation than Nafion ones. The presence of acids such as phosphoric promotes the oxidation of carbon and graphite to CO_2 and the formation of carbonates, reducing the porosity and promoting the agglomeration of the material. The Pt-C interactions in the catalytic layer also cause the oxidation of carbon, leading to the migration of free platinum particles. These particles also cause the synthesis of H_2O_2 by hydroxyl or hydroperoxyl ions and these compounds increase the corrosion and/or modification of the surface of PTFE, carbon, and PBI membrane, increasing the degradation of the GDL and decreasing its hydrophobicity. In HT-PEMFCs, the hydrophobicity of the layer is also important, since at high temperatures, the gases and ions circulating through the electrodes have higher humidity values. Hence, hydrophobicity improves the management of gases and prevents the degradation of the MEA components [30].
- **Carbon corrosion.** This process mainly occurs in the carbon fibers of the GDL and in the carbonaceous substrate of the MPL, which is not well coated with

fluoropolymer (Teflon). As mentioned above, the O_2, H_2O_2 and hydroxyl species present in the cathode are the major cause of the hydrophobicity losses of the GDL, being especially vulnerable the carbon black of the MPL as compared to the graphitic fibers of the GDB. As it was pointed out, hydrophobicity losses makes easier the attack of the oxidizing species to the carbon substrate, which is traduced in a faster degradation of the layer. Finally, the high voltage values during the start-up and shut-down procedures of the lifetime of the fuel cell have an important role in the degradation of the carbonaceous materials. Potentials over 0.21V vs RHE can produce carbon corrosion in moderate amount, but over 1.20 V, this potential corrosion achieves a very high importance [32, 33]. Thus, the development of new materials that can address the entire positive features that those carbon materials exhibit and, at the same time, which may minimize their negative characteristics is crucial.

- **Increased mass transfer resistance**. This increase is associated to different factors such as the formation of oxides of carbon or graphite or to the loss of hydrophobicity of the GDL. In addition, the porosity of the layer undergoes important changes due to the decrease of carbonaceous surface. These changes cause agglomeration in different regions, and this agglomeration avoids the correct diffusion of the reactants, decreasing the service lifetime and performance of the cell.
- **Surface oxides formation**. The previously described formation of oxidants may modify the surface characteristics and this modification generates long-term problems in the performance of the fuel cell in the polarization region, due to the lower conductivity of these oxides, which is traduced in an increase of the ohmic resistance of the electrodes and in a decrease of the activity of the catalyst.

2.4.2. Catalyst layer degradation

The catalyst layers are located between the gas diffusion layers and the electrolyte (one in the anode and other in the cathode). The Pt of the catalyst layer on the anode side dissociates the hydrogen molecules into protons and electrons according to Equation 2.2. Then, protons pass through the PBI membrane to reach the cathode, while electrons generated run through an external electrical circuit. On the cathode, protons, electrons and oxygen reacts to produce water, according to Equation 2.3.

$$H_2 \xrightarrow{Pt\ catalyst} 2H^+ + 2e^- \qquad (2.2)$$

$$O_2 + 4e^- + 4H^+ \xrightarrow{Pt\ catalyst} 2H_2O \qquad (2.3)$$

In addition to the expected reactions, another side reactions may occur on the cathode (Equations 2.4 and 2.5):

$$O_2 + 2e^- + 2H^+ \xrightarrow{Pt\ catalyst} H_2O_2 \qquad (2.4)$$

$$H_2O_2 + 2\,e^- \longrightarrow 2OH^- \qquad (2.5)$$

Both reactions may have a strong corrosion effect on the fuel cell components, especially on the carbonaceous materials and the fluoropolymers present in the MPL. Moreover, the interaction Pt-C may produce the degradation of the carbonaceous support of the metallic particles, which in turn promotes the agglomeration of the catalyst and the migration of the Pt particles over the catalytic layer. This fact, and the degradation of the MPL, produce two negative effects on the fuel cell performance. On one hand, the migration of the Pt particles over the catalytic layer decreases the active surface area of the catalytic layer, decreasing the service lifetime and the performance of the fuel cell. It also increases the degradation of the GDL, when these Pt particles start to catalyze the oxidation of the carbon fibers and the production of hydrogen peroxide into the GDL, which increases the corrosion of this layer. On the other hand, the agglomeration of the Pt particles also reduces the performance of the fuel cell due to the lower number of active Pt centers available in this catalyst layer. In addition, there is a lower porosity of the layer

due to the destruction of the porosity of the carbon support, same as explained for the carbonaceous substrate of the MPL [14].

2.5. Advanced materials for HT-PEMFC electrodes manufacturing

In order to overcome the limitations of the actual HT-PEMFCs technology, the development of new materials to improve the service lifetime of the electrodes in the hot acidic conditions of the fuel cell is required. In the last decades, some interesting carbonaceous and non-carbonaceous materials have been produced, with promising characteristics to be used in this field.

Nowadays, carbon blacks (CB, especially Vulcan XC-72) are the most commonly used supports for Pt and Pt-alloy catalysts for fuel cells. They are typically prepared by the pyrolysis of hydrocarbons. CB consists of nanometric near-spherical particles of graphite forming particle aggregates (and agglomerates), with a typical size around 250 nm. Due to their structure, CBs usually have polycrystallite structure. Each crystallite consists of several 'turbostratic' layers with an interplanar spacing of 0.35–0.38 nm. The specific morphology of carbon blacks is basically defined from the source material and the process of its thermal decomposition, but all CB present common characteristics such as high surface area (around 250 $m^2\ g^{-1}$ for Vulcan XC-72), low cost and easy availability, that help to reduce the overall cost of the fuel cell [34].

However, these materials present many problems in their use in HT-PEMFC technology, such as the presence of organo-sulfur impurities and deep micropores or recesses, which trap the catalyst nanoparticles making them inaccessible to reactants, thus leading to reduced catalytic activity. The pore size and pore distribution also affect the interaction between the polymeric ionomer and the catalyst nanoparticles. Furthermore, CB is thermochemically unstable, especially under the hot acidic conditions of the fuel cell, which

promotes the destruction of the catalytic and microporous layers [34]. Consequently, other more resistant materials have been investigated in order to overcome these limitations, attaining promising results in terms of catalytic activity and durability to be used in HT-PEMFC systems. In the following sections, a short review of the main studied materials is presented.

2.5.1. Carbonaceous materials

Graphene is an "atomically thin" sheet of hexagonally arranged carbon atoms, which has attracted a lot of interest since its discovery by Geim et al. in 2004 [34, 35]. It offers high conductivity and fast electron transfer capabilities. Due to all its interesting physicochemical and electrochemical properties, graphene has been object of research study for various applications including fuel cell catalyst support. The use of graphene and its oxide (graphene oxide, GO) in fuel cell is not only limited to its application as catalyst support but it is also being explored as material for conducting membranes (as a composite with polymers) and also as bipolar plate material. The 2-D planar structure of the carbonaceous sheets allows both the edge planes and basal planes to interact with the catalyst nanoparticles. This planar sheet structure also provides a very high surface area for the attaching of the catalyst nanoparticles. In order to improve some characteristics of this material, graphene has been doped or modified with different substances. For example, Nitrogen doped graphene has been shown to yield promising results especially for the sluggish cathodic ORR [36]. The disorders and defects created by the nitrogen particles in the graphene structure acts as active sites for the catalyst nanoparticles [37]. In other research studies, it was found that MEAs fabricated using Pt/N-G and Pt/G as the ORR catalyst into a LT-PEMFC system showed maximum power densities of 440 $mWcm^{-2}$ and 390 $mWcm^{-2}$, respectively [34]. Moreover, graphene oxide (GO), has also received much attention. Although GO has lower conductivity (a difference of two to three orders of magnitude as compared to graphene), it offers a different set of

properties (hydrophilicity or high mechanical strength, for example) as compared to graphene, which makes it suitable for a wide range of applications. Moreover, variable oxygen content enables tunable electronic conductivity for various applications.

Carbon nanofibers (CNF) are nanostructured materials produced from the thermal decomposition of hydrocarbons over metal particles. The basic difference between carbon nanotubes (CNTs) and CNFs is that unlike CNT, CNFs have no hollow cavity. The diameters of CNFs are much larger than CNTs and may go up to 500 nm while the length can be up to a few millimetres. Attending to the structure and orientation of their graphitic planes respect to their growth axis, CNFs have been classified into three types: Ribbon, Platelet and Herringbone, which are known to have intermediate characteristics between parallel and platelet types, thereby exhibiting higher catalytic activity than the parallel and better durability than the platelet forms [34].

Attending to their synthesis conditions, the physicochemical characteristics of the CNF can be adapted to their final application [34, 37]. Highly graphitic CNFs, obtained at higher temperatures, show better catalytic activity, despite its lower surface area and pore volume as compared to CB [34]. In addition, the high dispersion was promoted by terminal amine functional groups, which provided uniform preparation of size monodisperse catalysts and assisted controlled dispersion. One of the biggest differences between the CNTs and the CNFs is the exposure of the active edge planes. Unlike the CNTs, where a predominant basal plane is exposed, in the case of CNFs only the edge planes (which present potential anchoring sites), are exposed. Furthermore, various acid treatments also help to remove the residual metal impurities left behind during the synthesis of CNFs.

Finally, **Carbon Nanospheres** (CNSs) were observed for first time in the 1980s, where Inagaki et al. and Yamada et al. [38, 39] recognized the presence of carbon spherules during carbonization and shock-wave processes. In order to achieve a uniform targeted nano-size of the carbon nanospheres, a number of thermal, catalytically assisted, templated and

supercritically conditioned routes have been described in the literature [40]. The wide variety of production techniques used in the synthesis of these nanostructures has produced a range of carbon spheres with different sizes and textural properties. Inagaki [38, 40] classified these spherical nanostructures according to their nanometrical texture, proposing three categories: concentric, radial or randomly oriented carbon layers. According to their size, CNSs can be divided into three groups: in first place, the graphitic carbon onions, with diameters in the range 2–20 nm. In second place, less graphitic carbon spheres with diameters in the range 50 nm–1 μm, and, finally, the carbon beads, with diameters from one to several microns. In its spherical arrangement, the graphite sheets that form these structures are normally unclosed shells with waving flakes that follow the curvature of the sphere, creating many open edges at the surface. This creates reactive ‘‘dangling bonds’’ that give the spheres a high chemical activity, establishing them as suitable candidates for catalyst supports in composite materials, in energy storage or for electrochemical applications [40].

2.5.2. Non-Carbonaceous materials

The usage of nanostructured carbon materials has increased the performance and durability of the catalyst supports used in PEMFC technology, as they exhibit strong influence on the catalyst durability and behavior. However, because of their nature, carbon corrosion still exists for these systems, making impossible the complete avoiding of the electrochemical corrosion of these materials. Furthermore, functionalization of the carbon support (typically made to improve the anchorage of the catalyst nanoparticles on the support and reduce agglomeration) can make the support more susceptible to electrochemical oxidation [34]. Consequently, explore other non-carbonaceous supports is necessary. The inertness of some non-carbonaceous oxides and carbides of metals, such as titanium, silicon or tungsten, makes them very attractive materials for applications in relatively strong oxidative conditions.

Titanium oxide or titania materials have been evaluated as conductive metal oxides due to their excellent corrosion resistance in various electrolyte media. This fact, demonstrated even in acid media, makes titania based materials as a promising material for their evaluation as catalyst supports in fuel cells [34, 41]. Additionally, the production costs are low and the materials are easily available. Titanium can be presented in three main crystallographic forms: rutile, anatase and brookite. Stoichiometric titania (band gap 4.85 eV) is resistive and the presence of Ti^{3+} ions is essential for electronic conductivity. Ti^{3+} ions can either be generated by creating oxygen deficiency by heating TiO_2 in reducing atmosphere (to obtain TiO^{2-x} or $TinO^{2n-1}$) or by introducing dopants. However, when is exposed to the cell environmental conditions , the sub-stoichoimetric titania change into a stoichiometric state, and forms a resistive TiO_2 layer at the three-phase reaction interface.

Another Ti based material studied is TiN. This triple bond transition metal compound is very inert and it has high mechanical hardness, high melting point and high-electrical conductivity (4000 S m^{-1} compared with 1190 S m^{-1} for carbon black) [42]. Its resistance to corrosion and high conductivity make it an excellent candidate for the synthesis of durable electrocatalysts and electrocatalyst support. However, during some ex-situ tests performed, it was observed a decrease on the performance of Pt catalysts supported on this material, probably due to the formation of corrosion product on the nitride surface of TiN. Formation of positively charged corrosion products further led to adsorption of other negatively charges anions, covering the surface area of TiN nanoparticles with a layer of oppositely charged ions and making the electrode more passive (and hence decreasing its electrical conductivity).

Titanium diboride is another relatively new titanium based support, which has been investigated with a great deal of interest. TiB_2 is a ceramic material, which exhibits excellent thermal and corrosion stability and good electrical conductivity in acidic media [43]. TGA studies revealed that TiB_2 begins to oxidize as temperature approaches 532.2 ºC, and cyclic

voltammetry shown negligible changes in the redox region after several cycles, which confirms the high electrochemical stability in acid media of this material [43].

Finally, silicon carbide is a covalent carbide with stoichiometry 1:1, which exhibit a diamond structure. Thus, each Si atom is linked tetrahedrally with four carbon atoms, and each tetrahedron is linked with an adjoining being. This net distribution results into several crystal interrelated structures called "polytype". There are more than 200 different polytypes, being the most common the polytypes called 3C, 4H, 6H and 15R n-H, where (C), (H) and (R) are the basic crystal structures cubic, hexagonal and rhombohedral, respectively [44]. 4H, 6 H, and R-15 polytypes correspond to the α-SiC, and they are characterized by a greater presence and stability at high temperatures (more than 1973 K). Opposite, polytype 3C corresponds to β-SiC and it is characterized by a higher surface area (more than 500 $m^2\ g^{-1}$) as compared to that of α-SiC, low bandgap (≈2.4 EV) and high electron mobility (≈800 $cm^2\ V^{-1} \cdot s^{-1}$) [45]. In addition, it exhibits high availability and low cost, which make it interesting to be used in fuel cells. Attending to its particular politype, SiC may present a high porosity, with pore volume values of about 0.7 mL g^{-1}, and is a promising material as catalyst support [46].

2.6. Bibliography

[1] G. D. Southall, A. Khare, Sustainable Cities and Society 26 (2016) 134.

[2] Shaojie Wang, Ting Zhang, Haijia Su, Renewable Energy 96 (2016) 1135.

[3] L. Protasova, F. Snijkers, Fuel 181 (2016) 75.

[4] G. K. Dalapati , C. S. Chua, A. Kushwaha, S. L. Liew, V. Suresh, D. Chi, Materials Letters 183 (2016) 183.

[5] L. J. M. J. Blomen, M. N. Mugerwa, Fuel Cell Systems, Plenum Press, New York, 1993.

[6] J. Appleby, F. R. Foulkes, Fuel Cell Handbook, Krieger Publishing, Malabar, 1993.

[7] F.J. Pinar, Desarrollo de nuevas membranas poliméricas basadas en polibenzimidazol para su aplicación en celdas de combustible PEM de alta temperatura, Degree Thesis, University of Castilla-La Mancha, 2012.

[8] G. Hoogers, Fuel Cell Technology Handbook, Vol. 11, CRC Press, Florida, 2003.

[9] Q. Li · D. Aili, H. A. Hjuler · J. O. Jensen, High Temperature Polymer Electrolyte Membrane Fuel Cells. Approaches, Status and Perspectives, Springer, ISBN: 978-3-319-17081-7, New York, 2016.

[10] A. S. Woodman, E. B. Anderson, K. D. Jayne, M. C. Kinble, Proceedings in American Electroplaters and Surface Finishers Society 6 (1999) 21.

[11] N. P. Brandon, Encyclopedia of Materials: Science and Technology, Elsevier Ltd., Amsterdam, 2004.

[12] G. G. Park, Y.-J. Sohn, T.-H. Yang, Y.-G. Yoon, W.-Y. Lee, C.-S. Kim, J. Power Sources 131 (2004) 182.

[13] L. Cindrella, A. M. Kannan, J. F. Lin, K. Saminathan, Y. Ho, C. W. Lin, J. Wertz, J. Power Sources 194 (2009) 146.

[14] F. N. Büchi. M. Inaba, T. J. Schmidt, Polymer electrolyte fuel cell durability, ISBN 978-0-387-85534-9, 2009.

[15] S. Park, J.W. Lee, B. N. Popov, Journal of Power Sources 163 (2006) 357.

[16] F.Weng, C.Hsu, M.Su, International Journal of Hydrogen Energy 36 (2011) 13708.

[17] J. H. Chun, D. H. Jo, S. G. Kim, S. H. Park, C. H. Lee, E. S. Lee, J. Jyoung, S. H. Kim, Renewable Energy 58 (2013) 28.

[18] T. Haolin, W. Shenlong, P. Mu, Y. Runzhang, J Power Sources 166 (2007) 41.

[19] S. Litsler, G. Malean, J. Power Sources 130 (2004) 61.

[20] A. Serov, C. Kwak, Appl. Catal., B 90 (2009) 313.

[21] P. Costamagna, S. Srinivasan, J. Power Sources 102 (2001) 242.

[22] E. Antolini, J. App. Electrochem. 34 (2004) 563.

[23] G. Sasikumar, J. W. Ihm, H. Ryu, J. Power Sources 132 (2004) 601.

[24] G. Inzelt, M. Pineri, J. W. Schultze, M. A. Vorotyntsev, Electrochim. Acta 45 (2000) 2043.

[25] C. E. Carraher, G. G. Swift, Functional Condensation Polymers, Ed. Kluwer Academic, New York, 2002.

[26] U. B. Demerci, J. Power Sources 169 (2007) 239.

[27] P. Costamagna, S. Srinivasan, J. Power Sources 102 (2001) 242.

[28] R. Souzy, B. Ameduri, Prog. Polym. Sci. 30 (2005) 644.

[29] J. Lobato, P. Cañizares, M. A. Rodrigo, D. Úbeda, F. J. Pinar, Journal of Membrane Science 369 (2011) 105.

[30] J. Lobato, P. Cañizares, M.A. Rodrigo, D. Úbeda, F.J. Pinar, J. Power Sources 196 (2011) 8265.

[31] R. Kerr, H.R. García, M. Rastedt, P. Wagner, S.M. Alfaro, M.T.Romero, C. Terkelsen, T. Steenberg, H.A. Hjuler, International Journal of Hydrogen Energy 40 (2015) 16860.

[32] N. Linse, G. G. Scherer, A. Wokaun, L. Gubler, Journal of Power Sources 219 (2012) 240.

[33] J. Park, S. Yima, T. Kima, S. Parka, Y. Yoona, G.Park, T. Yanga, E. Park, Electrochimica Acta 83 (2012) 294.

[34] S. Sharma, B. G. Pollet, Journal of Power Sources 208 (2012) 96.

[35] K.S. Novoselov, A.K. Geim, S.V. Morozov, D. Jiang, M.I.K.I.V. Grigorieva, S.V. Dubonos, et al, Nature 438 (2005) 197.

[36] L. Qu, Y. Liu, J.B. Baek, L. Dai, ACS Nano 4 (2010) 1321.

[37] V. Jimenez, A. Nieto-Marquez, J. A. Díaz, R. Romero, P. Sánchez, J.L. Valverde, and A. Romero, Ind. Eng. Chem. Res. 48 (2009) 8407.

[38] M. Inagaki, K. Kuroda and M. Sakai, Carbon 21 (1983) 231.

[39] K. Yamada and S. Tobisawa, Carbon 27 (1989) 845.

[40] A. Nieto-Márquez, R. Romero, A. Romero, J.L. Valverde, J. Mater. Chem. 21 (2011) 1664.

[41] E. Antolini, E.R. Gonzalez, Solid State Ionics 180 (2009) 746.

[42] I. Milosv, H.H. Strehblow, B. Navinsek, M. Metikos-Hukovic, Surf. Interface Anal. 23 (1995) 529.

[43] B. Basu, G.B. Raju, A.K. Suri, Int. Mater. Rev. 51 (2006) 352.

[44] S. Gianella, D. Gaia, A. Ortona, Advanced Engineering Materials 14 (2012) 1074.

[45] A. Walcarius, Chem. Soc. Rev. 42 (2013) 4098.

[46] R. Dhiman, E. Johnson, E. Skou, P. Morgen, S. M. Andersen, Journal of Materials Chemistry A 19 (2013) 6030.

CHAPTER 3: Background, aims and scope of this work

One of the programs of the research portfolio of the Electrochemical & Environmental Engineering Laboratory of the Chemical Engineering Department (DIQ) of the UCLM aims at the development of efficient high temperature PEM fuel cells (HT-PEMFC). In this research program, important progresses have been made within the last few years, including the development and optimization of processes for the manufacture of several components of the PEMFC (polybenzimidazole (PBI) membranes, catalysts, gas diffusion layers, etc.), the design of more efficient bipolar plates and flow distribution channels and the evaluation of service lifetime under different operation conditions and with different fuels and oxidants. This experimental work has been complemented with CFD modelling, helping us to understand the performance of this complex type of electrochemical devices.

One of the most important elements of the fuel cell and, perhaps, the most sensitive on HT-PEMFC technology is the membrane. For this reason, the first challenge faced with our research group was to develop and optimize an efficient process to manufacture PBI membranes with good characteristics for being used in this type of devices. This issue was faced in the PhD of Dr. José Joaquín Linares (examined in 2010), in which a procedure for the manufacture of the doped membrane starting up from single monomers was obtained. This procedure was a real milestone because it meant having our own technology to produce the most sensitive component of the fuel cell. However, after this initial success, one of the main problems found was the fast degradation of the MEA components. Thus, in the first studies, using standard PBI membranes, an irreversible degradation of 6% of the voltage given by the cell fed with pure oxygen and hydrogen (at 150 ºC and 0.2 A cm^{-2}) was obtained, only after 700 hours of operation, which is around 10 times higher than the accepted value to be commercialized. Two mains causes were found: on one hand, the phosphoric acid losses undergone by the membrane, and on the other hand, the sintering and agglomeration processes on the catalyst particles, which opened two main ways to improve the technology:

- Improvement of the PBI membrane characteristics by increasing its acid retention capability
- Improvement of the catalysts.

The second PhD carried out in our group (Dr. Javier Pinar, examined in 2012) faced the first cause, by improving the mechanical properties and acid retention capability of the membranes. This was accomplished by casting composite PBI-TiO_2 membranes, which allowed improvement of over 90% in the acid retention capability in leaching tests and also in the chemical resistance, which results in much better operation behavior.

The other cause was faced in the PhD of Dr. Diego Ubeda (examined in 2013) in a work that was not only related to the development of single components of the cell but to the whole cell design, using CFD modelling and current distribution measurements. It was found that electrospray and airbrush deposition techniques for the catalyst resulted into a very different current density distribution, due to the irregular distribution of the Pt particles obtained by using each deposition technique and that more studies about the catalytic layer (and even about the gas diffusion layer) had to be performed, in order to get a ready-to-commercialized technology. Hence, the electrode is a very sensitive element and conclusions recommend to make efforts in order to optimize it.

With this background, the fourth PhD of this research program, contained in this document, is going to be focused on the improvement of the durability of the catalyst and the electrodes used in HT-PEMFC. Regarding to this goal, it is worth having in mind some points about two critical components of the electrodes, which have a strong influence of the durability of the fuel cell:

- The microporous layer (MPL), composed usually of a carbon black (such as Vulcan carbon XC72) and a hydrophobic agent (such as PTFE). This layer avoids the release of the Pt particles out of the catalytic layer, improving the durability and efficiency

of the fuel cell. Also, it improves the diffusion of the gas flow reactants provided by the gas diffusion backing (GDB), and makes easier the water management of the system (in low temperature PEMFC), due to its high hydrophobic character. The well-known thermal acidic corrosion of Vulcan carbon reduces considerably the durability of this layer, reducing the overall efficiency of the fuel cell. This decrease is associated to a worse distribution of the reactant gases (due to the agglomeration of the carbon during the degradation process of the material) and to an increase in the electrical resistance of the electrode (due to the oxides formation). Because of this, new materials must be studied in order to be used in the MPL manufacturing, trying to increase the stability of the system during longer period, increasing the service lifetime of the MEA and, hence, reducing the cost of the technology.

- The catalyst support of the catalytic layer, usually a carbon black. This material helps to obtain an adequate dispersion of the platinum particles, improving the active surface area of the catalyst. As for the MPL, the carbon corrosion is associated to problems with the durability and performance, because the corrosion of the carbonaceous support causes a decreasing of the catalytic activity, due to platinum agglomeration.

These problems may occur on both electrodes, although they are accentuated in the cathodic region, because of the potential formation of powerful radical oxidants during the reduction of oxygen, which accelerates the oxidation and corrosion processes of the electrode elements. Taking into account this fact, in the present work, the main objective is the development of optimized MPLs and catalysts supports to be used in cathodic electrodes of HT-PEMFCs based on PBI membranes doped with phosphoric acid. The target is to improve its durability and performance with respect to the standard and well-known Vulcan carbon based electrodes. Based on the state of the art of the technology in the moment of the starting

up this PhD, different carbonaceous and non-carbonaceous materials were proposed to substitute the Vulcan carbon black on both elements:

- Carbon nanospheres (CNSs)
- Carbon nanofibers platelet (CNFp)
- Silicon carbide (SiC)
- Binary silicon-titanium carbides (Si_xTi_yC)

This document will show the advantages and drawbacks of each of these promising materials. In order to achieve the main goal of this work, the following partial goals are going to be faced:

1) Physicochemical characterization of all materials studied, focusing the study in the most critical properties to be used as MPL and/or catalyst support (surface area, porosity, electrical conductivity, thermal corrosion in acidic media and electrochemical stability).
2) Assessment of the characteristics as cathodic MPL of the most promising materials found in the physicochemical characterization, using short life test in a single HT-PEMFC system and carrying out different characterization tests in order to evaluate the stability and performance. These tests involve polarization curves with air and oxygen, impedance spectroscopy, cyclic voltammetries and linear sweep voltammetries, with the objective to get all available information about the degradation of all MEA components, and how the new materials affects to the degradation rates, as compared to an standard Vulcan carbon based MEA. Results obtained with this methodology are expected to be worse of those which could be attain in real operation conditions, because the characterization procedure is expected to accelerate the degradation of the MEA, due to the stress caused during the different tests.

3) Assessment of the characteristic of the most promising new materials as catalyst support. Different Pt-based catalyst will be manufactured using the different new materials as catalyst support. All catalysts will be prepared using the same synthesis method in order to be properly compared. Real platinum content, platinum crystal and particle sizes, platinum dispersion, electrochemical active surface area (ECSA), activity towards the oxygen reduction reaction in RDE studies, and electrochemical stability in acidic conditions of the different catalyst will be studied. Obtained results will be compared to the results obtained with a commercial Pt/Vulcan catalyst, used as reference material.
4) Evaluation of the characteristic of the best catalysts in short life tests performed in a single HT-PEMFC system. Several characterization test will be carried out to evaluate the stability and performance using the selected materials as cathodic catalyst. These tests involve polarization curves with air and oxygen, impedance spectroscopy, cyclic voltammetries and linear sweep voltammetries, and they are targeted to attain all relevant information about the degradation of all MEA components, and how the new materials affects to the degradation rates, as compared to a standard Vulcan carbon based MEA. As pointed out in partial goal 2, results obtained with this methodology are expected to be worse of those which could be attain in real operation conditions, because the characterization is expected to accelerate the degradation of the MEA due to the stress caused during the tests.
5) Finally, according to the results achieved in the four previous partial goals, the best material for MPL and the best Pt-based catalyst will be used to manufacture an optimized cathode, evaluating its performance and stability in a HT-PEMFC lifetest, comparing the results with those obtained with a standard MEA. Same characterization tests performed in the previous tasks will be used to get information about the evolution of the MEA and about the degradation of its elements.

CHAPTER 4. Materials and experimental procedures

4.1. Materials

In this section, the different materials required for the manufacturing of the catalysts, electrodes, membrane-electrode assemblies and reactants to perform the different tests described on this work are presented.

4.1.1 Support materials.

Table 4.1 summarizes the materials evaluated as catalyst supports or raw materials for micro porous layer (MPL) preparation.

Table 4.1. Materials studied in the research reported in this document

Material	Acronym	Provided by
Carbon nanofibers platelet	CNFp	Lab-made [1]
Carbon nanospheres	CNSs	Lab-made [2]
Vulcan Carbon Black XC72	Vulcan XC72	Commercial (CABOTCorp.)
B-Silicon Carbide (high purity)	SiC	Commercial (SICAT)
Silicon-Titanium carbide with 10, 20 and 30% molar content of TiC	Si_xTi_yC	Commercial (SICAT)

4.1.2. Synthesis of Platinum based catalysts

Table 4.2 shows the reactants used in the manufacturing of the different Pt based catalysts tested in this work.

Table 4.2. Reactants used during the synthesis of the Pt based catalysts

Material	Purity [% wt.]	Provided by
Formic acid	98%	Sygma Aldrich
Deionized water	-	-
Hexachloroplatinic(IV) acid hexahydrate	>99.9%	Sygma Aldrich

Moreover, a commercial Vulcan XC72 catalyst (40% Pt/Vulcan XC72, E-TEK) was used with comparative purpose during the catalysts testing.

4.1.3. Membrane-electrode assembly (MEA) manufacturing

Table 4.3 summarizes other materials used in the electrodes and MEAs manufacturing process.

Table 4.3. Materials used in the electrodes manufacturing

Material	Purity [% wt.]	Provided by
2-Propanol	99.8	PANREAC
PTFE	60	ELECTROCHEM INC
Toray carbon paper 120 with 10% wet proofing on PTFE	-	FUELCELL STORE
PBI solution on N,N'-Dymethylacetamide	2.5	Lab-made
N,N'-Dymethylacetamide (DMA)	99.9	PANREAC
Toray carbon paper (GDL)+ 2 mg cm^{-2} Vulcan XC72 MPL	-	Freudenberg
PBI thermally treated membrane	-	Danish Power System
Nitrogen gas (packed at 200 atm)	>99.999	PRAXAIR
Phosphoric acid (PA)	85	Sygma Aldrich
Deionized water	-	-

4.2. Physicochemical characterization

4.2.1 X-Ray Diffraction (XRD)

The X-Ray diffraction was used to determine the degrees of crystallinity of the different catalysts and supports. This technique allows us to obtain information of crystallinity, crystal orientation, distance between crystallite planes, or polymeric nanostructure and molecular structure of the materials.

To analyze the different support materials, catalysts and electrodes, on the diffractogram of each sample, different peaks appear for each crystallite face of each compound of the sample, which allows the identification of the support and the catalyst active phase (Pt) in the catalyst, and which Pt crystallite face exhibit high preferential orientation. Also, this technique is very useful to evaluate if the samples have suffered a material loss, or generated new compounds like reduced or oxidized species during the electrochemical studies.

XRD measurements were performed using a diffractometer Philips PW-1700 with rotator anode and applying the copper transition constant for each samples. The sample radio corresponding to the angle 2θ is between 0° and 90° with a sweep speed of 0.1° 2θ s^{-1}. The crystal size and distance between planes were determined by the Scherrer and Bragg equations respectively (Eq. 4.1 and 4.2) [3], where *Lc* is the average crystallite size, λ [nm] is the wavelength corresponding to the copper constant (λ=0.15418 nm), β is the bandwidth peak at $I_{max}/2$ [rad], θ is the angle corresponding to I_{max} [rad] and d_{002}, the distance between planes.

$$Lc = \frac{0.89\lambda}{\beta \frac{1}{2}\cos(\theta)} \qquad [4.1]$$

$$d_{002} = \frac{\lambda}{2 \cdot sin(\theta)} \qquad [4.2]$$

4.2.2 Mass Spectrometry (ICP-MS)

The Inductively Coupled Plasma Mass Spectrometry is an analytical technique used for elemental determinations. It combines a high-temperature ICP (Inductively Coupled Plasma) source with a mass spectrometer. The ICP source transforms the atoms of the elements contained in the sample into ions. These ions are then separated and detected by the mass spectrometer.

The sample is typically introduced into the ICP plasma as an aerosol, either by aspirating a liquid or dissolved solid sample into a nebulizer or using a laser to directly convert solid samples into an aerosol. Once the sample aerosol is introduced into the ICP torch, it is completely desolvated and the elements in the aerosol are converted first into gaseous atoms and then they are ionized. Once the elements in the sample are converted into ions, they are brought into the mass spectrometer via the interface cones. The purpose of these cones is to sample the center portion of the ion beam coming from the ICP torch. Generally, it is recommended that samples have no more than 0.2% total dissolved solids (TDS) for best instrument performance and stability. Once the ions enter the mass spectrometer, they are separated by their mass-to-charge ratio and detected or counted by the detector. The fundamental purpose of the detector is to translate the number of ions striking the detector into an electrical signal that can be measured and related to the number of atoms of that element in the sample (via the use of calibration standards). Once the ion hits the active surface of the detector, a number of electrons is released, which then strike the next surface of the detector, amplifying the signal. The signal is compared to the ones of the known elements to study.

This technique is ideal to detect some traces of elements because it can analyze concentration until ppb. In this research, this equipment is very useful, because it allows us to know the exact platinum content in each different synthesized catalyst and also to verify

the occurrence of traces of that element in the phosphoric acid solution used in the electrochemical characterization process to study the degradation of the electrodes.

4.2.3 Brunnauer-Emmet-Teller area (BET)

In the field of solid catalysis, the surface area of catalysts is an important factor in catalytic activity. The BET method (Brunauer–Emmett–Teller) is commonly used in surface science for the calculation of surface areas of solids by physical adsorption of gas molecules. Physical adsorption results from relatively weak forces (Van Der Waals forces) between the adsorbate gas molecules and the adsorbent surface area of the test powder. The determination is usually carried out at the temperature of liquid nitrogen. The amount of gas adsorbed can be measured by a volumetric or continuous flow procedure.

This technique allows us to know the surface area of the different support and catalyst and also the pores size of the powder which will help us to understand the different phenomena occurring during the impregnation (synthesis process). This is really important to know how that parameter influenced directly on the efficiency of the catalyst. In this PhD, BET surface area of different samples and total pore volume were obtained using N_2 adsorption-desorption at 77 K (QUANTACHROME, model QUADRASORB 3SI)

4.2.4 Scanning Electron Microscopy (SEM)

The scanning electron microscopy (SEM) is an instrument that allows the observation and surface characterization of inorganic and organic materials, giving morphologic information of the analyzed material. A scanning electron microscope creates an enlarged image of the surface of an object. SEM scans the surface of the image point by point. It applies a very concentrated electron beam on the sample. The electron beam can disperse the sample or cause the appearance of secondary electrons. The lost electrons and secondary one are collected and counted by an electronic device located on the sides of the sample. Each read point of the sample corresponds to a pixel on a monitor. The larger the number of electrons

counted by the device, the greater the pixel brightness on the screen. As the electron beam scans the sample, the entire image thereof is displayed on the monitor. Scanning electron microscopes can magnify objects 10^5 times or more. This type of microscope is very useful because, unlike the TEM (transmission electron microscopy) or optical microscopes, it produces realistic three-dimensional images of the object surface. All micrographs shown in this work were performed using an electron microscope Philips XL30-CPDX4i.

4.2.5 Transmission Electronic Microscope (TEM)

The transmission electronic microscope is a powerful tool which allows the material characterization by using high power electron beam interacting with the sample. This technique is based on the transmission/dispersion of electron beam passing through electromagnetic lenses and projected on a very thin sample in a vacuum column (no more than 100 nm to be transparent to the electrons and obtain a good picture resolution). One part of the electrons is passing through the sample and the other part is crashed on the electrodes atoms. The X-ray emission is coupled to have information on the composition of the sample. This technique permits to obtain specific structural information of the sample thanks to the loss of the electrons from the beam. The groups of electron which pass through the sample are projected on a fluorescent screen and formed a visible picture. Depending on the type of dispersion of the electrons, it is possible to obtain three kind of contrast on the picture: 1) the picture amplitude contrast, given by low angle electrons; 2) the picture phase contrast, for crystalline samples, where electrons are dispersed in different directions depending on the crystal structure; and 3) the picture diffraction contrast, which is the most important factor to form the pictures of crystalline samples.

This technique has been used to study the particles dispersion and the average size on the active phase of each sample. Pictures were obtained and filtered with the DigitalMicrograph software. The TEM study was carried on the catalyst powder such as the prepared electrodes. In the case of the electrodes, as in the XRD experiments, the analyses

were performed on the fresh electrodes and after the electrochemical characterization to determine the platinum particles dispersion.

TEM analyses were carried out on a Jeol JEM 2100 TEM operating at 200 kV with an Orius (2x2 MPi) Gatan Digital Camera. Specimens were prepared by dispersing the samples in acetone and depositing a drop onto a C-coated Cu grid.

4.2.6 Temperature Programmed Reduction (TPR)

Temperature-programmed reduction (TPR) is a technique for the characterization of solid materials and it is often used in the field of catalysis to find the most efficient reduction conditions. The oxidized catalyst precursor undergoes a programmed temperature rise while a reducing gas mixture is flowed over it.

The technique consists in filling a simple container (U-tube) with the solid catalyst (0.1 g). The sample vessel is positioned in a furnace with temperature control equipment. A thermocouple is placed in the solid for temperature measurement. To remove the present air the container is filled with inert gas, applying a constant flow of 20 mL min^{-1} of Ar with 5% wt. H_2 which acts a reducing agent. Hydrogen consumed is determined with a thermal conductivity detector (TCD), but in practice the production of water is a more accurate way of measuring the reduction. The sample in the oven is heated at 5 ºC min^{-1}, up to 900°C. If a reduction process takes place at a certain temperature, hydrogen is consumed and the detector records it.

This experiment is performed to collect information about the different oxide metallic species which could be present of the catalyst surface depending on the reduction temperature and contribute to estimate the relative amount of each species depending on the hydrogen consumption. In this PhD, TPR experiments were carried out in a Micromeritics AutoChem Hp Chemisorption Analyzer.

4.2.7 Degree of hydrophobicity

The degree of hydrophobicity is an important parameter to be analyzed in the MPL of the HT-PEM fuel cells, especially at the cathode, where water is produced during operation. For determination of the hydrophobicity of the prepared electrodes, the angle contact method is used. On a small sample of each electrode a water drop of 20 μL is deposited and allowed to stand for 1 hour. Then, with a camera, a shooting with zoom of each of the samples is taken and the angle contact is measured between the droplet and the electrode surface. The higher the contact angle, the greater will be the hydrophobicity of the electrode [4]. In order to evaluate the uniformity, right and left angles were measured. The comparison between the values of those angles for the same sample gives an idea of the homogeneity of the surface. Figure 4.1 shows a graphic outline of the procedure.

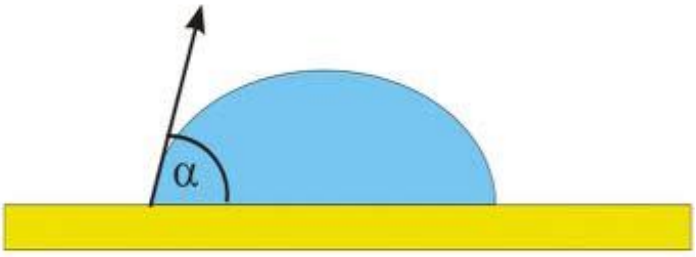

Figure 4.1. Scheme of drop water hydrophobicity degree characterization method

4.2.8 MPL Permeability of the reactive gases

One of the characteristics that must fulfill any gas diffusion layer is to allow the access of gases to the catalytic layer. One way to assess the suitability of the carbonaceous support is by determining the gas permeability using Darcy's law (eq. 4.3), which relates the flow through a porous media (Q) [$m^3\ s^{-1}$] with the variation of differential pressure (ΔP) [Pa], the cross section available (S) [m^2], the thickness of the porous medium (L) [m] and the fluid viscosity (μ) [Pa s].

$$Q = \frac{K \cdot S \cdot \Delta P}{\mu \cdot L} \qquad [4.3]$$

The proportionality constant *K* corresponds to the permeability of the medium. Permeability of the MPLs to the different reactive gases was calculated using the system represented in Figure 4.2. The flow is regulated by a flow controller while the pressure loss is evaluated with a manometer U filled with water. The pressure difference was measured in a pipe of 1.5 cm diameter, and flow rates of 5.0, 4.3, and 2.0 L min^{-1} of air, hydrogen and oxygen, respectively. By representing Q vs ΔP, and knowing the cross section area ($1.76.10^{-4}$ m^2), the thickness of each electrode and the viscosity of the gases in Pa.s (μ_{air} = 18.6 10^{-6}; μ_{O2} = $20.5.10^{-6}$; μ_{H2} = 8.92 10^{-6}), the value of K can be obtained.

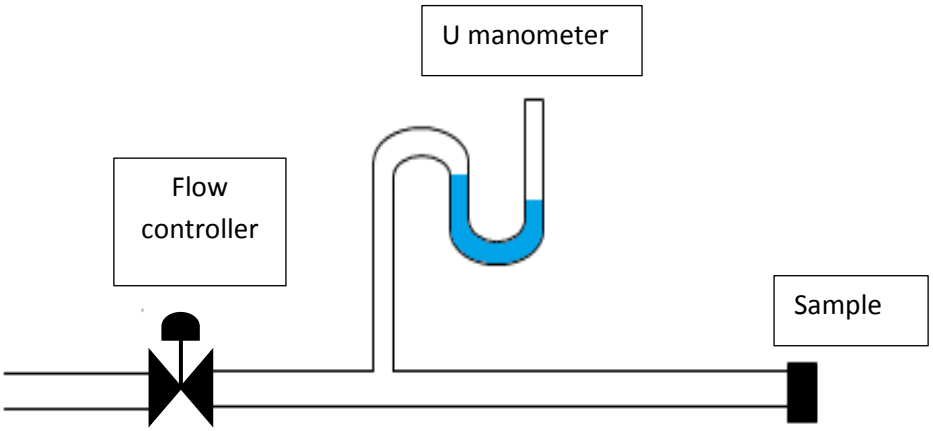

Figure 4.2. Experimental setup used for the determination of the gas permeability

4.2.9 Longitudinal Electronic Conductivity

Electronic conductivity evaluates the transport capacity of electrons into the electrode. This is one of the fundamental parameters because the electrons liberated by the anode and received by the cathode will flow through the electrodes. That is why a good conductivity value will ensure correct operation of Fuel Cells. Figure 4.3 shows the 4 point experimental device used to measure the electrical conductivity. The system consists of a

basic device of two plates (2x8 cm² and 1cm of thickness) on which electrodes are disposed. The plate which supports electrodes is made of compressible Teflon to insulate electrically the device. Measurement consists of disposing sample of 5x1cm² on the Teflon and then two gold wires are disposed on the corners of the electrode to apply the electrical current and two others gold wires in the center of the electrode to measure the potential difference. Then the device is closed by the other Teflon plate in contact with a controlled electrical resistance to heat the system.

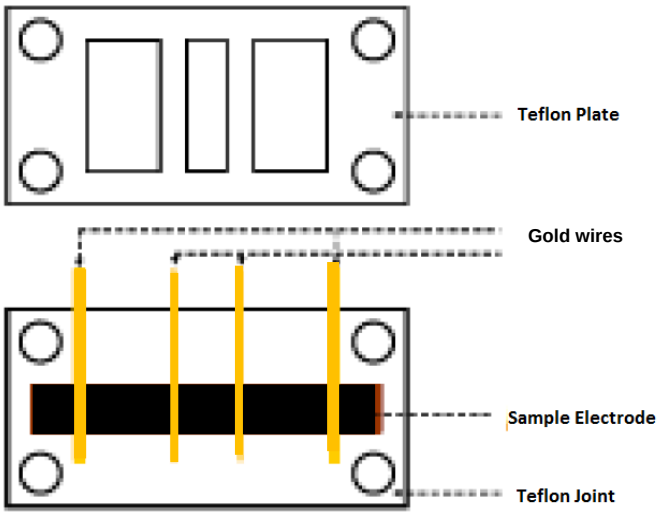

Figure 4.3. Four points device to measure the electrical conductivity of the samples

Conductivity of each electrode is calculated at 125, 150 and 175°C (operational HTPEMFC temperature range) using a potenciostat/galvanostat AUTOLAB PGSTAT 30 with the working module FRA (Frequency Response Analysis), shown in Figure 4.4.

Resistivities are measured in frequency range between 10000 and 100 Hz with a potential difference of 0.00 V and amplitude of 0.01 V in order to obtain the resistivity of each electrode expressed in ohms. It is necessary to calculate first the values of resistances to calculate then the values of conductivities. Resistance is obtained by drawing a Nyquist plot representing –Z(Ω) in function of Z (Ω).

Figure 4.4. Potentiostat/Galvanostat AUTOLAB used for conductivity and electrochemical measurements.

Figure 4.5 shows a Nyquist plot as example. The electrical resistance value is given by the interception with X axis, when imaginary part of the resistance is 0. Then, the conductivity was calculated with the equation 4.4, where σ is the electrical Conductivity (S cm^{-1}), L is the distance between the sensor and reference gold wires (1cm), R is the ohmnic Resistance (Ω) and S is the transversal section of the electrode.

$$\sigma = \frac{L}{R.S} \qquad (4.4)$$

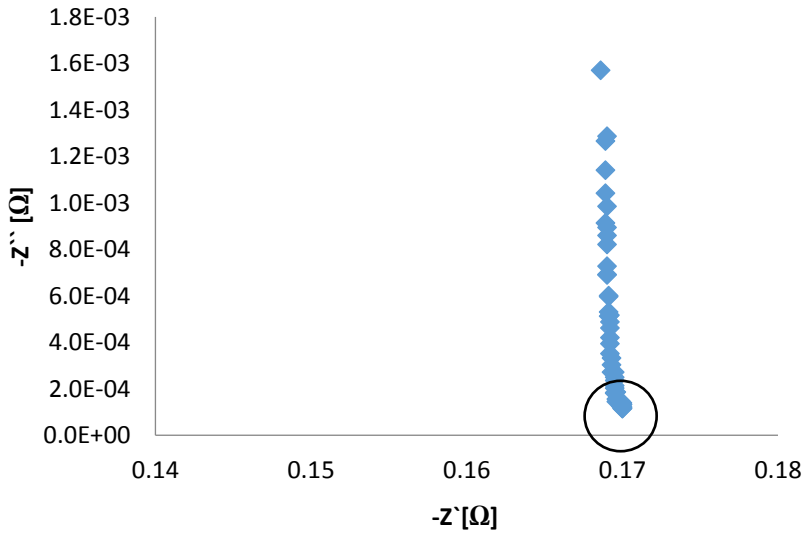

Figure 4.5. Typical shape of a Nyquist plot

4.2.10 Thermal Resistance

Generally, there are not expected problems in the electrodes related to operation at high temperatures because the operation temperatures of HT-PEMFC are quite low (maximum 200°C) and the material is robust. However, as HT-PEM Fuel Cells are operating in an acid environment (because of the PBI membrane), and the combination of acidic conditions and temperature could damage the electrodes, degradation tests were performed in an aggressive environment which simulates the worst fuel cells environment. The test consisted of impregnating the sample electrode with 85% phosphoric acid and, then, introduced it into an oven for 8 hours at 185°C. The sample was analyzed with XRD before and after the process to verify the degradation suffered by the electrode during the process.

4.3. Electrochemical Characterization

4.3.1. Voltammetric studies in half cell system with fixed electrodes

The electrochemical behavior of the different catalysts was studied via hydrogen adsorption/desorption in aqueous acidic media using a three-electrode setup. It is a quantitative analysis, frequently used to characterize an electrochemical system. From this experiment, it can be obtained information about the redox system and it can also be evaluated the electrochemical stability, which is here the most important aspect to focus on. The technique consists of changing the working electrode potential from an initial value E_0 to a final value E_F, performing oxidation-reduction cycles. The potential variation (scan speed) has to be maintained constant during the process. The scan can start from both sides, high potential (anodic) or low potential (cathodic), repeating the cycles. This potential variation is referred to a well-known reduction potential registered by a reference electrode whose function is to control the working electrode's potential. Figure 4.6 shows a simplified scheme of the experimental set up used during the experiments. Information obtained is expressed by representative diagrams called voltammograms, which are the graphical representation of the

registered electric current versus the working electrode's potential. Figure 4.7 shows an example of a cyclic voltammograms.

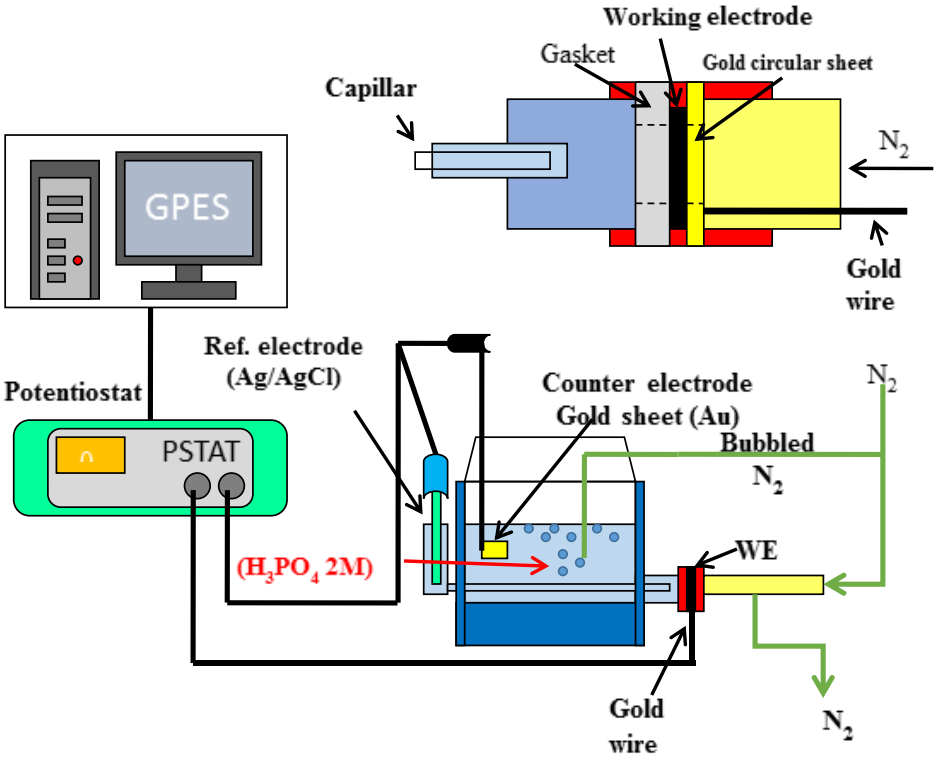

Figure 4.6. Scheme of the system used in the electrochemical ex-situ characterization.

According to Figure 4.7, it is possible to identify many phenomena, which take place on the electrode during the voltammetric study, such as the oxidation or reduction of platinum present on the electrode's surface. Reverse scan also gives relevant information. Then, corresponding peaks to reverse reaction of oxidation curve appear for the corresponding reduction current (reversible systems). In case of irreversible reactions, or changes on the surface of the electrode, new peaks of oxidation with different current densities would appear due to the modification of the electrode superficial properties. One of the most important aspects of electro catalyst characterization is the catalyst activity analysis. In acid media, the active faces of the deposited catalyst react with the hydrogen present in the media and series

of characteristics peaks appear, corresponding to the hydrogen adsorption and desorption process on the active centers of the Pt particles.

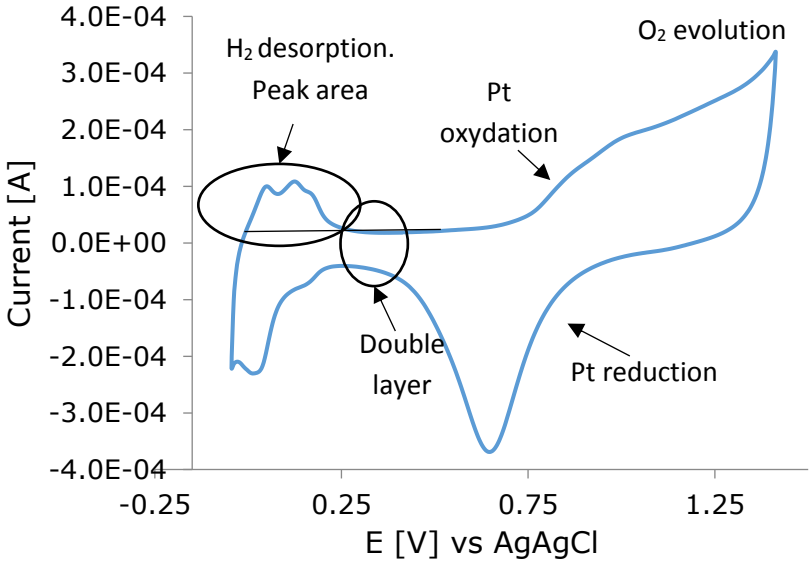

Figure 4.7. Example of cyclic voltammogram in which some relevant processes are highlighted

Total active area of the catalyst is determined by the calculation of the Electrochemical Surface Area (ECSA). By studying the evolution of this parameter, it is possible the quantification of the degradation suffered by the catalyst during a determined operation period. Equation 4.5 [5] allows us to calculate the $ECSA$ [$m^2\ g_{Pt}^{-1}$], where $A_{(Pt)}$ is the surface under the hydrogen desorption peak [$A\ V\ cm^{-2}$], v is the scan rate [$V\ s^{-1}$], C is the required load to reduce the proton layer on the active platinum [0.21 $mC\ cm^{-2}$] and L is the platinum load in the catalyst layer [0.3 $mg_{Pt}\ cm^{-2}$].

$$ECSA = \frac{A_{(Pt)}}{v \times C} \times \frac{1}{L} \qquad (4.5)$$

All ex-situ cyclic voltammetries using fixed electrodes were carried out in a highly acid environment using phosphoric acid (H_3PO_4 2.0 M) as electrolyte, in order to work with the same acid that it will be found inside the fuel cell. Support electrochemical evaluation was performed at room temperature, but for the catalysts evaluation, they were performed at

a constant temperature of 50°C (thermostatic bath) in order to facilitate the oxygen removal in the media, and also accelerate the degradation of the catalytic layer. In all cases, nitrogen was bubbled inside the electrolyte in order to obtain an inert atmosphere. The used reference electrode was an Ag/AgCl Metrohm AutolabB.V, with a potential of 0.21V vs RHE. The counter electrode was a thin gold sheet and measurements were performed with a potenciostat/galvanostat Autolab PGSTAT30. The selected scan speed was 20 mV s^{-1} for the analysis of supports, and 50 mV s^{-1} for the analysis of the catalysts, adjusting the E_0 and E_F at values of E_0 = –0.25 V vs Ag /AgCl and E_F = 0.79 V vs Ag/AgCl (supports)/1.00 V (catalysts), respectively.

4.3.2 ORR studies

The study of the oxygen reduction reaction was carried out by a technique linear sweep voltammetry, which allows knowing the catalytic activity of the catalyst. With this method of electrochemical characterization, the curve current density (j) is related to the potential (E) with a sigmoidal shape (Figure 4.8) for each rotational speed (ω). This curve can be divided into three different regions [6]:

- Diffusional control. The current density depends only on the mass transport rate and the total current is proportional to $\omega^{1/2}$. The plateau corresponds to the limiting current.
- Mixed control. The current density is associated to kinetic control and to mass transport, and j varies in a nonlinear fashion with $\omega^{1/2}$.
- Kinetic control. The current density is totally controlled by the kinetics of electron transfer and the speed of mass transport will have no effect current density. That is, j is independent of ω.

From the kinetic data obtained from oxygen reduction reactions, Koutecky-Levich analysis and Tafel slope evaluation were performed to analyze the activity of the catalyst

[6,7]. The electrochemical process consists of two consecutive steps, the mass transfer and load transfer, and, at certain times, one behaves as limiting step.

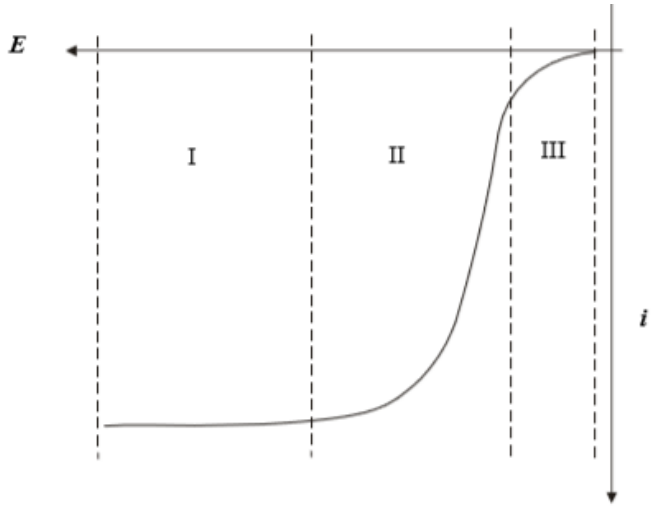

Figure 4.8. Example of current density vs potential linear sweep voltammetry in at a rotating disk electrode, when the three regions are clearly appreciated.

When the applied potential is small, the load transfer is slow and this fact is the limiting factor of the process. However, at high overpotentials, the load transfer is the fastest step and the process is limited by the mass transport. The current obtained at this point is independent of potential and is called limiting current or limiting current density (j_L) when it is expressed per unit area of electrode (A cm $^{-2}$). Therefore, the current density observed in the process (eq. 4.6) will consist of the charging current density (j_K) (Eq. 4.7) plus the limiting current density (j_L) (eq. 4.8).

$$\frac{1}{j} = \frac{1}{j_K} + \frac{1}{j_L} \qquad (4.6)$$

$$i_K = k \cdot n \cdot A \cdot F \cdot C_{O_2} \qquad (4.7)$$

$$i_L = 0.62 \cdot n \cdot F \cdot A \cdot D^{\frac{2}{3}} \cdot \omega^{\frac{1}{2}} \cdot \upsilon^{-\frac{1}{6}} \cdot C_{O2} \qquad (4.8)$$

Considering Equations 4.7 and 4.8, the total current density is defined by the equation Koutecky-Levich (Eq. 4.9).

$$\frac{1}{j} = \frac{1}{k \cdot n \cdot A \cdot F \cdot C_{O_2}} + \frac{1}{0.62 \cdot n \cdot F \cdot A \cdot D^{2/3} \cdot \omega^{1/2} \cdot \upsilon^{-1/6} \cdot C_{O2}} \qquad (4.9)$$

Where:

- j_L is the limiting current density (A cm^{-2}).
- ω is angle frequency (rad·seg^{-1}) calculated from rotating speed (rpm).
- n is the amount of electrons transfered (theoretical value should be 4).
- F is the Faraday constant (96485 C·mol^{-1}).
- A is the electrode area 0.196 cm^2.
- D is the oxygen diffussion coefficient in the electrolite ($2.1 \cdot 10^{-5}$ $cm^2 \cdot s^{-1}$).
- ν is the cinematic viscosity of the electrolite (0.011 $cm^2 \cdot s^{-1}$).
- C_{O2} saturated oxygen concentration in the electrolite media ($1.03 \cdot 10^{-6}$ mol·cm^{-3}).

Representing j^{-1} vs $\omega^{-1/2}$ two relevant parameters can be obtained: n, the number of exchanged electrons and j_K. The linearity of this graph indicates that the studied reaction is first order. When experiments at different potentials are performed, it can be obtained the dependence between the potential and j_K by Tafel equation. This equation describes the anodic and cathodic limits by the Bulter-Volmer equation (Eq. 4.10), allowing the characterization of the electrode reaction.

$$E = \frac{2.303 \cdot R \cdot T}{\alpha \cdot n \cdot F} \cdot \log j_0 - \frac{2.303 \cdot R \cdot T}{\alpha \cdot n \cdot F} \cdot \log j_K \qquad (4.10)$$

According to equation 4.9, Tafel slope (-2.303RT / αnF) can be calculated representing the log (J_K) against the potential in the area of kinetic control, which allows us to determine the exchange current density. The load current density can be obtained using the Equation 4.11.

$$j_K = \frac{j \cdot j_L}{j_L - j} \qquad (4.11)$$

The rotating disk electrode (RDE) is one of the hydrodynamic systems used in kinetic studies. This is able to vary the rate of mass transport in a very wide range. RDE consists of a disc with an electro catalytic material surrounded by a non-conductive tube material (polyethylene, Teflon, etc.), constructed so that only the surface of the disc-shaped electrode is in contact with the electrolyte solution. The electrode is rotated perpendicularly to the axis of the disc face, so that flow patterns established well-defined direction.

To deposit the catalyst on the surface of the 5 mm glassy carbon (GC) electrode (previously polished with a Al_2O_3 suspension and rinsed with deionized water to achieve a mirror finish effect), a catalyst ink was prepared with 6 mg of catalyst powder, using 4.8 mL of deionized water, 1.2 mL of 2-Propanol as dispersing agent, and 40 µL of Nafion solution (5% wt. on 2-propanol, Sygma Aldrich). Ink was sonicated for 20 min and then, 10 µL of the ink were placed on the surface of the GC electrode. Ink was dried at 500 rpm during 30 min.

Cyclic voltammetries and ORR analysis were carried out using sulfuric acid (H_2SO_4), 0.5 M as electrolyte. First, cyclic voltammetries were performed. To do this, the media was bubbled with nitrogen for 30 minutes in order to remove all oxygen present in the media. Then, 25 cycles were performed at 200 mV s^{-1} with no rotation speed, in order to polish the electrode surface. After that, 3 cycles were performed at 200, 150, 100 and 50 mV s^{-1} to calculate ECSA values. Subsequently, the system was saturated with oxygen for 30 min and ORR tests were performed. A low flow of oxygen was maintained throughout the experiment, in order to keep the complete saturation of the system. The ORR was conducted at four rotation speeds of 400, 900, 1200 and 1600 rpm.

4.4. Experimental procedures

In this section, all manufacturing and evaluation devices, and the experimental procedures used in this work are described.

4.4.1. Catalyst synthesis

The catalyst synthesis was conducted by the Formic Acid Method (FAM) [8]. This method consists of the deposition of platinum from a precursor salt (chloroplatinic acid hexa-hydrate, Sigma-Aldrich). To prepare a batch of 1.0 g of catalyst, the desired amount of the powder used as support (SiC, SiCTiC, CNFp, CNSs or Vulcan XC72) was added to a stirred reactor containing 500 mL of 0.1 M formic acid solution (98 %, Panreac), heating the system up to 80 °C. Then, a fixed volume of 50 mg ml^{-1} chloroplatinic acid hexahydrate solution was added drop by drop during 15 minutes approximately, and the mixture was kept under agitation at 80 °C for one hour. Then, the suspension was left to cool at room temperature, and the solid was filtered and dried during 12 hours in an oven.

4.4.2. MPL preparation

To manufacture the different MPLs, the selected material (CNSs, CNFp, SiC, Si_xTi_yC or Vulcan XC72, depending on the tests) was deposited onto a gas diffusion media (Toray Carbon Paper -PTFE wet proofing 10% wt., Fuel Cells Store, USA) by air-spraying a microporous ink consisting of the material and 10% wt. PTFE (Teflon™ Emulsion Solution, Electrochem Inc.), using 2-propanol as a dispersing agent. In order to achieve a good dispersion and homogeneity of the ink, vials were sonicated for 30 minutes. Airbrush device was fed with a pure nitrogen flow, in order to avoid the oxidation of the components during the deposition. When target loading of the MPLs was achieved, sintering process of the PTFE and removal of residual solvent on the surface of the electrodes were attained by heating the electrodes at 360 ºC for 30 min.

4.4.3 Catalyst layer deposition

The catalyst layers were deposited by airbrush method, spraying the catalyst ink over 5x5 cm^2

electrodes with commercial MPL (Freudenberg Vliesstoffe, H23C2) for the anode side. The catalyst ink for the cathode electrodes consisted of a 20% or 40% wt. Pt/X (being X the different supporting materials, i.e. CNSs, CNFp, SiC, Si_xTi_yC and commercial Pt/Vulcan carbon XC72), PBI ionomer (1.5 wt. % PBI in N,N-dimethylacetamide, DMAc, 1-20 PBI/support ratio), and DMAc as a dispersing agent. These Pt amounts on the catalyst powder were fixed according to the optimization results of the catalyst layer for HT-PEMFCs achieved in previous results performed by our research group [9] and they are in agreement with the ratios used in other works shown in the literature [10]. For the anode, the commercial catalyst, Pt/C, was used. In all cases, the Pt loading on the two electrodes (anode and cathode) was 0.6 mg Pt cm^{-2}, otherwise is mentioned. After the deposition of the catalyst layer, the electrodes were dried at 190 °C for 2 h, with the purpose of removing traces of DMAc. The electrodes were then wetted with a solution of 10% PA. Electrodes were left to adsorb the acid for one day.

4.4.4. MEA manufacturing

For the preparation of the MEA, a 7x7 cm^2 PBI thermally treated membrane (DPS, Denmark), according to the provider's specifications, was doped in 85 wt. % PA for 4 days at least, in order to achieve good proton conductivity values. The doping level acquired by the membrane was located between 9-10 molecules approx. of acid per polymer repeating unit in all cases. The corresponding thickness of the doped membranes was around 80 μm. The superficial acid on the membrane was thoroughly wiped off with filter paper and the membrane was used to prepare the MEA. Manufacturing process consisted on place the doped membrane sandwiched between a couple of electrodes (one anode and one cathode), and the whole system was hot-pressed at 130 °C and 1 MPa for 15 min. The completed MEA was inserted into the cell between bipolar plates of graphite (with a five serpentine channels frame in each plate). The geometrical area of each electrode was 25 cm^2.

4.4.5. MEA testing

In order to evaluate the behavior of the new materials in a real HT-PEMFC system, preliminary long-term testing studies were performed to the different MEAs prepared. All tests were carried out into a in a commercially available Cell Compression Unit (CCU) provided by Baltic fuel cells GmbH (Germany), connected to an AUTOLAB 302 potentiostat with a 20A booster. These parts and additional elements such as flow meter control or temperature control devices used in the test station are shown in Figure 4.9.

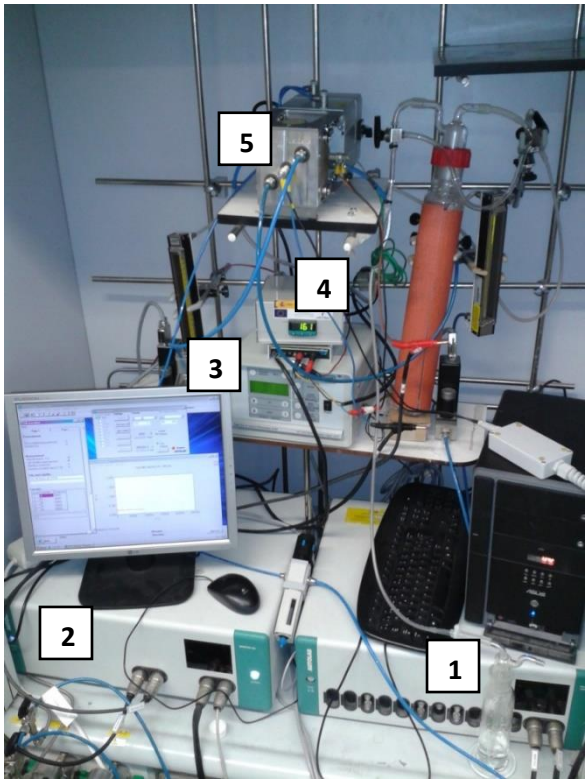

Figure 4.9. MEA test station.1) Potentiostat; 2) 20A booster; 3) four channels flow meter control; 4) Temperature control system; 5) Baltic test compression unit

All MEAs were compressed at 1.00 MPa into the Baltic unit. During the heating process carried out up to 120 ºC, 50 mL min^{-1} were fed to both sides of the fuel cell in order to remove the oxygen and residual materials over the fuel cell. When a temperature of 120 ºC was reached, break-in procedure started, consisting of operation at 0.1 A cm^{-2}, feeding the cell with H_2 as fuel and air as oxidant, using excess stoichiometric coefficients of $\lambda_{H2/air}$ of 1.5

and 2.0, respectively, for 48 hours. This break-in was carried out in order to conditioning the MEA and activate the catalyst before the test.

After the break-in procedure, temperature was increased up to 160 ºC. Short preliminary life test was conducted by increasing the current density to 0.2 A cm^{-2} and working at constant stoichiometric coefficients (λ_{H2} of 1.5 and λ_{air} of 2). For further characterization, a protocol test was carried out every 48 h, performing the first one at the end of the break-in procedure. This protocol test consists of the following routine:

- Galvanostatic polarization curves. They were performed from the OCV to 0.40 V. First with air at constant $\lambda_{H2/air}$ =1.5/2 and then with oxygen at constant $\lambda_{H2/O2}$ =1.5/9.5.
- Electrochemical impedance spectroscopy (EIS) tests. These tests were performed at 0.10 A cm^{-2} with 10 mV AC disturbance amplitude and frequency range from 10000 to 100 Hz. This sequence of EIS tests was carried out with air as oxidant and then the same procedure was repeated with oxygen.
- Cyclic voltammetries (CV). The ECSA of cathode was estimated with this technique. The cathode side was purged with nitrogen and hydrogen flowed through anode side with flows of 0.1/0.1 L min^{-1} N_2/H_2, during 8 minutes before to start the measurements and during measurements itself. In these conditions, 8 cycles were carried out from 0.05 V to 1.00 V with a scan rate of 100 mV s^{-1}, taking the 6^{th} for the ECSA determination.
- Linear sweep voltammetry (LSV). This technique was performed to evaluate the crossover of gas flow through MEA. The same gases of the CV were fed with flows of 0.3/0.3 L min^{-1} N_2/H_2 during 8 minutes, and then, with the same flows, one LSV was performed from 0.20 to 0.50 V at 2.0 mV s^{-1}. From the corrected linear sweep voltammetry, as it is shown in Figure 4.10, by removing the influence of the internal resistance of the system (calculated from the slope of the linear sweep in the linear section between 0.30 and 0.40 V using Equation 4.12), crossover values were calculated for each LSV performed.

$$R_{int}(\Omega) = \frac{1000}{LSV\ slope\ (mAV^{-1}cm^{-2}) * Electrode\ area(cm^2)} \qquad (4.12)$$

Because of the high number of the tests performed during the PhD, and taking into account the long time and resources consuming with these tests, only 100 hour-tests were performed of each MEA (excluding the break-in procedure) during the evaluation of the materials. This time was assumed to be long enough for a preliminary selection of the best materials tested.

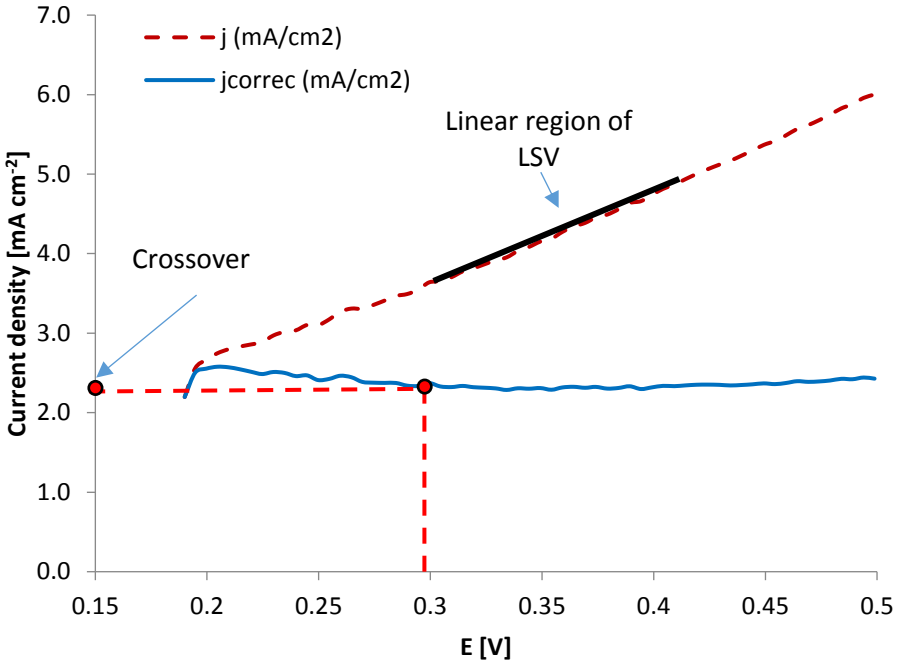

Figure 4.10. Example of calculation of the internal resistance and crossover using corrected LSV values

4.5. Bibliography

[1] V. Jiménez, A. Nieto-Márquez, J. A. Díaz, R. Romero, P. Sánchez, J.L. Valverde, and A. Romero, Ind. Eng. Chem. Res. 48 (2009) 8407.

[2] A. Nieto-Márquez, I. Espartero, J. Lazo, A. Romero, J.L. Valverde, Chemical Engineering Journal 153 (2009) 211.

[3] D. Singha, I. I. Soykal , J. Tiana, D. von Deaka, J. Kinga, J. T. Miller, U. S. Ozkan, Journal of Catalysis 304 (2013) 100.

[4] E. Nowak, P. Robbins, G. Combes, E. H. Stitt, A.W. Pacek, Powder Technology 250, (2013) 21.

[5] J. Lobato, P. Cañizares, M.A. Rodrigo, D. Úbeda, F.J. Pinar, J.J. Linares, Fuel Cells 10 (2010) 770.

[6] A.J. Bard, and L. R. Faulkner, Electrochemical Methods: Fundamentals and Applications (2001) ISBN: 978-0-471-04372-0, Wiley.

[7] C. Song, J. Zhang, PEM fuel cell electrocatalysts and catalyst layers. Fundamentals and applications, Chapter 2 (2008) ISBN: 978-1-84800-935-6, Springer.

[8] F. Colmati, E. Antolini, E. R. Gonzalez, Electrochimica Acta 50 (2005) 5496.

[9] J. Lobato, P. Canizares, M.A. Rodrigo, J.J. Linares, D. Úbeda, F.J. Pinar, Fuel cells 10 (2010) 312.

[10] A.S. Pushkarev, I.V. Pushkareva, S.A. Grigoriev, V.N. Kalinichenko, M.Yu. Presniakov, V.N. Fateev, International Journal of Hydrogen Energy 40 (2015) 14492.

CHAPTER 5: Study of carbonaceous based materials as Microporous Layer in HT-PEMFCs

5.1. Introduction and Objectives

The Gas Diffusion Layer (GDL) of the electrodes of HT-PEMFCs is situated between the catalyst layer and bipolar plate and it is subdivided into the Gas Diffusion Backing (GDB) and the Micro-Porous Layer (MPL). GDB is composed of carbon fibers, usually carbon cloths or papers substrates. Its main function is to promote an adequate diffusion of the gases through the entire electrode surface, and also to collect and transport the current to bipolar plates. On the other hand, the MPL, consisting of porous nano-sized carbon powders, improves the diffusion of reactant gases and liquids, minimizing electric contact resistance between the catalyst layer and bipolar plates, and managing the water balance during production, expulsion, supply and evaporation [1-4]. This later point is more important for low temperature PEMFC, where liquid water is produced during operation, but it is also significant in HT-PEMFC, where only gaseous water is found.

Extensive studies on the MPL have been carried out to investigate the effects of carbon powder type on PEM fuel cell performance [5-7]. For example, Passalacqua et al. prepared MPLs using different types of carbon blacks, in order to determine the effect of porous carbon structure on fuel cell performance. Performance improvement obtained with acetylene black was attributed to higher pore volume and smaller pore size, which facilitate gas diffusion and reduce the amount of water accumulation inside the MPL [5-7].

Carbon blacks (CB) like the Vulcan Carbon XC72 are typically used as supports for Pt and Pt-alloy catalysts for fuel cells and MPL usually contains Vulcan XC-72, as well. The high surface area (250 $m^2\ g^{-1}$ for Vulcan XC-72), low cost and availability of carbon blacks serve to reduce overall fuel cell costs. However, carbon blacks also have some well-known drawbacks including: 1) thermochemical instability; 2) corrosion under acidic conditions and high potentials; 3) pore size and pore distribution that may interact with ionomer and catalyst particles, and 4) presence of organosulfur impurities, which may reduce the catalyst activity [8-10]. Likewise, the high voltage values reached during the start-up and shut-down of the

fuel cell may have an important role in the degradation of the carbonaceous materials. Potentials over 0.21 V vs RHE can produce carbon corrosion in moderate amount and over 1.20V the corrosion achieves high importance [11-12]. Thus, the development of new materials that can address the entire positive features that those carbon materials exhibit and, at the same time, which may minimize their negative characteristics is crucial.

Therefore, carbon nanostructures formed by rolled-graphene sheets are currently being examined in order to overcome these limitations. Typically, nanostructures can be divided into:

1) Carbon nanotubes (CNT), 2-D nanostructures that may be single walled or multi-walled;
2) Carbon nanofibers (CNF), filamentous and graphene sheets that form fibers, sometimes having a hollow interior. Based on the disposition angle of the graphene axis, these fibers are classified as Platelet (CNFp), Fishbone and Parallel [13].
3) Carbon nanospheres (CNS), formed by graphene sheets in the form of hollow spheres, presenting different morphology and characteristics attending to their synthesis procedure and carbon precursor source [14].

All of these nanostructured materials have revealed improved electrochemical and thermochemical resistances when they have been tested in PEMFC systems [15,16]. It should be noted that PBI based HT-PEMFC system differs from the Nafion-based PEMFC, since it only has one gaseous phase on the cathode side and the electrode surface environment is more aggressive because of the combined effect of the high temperatures (100-200 ºC) and the presence of phosphoric acid. It must be pointed that usually, the investigation of these materials is focused on their application in the catalytic layer, but the GDL itself has not received much research attention. In this sense, our research group has been referenced as the main group that focused the study also on the improvement of this layer [3].

Taking into account this background, the main objective of this Chapter is the evaluation of carbon nanofibers Platelet (CNFp) and carbon nanospheres (CNS), both nanocarbonaceous materials synthesized in our facilities according to the procedures reported in literature [17, 18], to be used as raw material of the cathodic MPL electrode for HT-PEMFCs, comparing their properties with those of a Vulcan carbon XC72, proposed as reference material.

5.2. Methodology

SEM micrographs were performed to both nanocarbonaceous materials to evaluate their particle size distribution and aspect with more detail. Figure 5.1 shows the SEM micrographs obtained for each nanomaterial.

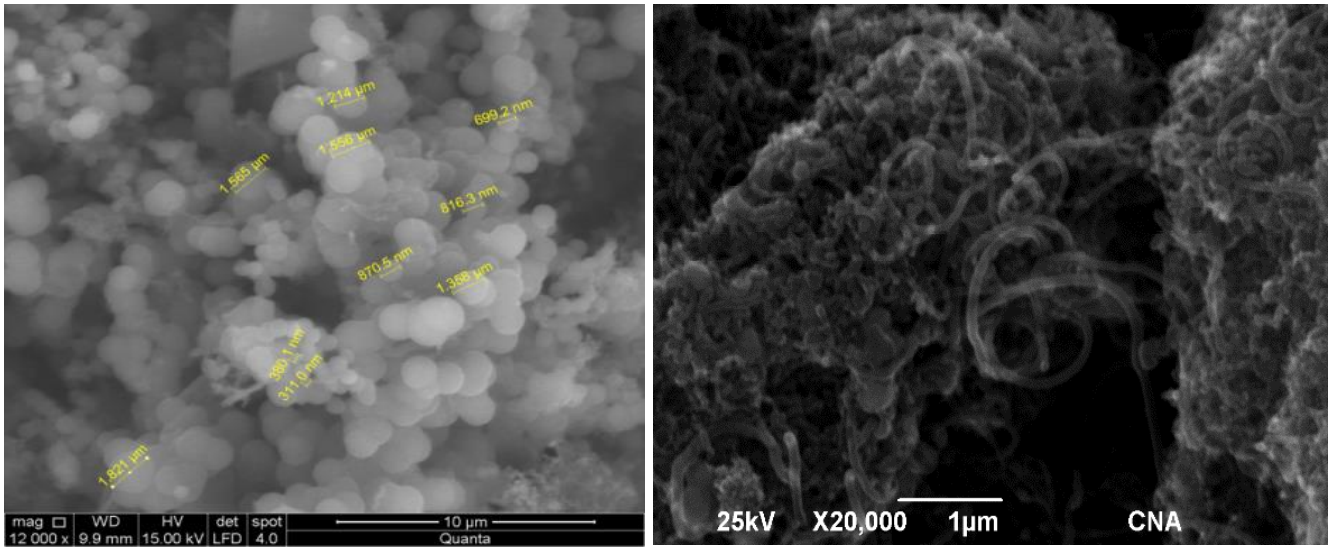

Figure 5.1. SEM micrographs of both nanocarbonaceous material studied: Carbon nanospheres (left) and Carbon nanofibers platelet (right)

As it can be observed, lab-made CNSs manufactured have not uniform sizes, presenting particle size ranging between 300-1500 nm. The spherical shape is clearly observed, which means that CNSs have been successfully synthesized. On the other hand, carbon nanofibers exhibit uniform aspect, with diameter around 100 nm and variable lengths.

The different carbonaceous materials in powder form were analyzed by XRD, according to the procedures described in the Chapter 4, in order to get more information about their crystallinity. BET surface area of different samples and total pore volume were obtained using N_2 adsorption-desorption at 77 K, to get more information about the surface area and the porosity of the samples.

To manufacture the different MPLs, CNSs, CNFp or Vulcan XC72 material (depending on the tests) was deposited onto a gas diffusion media (Toray Carbon Paper - PTFE 10%, Fuel Cells Store, USA) by air-spraying a microporous ink consisting of the carbonaceous material and 10% PTFE (Teflon™ Emulsion Solution, Electrochem Inc.). After the deposition of the MPLs (2.0 mg cm^{-2}), sintering is attained by heating the electrodes at 360 ºC for 30 min. MPLs were characterized by XRD first, to evaluate changes in the crystallite properties of the materials. Hydrophobicity of the samples was evaluated by the drop water method. Electrical conductivity was determined by EIS, using the four-point method. Permeability of the reactive gases was also evaluated by studying the pressure drop at different hydrogen, oxygen and air flows. All these experimental procedures were described in Chapter 4.

The stability is a critical challenge to be overcome in the field of proton exchange membrane fuel cells. Thus, accelerated thermal tests were performed placing 1x1 cm^2 samples, impregnated with 13 mg of 85% phosphoric acid (PA) in a furnace at 190 ºC during 8 hours, analyzing the crystallite changes by XRD to evaluate the stability of the materials.

Finally, to complete the ex-situ characterization, electrochemical degradation in PA media was evaluated by voltammetric tests, that were used to analyze the stability of the different advanced materials tested under the same operation conditions. These tests were performed in half-cell system, at 25 ºC, using 2M PA solution as electrolyte, an Ag/AgCl electrode as reference electrode, and a gold foil as counter electrode. Nitrogen was bubbled during all experiment into the reactor in order to remove the oxygen of the media. Under

these conditions, 350 cycles were performed for each sample, from -0.21 to 0.79 V (vs Ag/AgCl) at 20 mV s^{-1}. This lower speed rate was selected to promote the corrosion of the electrodes.

In the second part of the Chapter, electrodes containing MPLs prepared with each material were used as cathodes and tested in a single HT-PEMFC system. MPLs of the electrodes were manufactured by the same procedure described in the ex-situ experiments. The catalyst layer was deposited by spraying the catalyst ink on the electrodes. The catalyst ink consisted of a 40% Pt/C catalyst on Vulcan XC-72R Carbon Black (Fuel Cell Store, USA), PBI ionomer (1.5 wt. % PBI in N, N-dimethylacetamide, DMAc), and DMAc as a dispersing solvent. In both cases, the Pt loading on each electrode was 0.6 mg Pt cm^{-2}. After the deposition of the catalyst layer, the electrodes were dried at 190 °C for 2 h, with the purpose of removing traces of DMAc. The electrodes were then wetted with a solution of 10% PA. Electrodes were left to adsorb the acid for one day. For the preparation of the MEA, a thermally treated PBI membrane was provided by Danish Power Systems®. This membrane was doped in 85 wt. % PA for 5 days, in order to achieve good proton conductivity. The doping level acquired by the membrane was approx. 10 molecules of acid per polymer repeating unit. The corresponding thickness of the doped PBI membrane used was 83.2 μm. The superficial acid on the membrane was thoroughly wiped off with filter paper and the membrane was used to prepare the MEA. In order to fabricate the membrane-electrode assembly (MEA), the doped membrane was sandwiched between a couple of electrodes and the whole system was hot-pressed at 130 °C and 1 ton for 15 minutes. Vulcan carbon was always used for the MPL of the anodes, taking into account that cathodic reaction is the bottleneck in the overall process, in particular in terms of the dragging of catalyst components. The completed MEA was inserted into the cell between the end plates of graphite (with a five serpentine channels frame in each plate). The geometrical area of each electrode was 25 cm^2.

MEAs were mounted and characterized in a commercially-available Cell Compression Unit (CCU) provided by Baltic Fuel Cells GmbH (Germany). The break-in procedure consists of the operation at 0.1 A cm^{-2}, and λ (H_2) 1.5 and λ (air) 2 for 70 hours. Then, a preliminary stability test was conducted by increasing the current density up to 0.2 A cm^{-2} (160 °C). For further characterization, a protocol test was carried out every 48 h, during the 100 hours of the short tests performed, since the end of the break-in procedure. This test, already described from a generalist viewpoint in Chapter 4, consists of the following routine:

- Galvanostatic polarization curves.
- Electrochemical impedance spectroscopy (EIS)
- Cyclic voltammetries (CV).
- Linear sweep voltammetry (LSV).

The conditions of each test of the characterization routine were described in the Chapter 4 of this document (see page 86).

5.3. Ex-situ characterization of carbonaceous based materials

5.3.1. Powder characterization.

XRD analyzes were performed to evaluate crystallite size and crystallinity. Figure 5.2 shows the XRD patterns of different carbon materials. It may be observed that they all have a characteristic graphite (0 0 2) peak at 2θ = 26° [17, 18, 19], and another one located approx. at 2θ = 41 º.

Table 5.1 shows the crystallite sizes (L_C), and the average interlayer spacing (d_{002}). L_C and d_{002} were calculated according to the equations 4.1 and 4.2, respectively, described in Chapter 4. The average interlayer spacing, d_{002}, may be related to the graphitization index, which indicates the similitude of the measured carbon with graphite (which presents a d_{002} value of 0.335 Å).

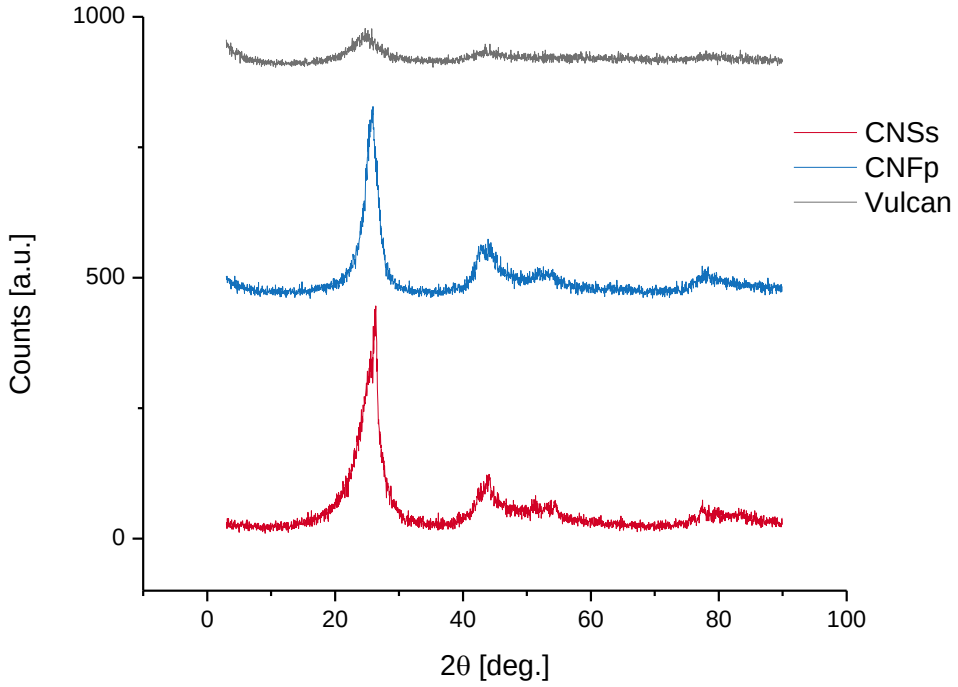

Figure 5.2. XRD from different carbonaceous powders tested

Table 5.1. XRD and BET results obtained for each carbonaceous material studied

Sample	Lc [nm]	d_{002} [Å]	BET area [$m^2\ g^{-1}$]	Pore Volume (for pores smaller than 1136.8 Å) [$cm^3\ g^{-1}$]	Average pore size [nm]
Vulcan XC72	**2.32**	**3.48**	**220.4**	**0.442 0.043 mp**	**12.2**
CNFp	**3.85**	**3.43**	**144.2**	**0.549 [0.004 mp]**	**7.6**
CNS	**3.33**	**3.38**	**9.2**	**0.042 [0.00 mp]**	**9.0**

Respect to the BET surface area, Figure 5.3 shows the adsorption/desorption isotherm for each carbonaceous sample, whereas BET area, pore volume, micropore volume (mp) and average pore size are also shown in Table 5.1.

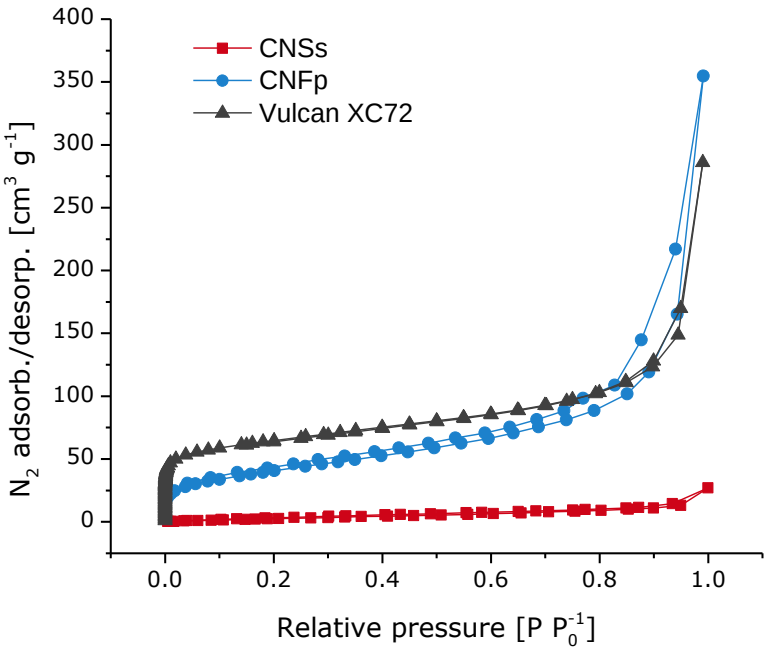

Figure 5.3. BET isotherms obtained for the different carbonaceous materials studied.

CNFp sample exhibits a type IV Langmuir adsorption/desorption isotherm, with a clear hysteresis phenomenon that can be associated to the surface micro and mesoporosity, [20] which it also noticed in Table 5.1, in which it can be observed that CNFp exhibited the highest pore volume. CNS exhibits a shape closely to a type II Langmuir plot, which corresponds to materials with no microporosity surface and although Vulcan carbon also exhibits a very small hysteresis on the desorption curve, it could also be considered as a type II isotherm, suggesting behavior as mesoporous and/or non-porous materials [20].

Carbon nanofibers had the greatest crystal size while the Vulcan Carbon had the smallest one. All materials presented values within the range typically found in literature [16, 17]. Parameter d_{002} was similar in all cases, being the lowest value for the carbon nanospheres (CNS), suggesting a more graphitic structure for these materials. Respect to the BET areas, it can be observed that carbon nanostructures presents lower surface areas compared with Vulcan carbon, being CNS the material with the lowest BET area. This fact has to be related to their structure, more compact and less porous than in the other carbonaceous materials. At

this point, it must be reminded that the sphere is the geometrical morphology with less surface exposed, which also justify this lower value [18].

5.3.2 MPL Characterization

As a starting point, the different MPLs were characterized by XRD analyses, in order to study the surface of the layer containing the different carbon materials. XRD patterns of the MPLs are shown in Figure 5.4.

Apparent crystallite size and apparent distance between planes d_{002a}, were calculated in the same manner as for the powders. The values obtained for the different MPLs are shown in Table 5.2, together with other information that will be later discussed but that it is included here to favor further comparison and discussion.

In comparing results, it can be noticed that values obtained for LC and d_{002} differ significantly from the values shown in Table 5.1.

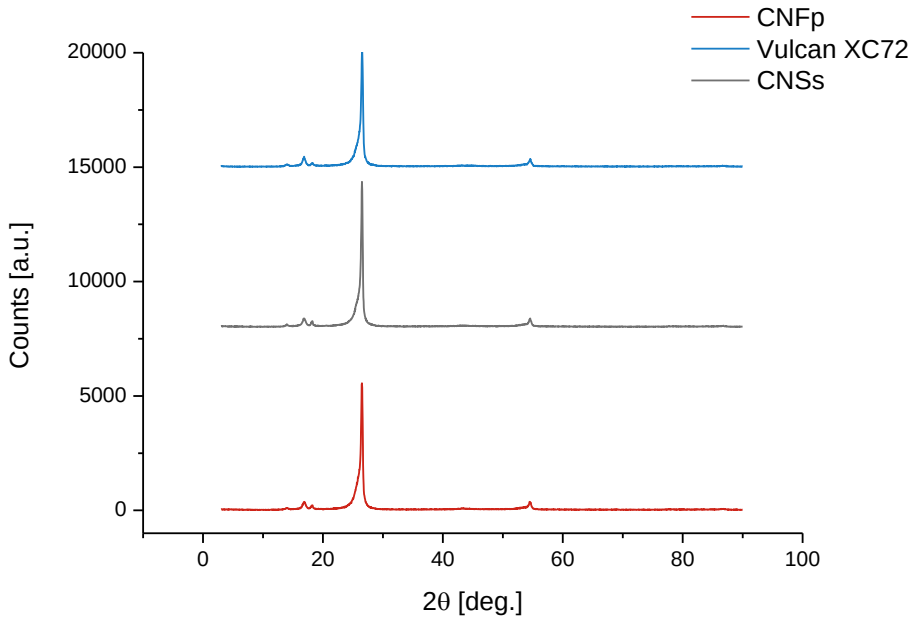

Figure 5.4. XRD patterns for different electrodes with MPLs prepared with each carbonaceous material

Initially, this difference can be explained in terms of the addition of PTFE in the microporous layer, which causes agglomerations, that is why the values are considering as

"apparent". However, the effect of the GDL (below the MPL) should not be neglected. At this point, it is important to take in mind that this GDL was also analyzed by the XDR technique, and perhaps this point is the most influential fact in the changes of the crystallinity observed.

Table 5.2. XRD patterns for different MPLs before and after the stability assessments

Material	LC_a [nm]	$d002_a$ [nm]	% Increase
Vulcan	18.48	0.335	-
CNF_P	21.45	0.336	-
CNSs	24.56	0.336	-
Vulcan post TT*	20.88	0.336	12.96
CNF_P post TT*	24.20	0.336	12.82
CNS post TT*	25.59	0.337	4.20
Vulcan post CV**	23.33	0.338	26.24
CNF_P post CV**	24.79	0.338	15.58
CNS post CV**	24.80	0.336	0.94

* Post TT: after thermal treatment; ** Post CV: after the voltammetric test

Therefore, these values do not represent the real size of crystals and distance between planes and they have to be considered only as apparent first approach, that shall be used only for comparative purposes when making stability assessments (as described later on in this Chapter).

The surface appearance of the different electrodes was studied using SEM micrographs. Figure 5.5 shows the SEM of the MPLs manufactured with the different carbonaceous materials.

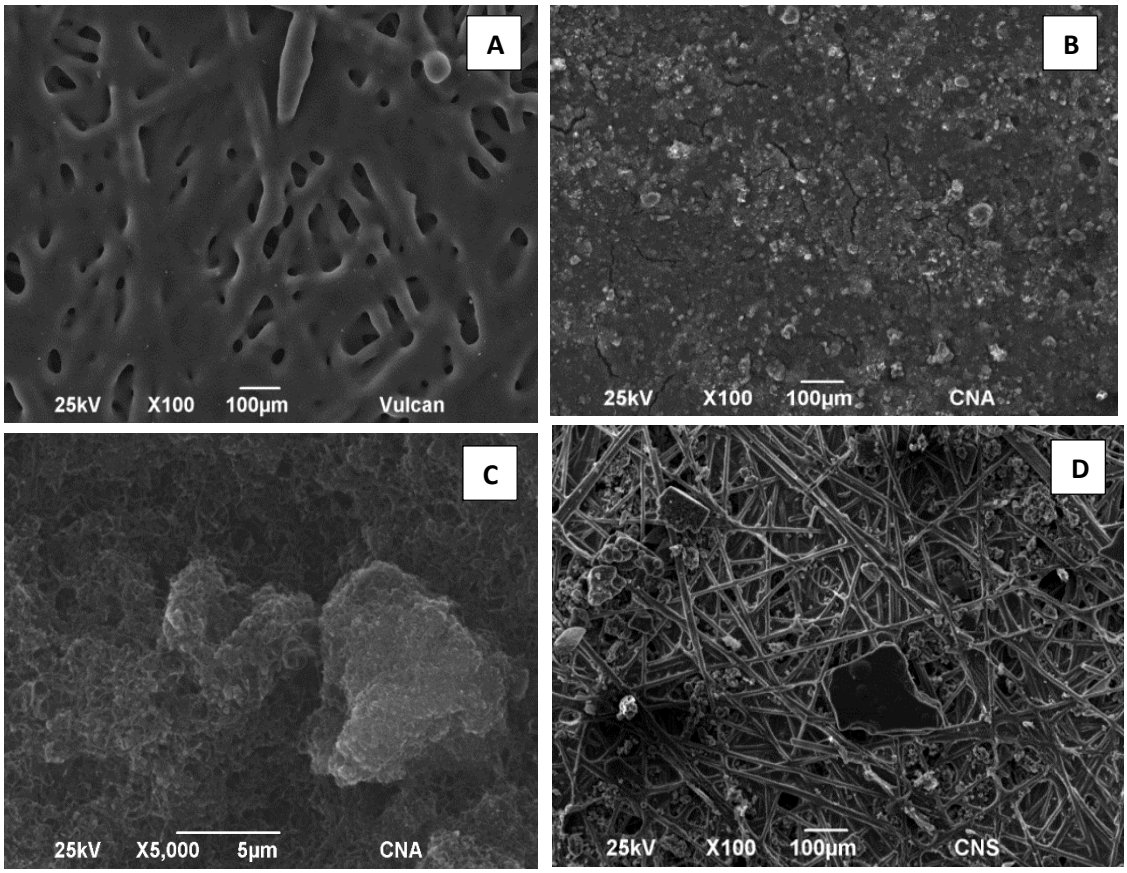

Figure 5.5. SEM micrographs of the different MPLs analyzed: A) Vulcan XC72; B) CNFp; C) CNFp (higher magnification of CNFp MPL); and D) CNSs

Vulcan has a homogeneous surface, since the powder is somewhat thinner and is distributed more uniformly along the surface. Carbon nanofibers based MPL exhibits a very compact structure, with no signal of the carbon network of the GDB, and presenting a grainy surface, similar to that observed in carbon nanotubes [21]. At higher magnifications (Part C), it is possible to distinguish the different morphologies of the carbon fibers in the case of CNF_P [17] can be distinguished. The spherical shape of the CNS is clearly appreciated in Part D, but as it can be observed, most of CNSs are situated into the spaces between the GDB network, and not just covering them, such as in Vulcan carbon based MPL. The image

obtained for the Vulcan is quite similar to those obtained by other authors [22]. Nevertheless, in all cases, the MPL surfaces were found to be homogenous at naked eye.

The degree of hydrophobicity was measured following the procedure described in the Chapter 4. Table 5.3 shows the left and right contact angles of each sample and also those obtained in a non-modified GDB labelled as GDL (measured for comparative purposes).

Table 5.3. Left and right contact angles measured for different MPLs

Sample	Left angle [°]	Right angle [°]
GDL	39	40
CNFp	143	144
CNS	142	142
Vulcan XC 72	133	132

MPLs with nanocarbonaceous materials exhibited higher hydrophobic character as compared to the Vulcan carbon one. Likewise, it is confirmed that the MPL significantly contributes to the increase in the hydrophobicity of the electrodes [23], since the non-modified GDL is considerably less hydrophobic, as clearly indicates its lower angle contacts [24]. The higher hydrophobicity of MPL means an expected better water management, leading to lower fuel cell degradation [23]. In all cases, the left and right angles have the same value approximately, so it may be considered that the surfaces are quite homogeneous and regular.

The reactive gas permeability was assessed using Darcy's law (equation 4.3, described in Chapter 4) [25]. Figure 5.6 shows the flow vs differential pressure curves obtained for each sample for the different reactive gases tested and Table 5.4 shows the permeability constant values of air, oxygen and hydrogen for the different MPLs.

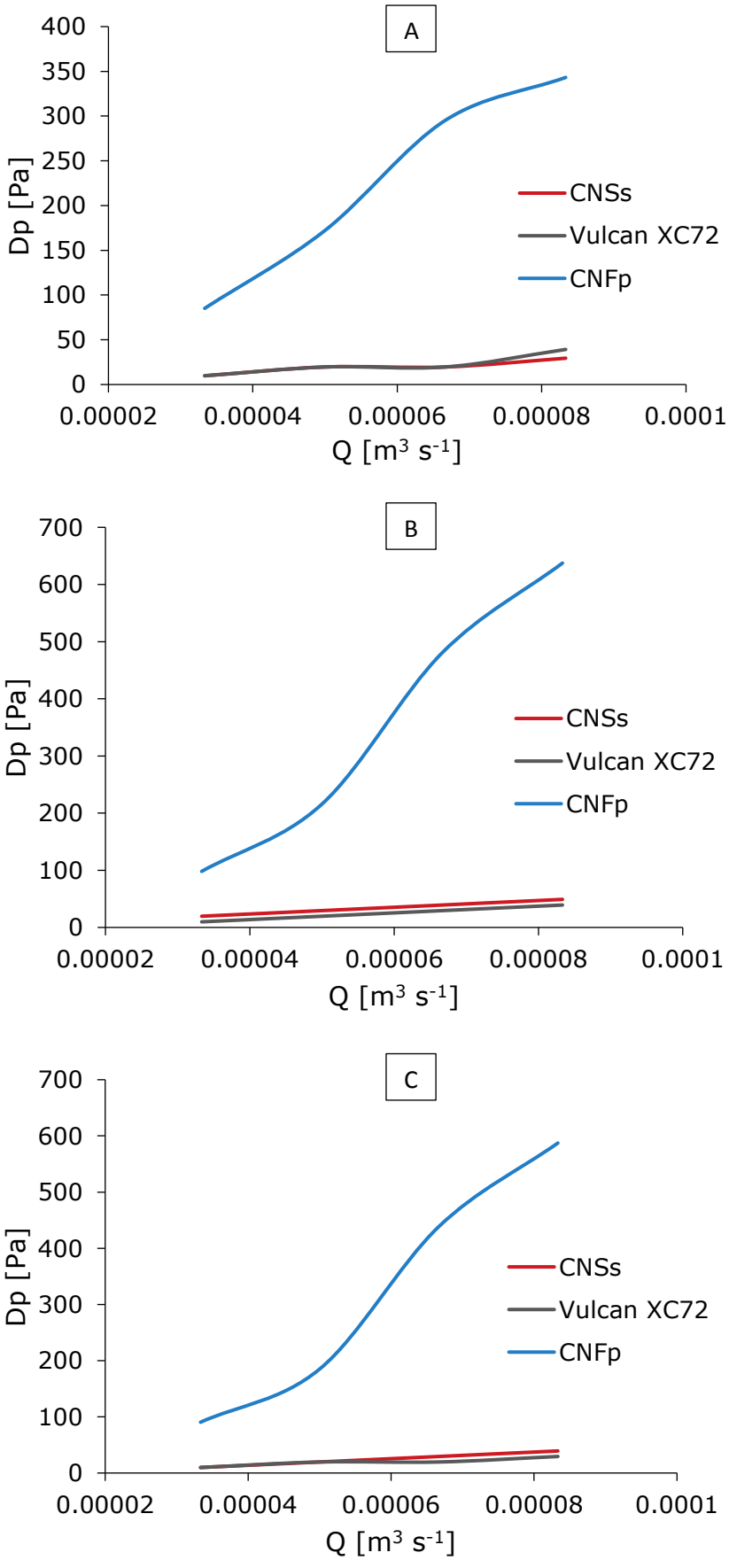

Figure 5.6. Permeability curves obtained for each reactive gas: A) Hydrogen; B) Oxygen; and C) Air

As it can be observed, CNFp-MPL exhibits much higher pressure drops as compared to the rest of MPL tested (for all reactive gases), and this means much higher problems of gas diffusion and, hence, a much worse expected performance during fuel cell operation, with a worse distribution of reagents on the electrode surfaces. CNS behaves as Vulcan XC72 and no significant differences are observed between both MPLs.

Table 5.4. Permeability constant values for different reactive gases obtained for each MPL tested

Sample	K_{Air} [m^2]	K_{O2} [m^2]	K_{H2} [m^2]
CNFp	$3.95 \cdot 10^{-12}$	$3.68 \cdot 10^{-12}$	$4.01 \cdot 10^{-12}$
CNS	$9.51 \cdot 10^{-11}$	$5.27 \cdot 10^{-11}$	$1.03 \cdot 10^{-10}$
Vulcan XC 72	$8.44 \cdot 10^{-11}$	$9.35 \cdot 10^{-11}$	$1.02 \cdot 10^{-10}$

In comparing gases, the permeability of hydrogen is the highest, as it may be initially expected, since it is the smallest specie. Air and oxygen behave in a more similar way and the lower size of the nitrogen molecules contained in air can help to explain the small differences noticed. Respect to the permeability coefficients, fitting values confirm that MPLs prepared with CNS and the carbon Vulcan XC72 are more permeable to the different gases than those prepared with CNFs, which present diffusion coefficients one log-unit below the rest of material tested. All values have been found to be quite similar to those found in literature [26]. The lower diffusion coefficient and, hence, worse performance of CNFs can be explained in terms of the more compact surfaces found in the MPLs seen in Figure 5.5, which may hinder the flow of gases.

In addition to provide an appropriate structure to enhance gas diffusion of the reactants and products, the MPL must also provide also good electrical conductivity, meaning that electrodes must have low resistivity (high electrical conductivity) in order to promote the

transfer of electrons from the electrode to the bipolar or end plates. In order to know more about the influence of the new carbonaceous materials on this conductivity, resistivity measurements were performed on the MPL with the different carbon materials at three different temperatures. Furthermore, for comparative purposes, the electrical conductivity of a commercial GDL coated with an MPL was also measured. Figure 5.7 shows the evolution of solid phase conductivity with temperature for each sample.

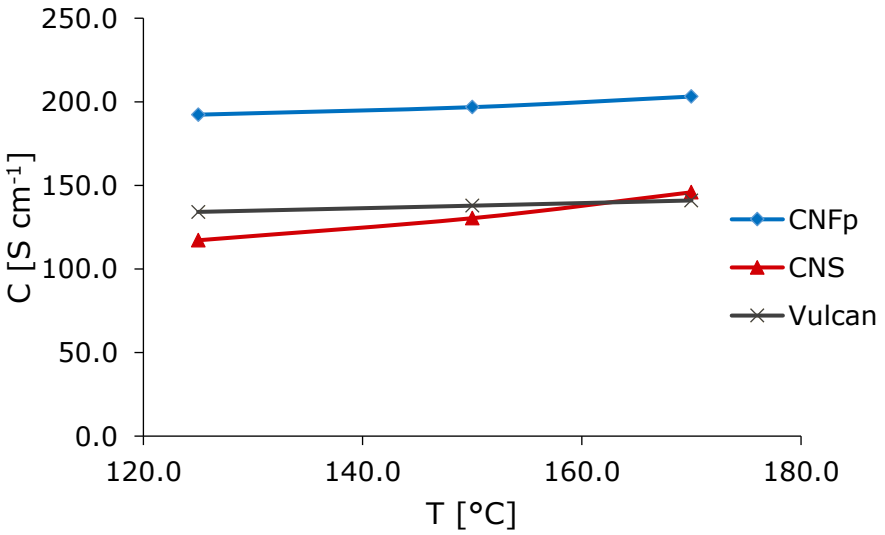

Figure 5.7. Electrical conductivity measurements performed at different temperatures for each material tested.

It can be seen that the conductivity in all cases is between 125.0 and 200.0 S cm^{-1}, similar to the values found in literature in other research works [27]. Those values are much higher than the values observed for the gas diffusion layers (GDLs) based on carbonaceous materials, which are approximately around 7.0 S cm^{-1} [28]. Therefore, it may be stated that all prepared MPLs provide less ohmic resistance, possibly due to more compact structure, added to a greater structural stability and improved interlayer contact. The MPL having CNFs shows the highest electrical conductivity in the whole range of temperatures tested and this may be explained in terms of the more compact structure observed in Figure 5.5. Initially, these values are surprising, because the electrical conductivity values for carbon nanofibers were reported to fall within a range between 0.5 and 30.0 S cm^{-1} and, in fact, CNFs may be classified as being at an intermediate range between high conductive carbon blacks and highly

graphitic carbons, in terms of conductivity. However, it should be taken into account that the apparent electrical conductivity in the MPL also depends on the packing and porosity [29] and this is the key to explain the high values observed here. At this point, it is important to take in mind that, in this study, electrical conductivities are measured for the microporous layer, not for powders. The MPL with the CNSs exhibits conductivity values that are similar to those of the MPL based on Vulcan XC72, around 135 S cm^{-1} at 160 ºC, and only slight differences are noticed at the highest temperature. Consequently, it may be concluded that these advanced carbon materials are good candidates to form a part of the electrode MPL for HT-PEMFCs, from an electrical conductivity perspective, because they do not produce any negative effect but even they promote this electron transport. In this case, opposite to what it was observed regarding the diffusion of gases, the CNFs are the material showing the most promising characteristics.

Thermal degradation tests were conducted in phosphoric acid (PA) media. After completing the thermal degradation assays, XRD analyses were performed in order to examine changes in surface structure of the different MPLs. Figure 5.8 shows the XRD patterns achieved for each sample before and after the assessment and Table 5.2 shows the values that were obtained for the LC and d_{002}.

From the comparison of the results, it is evident that the MPL with the CNSs shows negligible changes in the form of the pattern, with an increase of the apparent crystallite size (LC_a) of only 4.2%, which indicates a low degradation process for this surface and the GDB. This means that CNSs exhibit a very good stability and protects the macroporous layer situated under it. On the other hand, MPLs prepared with CNFp and Vulcan carbon show larger changes on their crystallinity properties, meaning that these electrodes suffer from greater thermal degradation in the phosphoric acid media. The highest value of degradation corresponds to Vulcan carbon, with an increase in apparent crystal size by 12.95%. The

increase in the crystal size could be attributed to agglomeration processes of the particle materials [23].

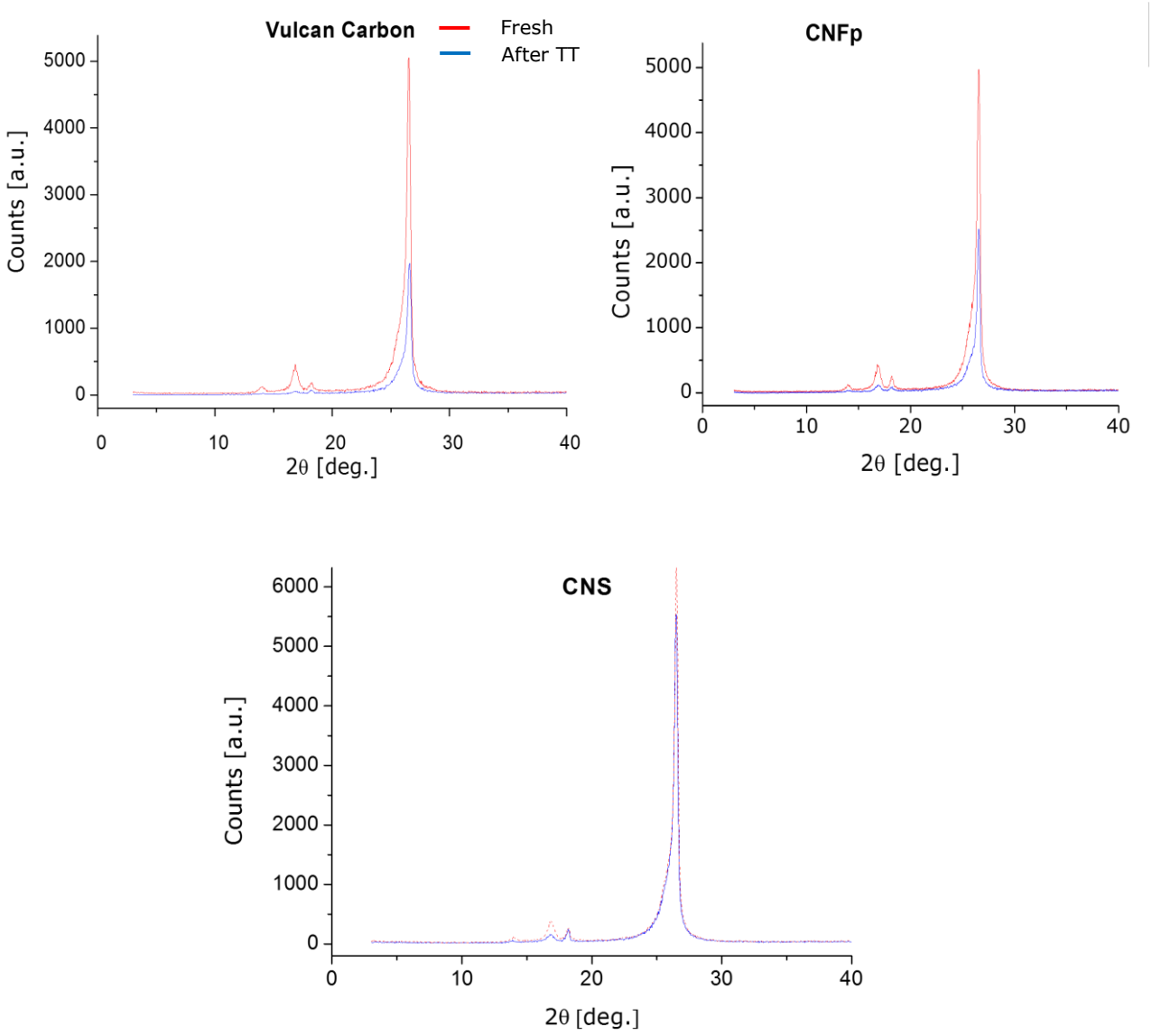

Figure 5.8. XRD patterns before and after the thermal stability assessment for each electrode tested.

Electrochemical assays were performed in order to establish the electrochemical stability of the MPLs prepared with different advanced carbon materials, according to the method described in Chapter 4. Cyclic Voltammetry (CV) is an important electrochemical tool that may reveal evidence of surface oxidation in different carbon materials. It should be noted that the cyclic voltammetries (CVs) were carried out by immersing the electrodes in a

2.0 M phosphoric acid solution, since the electrolyte used in the HT-PEMFC is phosphoric acid doped PBI based membranes. Therefore, all MPL surfaces were exposed to the phosphoric acid media, whereas in an actual fuel cell, an extra layer (catalyst layer) exists between the MPL and the electrolyte. Thus, in the CV tests, the degradation process is expected to be accelerated.

Figure 5.9 shows the cyclic voltammograms number 1 and 350 for all samples prepared in this study, recorded during the potential cycling (-0.40 V to 0.80 V approx. vs Ag/AgCl electrode; -0.25 V to 0.80V for Vulcan carbon, because this sample let to observe clearly the hydrogen evolution peak at lower potential).

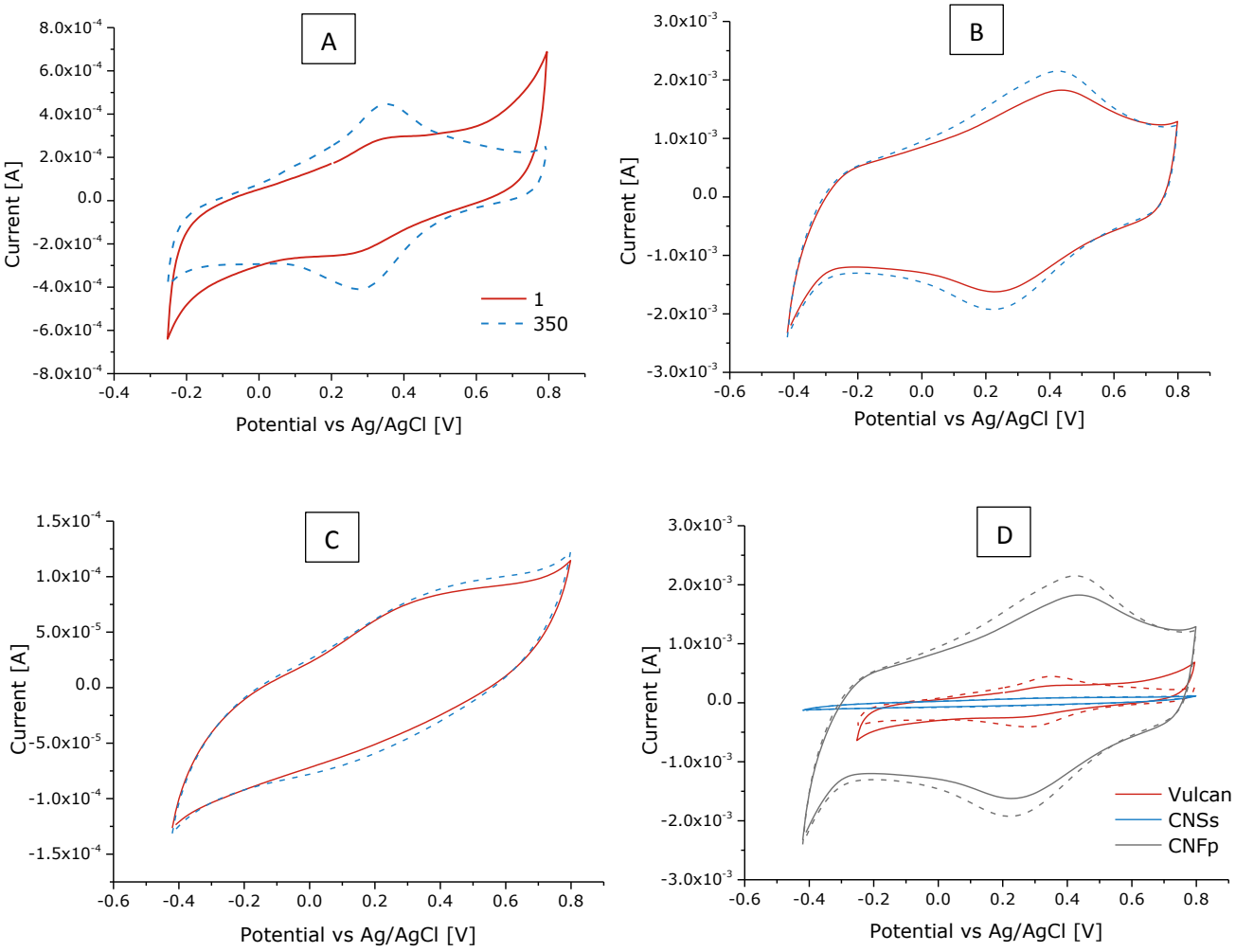

Figure 5.9. Cyclic voltammetries obtained for different electrodes tested. A) Vulcan XC72; B)CNFp; C) CNS; and D) comparative of cycles aspect of the different materials tested (same y-axis).

The initial cycle of the MPL prepared with the commercial Vulcan carbon black, shows high oxidation currents at high potential value, approximately 0.80 V (vs RHE). This increased current may be associated to easy-to-oxidize impurities [30], and also, to the presence of oxygen, which means that nitrogen did not removed it completely when the test started.

In addition, these voltammetric current peaks may also be attributed to oxidation caused by defects on the particle surfaces [31]. The oxidation of carbon surface of carbon blacks in hot phosphoric acid has been reported at potentials nearing 0.60 V (vs RHE) [32]. Although, this observation was made for a Pt catalyst on Vulcan XC72 (not the case in our study). Thus, the formation of a surface oxide and the oxidation of carbon may be illustrated using the sequence of reactions shown in eqs. 5.1 and 5.2 [33].

$$C + H_2O \rightarrow CO_{surf} + 2H^+ + 2e^- \qquad [5.1]$$

$$CO_{surf} + H_2O \rightarrow CO_2 + 2H^+ + 2e^- \qquad [5.2]$$

In the absence of Pt, as in our study, the further oxidation of CO_{surf} to carbon dioxide should have a very slow kinetic rate, potentially explaining the lack of CO_2 bubbles on the surface of the electrode during the CV tests.

The voltammograms of the two carbon nanostructures are similar to one another and differ from that obtained for the Vulcan XC72. In this case, the hydroquinone-quinone (HQ-Q) peak at 0.40 V approx. (vs AG/AgCl) observed in the anodic CV curve is indicative of surface oxidation. It is easy to see how surface charge density increases with the number of cycles, due to the surface reaction of the electrodes prepared with both carbon nanostructures. This change may be calculated by subtracting the pseudocapacitance charge from the total charge in the HQ-Q region [30, 34] and integrating the area under the peak. According to various authors, [35-37] the calculated charge is assumed to be a faradaic charge generated from the one electron HQ-Q redox reaction (eq. 5.3).

$$>C=O + e^- + H^+ \leftrightarrow C–OH \qquad [5.3]$$

Thus, in the MPL with CNF_P, the first cycle had area of 1.277 mC, and in the 350th cycle, the area increased by 16.5 % (1.488 mC). Therefore, it is clear that the carbon nanofibers with a platelet structure, suffer from higher electrochemical degradation. The greater edge plane exposure and number of defected sites of the CNFp could be responsible for the higher degradation, because the corrosion of carbon materials begins at these edge planes. The MPL prepared with CNS does not show significant changes in voltammograms during the 350 cycles, indicating a good electrochemical stability under those operating conditions.

All of the carbonaceous electrodes were analyzed by XRD after the electrochemical degradation tests and results obtained are also presented in Table 5.2 (together with those of the raw materials and those of the materials after the thermal degradation tests, for comparison purposes). As expected, the surface of the MPL prepared with carbon nanospheres did not change based on the parameters calculated from XRD analyses. However, CNFp shows large increases in Lc_a crystallite size (15.57%) and the MPL prepared with the commercial carbon black, Vulcan XC72 had the largest increase in the parameter Lc_a,, indicative of a large change on the surface tested. All these comments were confirmed by SEM analyses. Figure 5.10 shows images of the MPL surfaces after the CV tests in acid media.

Large cracks may be seen on the surfaces of the MPL prepared with Vulcan XC72 and on the surface of the MPL prepared with the carbon nanofibers, whereas no appreciable changes were evident on the surface of the CNSs based MPL, being these observations in agreement to the variation of the crystallite parameters calculated from the XRD analyses.

The low electrochemical degradation showed by the CNSs may be explained by their low BET surface (shown in Table 5.1), and their spherical shape, free of edges or having lower edge plane exposure, leading to a lower number of defected sites that may result in carbon corrosion. This makes it hard for the acid media to attack the carbon surface.

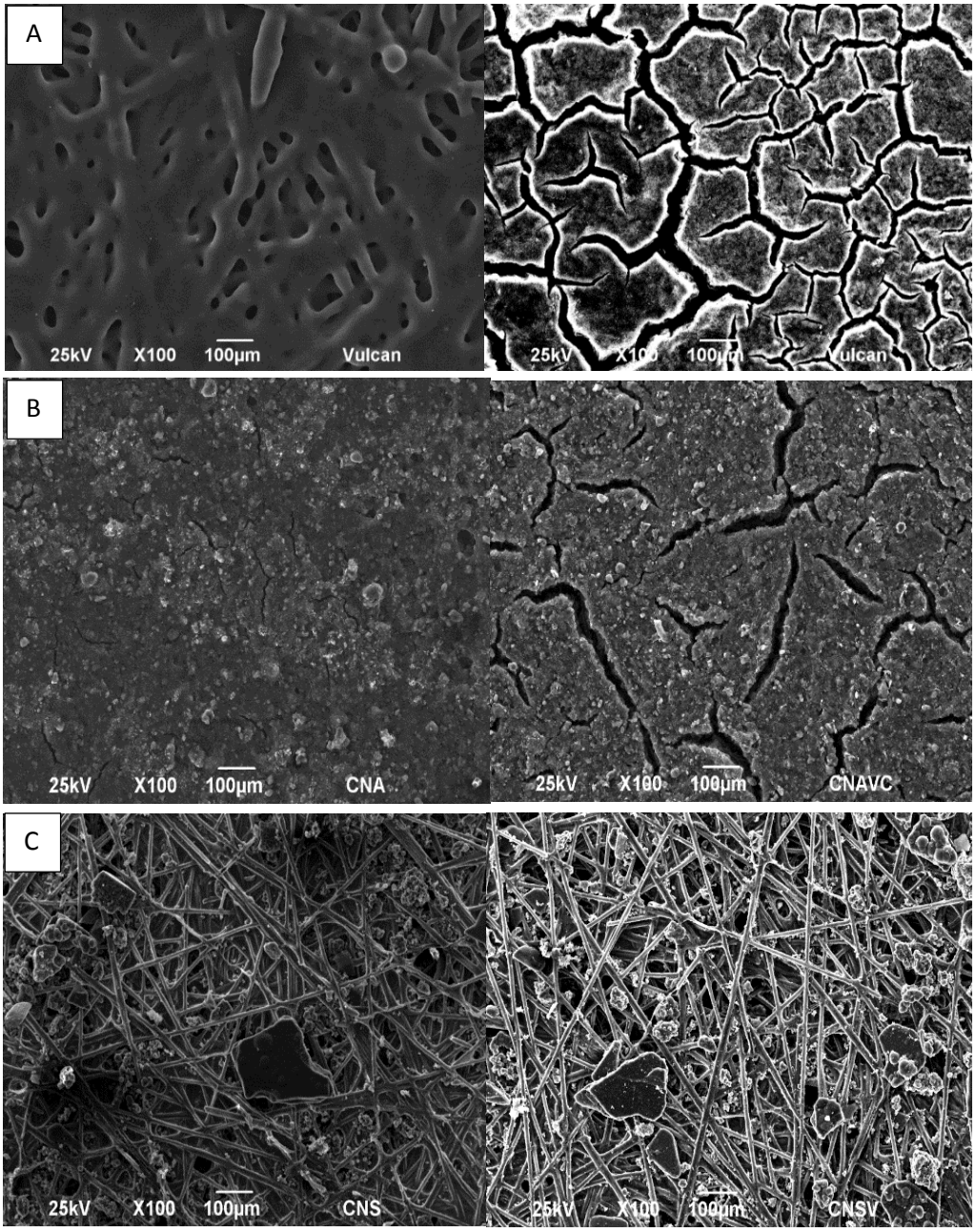

Figure 5.10. SEM micrographs performed to the different electrodes before (left) and after (right) the voltammetric study.

Another possible explanation may be the greater degree of graphitization (high ratio between the L_C and d_{002} parameters), meaning that CNSs are more stable than other materials [14, 18]. In other words, materials with higher values of BET surface (Vulcan Carbon and CNFp) may suffer from higher degradation than materials having lower BET values (CNSs) and they are not as appealing for the microporous layer as they would be if they were used as catalyst support. Therefore, BET value may directly influence on the chemical resistance of

the carbon materials, due to the larger area exposed to the acid media. It should be noted that the low BET value of the MPL with CNSs does not decrease the gas permeability of this layer, which could be easily understood by observing the distribution of the spheres shown in SEM micrographs. Furthermore, the excellent graphitic character of CNSs [14, 18] makes this material more resistant to the corrosion. This may not only explain the high resistance to the electrochemical corrosion in acid media but also the high heat resistance of the MPLs prepared with CNSs.

5.4. HT-PEMFC performance

In order to evaluate the performance of the nanomaterials based MPLs in a HT-PEMFC environment, short lifetests of approximately 100 hours in a single cell were carried out. Figure 5.11 shows the changes in the cell voltage observed during the lifetests of the MEA prepared with the MPL with the different carbonaceous materials. Throughout the lifetest, three characterization tests were carried out (as detailed in the Section 5.2) and their effect is clearly observed in the plot with the discontinuities in the value of the cell voltage, that rapidly settle down to the expected cell voltage value.

In the case of the CNS based MEA, the initial voltage was 0.48 V and it increases continuously during the break-in period until a value close to 0.59 V. After this initial stage, the performance improves over the first 45 hours with an activation of 113 $\mu V\ h^{-1}$ but then, after this first stage, degradation becomes more significant and at the end of experiment, the total degradation rate of the fuel cell was around 13 $\mu V\ h^{-1}$ (taking into account just the degradation in steady state). In comparing this value with other results previously shown in the literature, it can be noticed that the CNSs based MPL is improving the stability of the HT-PEMFC with values much better than other reported in similar tests with Vulcan carbon MPL. Thus, for PBI-based membranes, degradation rates measured in previous studies were 250 $\mu V\ h^{-1}$ [38] and 194.2 $\mu V\ h^{-1}$ [39].

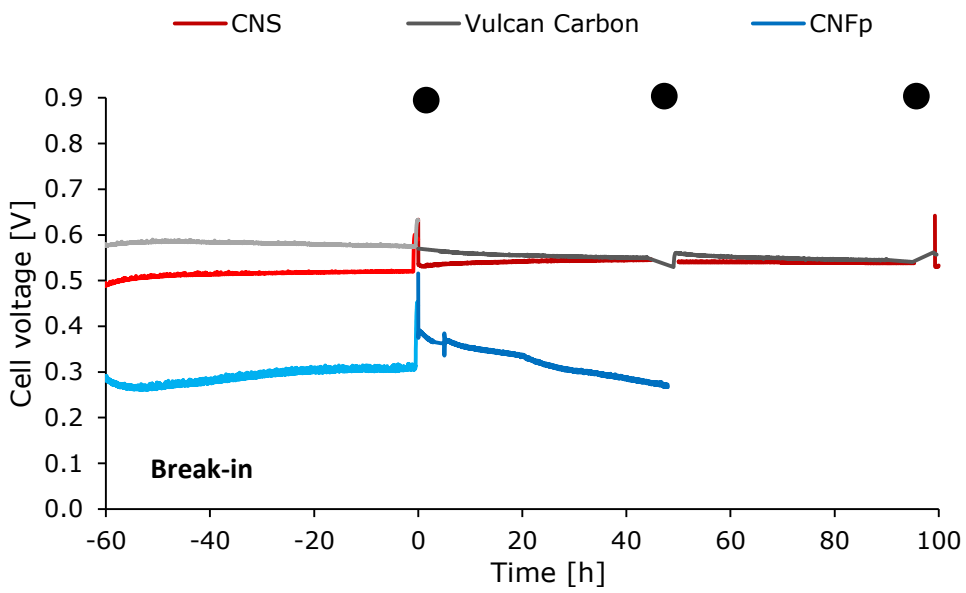

Figure 5.11. Short Lifetest performed to MEAs with different MPL raw materials. Black dots indicate the different characterization tests performed.

The low degradation rate noticed for the CNS based MEA could be explained by the high electrochemical and thermal stability exhibited by carbon nanospheres in the ex-situ characterization, which could be related, as it was pointed out before, to the low BET surface area and high graphitic character shown by CNS, which make harder the physicochemical deterioration of this material.

The standard MEA (made of Vulcan carbon) shows a break-in voltage around 0.58 V, starting the steady state at 0.57 V and, at the end of the preliminary lifetest, the voltage drop measured was 293 $\mu V\ h^{-1}$, much higher than CNS based MEA.

The MEA manufactured with the CNFp based MPL shows a very low voltage during the break-in process, and after the first test, the performance decreased faster. For this reason, the lifetest was turned off just after the second protocol test, only after 48 hours of operation. This experiment was repeated to confirm the bad results, resulting in the turn-off the cell after 10 hours, due to the high voltage drop suffered during the break-in protocol, which clearly indicates that carbon nanofibers present problems to be used as MPL. This fact could be

related to the compact surface observed in the SEM micrographs shown in Figure 5.5, and also the very low gas permeability coefficients obtained during the ex-situ characterization, which could prevent the correct diffusion of the gases throught the MEA, resulting in the fast degradation of the components when a current density is applied, associated to the high mass transfer limitation problems.

In order to know more about the electrochemical characteristics of the different MEAs, several polarization curves were performed in the HT-PEMFC at different times fed with air and pure oxygen and they are shown in Figures 5.12 and 5.13, respectively.

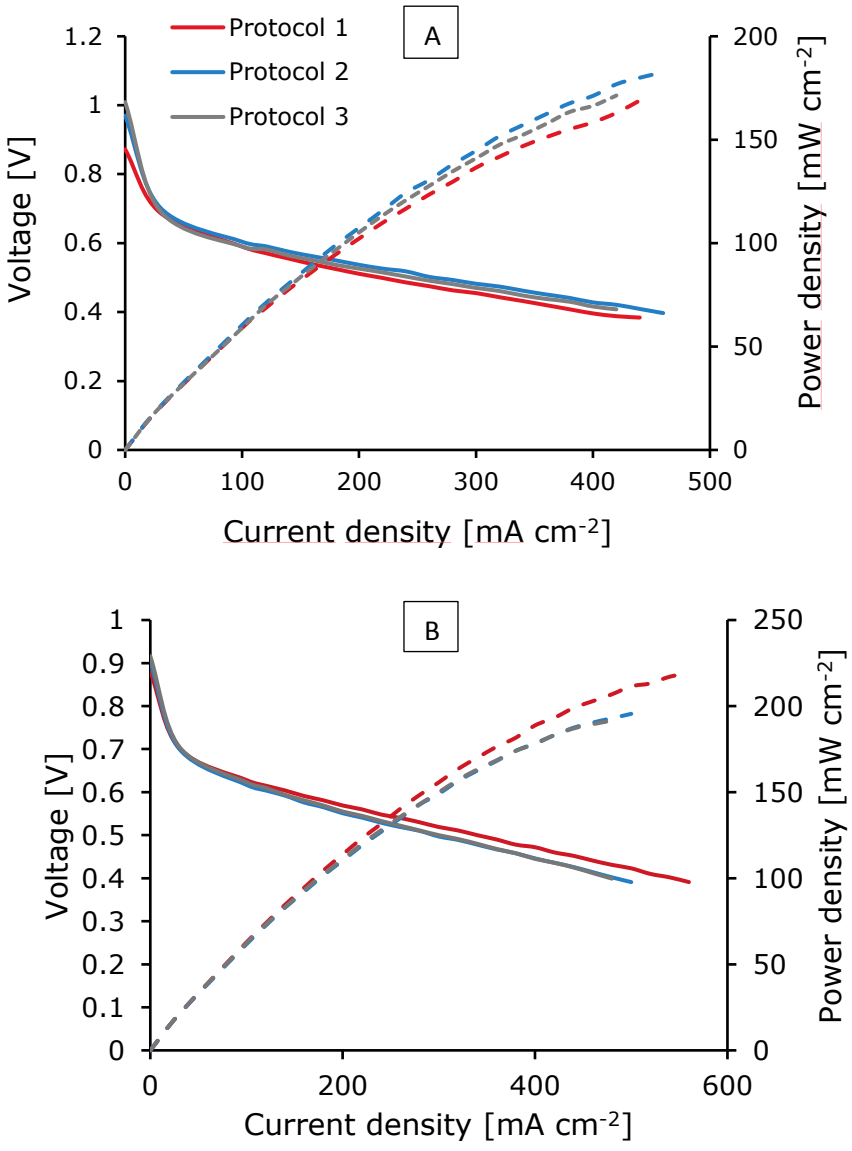

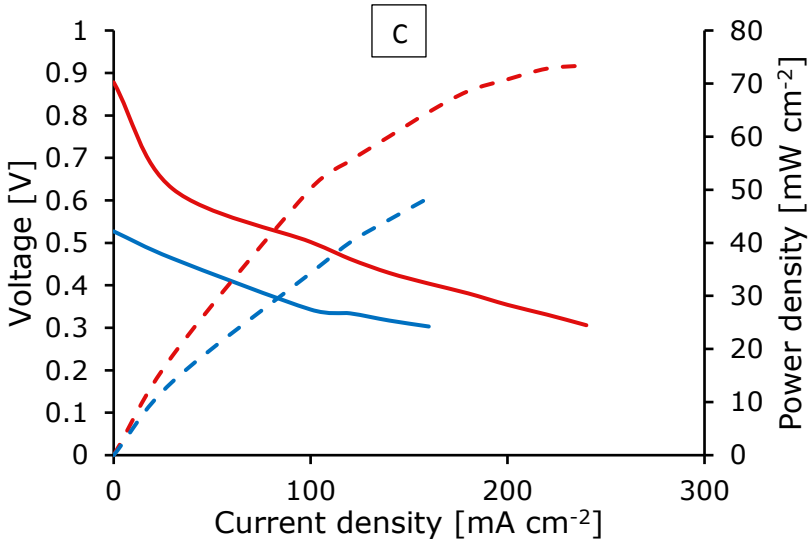

Figure 5.12. Polarization curves performed with Air and Hydrogen for each MEA tested. A) CNS; B) Vulcan Carbon; and C) CNFp

The maximum power density reached by CNS based MEA is about 180 mW cm^{-2} when was fed with air, and 380 mW cm^{-2} using oxygen as oxidant, respectively, which means that the system undegoes an important gain working with pure oxygen, as it was expected taking into a count that the stoichiometric coefficient applied in the case of O_2 is 9.5, feeding the system with a much higher flow respect to the theoretical. These values are slightly lower than values obtained by our research group (219 and 400 mW cm^{-2}) [39] using a standard Vulcan carbon support, which are closely similar to values achieved by the standard MEA tested.

On one hand, CNFp, as it was expected, exhibits a low performance and a high decrease between polarization curve 1 and 2. On the other hand, power density values obtained for CNS based MEA are similar than others reported recently in the literature in which new nanocarbonaceous materials have been tested. Thus, Duan [40] reported power densities around 250 mW cm^{-2} operating with air, at 70 °C using a CNF sheet based MPL into a 5 cm^2 fuel cell system. Hunsom [41] reported values around 350 mW cm^{-2} operating at 60 °C using Hicon carbon black as MPL into a 5 cm^2 fuel cell fed with pure oxygen. No

information about the usage of new nanocarbonaceous materials in HT-PEMFC systems has been found.

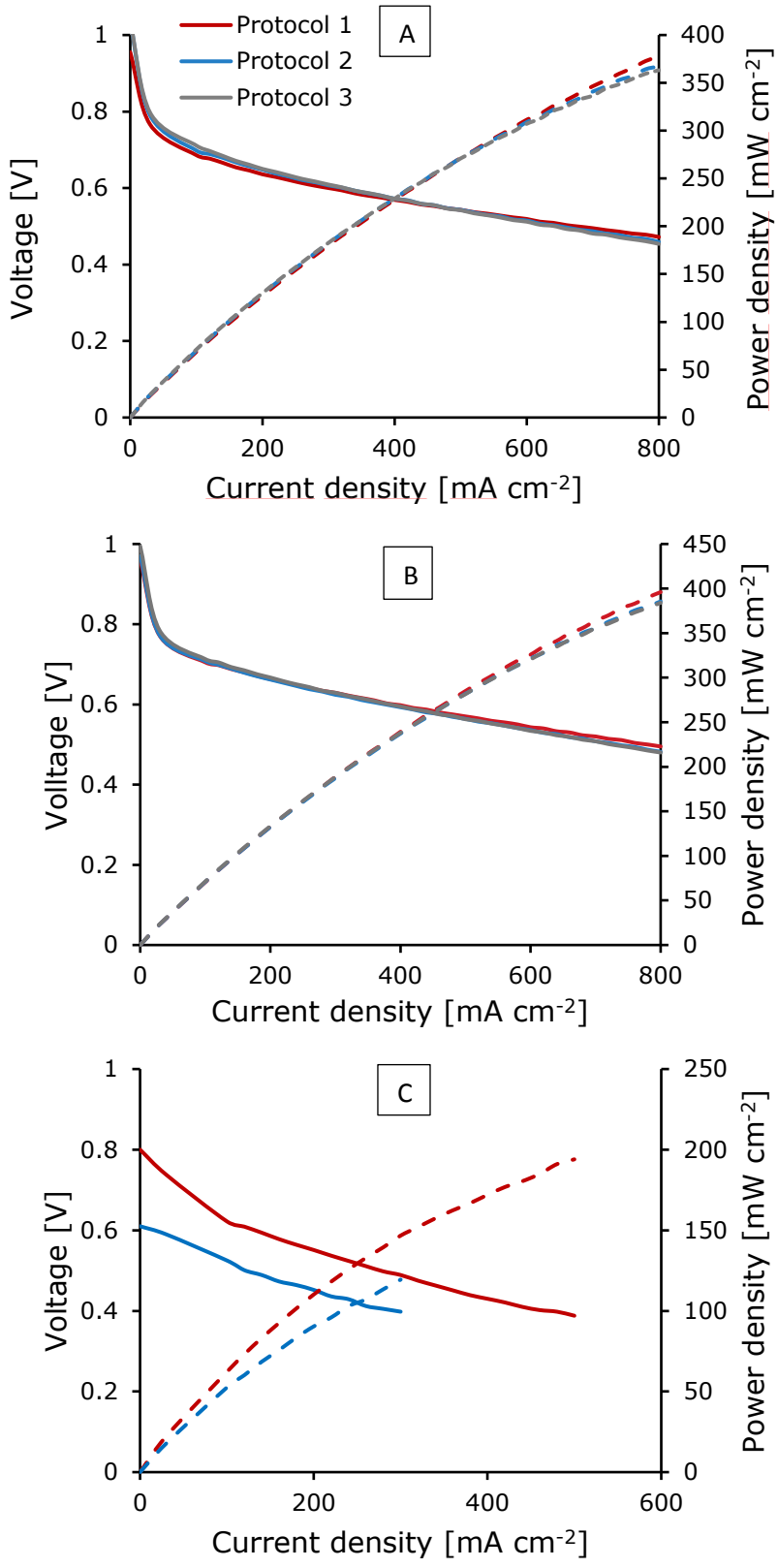

Figure 5.13. Evolution of polarization curves performed during the life test with Hydrogen and Oxygen for each MEA tested. A) CNS; B) Vulcan Carbon; and C) CNFp.

During the lifetests, the power density decreased slightly, 13% with air and 8% with oxygen (thus, being the degradation higher with air). Moreover, during the lifetest the MEA showed very good open-circuit voltage values (at 0.0 A cm^{-2}), indicating that no short circuits, electrical losses or damages in the membrane occurred.

As it was pointed out above, during the lifetest, impedance analyses were carried out at different operation times. As an example, Figure 5.14 shows the Nyquist plots of the MEA with CNS based electrodes.

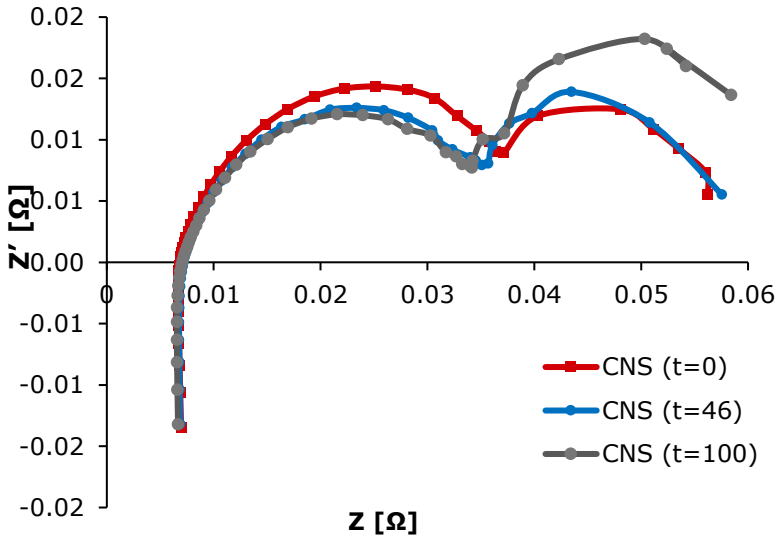

Figure 5.14. EIS evolution for CNS based MEA during the preliminary life test.

In order to know the resistance values originated in the fuel cell, an equivalent circuit R (RQ) (RQ) was used to simulate the impedance data in this work [41, 42, 43]. The parameters obtained by matematical fitting of experimental results are shown in Table 5.5.

No great changes can be observed in the values of the parameters calculated at the different times for which the impedance analysis were carried out, for any of the two MEA tested (with CNS or Vulcan Carbon). In the case of the MEA containing CNFp, the rapid deterioration avoided obtaining relevant transient information.

With respect to parameters obtained operating with air, the high frequency resistance is typically explained in terms of the sum of the ohmic resistances of the membrane electrolyte and the electric resistance of the electrode (GDL + MPL, mainly).

Table 5.5. Evolution of the internal resistance parameters obtained from the fitting of the EIS data performed at 0.2 A cm^{-2} to equivalent circuit R (RQ) (RQ)

		Air			Oxygen		
MPL	Time (h)	Rohm	Rct	Rmt	Rohm	Rct	Rmt
		mΩ cm^2	mΩ cm^2	mΩ cm^2	mΩ cm^2	mΩ cm^2	mΩ cm^2
CNS	0	173.8	800.0	561.3	175.5	575.5	0
	46	185.0	632.8	620.5	174.8	653.8	0
	100	182.0	735.5	606.3	177.0	722.8	0
Vulcan XC-72	0	184.0	402.3	867.5	182.0	446.5	0
	46	194.0	488.3	707.0	198.3	465.0	0
	100	203.5	514.8	576.0	199.8	458.5	0
CNFp	0	156.0	1722.5	0	137.3	505.0	0
	46	-	-	0	144.0	596.3	0
	100	-	-	-	-	-	-

It can be observed that this high frequency resistance is very similar between CNSs based MEA and Vulcan XC72 based MEA, with a value around 0.2 Ω cm^2. Anyhow, the ohmic resistance of the CNSs based one is slightly lower than that of Vulcan XC-72. In the case of CNFp based MEA, due to the higher electrical conductivity shown by this material during the ex-situ characterization, it can be observed that ohmnic resistance is lower as compared with the other MEAs containing the other two carbonaceous materials.

Furthermore, the semicircle observed in the Nyquist plot may be explained in terms of the charge transfer resistance (R_{CT}) or by oxygen reduction reaction (ORR) activation in

the cathode catalyst layer. The electrodes prepared with the CNS based MPL show a higher R_{CT} as compared to the Vulcan supported MPL (0.7 Ω cm^{-2} vs 0.5 Ω cm^{-2} for the standard one). These values are higher and they could explain the lower performance achieved by the MEA prepared with the CNSs. Thus, it has to be accounted that the novel CNSs based electrodes are not optimized in terms of the overall composition, particle size, ratio ionomer/CNSs, amount of phosphoric acid, etc. CNFp achieved an intermediate value between the other two MEAs.

At low frequency, another arc could appears on the EIS that may be related to the mass transport limitations. From that arc it can be pointed out that the mass transfer resistances in the case of the CNS based electrodes are lower than Vulcan XC-72 based electrodes. Mass transfer resistance was not noticed in the case of CNFp based MEA.

Next parameter evaluated during the characterization tests was the active area of the catalyst, through cyclic voltammetry characterization. Table 5.6 shows the ECSA values obtained at different times of the essay. At the beginning, a value of 17.2 m^2 g^{-1} is obtained for the CNS based MEA. In comparing this value with other shown in the literature, it can be observed that it is similar to the ECSA calculated by Modestov (above 19.4 m^2 g^{-1}) [44].

Table 5.6. ECSA evolution during the lifetests carried out for each MEA tested

Sample MPL	1st Protocol ECSA [m^2 g^{-1}]	2nd Protocol ECSA [m^2 g^{-1}]	3th Protocol ECSA [m^2 g^{-1}]	ECSA degradation [%]
CNS	17.22	15.96	15.18	**11.85**
Vulcan XC72	27.88	22.87	22.58	**19.01**
CNFp	10.6	-	-	-

However, there is a slight decrease throughout the test obtaining a non-negligible percentage of degradation of 11.8 %, as it has been stated previously. This value, is lower than the one (19.0%) obtained by the electrode prepared with the standard MPL (Vulcan

carbon), which means that the CNS based MPL contributed to a better stabilization of the catalyst layer. Figure 5.15 shows the voltammograms obtained during the different tests.

It can be observed that CNFp based MEA shows a strange change in the shape of the cycle obtained during the second protocol. This fact confirms the membrane damaging, with the subsequent crossover, which also explain the fast decreasing of the voltage during the lifetest. Nevertheless, the first voltammogram confirms that at the start of the experiment, the membrane did not present damages, and the catalytic activity was acceptable, which confirms that the MPL was the responsible of the lower performance achieved during the break-in period.

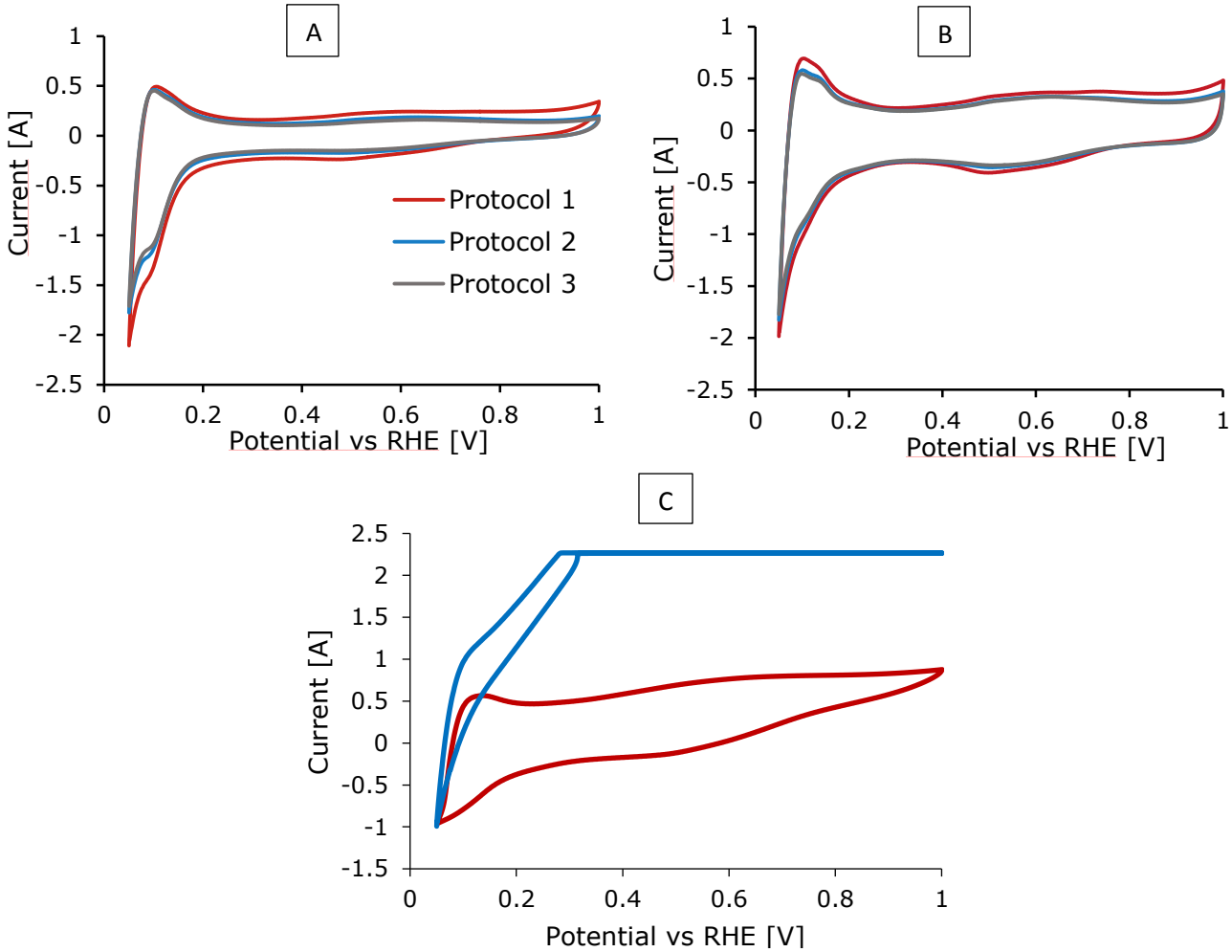

Figure 5.15. Cyclic voltammetries obtained for each MEA during the protocol tests. A) CNS; B) Vulcan XC72; and C) CNFp

The crossover in the case of the CNFp based MEA was confirmed by the parameters calculated from LSV, shown in Figure 5.16. It can be observed that in the case of the CNFp

based MEA, the crossover values are much higher at the second test performed, which is in agreement with the decreasing of the internal resistance of the system. Respect to the CNS and Vulcan XC72 based MEAs, both exhibit similar crossover, around 0.4 and 0.3 mA cm^{-2} respectively, which means, in accordance to the high internal resistance of the system, that the PBI membranes of these MEAs exhibit no signs of damaging in both cases. Furthermore, both parameters were still around the same values during all experiment, which means that not severe changes nor degradation of the materials appeared during the tests.

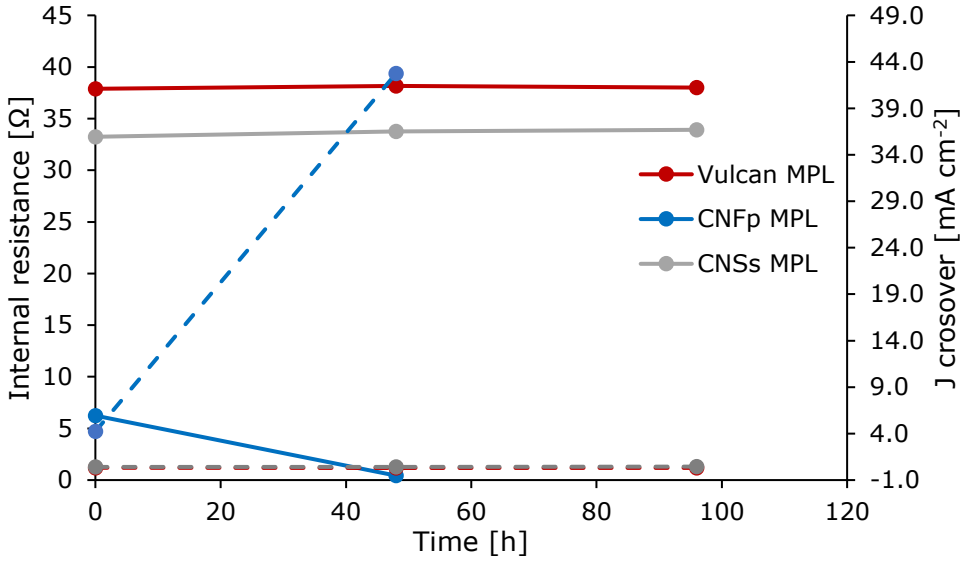

Figure 5.16. Crossover and internal resistance evolution of the different MEAs tested. Continuous lines represent the evolution of the internal resistance; discontinuous lines represent the evolution of the crossover values, both parameters calculated at V = 0.3 V.

Respect to the lower ECSA (compared with the standard Vulcan XC72 based MEA) values achieved by the CNS based MEA (that was pointed out in Table 5.6), it should be taken into account that the CNSs particles are higher than Vulcan ones. Then, some of the catalyst particles, (much smaller than CNSs) could be deposited between the space of the CNSs during the deposition of the catalyst layer onto the MPL and they would not be available for the electrochemical reaction because those catalyst particles would not be in contact with the PBI membrane (electrolyte). This could contribute to achieve high values of R_{CT} and low values of ECSA. Nevertheless, the fact that the CNSs have a bigger particle size than the Vulcan ones, could originate a less compact and a more porous structure and the access of the gases to the active sites of the catalyst layer would be favoured and hence, the

mass transport resistance would be lower in the case of the MPL with CNSs. These effects are more noticeable when air is used as it can be observed in Table 5.4, because the oxygen concentration is lower. To clarify this explanation, Figure 5.17 shows a scheme of the structure of the MPL formed by the CNSs, where some catalyst particles (Pt/C) are deposited between the CNSs are observed. As illustrated, they would not be available for the electrochemical reaction and this fact could explain the lower values of ECSA and higher values of R_{CT} obtained by the electrodes prepared with the MPL with CNSs [45].

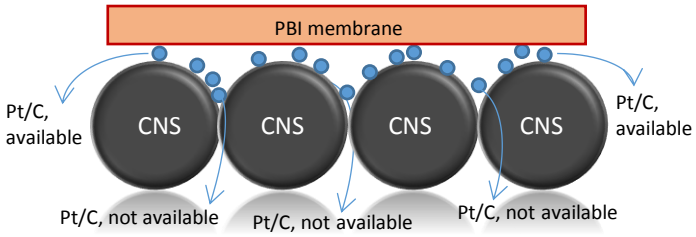

Figure 5.17. Scheme of the structure of the MPL prepared with CNS, where some Pt particles are deposited in the deep space between CNS particles and do not participate in the electrochemical reaction

5.4 Conclusions

According to the results achieved in this Chapter, the following main conclusions can be drawn:

- Nanocarbonaceous materials can be successfully used in the MPL of HT-PEMFC, as substitutes of the widely used Vulcan Carbon.
- Carbon nanospheres exhibit very good electrochemical and thermal stability when they were ex-situ characterized, probably related to their low BET surface area caused by the spherical shape and high graphitic character.
- Carbon nanofibers present high electrical conductivity, much better than those obtained by CNS and Vulcan Carbon.

- CNS based MEA shows a very good stability in the preliminary short lifetest, with voltage drops after 100 hours of only 13 $\mu V\ h^{-1}$, much lower that the voltage drop achieved from a standard MEA with Vulcan based MPL.
- Carbon nanofibers presents several problems for being used in the MPL in HT-PEMFC, associated to their compact surface, which prevents the correct diffusion of the reactive gases and results in a very low performance.

5.5. Bibliography

[1] A. Minjeh, C. Yong-Hun, C.Yoon-Hwan, K. Jinho, J. Namgee, S. Yung-Eun, Electrochimica Acta 56 (2011) 2450.

[2] J. Lobato, P. Cañizares, M. A. Rodrigo, D. Úbeda, F. J. Pinar, J. J. Linares, Fuel Cells 10 (2010) 770.

[3] A. Chandan, M. Hattenberger, A. El-kharouf, D. Shangfeng, A. Dhir, V. Self, B.G. Poller, A. Ingram, W. Bujalski, Journal of Power Sources 231 (2013) 264.

[4] Q. Li, D. Aili, H. A. Hjuler, J.O. Jensen, High temperature Polymer Electrolyte Membrane Fuel Cells (Chapter 14), Springer, 2016, ISBN 978-3-319-17081-7

[5] P. Sehkyu, L. Jong-Won, B. N. Popov, Journal of Power Sources 16 (2006) 357.

[6] L.R. Jordan, A.K. Shukla, T. Behrsing, N.R. Avery, B.C. Muddle, M. Forsyth, J. Appl. Electrochem. 30 (1999) 641.

[7] E. Passalacqua, G. Squadrito, F. Lufrano, A. Patti, L. Giorgi, J. Appl. Electrochem. 31 (2001) 449.

[8] Y.Park, K. Kakinuma, M. Uchida, H. Uchida, M. Watanabe, Electrochimica Acta 123 (2014) 84.

[9] A. Witkowska, G. Greco, S. Dsoke, R. Marassi, A. Di Cicco, Journal of Non-Crystalline Solids 401 (2014) 169.

[10] B. Avasarala, R. Moore, P. Haldar, Electrochimica Acta 55 (2010) 4765.

[11] N. Linse, G. G. Scherer, A. Wokaun, L. Gubler, Journal of Power Sources 219 (2012) 240.

[12] J. Park, S. Yima, T. Kima, S. Parka, Y. Yoona, G.Park, T. Yanga, E. Park, Electrochimica Acta 83 (2012) 294.

[13] N.M. Rodriguez, Journal of Materials Research 8 (1993) 3233.

[14] A.Nieto-Márquez, R. Romero, A. Romero, J. L. Valverde, J. Mater. Chem. 21 (2011) 1664.

[15] D.A Stevens, M.T Hicks, G.M Haugen, J.R Dahn, Journal of the Electrochemical Society, 152, Issue 12 (2005) A2309.

[16] D. Sebastian del Río, Degree Thesis, ISSN: 2254-7606, Zaragoza (Spain), April 2011.

[17] V. Jiménez, A. Nieto-Márquez, J. A. Díaz, R. Romero, P. Sánchez, J.L. Valverde, and A. Romero, Ind. Eng. Chem. Res. 48 (2009) 8407.

[18] A. Nieto-Márquez, I. Espartero, J. Lazo, A. Romero, J.L. Valverde, Chemical Engineering Journal 153 (2009) 211.

[19] D. Singha, I. I. Soykal , J. Tiana, D. von Deaka, J. Kinga, J. T. Miller, U. S. Ozkan, Journal of Catalysis 304 (2013) 100.

[20] V. Gómez-Serrano a,), C.M. González-García, M.L. González-Martín, Powder Technology 116 (2001) 103.

[21] H. Gharibi, M. Javaheri, R. Abdullah Mirzaie, International Journal of Hydrogen Energy 35 (2010) 9241.

[22] S.K. Kamarudina, N. Hashima, Renewable and Sustainable Energy Reviews 16 (2012) 2494.

[23] F. N. Büchi. M. Inaba, T. J. Schmidt, Polymer electrolyte fuel cell durability, ISBN 978-0-387-85534-9, 2009.

[24] J.J. Linares, Degree Thesis, University of Castilla – La Mancha, January, 2010.

[25] J. Lobato, P. Cañizares, M.A. Rodrigo, C. Ruiz-López, J.J. Linares, J. Appl. Electrochem. 38 (2008) 793.

[26] G. Park, Y.Sohna, S.Yima, T.Yanga, Y. Yoona, W. Leea, K. Eguchib, C. Kima, Journal of Power Sources 163 (2006) 113.

[27] M. Çelik, G. Özışık, G. Genç, and H. Yapici. J Appl Mech Eng 3:1 (2014) open access journal.

[28] A.Z. Weber and J. Newman, J. Electrochem. Soc. 152 (2005) A677.

[29] D. Sebastián, A.G. Ruiz, I. Suelves, R. Moliner, M.J. Lázaro, J. Mater. Sci. 48 (2013) 1423.

[30] K.H. Kangasniemi, D.A. Condit, T.D. Jarvi, J. Electrochem. Soc. 151 (2004) E125.

[31] B. Avasarala, R. Moore, P. Haldar, Electrochimica Acta 55 (2010) 4765.

[32] T. Maoka, Electrochimica Acta 33 (1988) 379.

[33] E. Passalacqua, P.L. Antonucci, M. Vivaldi, A. Patti, V. Antonucci, N. Giordano, K. Kinoshita, Electrochimica Acta 37 (1997) 2725.

[34] M.F. Mathias, R. Makharia, H.A. Gasteiger, J.J. Conley, T.J. Fuller, C.J. Gittleman, S.S. Kocha, D.P. Miller, C.K. Mittelsteadt, T. Xie, S.G. Yan, P.T. Yu Electrochem. Soc. Interface, 14 (2005) 24.

[35] J.H. Chen, W.Z. Li, D.Z. Wang, S.X. Yang, J.G. Wen, Z.F., Ren, Carbon 40 (2002) 1193.

[36] J.S. Ye, X. Liu, H.F. Cui, W.D. Zhang, F.S. Sheu, T.M. Lim, Electrochem. Commun. 7 (2005) 249.

[37] P.N. Ross Jr, L. Lipkowski, P.N. Ross (Edds) Electrocatalysis, Wiley-VCH, New York (1998) 54.

[38] S. Yu, L. Xiao, B.C. Benicewicz, Fuel Cells 165 (2008) 3.

[39] J. Lobato, P. Cañizares, M.A. Rodrigo, D. Úbeda, F.J. Pinar, J. Power Sources 196 (2011) 8265.

[40] Q. Duan, B. Wanga, J. Wang, H. Wanga, Y. Lu, Journal of Power Sources 195 (2010) 8189.

[41] M. Hunsom, P.Piumsomboon, K. Pruksathorn, N. Tantavichet, S. Endoo, K. Charutavai, K. Poochinda, Renewable Energy 36 (2011) 369.

[42] J. Zhang, Y. Tang, C. Song, J. Zhang, J. Power Sources 172 (2007) 163.

[43] X. Yuan, H. Wang, J.C. Sun, J. Zhang, Int. J. Hydrog. Energy 32 (2007) 4365.

[44] A.D. Modestov, M.R. Tarasevich, V.Y. Filimonov, N.M. Zagudaeva, Electrochim. Acta 54 (2009) 7121.

[45] H. Zamora, J. Plaza, J. Lobato, M.A Rodrigo, ChemSusChem 9 (2016) 1187.

CHAPTER 6. Evaluation of carbonaceous materials as catalyst support for HT-PEMFC

6.1 Introduction and Objectives

Once studied the influence of the use of nanocarbonaceous materials in the Micro Porous Layer (MPL) of HT-PEMFCs, it is necessary to face how these materials can affect to the performance of the electrocatalyst, the other critical component of the electrode. At this point, it is important to take in mind that nowadays, the main challenge of HT-PEMFC is to get high performance and durability with low-cost catalysts and this fact is becoming a bottleneck for the technology, because of the high price of platinum, which, unfortunately, is the key and almost the only catalyst available today for HT-PEMFC. Evaluation of non-precious metal-based materials as catalyst is a hot topic of research nowadays, but the performance of these materials in this moment is so bad as compared with precious materials such as Pt or Pd at the operational temperature ranges of PEMFCs [1] and, hence, they are not a real alternative now.

Just on the contrary, the most interesting topic of research deals with the reduction of the platinum content in the electrocatalyst. At this point, two main ways are usually studied to reduce the platinum content and, hence, to optimize the electrocatalyst. The first way consists of increasing the platinum utilization in the catalyst layers, improving the bounding and active area of the metal particles by improving the synthesis method or the catalyst support, allowing the use of lower Pt amounts in the MEA manufacturing. The other way consists of reducing the platinum load by alloying Pt with inexpensive metals such as Co, Fe, etc. In supported electrocatalysts, platinum is typically dispersed into carbonaceous materials, being the preparation of this mixture carbon-platinum very important because it may affect the performance of the whole HT-PEMFC. Surface area, porosity, electrical conductivity, electrochemical stability and surface functional groups are the key characteristics to be optimized in order to get a good electrocatalyst support [2]. In addition, it is very important to manage a significant problem associated to the conventional used carbon support materials and that was also faced for the MPL in the previous Chapter: the several corrosion processes

under typical operation conditions suffer by the raw materials of the MPL and catalyst support in both electrodes in the HT-PEMFCs, being more significant those happening on the cathode. This corrosion is caused by the hot acidic conditions provided by the PBI membrane doped with phosphoric acid (PA), and the high voltages achieved by the MEA during the start-on and shut-down operations [2-6].

Thus, this Chapter is going to be focused on the replacement of the standard carbon black material used as catalyst support by new nanocarbonaceous materials, which exhibit the same good properties of the carbon blacks but show a lower corrosion effect. It is looked for better stability and durability at the operational conditions required by this type of fuel cells. An interesting overview about different materials and the state of the art of the technology studied to be used as catalyst support can be found elsewhere [2, 7-9]. This information, together with the information obtained in Chapter 5 about the use of carbon nanofibers and carbon nanospheres is the base of the research carried out here. Hence, in this Chapter, two nanocarbonaceous materials (Carbon nanofibers platelet (CNFp) and Carbon nanospheres (CNS)) have been tested as catalyst supports for the cathode of HT-PEMFC, operating with phosphoric acid doped PBI membranes. It is aimed to evaluate if they can substitute the commonly used Vulcan Carbon XC72 as catalyst support, by keeping the same good operation properties of the electrodes made with this product but, at the same time, enhancing the stability and durability of the fuel cells.

6.2. Methodology

6.2.1. Catalyst synthesis

The catalyst synthesis method consists of the deposition of platinum from a precursor salt (chloroplatinic acid hexa-hydrate, Sigma-Aldrich). To prepare a batch of 1.0 g of catalyst, 600 mg of support (CNFp, CNS or the Vulcan Carbon used as the reference) were added to a 500 mL of 0.1 M formic acid solution (98 %, Panreac) keeping temperature at 80 °C during

this operation. Then, 21.2 mL of a 50 mg ml^{-1} chloroplatinic acid hexa-hydrate solution was added very slowly, and the mixture was kept under agitation at 80 °C for one hour. Then, the suspension was left to cool at room temperature and the solid filtered and dried. After the drying process, the catalyst powders were weighted and characterized. The target concentrations of platinum in the catalyst was 40% wt., in order to achieve comparable results with the commercial carbonaceous catalyst used also as reference material (40% wt. Pt/Vulcan carbon).

6.2.2 Physicochemical characterization

Inductively coupled plasma mass spectrometry (ICP-MS) was carried out to obtain the real Pt content deposited on the catalysts. In order to evaluate the crystallite properties of the Pt particles of different catalysts, X-Ray Diffraction (XRD) analyses were performed on a Philips PW-1700 diffractometer with rotating anode, applying Kα corresponding to the transition from copper radiation for different samples. Transmission Electron Microscopy (TEM) was used to get more information about the dispersion of the Pt particles through the catalyst support. TEM analyses were carried out on a Jeol JEM 2100 TEM operating at 200 kV with an Orius (2x2 MPi) Gatan Digital Camera. Specimens were prepared by dispersing the samples in acetone and depositing a drop onto a C-coated Cu grid. TEM images were analyzed using Digital Micrograph software from Gatan. Temperature Programmed Reduction (TPR) was used to evaluate the presence of Platinum oxides, which indicates the efficiency of the synthesis method in terms of metal reduction of the Pt precursor. More details about this characterization can be found in Chapter 4.

6.2.3 Electrochemical characterization

A voltammetric study was carried out in a half-cell system, using different electrodes manufactured with the target catalysts. The electrodes consisted of commercial carbon cloth

with a deposited Micro Porous Layer (Freudenberg Vliesstoffe, H23C2) and a catalyst layer deposited onto it made with the catalyst to be tested. The voltammetric tests consisted of 400 cycles (-0.20 – +1.00 V vs. Ag/AgCl) at 50 mV s^{-1}, using a 2.0 M phosphoric acid solution as electrolyte at 50 °C, with a gold sheet as counter-electrode. Before each test, nitrogen was bubbled for 20 minutes in order to remove the O_2 of the electrolyte. Luggin capillary tube was used to connect reference electrode to the half-cell. More details about the set up can be found elsewhere [13]. After that, degradation of tested catalysts was studied by the evaluation of the Electrochemical Surface Area (ECSA). The technique for determining the ECSA of fuel cell electrodes by CV involves cycling over a voltage range where charge transfer reactions are adsorption-limited at the activation sites. ECSA values were obtained by the H_2 desorption peak area, by the equation 4.5 (described in Chapter 4) [14].

To evaluate the electrochemical behavior of the different produced catalysts, Oxygen Reduction Reaction (ORR) studies were performed on rotating disk electrode (RDE), using an AUTOLAB RDE with a 5 mm Glassy carbon (GC) electrode, and using a gold sheet as counter electrode. Catalyst inks were prepared with 1 mg of catalyst powder, solved in 0.75 mL of deionized water and 0.25 mL of isopropanol. The catalyst ink was sonicated for 10 min. To prepare the electrode, the GC head was polished for 5 min in Alumina surface, cleaned with deionized water and dried. Then, 10 µL of catalyst ink were placed on the GC surface, drying at room temperature for 30 min. at 500 rpm. After that, a second deposition was performed with the same procedure, depositing 8.8 µL of ink in this case.

The RDE studies consisted of:

- Cyclic voltammetries: 25 cycles from -0.25 to 1.20 V (vs Ag/AgCl reference electrode), with a scan rate of 200 mV s^{-1}, using 0.5 M H_2SO_4 solution as electrolyte, in order to polish the electrode before the ORR measurements. Before the measurements, N_2 was bubbled to remove the oxygen and 3 cycles were performed at 200, 150, 100 and 50 mV s^{-1}, to calculate the ECSA at different scan rates.

- Oxygen reduction reaction: linear sweep voltammetries were carried out from 0.90 to 0.05 mV (vs Ag/AgCl) at 5 mV s^{-1}, at 400, 900, 1200 and 1600 rpm, to analyze the activity of the different catalysts tested after bubbling O_2 during 30 min in order to saturate the electrolyte. Tafel slopes and number of electrons transferred were calculated according to the procedure and equations described in Chapter 4.

6.2.4. Preliminary Short lifetest performance

A catalyst layer was deposited by spraying the catalyst ink over the commercial electrodes (Freudenberg Vliesstoffe, H23C2). The catalyst ink for the cathode electrodes consisted of a 40% wt. Pt/X, being X the different nanocarbonaceous materials (or a commercial Pt/Vulcan carbon XC72 (Fuel Cell Store) used as reference material), PBI ionomer (1.5 wt. % PBI in DMAc, 1-20 PBI/support ratio), and DMAc as a dispersing agent. This Pt amount on the catalyst powder was fixed according to previous results obtained by our group in studies for the optimization of the catalyst layer of HT-PEMFCs [15] and it is in agreement with the ratios used in other works found in the literature [16]. For the anode, the commercial catalyst, Pt/C, was used. In all cases, the Pt loading on the two electrodes (anode and cathode) was 0.6 mg Pt cm^{-2}. After the deposition of the catalyst layer, the electrodes were dried at 190 °C for 2 h, with the purpose of removing traces of DMAc. The electrodes were then wetted with a solution of 10% PA. Electrodes were left to adsorb the acid for one day. For the preparation of the MEA, a thermally cured PBI membrane was doped in 85 wt. % PA for 5 days, in order to achieve good proton conductivity. The doping level acquired by the membrane was 9 molecules approx. of acid per polymer repeating unit. The corresponding thickness of the doped membrane was 83.2 μm. The superficial acid on the membrane was thoroughly wiped off with filter paper. In order to fabricate the MEA, the doped membrane was sandwiched between a couple of electrodes and the whole system was hot-pressed at 130 °C and 1 MPa for 15 min. The completed MEA was inserted into the cell between end

plates of graphite (with a five serpentine channels frame in each plate). The geometrical area of each electrode was 25 cm^2. MEAs were mounted and characterized in a commercially available Cell Compression Unit (CCU) provided by Baltic fuel cells GmbH (Germany). The break-in procedure consists of operation at 0.1 A cm^{-2} and $\lambda_{H2\ /\ air}$ excess stoichiometric coefficients of 1.5/2.0 for 48 hours. A preliminary stability test was conducted by increasing the current density to 0.2 A cm^{-2} (160 °C) and working at constant stoichiometric coefficients (λ_{H2} of 1.5 and λ_{air} of 2.0). For further characterization, a protocol test was carried out every 48 h since the final of the break-in procedure as reported elsewhere [12]. This protocol test (described in Chapter 4 and repeated here for the sake of clarity) consists of the following characterization techniques:

- Galvanostatic polarization curves. They were performed from the OCV to 0.40 V. First with air at constant $\lambda_{H2/air}$=1.5/2.0 and then with oxygen at constant $\lambda_{H2/O2}$ =1.5/9.5.
- Electrochemical impedance spectroscopy (EIS) tests. The EIS tests were performed at 0.1 A cm^{-2} with 10 mV AC perturbation amplitude and frequency range from 100 kHz to 100 MHz. This sequence of EIS tests was carried out with air as oxidant and, then, the same procedure was repeated with oxygen.
- Cyclic voltammetries (CV). The Electrochemical surface area (ECSA) of cathode was estimated with this technique. The cathode side was purged with nitrogen and hydrogen flowed through anode side with flowrates of 0.1/0.1 L min^{-1} N_2/H_2. The CV was carried out from 0.05 V to 1.00 V with a scan rate of 100 mV s^{-1}.
- Linear sweep voltammetry (LSV). This technique was performed to find out any crossover of gas flow through MEA. The same gases of the CV were fed with flowrates of 0.3/0.3 L min^{-1} N_2/H_2.

This protocol means the application of important disturbances in the normal operation of the HT-PEMFC and, consequently, it could be considered that it induces accelerate stress conditions which may affect importantly to the service life of the fuel cell.

6.3. Results and Discussion

6.3.1. Preparation of the catalysts

To evaluate the potential substitution of Vulcan carbon by CNS or CNFp as supporting materials, two catalysts were prepared in the lab with a target content of Pt of 40% wt. Characteristics of these three materials were compared among them and with a commercial 40% Pt/Vulcan catalyst, in order to determine the influence of the supporting material and also if the lab-made preparation of the electrodes influences on the results. After the synthesis process, real Pt (% wt.) content was determined by ICP method for all catalyst prepared. Results are shown in Table 6.1, besides the other characterization parameters of the catalysts that will be presented and discussed afterwards. This table also shows the BET area of the support, since this parameter is relevant for the discussion.

Table 6.1. Pt content, Pt crystallite sizes obtained from XRD analyses, Average Pt particle size determined from TEM micrographs and BET values of the supports for the different catalyst evaluated

Catalyst	Real Pt Content [% wt]	(2 2 0) Pt Crystal size [nm]	Average Pt particle size [nm]	Support BET area [$m^2\ g^{-1}$]
40% Pt/CNS	30.0 ± 0.5	4.4	-	9.22
40% Pt/CNFp	39.8 ± 0.4	4.0	3.7 ± 0.7	144.16
40 %Pt/Vulcan XC-72 (commercial)	40.1 ±0.2	4.2	3.6± 1.1	220.34
40 %Pt/Vulcan XC-72 (labmade)	39.9 ±0.1	4.8	4.1± 1.1	220.34

It can be observed that commercial Vulcan XC72, lab-made Vulcan XC72 and CNFp based catalysts have a Pt content close to the target one, but this is not in the case of the catalyst prepared with CNS. In this case, the analyzed platinum amount was around 10% lower than the expected, which means 25% of the Pt was not successfully deposited with the experimental procedure applied.

As it was pointed out in the physicochemical characterization of the different carbonaceous materials used shown in Chapter 5, CNS has a very low area (around 10 $m^2 g^{-1}$), which means that there are not available active centers of the surface of the CNSs to deposit the high Pt amount required, and this could explain the obtained results.

In order to confirm this point, SEM analysis was carried out. Figure 6.1 shows a comparative between the SEM micrograph obtained from Pt/CNS and other obtained with the commercial Pt/Vulcan catalysts (used as a reference). In comparing both pictures, it is confirmed the very irregular deposition of the metallic particles (white agglomerated parts) on the CNS, as compared to the very uniform dispersion of the Pt particles on commercial catalyst, which covers a high percentage of the surface of the support.

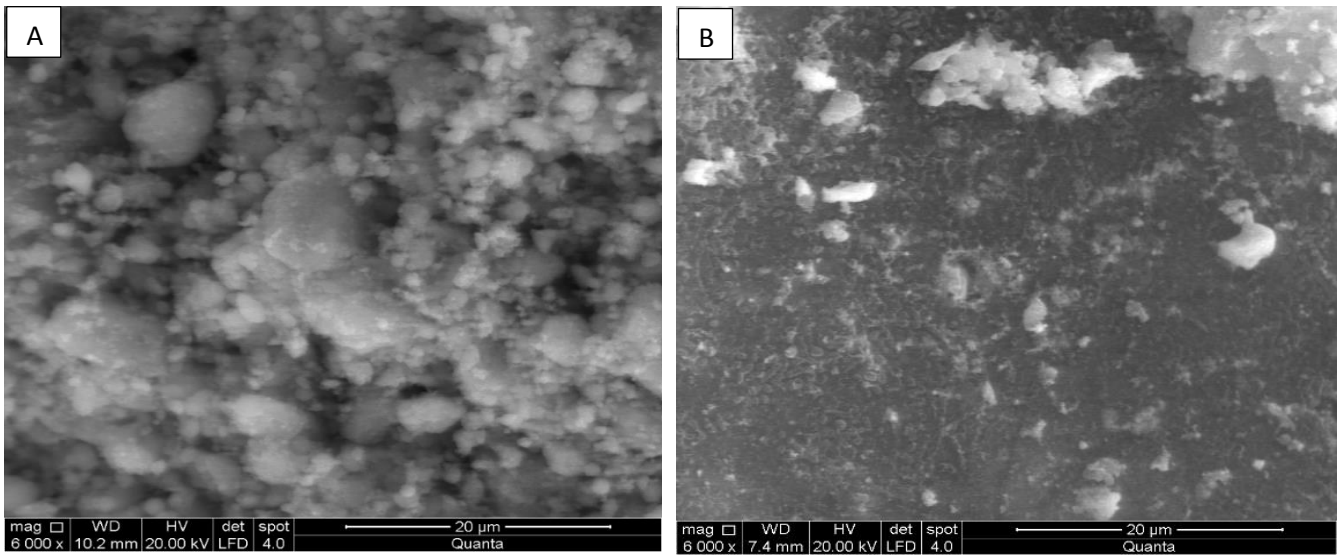

Figure 6.1. SEM images of commercial Pt/Vulcan (A) and Pt/CNS (B) based catalysts

Figure 6.2 shows the XRD patterns of the different catalysts. The main diffraction peaks of carbon, located at 2θ=26º [17], are much lower than those obtained for the raw carbonaceous materials (shown in Chapter 5) and, even, they are almost non-detectable for the Vulcan carbon based catalysts.

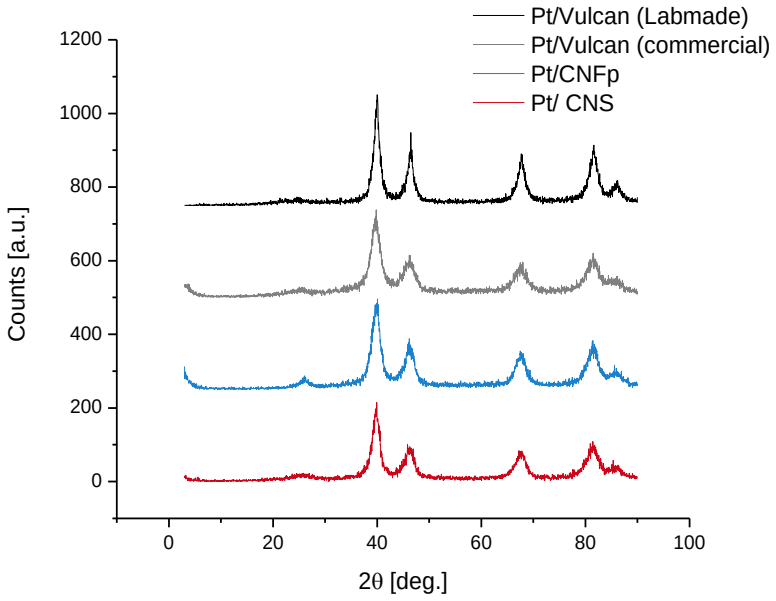

Figure 6.2. XRD patterns obtained for Pt based catalysts manufactured using the different carbonaceous materials tested in this work.

The platinum peaks are assigned according to the International Centre for Diffraction Data PDF 00-004-0802 and show a face-centered-cubic crystal structure for platinum. Moreover, the main peak for the Pt is located at 39.6º (111) plane, and the next one, (200) plane, is located at 41.3º. Both peaks are close to each other, and this proximity, in addition to the interferences with other catalyst support peaks, may affect to the crystallite parameters calculation. For this reason, Pt (220) plane peak, located at 68º, is often used to calculate the crystallite size of Pt based catalysts [18, 19]. Table 6.1 shows the Pt crystallite size calculated using the Scherrer formula. All lab-made catalysts exhibit similar Pt crystal and particle size to the commercial catalyst ones, being slightly higher the Pt particles obtained for the Pt/Vulcan lab-made catalyst than the one of the commercial catalyst, which means that the

synthesis method may have only a very slight influence on the final catalyst properties. It can be observed that the very low surface area of CNS, and the lower Pt content achieved during the synthesis process, does not have a remarkable effect on the platinum crystal size. CNFp based catalyst exhibited similar crystallite parameters to commercial catalyst, presenting the lowest Pt crystal size.

In order to get further information about the platinum dispersion, TEM analysis was used to characterize the different catalysts studied and resulting micrographs are shown in Figure 6.3. According to SEM (Figure 6.1) Pt/CNS had a very bad Pt dispersion, and for this reason it was decided that TEM analysis was not necessary for this catalyst. Regarding the other catalyst, the Figures 6.3B and 6.3C show, no significant differences in the particle size distribution can be observed between the lab-made and the commercial catalyst with the Vulcan carbon support. This observation indicates that the procedure applied in the manufacturing process is robust and well-done and that the particle size distribution depends on the support rather than on the experimental methodology applied. The differences achieved in the XRD could be attributed to the fact that the powders analyzed by XRD in the case of lab-made Vulcan contained more agglomerated particles. This is reflected in Figure 6.3 with a non-homogenous distribution, which shows agglomerated particles in certain regions. On the other hand, Pt/CNFp catalyst (Figure 6.3A) shows a very nice homogeneous distribution of the platinum particles, with very low presence of agglomerated particles. This is very important, especially if it is taken into account that the surface area of this support is around 40% lower than Vulcan XC72 (as it was shown in Table 6.1). This fact might be explained in term of a higher presence of acid groups, with allow the platinum particles to fix in better conditions to the support, as it will be discussed later. Table 6.1 also shows the values of the average Pt particle size obtained for each catalyst (by counting 80 particles of each catalyst). It can be concluded that these results are in agreement with those obtained from the XRD analyses.

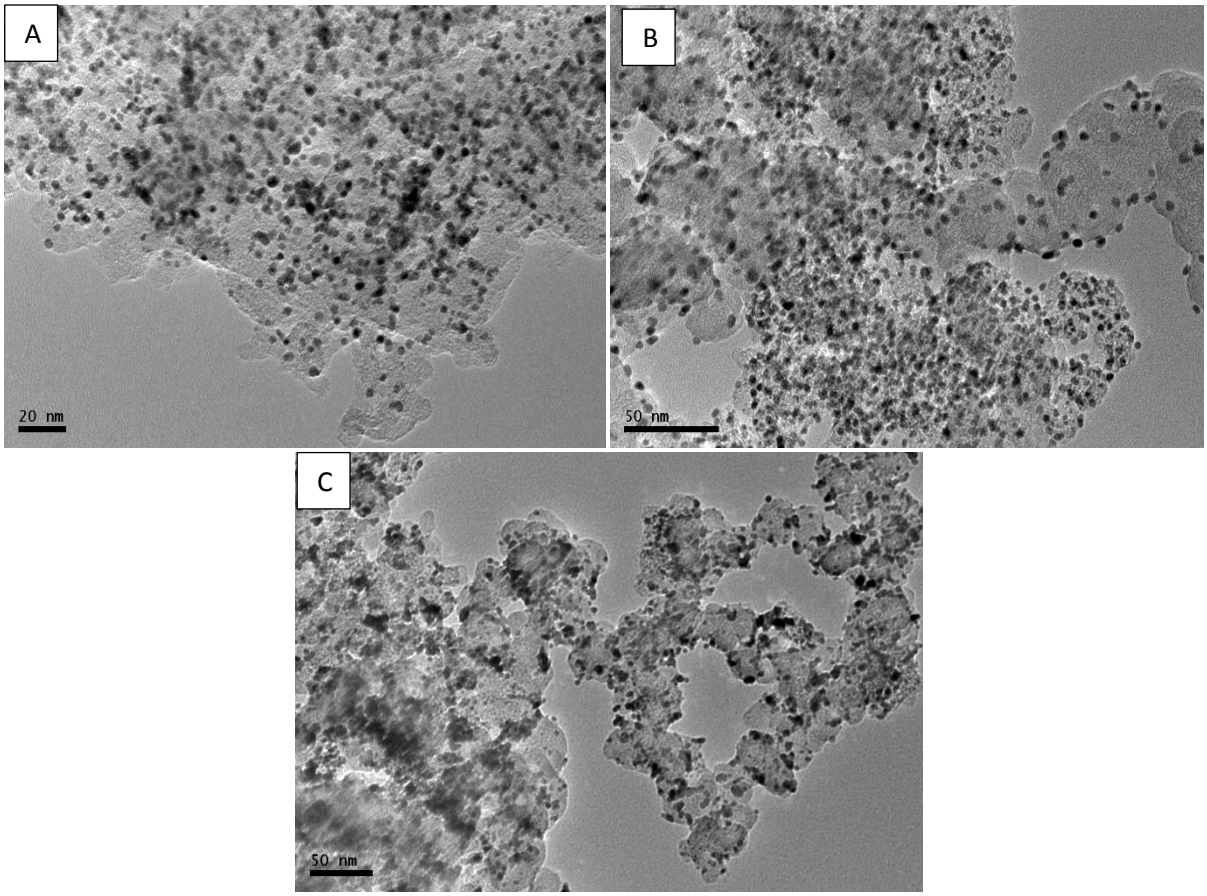

Figure 6.3. TEM micrographs of different catalyst: A) Pt/CNFp; B) Commercial catalyst Pt/Vulcan. C) Pt/Vulcan (homemade)

However, in comparing the crystal size and the particle size results, it can be observed that sizes calculated by TEM are slightly smaller than crystal size values. This fact can be explained in terms of:

- The crystallite size is calculated for a determined platinum face, which means that it must not necessary be similar to the particle size if the shape of the particle is not regular.
- XRD analysis are performed to large amounts of samples, and the value obtained (that could be taken as a global value) could be affected by the agglomeration of material during the sample preparation for the analysis. This means that the experimental error is higher in the XRD than TEM analysis, which calculates the

average particle size by the individual counting of 80 particles, avoiding agglomerates or other error sources.

Rotating disk electrode (RDE) analysis were performed in order to evaluate the activity and the ECSA of the different catalysts synthesized. Figure 6.4 shows the voltammograms obtained at different scan rates for the four Pt based catalysts studied.

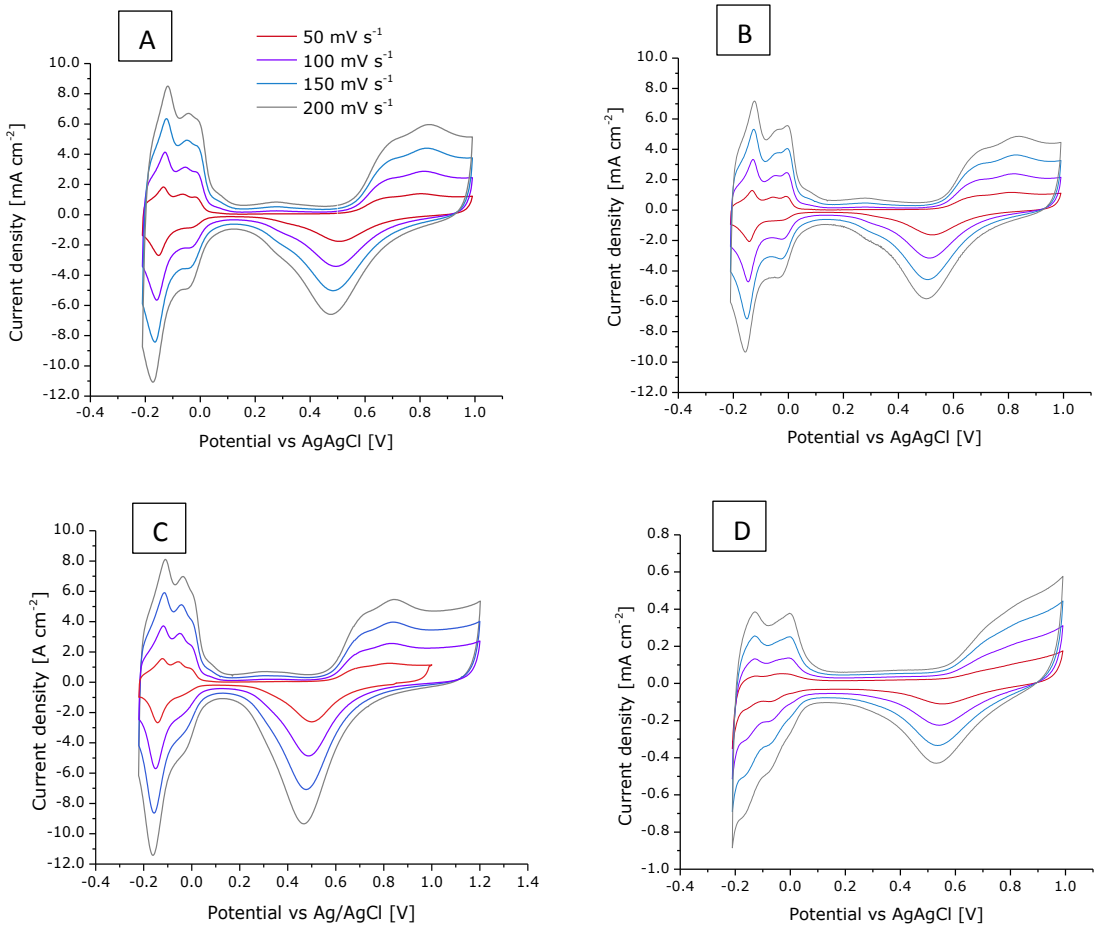

Figure 6. 4. Cyclic voltammograms obtained a different scan rates during the RDE measurements for all catalyst tested. A) Pt/Vulcan (commercial); B) Pt/CNFp; C) Pt/Vulcan (handmade); and D) Pt/CNS

In the high voltage region (0.6-1.0 V vs. Ag/AgCl electrode), an increase of the current appear, associated with the Platinum oxides formation [20], followed by a stabilization of the current. This stabilization can be explained in terms of the lower conductivity of the Pt oxides as compared to metallic Pt and because they also present lower catalytic activity, reducing the current density in the 0.9-1.0 V vs Ag/AgCl. In addition, it can be observed that CNFp and Vulcan based catalysts exhibit similar double layer contribution.

However, this fact changes when higher CNFp amounts are used in the electrode preparation (as it will be shown later in the voltammetry analysis in half-cell with fixed electrodes), since the high mesoporous character of the CNFp gives this material a high capacitive character, which also increases the double layer contribution of the material. As expected, Pt/CNS exhibited a very low active adsorption/desorption peaks, one log-unit lower than the others.

Moreover, important differences in the shapes of the voltammograms attending to the scan rate can be observed. The higher the scan rate, the higher is the current density, which is in agreement to the expected proportionality between current and root square of scan rate, stated by Randles-Sevcik equation (Equation 6.1) [21].

$$i_p = 0.4463\, nFAC \left(\frac{nFvD}{RT}\right)^{1/2} \quad (6.1)$$

where i_p is the maximum current in amps, n is the number of electrons transferred in the redox event, A is the electrode area in cm^2, F is the Faraday Constant in C mol^{-1}, D is the diffusion coefficient in $cm^2\ s^{-1}$, C is the concentration in mol cm^{-3}, v is the scan rate in V s^{-1}, R is Gas constant in J K^{-1} mol^{-1}, and T is the temperature in K

Respect to the orientation of the platinum particles, it can be observed that faces (1 0 0) and (1 1 1) can be distinguished perfectly, observing similar behavior respect to the preferential orientation of the Pt through the (1 1 1) face [22, 23]. Using the area of these desorption peaks, ECSA values were calculated for each catalyst using Equation 4.4 and results are shown in Table 6.2.

As it can be observed, commercial and homemade Pt/Vulcan catalysts exhibit almost the same values of the ECSA. This fact points out again the robustness of the synthesis methodology applied in this work. Furthermore, Pt/Vulcan based catalysts exhibited the highest ECSA value of all carbonaceous catalyst studied. Pt/CNFp presents ECSA values around 15-20% lower, but this fact can be explained taking into account that the Pt/CNFp

powder presents large particle sizes, which make difficult to prepare a perfect homogeneous ink. This fact means that this difference could be related to the concentration of the ink deposited on the GC electrode could be not exactly 0.4 mg Pt mL^{-1}.

Table 6.2. ECSA values measured from H_2 desorption peaks of the different voltammograms obtained during the RDE measurements

Catalyst	ECSA (50 mV s^{-1}) [m^2 g^{-1}]	ECSA (100 mV s^{-1}) [m^2 g^{-1}]	ECSA (150 mV s^{-1}) [m^2 g^{-1}]	ECSA (200 mV s^{-1}) [m^2 g^{-1}]
Pt/CNFp	43.25	50.54	58.99	66.93
Homemade Pt/Vulcan	66.84	73.91	77,59	81.22
Commercial Pt/Vulcan	68.56	76.46	79.68	84.57
Pt/CNS	2.31	3.18	4.40	5.30

Nevertheless, the ECSA values achieved by the Pt/CNFp are high enough to be used in HT-PEMFC. Finally, Pt/CNS exhibits very low ECSA values, around 15 times lower than the other catalysts tested and this observation confirms the bad prospects of this material for being a replacement of Vulcan carbon as a supporting material in the catalyst.

In the case of the RDE studies, ORRs were performed in order to evaluate the activity of the catalysts through the cathodic reaction [24]. Figure 6.5 shows the ORR curves obtained at different rotating speeds for all catalysts tested. As it can be observed, commercial catalysts and handmade Pt/Vulcan exhibit slight differences between their limiting current densities achieved in the diffusional region [21, 24], at lower potential values. This means that the synthesis method could have had a slight effect on the properties of the synthesized catalyst. Pt/CNFp exhibits intermediate values between both Pt/Vulcan catalyst, which means that the difference between the ECSA of this catalyst and Pt/Vulcan catalyst does not have a strong effect on the activity of the catalyst. Opposite, Pt/CNS catalyst exhibits, as it was expected due to their negligible ECSA, the worst performance of four catalysts tested.

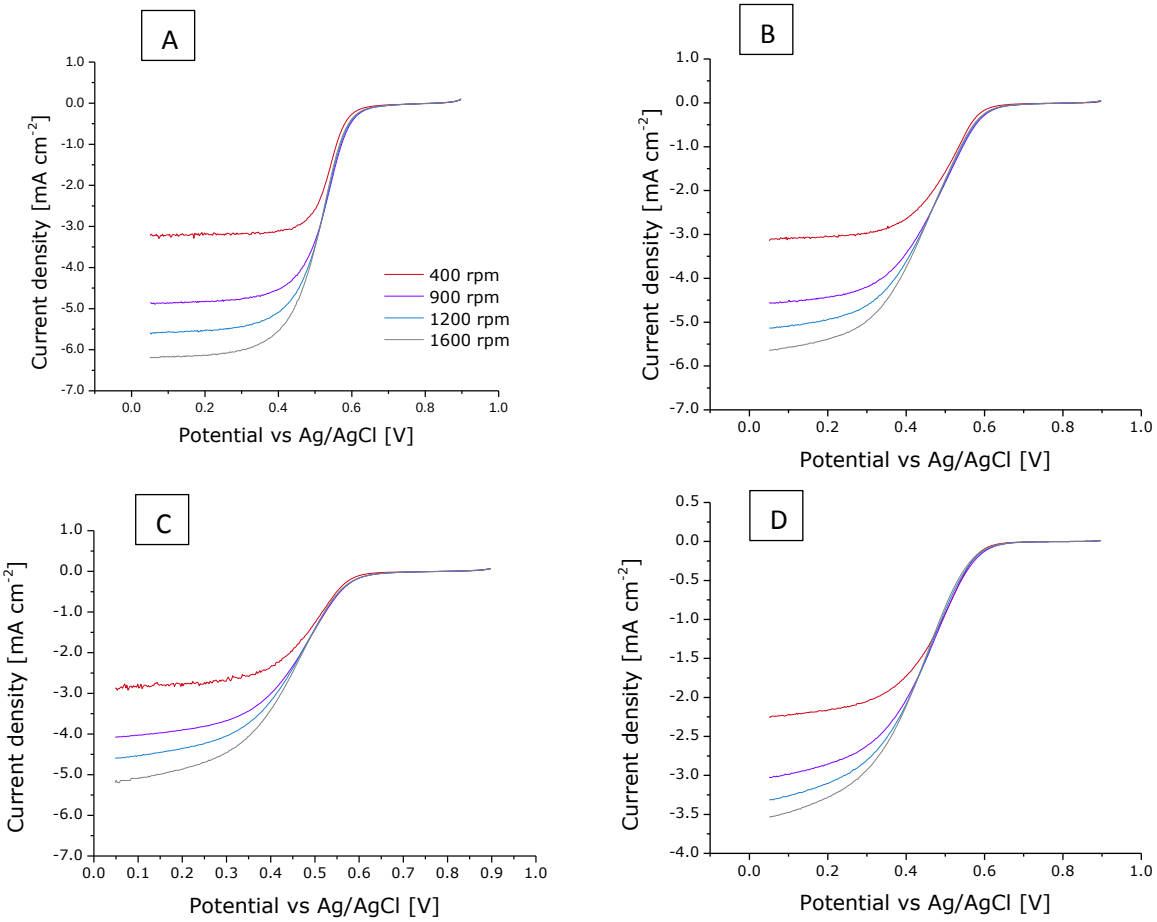

Figure 6.5. ORR performed at different scan rates for the different catalysts tested. A) Commercial Pt/Vulcan; B) Pt/CNFp; C) Pt/Vulcan (handmade); and D) Pt/CNS

Representing the 1/j values versus the inverse of the root square of the rotating speeds (given in rad s-1), real electrons transferred can be obtained from the slope of the linear plot, according to the Koutecky-Levich Equation (Equation 6.2, described in Chapter 4) [21, 25], where j_L is the limiting current density (A cm^{-2}), ω is angle frequency (rad·seg^{-1}) calculated from rotating speed (rpm), n is the amount of electrons transfered (theoretical value should be 4), F is the Faraday constant (96485 C·mol^{-1}), A is the electrode area 0.196 cm^2, D is the oxygen diffussion coefficient in the electrolite ($2.1 \cdot 10^{-5}$ $cm^2 \cdot s^{-1}$), ν is the cinematic viscosity of the electrolite (0.011 $cm^2 \cdot s^{-1}$) and C_{O2} is the saturated oxygen concentration in the electrolite media ($1.03 \cdot 10^{-6}$ mol·cm^{-3}).

$$\frac{1}{j} = \frac{1}{k \cdot n \cdot A \cdot F \cdot C_{O_2}} + \frac{1}{0.62 \cdot n \cdot F \cdot A \cdot D^{2/3} \cdot \omega^{1/2} \cdot \upsilon^{-1/6} \cdot C_{O2}} \qquad (6.2)$$

In Figure 6.6 can be observed the Koutecky-Levitz plots of the different catalysts tested, and Table 6.3 shows the number of electrons calculated for each catalyst. Since in all cases the catalyst is platinum, all samples exhibit number of electrons close to 4, which means that the complete reduction of the oxygen is performed. Lowest value is attained with Pt/CNS, as it was expected.

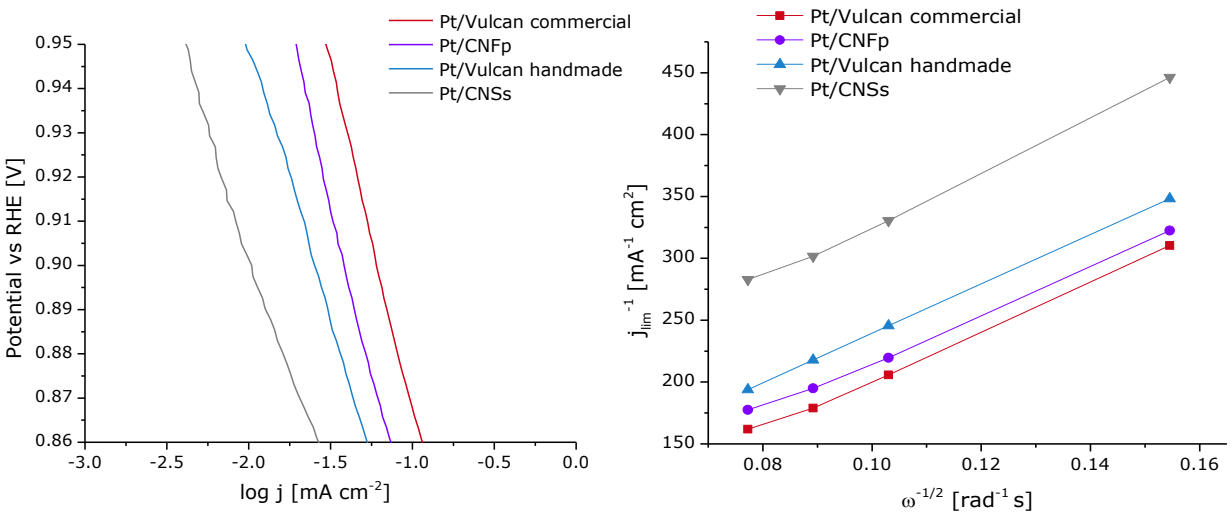

Figure 6.6. A) Comparison of Tafel plots of the different catalysts tested at 1600 rpm. B) Comparison of the Koutecky-Levich plots of the different catalysts tested.

From the current density values of the kinetic control region (+120 mV of over potential value) Tafel slopes can be calculated. The comparison of the Tafel plots of the four catalysts at 1600 rpm are shown in Figure 6.6A [21, 24]. Numeric values of the slopes calculated are available in Table 6.3. Values of specific current density (Specific activity) (SA) and Specific Mass Activity (SMA), calculated at 0.90 V vs RHE [26] from the LSV of the ORR measurements at 1600 rpm are also presented in Table 6.3.

As it can be observed, values for Pt/Vulcan and Pt/CNFp catalysts are slightly higher to the expected Tafel value (86 mV dec^{-1}) [27], but the plots are similar to the one shown in literature. SMA and SA values confirm that the best activity was achieved by the Pt/CNFp and commercial Pt/Vulcan.

Table 6.3. Additional parameters obtained from the Tafel and Koutecky-Levich plots for the different catalysts tested: number of transferred electrodes, Tafel slope, specific activity and mass activity.

Catalyst	Number of electrons	Tafel slope [mV dec^{-1}]	S A [mA cm^{-2}]	SM A [A gPt^{-1}]
Pt/CNFp	4.27	95.7	3.83E-02	0.99
Commercial Pt/Vulcan	4.14	93.2	6.03E-02	1.57
Homemade Pt/Vulcan	4.15	99.4	2.52E-02	0.66
Pt/CNS	3.72	113.8	1.05E-02	0.36

In comparing the data from both Pt/Vulcan catalysts, it can be observed that the commercial one presents higher values (more than double) than the lab-made Pt/Vulcan catalyst. Initially, this higher value may suggest that probably the batch could have suffered oxidation of the Pt particles. Alternatively, the difference can be explained by a bad deposition on the GC electrode. At this point, it was decided to exclude the Pt/CNS catalyst for further studies, since it was demonstrated that this catalyst presented the worst properties of all carbonaceous based catalysts evaluated and it had no sense to waste time on the study of its application as catalyst support.

To get more information about the oxidation state of the platinum particles of the catalysts, Temperature Programmed Reduction (TPR) analysis were carried out to the different 40% wt. Pt content catalysts prepared. Figure 6.7 shows the different spectra obtained. Three different regions can be appreciated for the three catalysts. In the first zone, located between 0 and 250 ºC, a small peak appears in all catalysts around 100 ºC, which could be attributed to the reduction of the rest of Pt complex precursor on the surface of the samples, corresponding to the change from Pt (IV) to Pt (II) [28-30]. As it can be observed, the Pt/Vulcan lab-made catalyst did not show a peak in this region, which means that the Pt complex were completely reduced during the synthesis process.

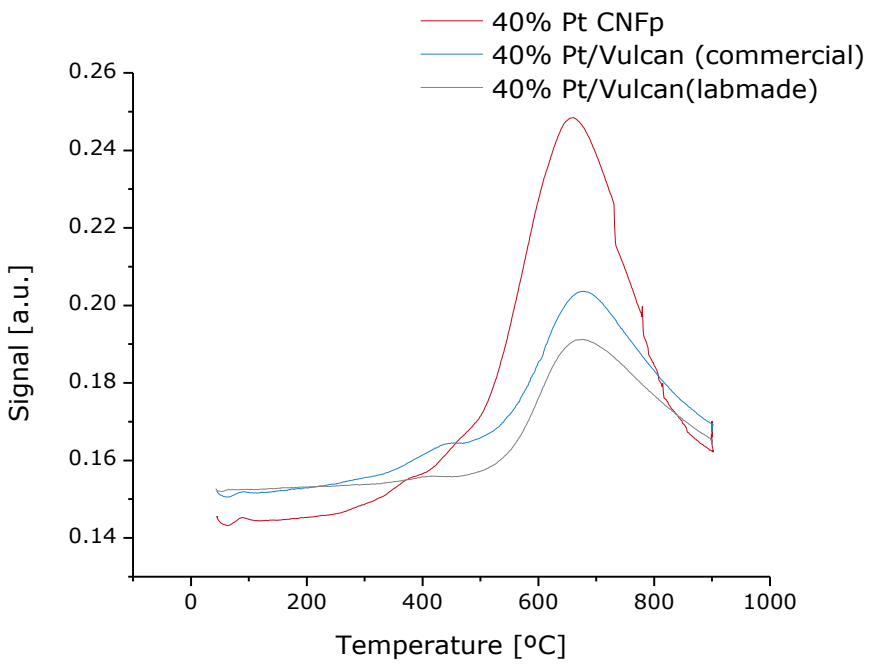

Figure 6.7. TPR spectra for different Pt based catalysts studied

On the other hand, the Pt/CNFp exhibited the highest peak in this region. Nevertheless, it can be considered that the formic acid method is robust, considering negligible the Pt complex presence in the final lab-made catalysts. In the region between 250 and 500 ºC, the slope of the plots starts to increase and another peak appears between 350 and 450 ºC, which corresponds to the reduction of Pt complex and Pt oxides bounded to the surface of the catalyst support, respectively. As it can be observed, lab-made Pt/Vulcan catalyst exhibited lower peak area than the commercial one, which means that the formic acid method achieves better Pt reduction rates than the method used to manufacture the commercial Pt/Vulcan catalyst. This means that after this point, all platinum contained in the catalyst should be present in zero valent state (metallic Pt). This peak could be also attributed to the hydrogen reaction with the reactive sites formed by desorption and transformation of CO_2 (formed due to the decomposition of carboxylic groups of the carbon surface) into CO due to the Pt activity [28-30]. After 550 ºC approx., a new huge peak appears [28-30], exhibiting a high intensity for the Pt/CNFp catalysts. This peak can be associated to CO

desorption caused for the decomposition of weak acid functional groups of the catalyst, which have a high presence in the synthesized CNFp used in this work [29].

6.3.2. Electrochemical characterization of the catalysts

To study the electrochemical behavior of the different catalysts, a voltammetric study was carried out to each of the different electrodes manufactured with them. Figure 6.8 shows the voltammograms, which compare the performances of the different catalysts prepared, containing the same platinum concentration (nominal content: 40% wt.) and Pt loading (0.3 mg Pt cm^{-2}) but different supports.

It can be observed an increasing of the current density on the high voltage region, due to the Pt oxides formation [20]. The changes on the oxygen evolution is related with this fact, and the complete removal of the oxygen media with time by the N_2 bubbling action. This slope decreases in all cases during the experiment, due to the platinum deactivation processes (formation of platinum oxide layers that decrease the activity of the catalyst) and the migration of the platinum particles into the electrolyte. This fact could also be observed in the platinum reduction region, which appears at 0.70 V vs. Ag/AgCl. Double layer does not suffer severe changes on its shape. On the other hand, the commercial Vulcan catalyst and CNFp catalyst exhibit a lower decrease of the double layer region (0.2-0.4 V), which may mean a very small decrease of the surface area of the catalyst support. This region could be related to the degradation of the carbonaceous support, because the degradation of the carbonaceous surface decreases the porosity and, as a consequence, the surface area and the capacitance character of the material, reducing the double layer contribution [31]. CNFp based catalyst exhibit the highest double layer contribution, since CNFp exhibits high capacitance character and electrical conductivity due to their mesoporous character.

The hydrogen adsorption/desorption peaks appear at same potential region for all samples studied (between -0.20/0.15 V vs Ag/AgCl electrode).

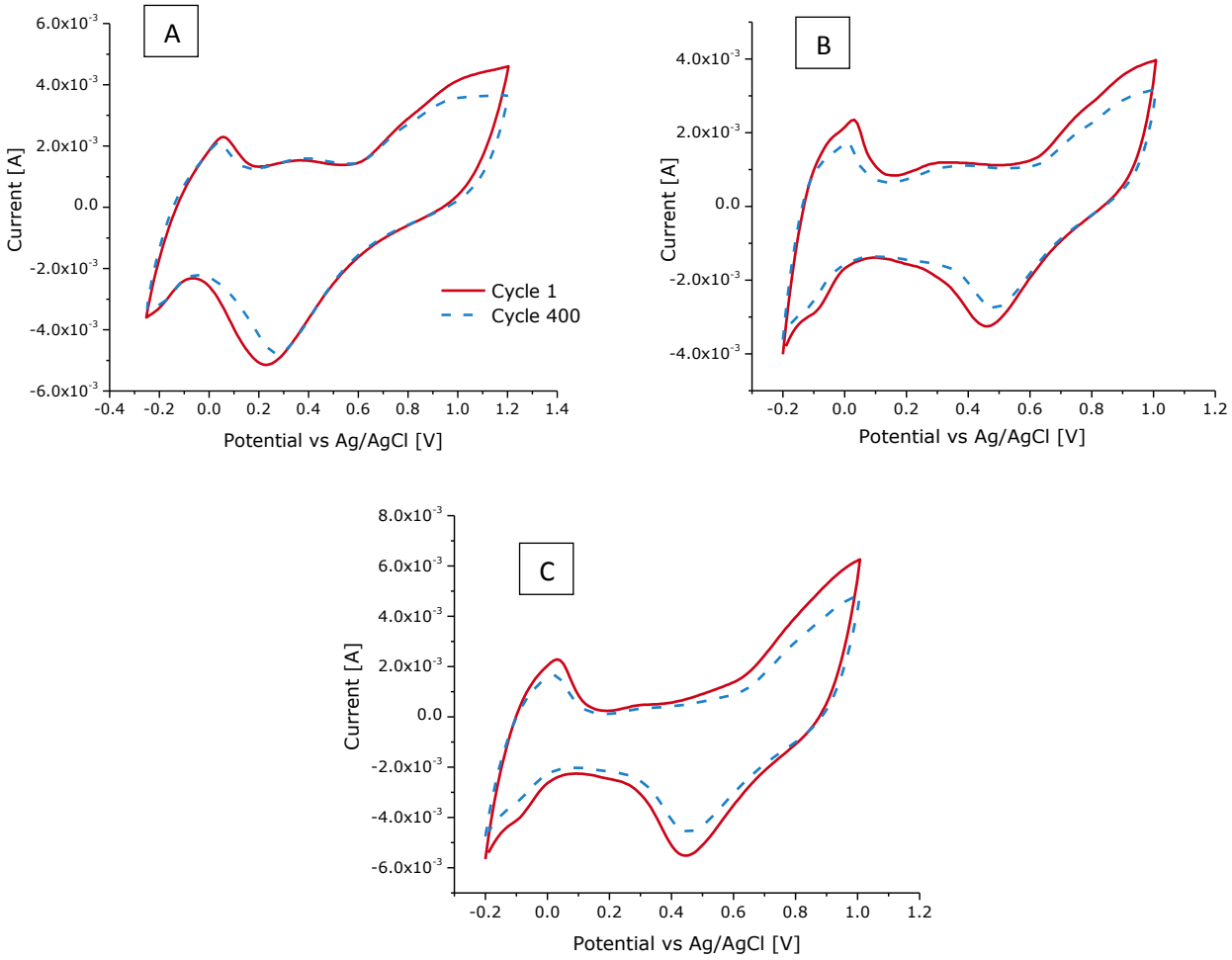

Figure 6.8. Cycle 1 and 400 of voltammograms of different catalyst tested: A) 40% wt. Pt/CNFp; B) Commercial catalyst, Pt/C; C) Homemade 40% wt. Pt/C.

Respect to the orientation of the platinum particles, it can be observed that faces (1 0 0) and (1 1 1) cannot be distinguished, exhibiting all catalysts one huge peak in the H_2 desorption region. However, in the adsorption region in the case of the commercial Vulcan catalyst, both peaks (corresponding each one to the different faces) are better appreciated [22, 23]. Using the area of these desorption peaks, ECSA values were calculated (with eq. 4.4) for each catalyst for cycles 1 and 400, in order to analyze the evolution of the active area of the catalyst during the experiment. The obtained values are shown in Table 6.4 where the degradation of the catalysts in terms of the variation of ECSA is also shown.

It can be observed that CNFp based catalyst exhibited lower ECSA values than commercial and lab-made Vulcan catalysts, but the higher double layer contribution effect in the case of carbonaceous catalysts, especially for the Pt/CNFp, could mask part of the H_2 adsorption/desorption peak, reducing the active area observed. Thus, taking into account the better platinum dispersion and the thickness of the observable hydrogen desorption peak, probably the real active surface area of this catalyst could be the same or even higher than the ECSA achieved for the Vulcan based catalyst. This explanation is in agreement with the highest current value achieved by this catalyst.

Table 6.4. ECSA values at different cycles for all catalyst tested in half-cell studies.

Catalyst	ECSA (Cycle 1) [$m^2\ g^{-1}$]	ECSA (Cycle 400) [$m^2\ g^{-1}$]	ECSA degradation [%]
40% Pt/CNFp	18.1	15.1	16.2
Commercial (40 % Pt/C)	29.3	19.5	33.6
Homemade (40% Pt/C)	31.4	21.7	27.6

Respect to the homemade Pt/C, the observable ECSA presented the highest values, which suggest that the synthesis method improves the active area of the homemade Pt/C catalyst as compared to the commercial one. This fact confirms that the worse performance of the Pt/Vulcan used during RDE measurements was due to partial oxidation of the Pt or to a bad deposition on the GC electrode. Nevertheless, as for the RDE studies, the obtained values are close to those of the commercial one. If the ECSA degradation of both commercial and labmade Pt/Vulcan, the value is slightly lower in the case of the labmade one. This fact could be explained in terms of the higher Pt particle size exhibited by the labmade Pt/Vulcan catalyst compared with the commercial one, which could be the responsible of the improvement of the stability. It is also remarkable that CNFp catalyst exhibited the lowest ECSA degradation, which could be attributed to the higher electrochemical stability of this

material as compared to the Vulcan carbon, as it was pointed out in Chapter 5 during the electrochemical characterization of the different materials. Furthermore, the high amount of acid groups observed in the TPR analysis of the Pt/CNFp could help to bind the platinum particles, avoiding the migration or agglomeration processes observed in carbon blacks materials.

6.3.3 Tests in a single HT-PEMFC

Taking into account the results obtained in the ex-situ characterization, 40% Pt/CNFp was selected to prepare a cathode to be used in a short lifetest of a HT-PEMFC (this cathode was then assembled in the so-called Pt/CNFp based MEA). Results obtained were compared to those obtained by a cathode made up with the commercial Vulcan catalyst (this cathode was assembled in the so-called Standard MEA). In order to attain comparable results, all experiments were carried out in the same cell and under the same operation conditions. Figure 6.9 shows the cell voltage versus time of MEAs prepared with the two catalysts studied in this work. The negative time values correspond with the break-in period, which lasted at approximately 70 h. Break-in periods in all tests were carried out at 120 ºC and 0.1 A cm^{-2}.

It can be observed that the standard MEA exhibited a decrease in the cell voltage during the first moments, which was overcome in less than 20 hours, most likely due to the activation of the catalyst. On the other hand, Pt/CNFp based MEA showed a very stable behavior during the break-in period, overcoming the performance of the standard MEA with voltages around 140 mV higher. When the break-in period ended, operation of the cell for 100 h was monitored. Although, it is not a long period, it can be considered long enough to evaluate the stability of new materials, above all, considering that at time 0, 50 and 100 h different electrochemical characterization tests (polarization curves with oxygen and air; impedance spectroscopy, linear sweep voltammetries, and cyclic voltammetries) were carried out. These techniques are known to contribute to accelerate the degradation of the MEA [32].

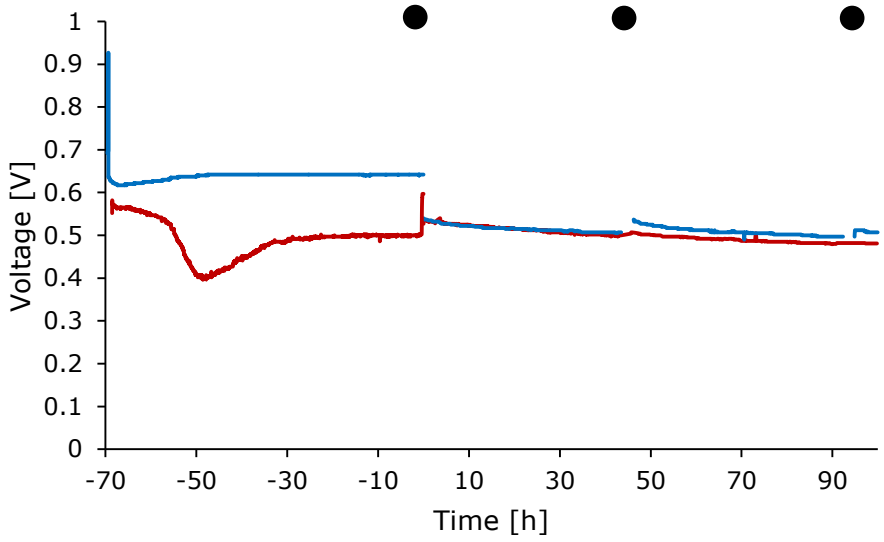

Figure 6.9. Evolution of cell voltage with time of MEAs with different catalysts. T= 160 °C; current density 0.2 A cm^{-2}. Break in period: 68 h at 120 °C and at 0.1 A cm^{-2}. Red line = Commercial catalysts (Pt/C); Blue line = Pt/CNFp; Black dots indicate the time when different characterization techniques were carried out.

From Figure 6.9, it can be observed that both MEAs tested exhibited a similar performance during the first 48 hours, with cell voltages over 0.51 V at 0.2 A cm^{-2}, but after the second characterization test, the Pt/CNFp based MEA increased its performance while the standard MEA continued a linear decreasing trend. This fact was also observed after the third characterization test, when a slight increase of the cell voltage of the Pt/CNFp MEA is noticed. In order to evaluate the degradation of the MEA, voltage at the start of the lifetests (after the first characterization test) and after 100 hours were used to calculate the voltage drops. For the standard MEA, an average decrease of -541 µV h^{-1} was obtained, while only -290 µV h^{-1} were obtained in the case of the Pt/CNFp based MPL (nearly 50% lower).

Figure 6.10 shows the evolution of the polarization curves that were performed during the different characterization tests performed to the MEAs evaluated and Table 6.5 shows parameters obtained from these polarization curves. As it was expected, both MEAs attained a better performance running with pure oxygen respect to the observed when they are fed with air.

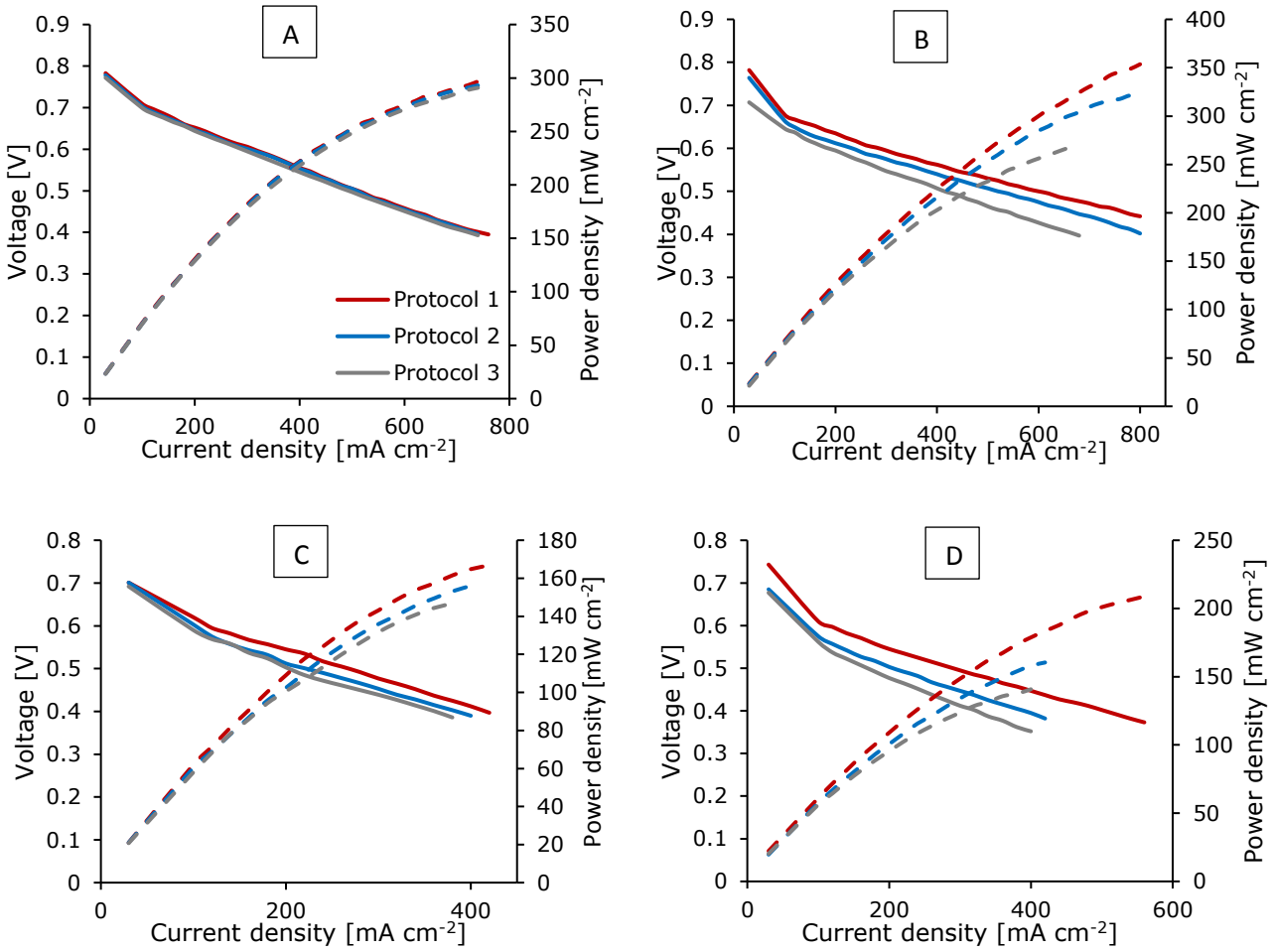

Figure 6.10. Evolution of polarization curves carried out with air and O_2 on the characterization tests performed during the life tests for both MEAs tested in this work at 160 ºC. A) Polarization curves performed to the CNFp based MEA with air. B) Polarization curves performed to the standard MEA with air. C) Polarization curves performed to the CNFp based MEA with oxygen; and D) Polarization curves performed to the standard MEA with oxygen. Protocol 1: t = 0 h; Protocol 2: t = 50 h; Protocol 3: t = 100 h

The oxygen gain, calculated at 0.2 A cm^{-2} from the data achieved in the polarization curves, was around 100 mV for both MEAs, which means that both catalysts underwent similar limitations, related to the oxygen transfer to the active sites. The performance is better for the standard MEA during the first characterization test, which means that when temperature was increased to 160 ºC at the end of the break-in process, the activity of the Pt/Vulcan catalyst was higher than Pt/CNFp. This fact is confirmed with the higher slope of the polarization curves of CNFp based MEA, which means that the Tafel slope value is higher for this catalyst than for the commercial one.

Table 6.5 Values of OCV and Peak power density at different times, obtained from the polarization curves at 160 °C with oxygen and air.

Catalyst	OCV (O_2) [mV]			OCV (Air) [mV]			Peak Power (O_2) [mW cm^{-2}]			Peak Power (Air) [mW cm^{-2}]		
	0 h	50h	100 h	0 h	50h	100 h	0 h	50h	100 h	0 h	50h	100 h
Pt/CNFp	1017	1025	1032	973	972	926	300.2	293.4	290.8	166.7	156.0	146.7
Pt/ Vulcan XC72	940	940	900	850	840	820	353.6	321.6	269.9	208.9	160.4	140.8

On the other hand, it can be observed that at the end of the lifetests, the performance of the standard MEA is worse than that of the CNFp based MEA. This fact confirms that the high stability of the Pt/CNFp demonstrated during the ex-situ characterization has a positive influence on the stability of the fuel cell. The standard MEA suffered a decrease around 23.7% and 32.6% in the maximum power density achieved with oxygen and air, respectively, while the Pt/CNFp only registered a decrease of 3.1% with oxygen, and 12% running with air.

The open circuit voltage (OCV) values exhibited very low variations during the test, as it can be observed in Table 6.5. This means that not important mechanical failures of the phosphoric acid doped PBI membranes occurred over the 100 hours of operation. In addition, Pt/CNFp MEA shows a slight increase of the OCV value during the first 48 hours, which could be explained in terms of a hydration process of the PBI membrane. Thus, the main degradation effects must be associated to the degradation of the electrodes. Recently, it has been pointed out different degradation mechanisms that may occur in PBI based HT-PEMFCs regarding the catalyst layer degradation and they can be found elsewhere [33]. In this work, in order to get more information about the degradation performed on the catalytic layer, ECSA values were calculated from the cyclic voltammetries tests. Table 6.6 shows the evolution of this parameter during the lifetests for both MEAs tested. It can be observed that the MEA prepared with Pt/CNFp as cathode catalyst exhibited a very low degradation rate (around 9.7 %) as compared to the commercial catalyst based MEA (21.70%). Both MEAs

exhibited similar values of initial ECSA, being slightly higher the values obtained for the standard one, but due to the high degradation rate of the commercial catalyst, the final ECSA was higher for the Pt/CNFp based MEA.

Table 6.6. Evolution of ECSA obtained from H_2 desorption peak of cyclic voltammetries performed during the different protocol tests.

Cathode catalyst	ECSA 1 [m^2g^{-1} Pt]	ECSA 2 [m^2g^{-1} Pt]	Final ECSA [m^2g^{-1} Pt]	Total degradation [%]
Pt/Vulcan XC72	17.05	14.69	13.36	**21.70**
Pt/CNFp	16.18	15.22	14.61	**9.70**

More information about the behavior of these MEAs is given by the impedance spectroscopy analyses that were carried out at different times during the lifetests (0 h, 50 h and 100 h). Figure 6.11 shows, as an example, the evolution of the different Nyquist plots of the Pt/CNFp based MEA, obtained at 0.2 A cm^{-2}.

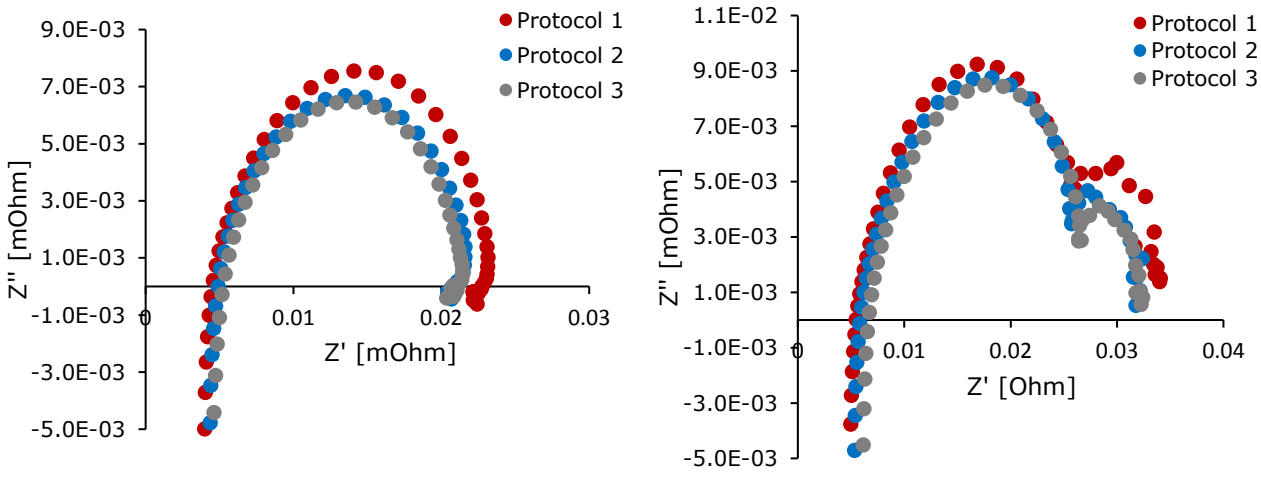

Figure 6.11. Nyquist plots obtained from the different protocol test performed at 0.2 A cm^{-2} for the Pt/CNFp based MEA

From this data, fitted to an equivalent circuit, the different resistances (ohmic, charge transfer and mass transfer) can be calculated [33, 34]. Ohmic resistance (R_{ohm}) is calculated at high frequencies, from the intersection point of the Nyquist plot with the X axis, when the imaginary resistance (Y axis) is 0 [33, 34]. A second resistance (R_{CT}) is calculated from the first arc, and it is related to the resistances provided by the electronic charge transfer during

the reaction. Finally, as it can be observed in Figure 6.11B, another arc appear at low frequency values in the case of the EIS obtained using air as oxidant, which is related with the mass transfer limitations (R_{MT}) [31,32]. Figure 6.12 shows the evolution of the different resistances obtained from the Nyquist plots data obtained at 0.2 A cm^{-2}, and fitted to the R_1 (R_2Q_1) (R_3Q_2) equivalent circuit, whose components correspond to R_{Ohm}, R_{CT} and R_{MT}, respectively [30,31]. Fittings were performed using the FRA software of AUTOLAB.

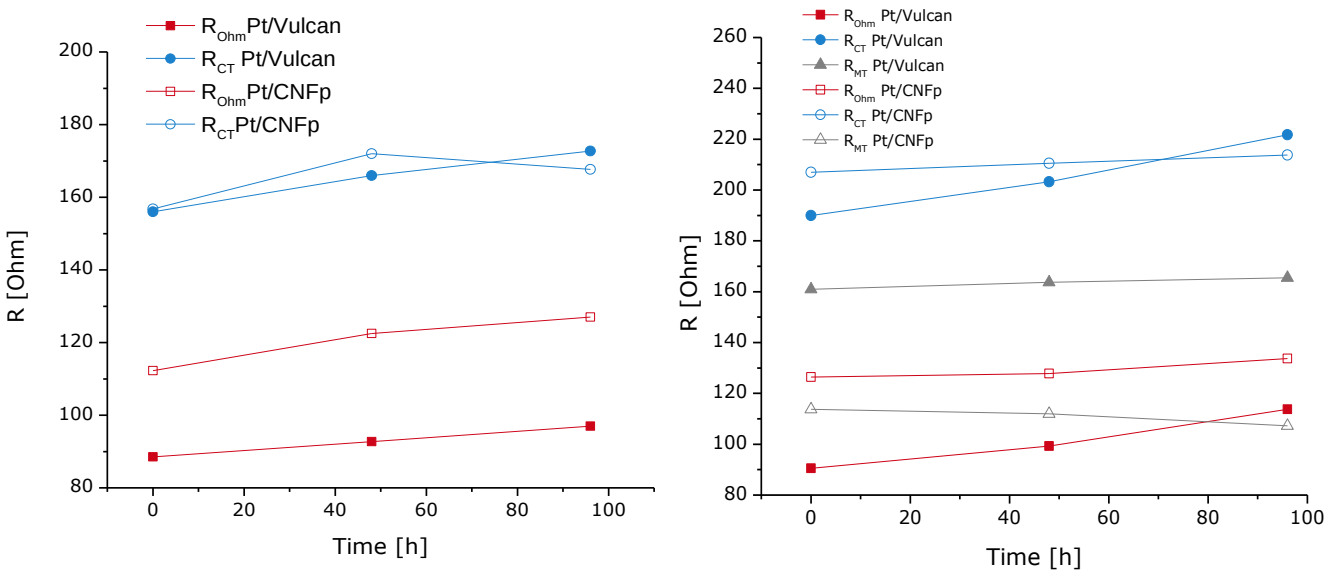

Figure 6.12. Evolution of the Ohmnic resistance (Rohm), Charge transfer resistance (R_{CT}) and Mass transfer resistance (R_{MT}) obtained from the fittings of the Nyquist plots to the equivalent circuit R (RQ) (RQ) from the EIS performed with oxygen (left) and air (right) for both MEAs tested.

The first parameter, R_1 (R_{Ohm}), undergoes only a slight increase during the lifetests for both MEAs, which means that not a high degradation of the PBI membrane occurred. In fact, the small increases of this value could be explained in terms of phosphoric acid loses [35].

The charge transfer resistance (R_{CT}) explains the better performance of the Pt/CNFp based MEA at the end of the experiment and the lower power densities achieved at the start of the life test. Thus, at the very initial moment of the lifetests, the charge transfer resistance is lower for the standard MEA, but this parameter undergoes a large increase during the test for the Vulcan carbon based MEA, and remains almost constant in the case of the Pt/CNFp,

being lower the R_{CT} of the Pt/CNFp MEA in the last test. Regarding the mass transfer resistance (R_{MT}), it must be pointed out that in the case of the tests running with oxygen, this resistance did not appear because of the high amount of oxygen available in the cell. The standard MEA exhibited the highest values, which means that the standard MEA suffers more mass transfer limitation problems, which could be due to the different porosity of the layers. This parameter remained constant during the lifetests for both MEAs studied.

Finally, Figure 6.13 shows the evolution of the different LSV parameters obtained from the linear sweep voltammetry plots.

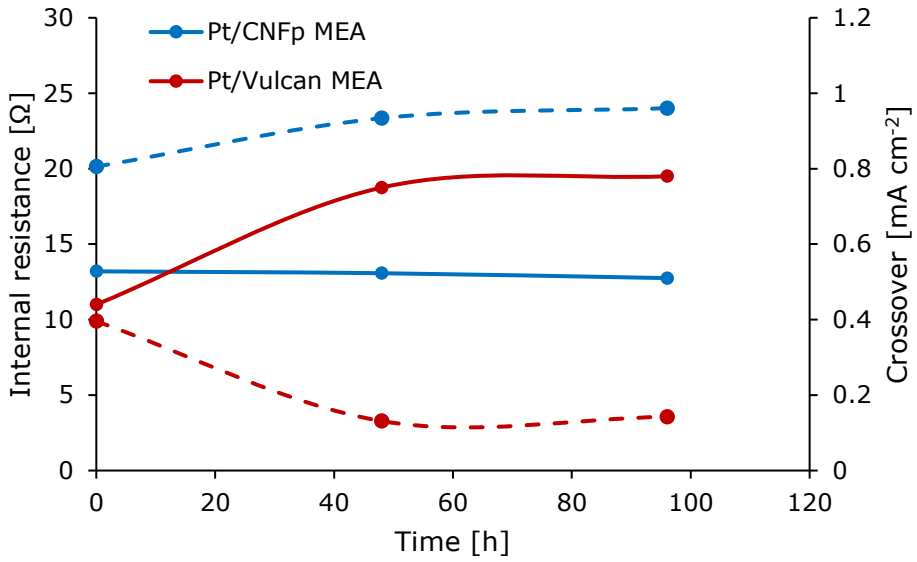

Figure 6.13. Evolution of the LSV parameters for the different MEAs tested during the lifetests. Continuous line: Evolution of internal resistance, expressed in ohms; discontinuous line: Crossover, expressed in mA cm^{-2}, both calculated at V = 0.30 V.

As it can be observed, for Pt/CNFp based MEA, negligible changes are observed in the evolution of both parameters. The internal resistance of the MEA is very high (over 20 ohms), which may mean that the membrane does not present any damage. In addition, the crossover is very low (between 0.50 and 0.55 mA cm^{-2}) which confirms the good status of the membrane during all experiment.

On the other hand, Pt/Vulcan XC72 MEA presents lower values of internal resistance (around 10 ohms at t=0 hours) and during the experiment it can be observed that after 48

hours the value decreases until 3.5 ohms, which is high enough to say that the membrane did not undergo any important damages during the test. The decrease could be attributed to a possible acid leaching in the membrane, which decreases its thickness. It can also be explained in terms of the formation of micro porous or holes in the PBI membrane. Anyway, crossover values still under 1 mA cm^{-2} during all preliminary life test, which allows us to consider that not severe damages on the membrane occurs during the experiment. This means the differences between the performances of both MEAs during the tests could be attributed to the different catalysts used and not to the membrane. This is also in agreement with the high OCV values achieved in the different polarization curves performed during the characterization tests.

6.4. Conclusions

The main conclusions drawn from the results shown and discussed in this Chapter are:

- Platinum supported on CNFp catalyst can be manufactured successfully by the formic acid method.
- Manufacture of high loading platinum supported on CNS catalyst is not successful because it cannot be attained the targeted Pt amount, most probably due to the very low surface area of this supporting material.
- CNFp based catalyst exhibited better stability compared with the standard Pt/Vulcan catalyst. The enhanced Pt dispersion of the Pt/CNFp catalyst could explain these good results. This fact could be explained in terms of the presence of more acid groups on the surface of the CNFp, which allows a better dispersion and bounding of the metallic particles.
- CNFp based MEA exhibits better performance at low current densities than standard MEAs prepared with a commercial catalyst based on Vulcan carbon black.

Furthermore, the degradation rate achieved for the CNFp based MEA is around 50% lower than values achieved for the standard MEA, presenting also a better performance respect to the Vulcan based MEA during the short lifetest carried out. This fact could be explained since the Pt/CNFp based MEA did not undergo several significant changes on their resistances (calculated from the EIS data), while the standard MEA undergoes an increase of its charge transfer resistance, traduced in worse catalytic activity.

6.5. Bibliography

[1] Z. Chen, D. Higgins, A. Yu, L. Zhang, J. Zhang, Energy & Environmental Science 4 (2011) 3167.

[2] S. Sharma, B.G. Pollet, Journal of Power Sources 208 (2012) 96.

[3] L.M. Roen, C.H. Paik, T.D. Jarvi, Electrochemical and Solid-State Letters 7 (2004) 19.

[4] R. Dhiman, E. Johnson, E.M. Skou, P. Morgen, S.M. Andersen, Journal of Materials Chemistry A 1 (2013) 6030.

[5] N. Linse, G. G. Scherer, A. Wokaun, L. Gubler, Journal of Power Sources 219, (2012) 240.

[6] J. Park, S. Yima, T. Kima, S. Parka, Y. Yoona, G.Park, T. Yanga, E. Park, Electrochimica Acta 83 (2012) 294.

[7] S.N. Stamarin, J. Speder, R. Dhiman, M. Arenz, E.M. Skou, ACS Appl.Mater. Interfaces 7 (2015) 6153.

[8] S. Yin, S. Mu, H. Lv, N. Cheng, M. Pan, Z. Fu, Applied Catalysis B: Environmental 93 (2010) 233.

[9] Y. C. Kimmel, L. Yang, T. G. Kelly, S. A. Rykov, J. G. Chen, Journal of Catalysis 312 (2014) 216.

[10] V. Jiménez, A. Nieto-Marquez, J. A. Díaz, R. Romero, P. Sánchez, J.L. Valverde, and A. Romero, Ind. Eng. Chem. Res. 48 (2009) 8407.

[11] A. Nieto-Márquez, I. Espartero, J. Lazo, A. Romero, J.L. Valverde, Chemical Engineering Journal 153 (2009) 211.

[12] J. Lobato, H. Zamora, P. Cañizares, J. Plaza, M.A. Rodrigo, Journal of Power Sources 288 (2015) 288.

[13] J. Lobato, P. Cañizares, M.A. Rodrigo, J.J. Linares, Electrochimica Acta 52 (2007) 3910.

[14] J. Lobato, P. Cañizares, M.A. Rodrigo, D. Úbeda, F.J. Pinar, J.J. Linares, Fuel Cells 10 (2010) 770.

[15] J. Lobato, P. Canizares, M.A. Rodrigo, J.J. Linares, D. Ubeda, F.J. Pinar, Fuel cells 10 (2010) 312.

[16] A.S. Pushkarev, I.V. Pushkareva, S.A. Grigoriev, V.N. Kalinichenko, M.Yu. Presniakov, V.N. Fateev, , International Journal of Hydrogen Energy 40 (2015) 14492.

[17] P. Nguyen, C. Pham, Applied Catalysis A: General 391 (2011) 443.

[18] J. Lobato, P. Cañizares, M.A. Rodrigo, J.J. Linares, Applied Catalysis B: Environmental 91 (2009) 269.

[19] J. Lobato, P. Cañizares, D. Ubeda, F.J. Pinar, M.A. Rodrigo, Applied Catalysis B: Environmental 106 (2011) 174.

[20] T. Reier, M. Oezaslan, P. Strasser. ACS Catal. 2 (2012) 1765.

[21] A.J. Bard, and L. R. Faulkner, Electrochemical Methods: Fundamentals and Applications, 2001, ISBN: 978-0-471-04372-0, Wiley.

[22] Q.He, X. Yang, W. Chen, S. Mukerjee, B. Koel, S. Chen, Phys. Chem. Chem. Phys. 12 (2010) 12544.

[23] K. Kinoshita, J. Electrochem. Soc. 137 (2010) 845.

[24] L. Zhang, H. Li, J. Zhang, Journal of Power Sources 255 (2014) 242.

[25] R. Vargas, C. Borrás, J. Mostanya, B. R. Scharifker, Electrochimica Acta 80 (2012) 326.

[26] A. Schenk, C. Grimmer, M. Perchthaler, S. Weinberger, B. Pichler , C. Heinzl, C. Scheu, F.A. Mautner, B. Bitschnau, V. Hacker, Journal of Power Sources 266 (2014) 313.

[27] H.A. Gasteiger, S.S. Kocha, B. Sompalli, F.T. Wagner, Appl. Catal. B - Environ. 56 (2005) 9.

[28] S.R de Miguel, O.A. Scelza, M.C. Román-Martínez, C. Salinas-Martínez de Lecea, D. Cazorla-Amorós, A. Linares-Solano, Applied Catalysis A: General 170 (1998) 93.

[29] M.A. Aramendía, J.C. Colmenares, A. Marinas, J.M. Marinas, J.M. Moreno, J.A. Navío, F.J. Urbano, Catalysis Today 128 (2007) 235.

[30] G.C. Torres, E.L. Jablonski, G.T. Baronetti, A.A. Castro, S.R. de Miguel, O.A. Scelza, M.D. Blanco, M.A. Pefia Jiménez, J.L.G. Fierro, Applied Catalysis A: General 161 (1997) 213.

[31] F. Büchi, N. Inaba, T.J. Schmidt, Polymer Electrolyte Fuel Cell Durability, Springer Science + Business Media 2009.

[32] G-B. Jung, K-Y. Chuang, T-C. Jao, C-C. Yeh, C-Y. Lin, Applied Energy 100 (2012) 81.

[33] M. Zhiani, S. Majidi, V. B. Silva, H. Gharibi, Energy 97 (2016) 560.

[34] X. Changjun, Q. Shuhai, Procedia Environmental Sciences 11 (2011) 589.

[35] F.J. Pinar, P. Cañizares, M.A. Rodrigo, D. Úbeda, J. Lobato, Journal of Power Sources 274 (2015) 177.

CHAPTER 7: Study of the application of non-carbonaceous materials as Microporous Layer in HT-PEMFCs

7.1. Introduction and Objectives

In Chapter 5, different carbonaceous materials were evaluated to be used as Microporous layer (MPL) for HT-PEMFC electrodes and it was concluded that carbon nanospheres were good carbonaceous candidates to replace the widely used Vulcan carbon, while the use of carbon nanofibers as MPL should be avoided, because they lead to bad performance in HT-PEMFC. In the search for materials that improve performance of the MPL of HT-PEMFC, in the present Chapter, different materials based on silicon carbide are going to be evaluated for the same purpose.

As it is known, the main function of the MPL is the improvement of the diffusion of reactant gases, minimizing electric contact resistance between the catalyst layer and bipolar plates, and in the case of LT-PEMFC, managing the water balance during production, expulsion, supply and evaporation. Consequently, it produces an improvement in the performance of the PEMFC [1-3], which is attributed to the improved distribution of pores, that, in turn, facilitates gas diffusion and, in the case of LT-PEMFC, reduces the amount of water accumulation inside the MPL [4,5].

As it has been pointed out in previous chapters, MPL of PEMFC usually contains Vulcan XC-72, because of its well-known good properties (high surface area, low cost and high availability), that serve to reduce overall fuel cell costs. However, this type of materials shows important drawbacks for being used in HT-PEMFCs based on phosphoric acid (PA) doped PBI membranes, because of its high corrosion rates at the typical operational conditions applied in this type of fuel cells [6, 7]. This negative fact is even promoted by the extreme voltage values reached during the start-up and shut-down procedures, which, nowadays, are known to present an important role in the degradation of the carbonaceous materials. Potentials over 0.21 V vs RHE can produce carbon corrosion in moderate amount, and for potentials over 1.20 V vs RHE, carbon corrosion achieves high rates [8, 9]. In addition, it is well-characterized that carbonaceous materials promote the reduction in the

catalyst activity because of the presence of sulphur impurities and the occurrence of micropores with suitable size to trap catalyst nanoparticles [6, 10].

Thus, it is crucial the development of new materials that can address the entire positive features that carbon materials exhibit and, at the same time, that could minimize the negative characteristics. One of most promising alternatives is the silicon carbide (SiC). Silicon carbide is covalent 1:1 stoichiometric carbide, keeping diamond structure, despite the different size of silicon (Si) and carbon (C). Attending to its crystalline structure, SiC is divided into different groups. The main groups are α-SiC and β-SiC [11-14]. The α-SiC is characterized by its greater occurrence and stability at high temperatures (above 1973 K). β-SiC is characterized by a higher surface area as compared to α-SiC, low band gap and high electron mobility. It is important to take into account that SiC is a hard, solid semiconductor and presents good stability under high temperature and voltage [11, 12]. Regarding other properties of interest, it shows a high porosity, with values of pore volume about 0.7 mL g^{-1}, and large surface area [13]. Recent research studies show that SiC is not the only non-carbonaceous material with potential application in HT-PEMFC. Tungsten carbide or titanium based materials [15-18] have been tested to be used as catalyst support for PEMFC systems achieving promising results in terms of stability and performance and these good prospects make them also good candidates for being tested in the MPL.

Taking into account this background, the main objective of the research shown in this Chapter is the characterization and evaluation of SiC and binary SiC-TiC materials (represented by their molecular formulas, Si_xTi_yC) in their application as microporous layer of HT-PEMFCs based on PA doped PBI membranes as electrolytes.

7.2. Methodology

High purity SiC, and Si_xTi_yC with percentages of TiC of 10, 20 and 30% (% mol), represented by their molecular formulas $Si_{0.9}Ti_{0.1}C$, $Si_{0.8}Ti_{0.2}C$ and $Si_{0.7}Ti_{0.3}C$, respectively, were gently provided by SICAT (Paris, France). According to the provider specifications, these materials also present impurities such as Fe, Al or Ca (200-900 ppm).

Powders were analysed by X-Ray diffraction (XRD) and BET (Brunauer-Emmet-Teller) to get more information about their surface and crystallite characteristics. Then, MPLs were manufactured depositing the different carbides onto a gas diffusion media (Toray Carbon Paper -PTFE 10%, Fuel Cells Store, USA) by air-spraying a microporous ink consisting of the non-carbonaceous material and 10% PTFE (Teflon™ Emulsion Solution, Electrochem Inc.). Previously, an optimization of the non-carbonaceous loading in the MPL preparation was performed, because of the expected very different characteristics of SiC as compared with those of carbonaceous materials. In particular, the thickness of the MPL was considered critical. Thus, 2.0, 4.0 and 6.0 mg cm^{-2} were the support loadings tested, evaluating the surface by Hg porosimetry (carried out by CSIC institution, Madrid) and XRD, in order to get an optimum value to be used with this type of materials. Graphical points of the Hg porosimetry results were calculated with the data obtained from the mercury intrusion porosimetry (MIP) process, according to Hager equation (Eq. 7.1), where ρ is material density; V_{tot} is total pore volume; τ is tortuosity which is defined as the ratio of actual distance travelled (l_e) to shortest distance (l) ($\tau > 1$), and $\int_{\eta=r_{c,}\,min}^{\eta=r_{c,}\,max} \eta^2 f v(\eta) d\eta$ is the pore volume distribution by pore size.

$$k = \frac{\rho}{24\tau^2(1+\rho V_{tot})} \int_{\eta=r_{c,}\,min}^{\eta=r_{c,}\,max} \eta^2 f v(\eta) d\eta \qquad [7.1]$$

After the deposition of the ink, sintering was attained by heating the electrodes at 360 ºC for 30 min. Other evaluated parameters were the hydrophobicity, and electrical conductivity of the different SiC based materials MPLs, with the methods described in Chapter 4.

As it has been pointed out, the stability of the MPL is the critical challenge to be overcome in the field of HT-PEMFC. Thus, the first studies consisted of the application of the same accelerated thermal and electrochemical tests used in Chapter 5 for the different non-carbonaceous based electrodes. Thus, the changes in the crystallite detected by XRD and the evolution of the shape of the cyclic voltammograms were used to evaluate the stability of these materials. Then, in the second set of tests, electrodes containing MPLs prepared with each non-carbonaceous material were used as cathodes to be tested in single HT-PEMFC system. MPLs of the electrodes were manufactured by the same procedure described in the ex-situ experiments, using the optimized load achieved in them. The catalyst layer was deposited by spraying the catalyst ink on the electrodes. The catalyst ink consisted of a 40% Pt/C catalyst on Vulcan XC-72R Carbon Black (Fuel Cell Store, USA), PBI ionomer (1.5 wt. % PBI in N, N-dimethylacetamide, DMAc), and DMAc as a dispersing solvent. In both cases, the Pt loading on each electrode was 0.6 mg Pt cm^{-2}. After the deposition of the catalyst layer, the electrodes were dried at 190 °C for 2 h, with the purpose of removing traces of DMAc. The electrodes were then wetted with a solution of 10% PA. Electrodes were left to adsorb the acid for one day. For the preparation of the membrane-electrode assembly (MEA), a thermally treated PBI membrane was provided by Danish Power Systems®. This membrane was doped in 85 wt. % PA for 5 days, in order to achieve good proton conductivity. The doping level acquired by the membrane was above 9 molecules of acid per polymer repeating unit. The corresponding average thickness of the doped PBI membrane used was 80 μm. The superficial acid on the membrane was thoroughly wiped off with filter paper and the membrane was used to prepare the MEA. In order to manufacture the MEA, the doped

membrane was sandwiched between a couple of electrodes and the whole system was hot-pressed at 130 °C and 1 MPa for 15 minutes. Same that in the carbonaceous material testing performed in Chapter 5, Vulcan carbon was always used for the MPL of the anodes. The completed MEA was inserted into the cell between end plates of graphite (with a five serpentine channels frame in each plate). The geometrical area of each electrode was 25 cm^2.

MEAs were mounted and characterized in a commercially-available Cell Compression Unit (CCU) provided by Baltic Fuel Cells GmbH (Germany). The break-in procedure consists of the operation at 0.1 A/cm^2, and λ (H_2) 1.5 and λ (air) 2 for 48 hours. Then, a preliminary stability test was conducted by increasing the current density to 0.2 A cm^{-2} (160 °C). For further characterization, a protocol test was carried out every 48 h, since the end of the break-in procedure. This test (applied in all previous Chapters) consists of the following routine:

- Galvanostatic polarization curves. They were performed from the OCV to 0.40 V, increasing the current of the system by 0.5A each 30 seconds. Polarization curves were performed first with air and then with oxygen, with the following stoichiometric parameters: [λ (H_2) = 1.5]; [λ (air) = 2]; and [λ (O_2) = 9.5].
- Electrochemical impedance spectroscopy (EIS) tests. The tests were performed at different current densities (0.03, 0.10, 0.20, 0.30 and 0.40 A cm^{-2}) with 10 mV AC perturbation amplitude and frequency ranging from 100 kHz to 100 MHz. This sequence of EIS tests was carried out first with air and, then, the same procedure was repeated with oxygen. After that, ohmic resistance ($\mathbf{R_\Omega}$), charge transfer resistance ($\mathbf{R_{CT}}$) and mass transfer resistance ($\mathbf{R_{MT}}$) were calculated, fitting the experimental data achieved in the EIS to the simulated electrical circuit **R (RQ) (RQ)** to obtain those parameters.
- Cyclic voltammetries (CV). The cathode side was purged with nitrogen and hydrogen flowed through anode side with flows of 0.1/0.1 L min^{-1} N_2/H_2. The CV was carried

out from 0.05 V to 1.00 V (scan rate of 100 mV s^{-1}). Obtained results were used to estimate the electrochemical surface area (ECSA) of the cathode.

- Linear sweep voltammetry (LSV). The same gases of the CV were fed with flows of 0.3/0.3 L min^{-1} N_2/H_2. This technique was performed to find out any crossover of gas flow through MEA.

7.3. Ex-situ characterization

7.3.1. Powder characterization

SiC based powders and MPLs were analyzed by XRD and BET analysis. Table 7.1 shows the main parameters achieved for each SiC and Si_xTi_yC based material tested.

Table 7.1. Crystallite parameters and surface and pore data for different SiC based materials

Material	SiCTiC-10% Ti	SiCTiC-20% Ti	SiCTiC-30% Ti	SiC
Surface Area (m^2/g)	99.54	54.42	23.25	31.41
Micropore Volume (cc/g)	0.008	0.001	0.000	0.000
Total pore volume (cc/g)	0.175	0.189	0.110	0.178
Average Pore diameter (nm)	4.1	6.9	9.5	11.3
Crystallite size (nm)	28.0 (2θ=35.6°) 20.8 (2θ=41.8°)	20.8 (2θ=35.6°) 22.3 (2θ=41.8°)	22.9 (2θ=35.6°) 23.3 (2θ=41.8°)	15.95 (2θ=35.6°) -
Distance between planes (nm)	0.252 (2θ=35.6°) 0.216 (2θ=41.6°)	0.252 (2θ=35.6°) 0.216 (2θ=41.8°)	0.252 (2θ=35.6°) 0.216 (2θ=41.8°)	0.252 (2θ=35.6°)

As it can be observed, the higher the TiC content, the lower is the surface area of the binary carbide, being the $Si_{0.9}Ti_{0.1}C$, the binary carbide material with highest BET

area. This large surface area of the best binary carbide is more than 3 times higher than BET showed by pure SiC, which exhibits moderate values of this parameter (slightly over 30 $m^2 g^{-1}$) and more than 4 times higher than that showed by the binary carbide $Si_{0.7}Ti_{0.3}C$, the binary carbide with 30% TiC. These results are higher than other BET values found in literature for SiC, around 20 $m^2 g^{-1}$ [13].

Regarding the porosity, pure SiC presents a pure mesoporous character, taking into account the absence of microporous volume and its average pore size (11 nm). As it can be observed, the TiC content of the binary carbide material has a strong effect on this parameter. Thus, the binary carbide $Si_{0.9}Ti_{0.1}C$ exhibits the highest microporous character of all non-carbonaceous materials, and the lowest average pore size. When TiC content is increased, average pore size increases and microporosity decreases, giving higher mesoporous character to the binary carbide. Taking into account the results obtained with pure SiC, this observation suggests that both carbides have low microporous character and that the differences found for this parameter in the binary carbide material can be attributed to the interstitial region between SiC and TiC.

Figure 7.1 shows the different adsorption-desorption curves obtained for each material during the BET test. It can be observed that all materials fits well to a type 4 Langmuir isotherm, which means that they combine microporous and mesoporous character on their surface. The characteristic hysteresis phenomenon, observed in all curves, is in agreement with the porosity values shown in Table 7.1. The hysteresis of the plots decreases with the amount of Ti on the binary carbides. This fact confirms that higher amounts of TiC decreases the porosity of the material and increases the average pore size, as it was also showed in Table 7.1. This fact affects especially to the microporosity, and it could justify the severe decrease observed in the BET area of the

binary carbide $Si_{0.7}Ti_{0.3}C$, with 30% TiC. Regarding to the pure SiC, the high mesoporous character increases the hysteresis phenomena, as it can be clearly observed in Figure 7.1.

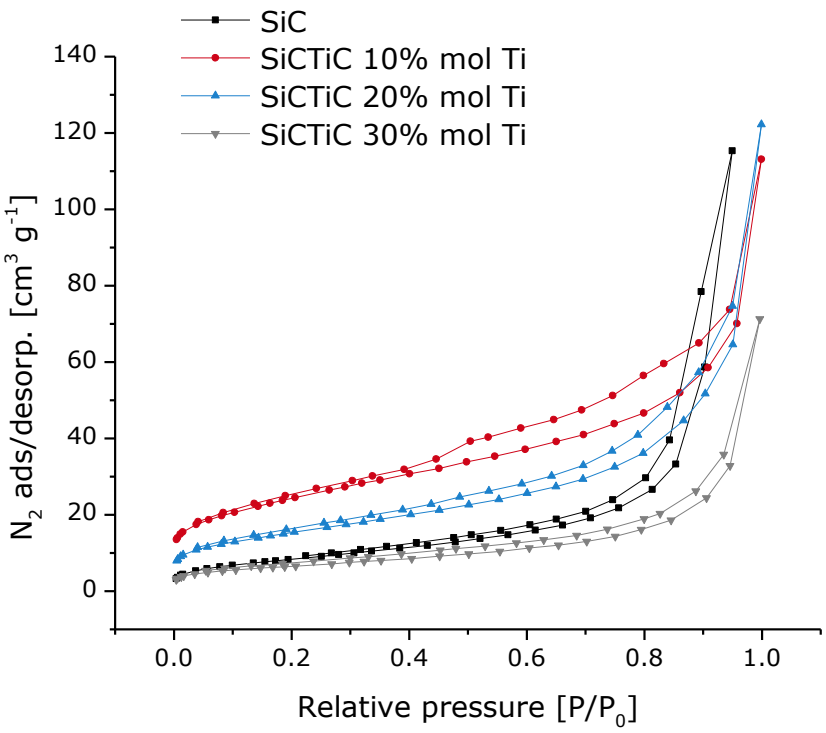

Figure 7.1. BET plots obtained for different SiC based materials

Figure 7.2 shows the XRD patterns of the different SiC based materials tested. It can be observed that SiC based materials present characteristics peaks at 2θ of 36º, 41º, 60º and 74º, being 36º the main peak, which may be attributed to the face (111) [19]. The peak located at 2θ = 41º is the main peak associated to TiC. This can be confirmed by the increase observed in the intensity of this peak with the Ti content in the binary carbide.

Crystal size (L_c) and distance between planes (d_{002}) shown in Table 7.1 were calculated for each sample using equations 4.1 and 4.2, respectively (Chapter 4). Table 7.1 shows the XRD crystal size and d_{002} values for each powder sample, obtained for 2θ = 35.6 º peak. In addition, Si_xTi_yC samples also present the values of these parameters for main peak of TiC (2θ = 41.8 º).

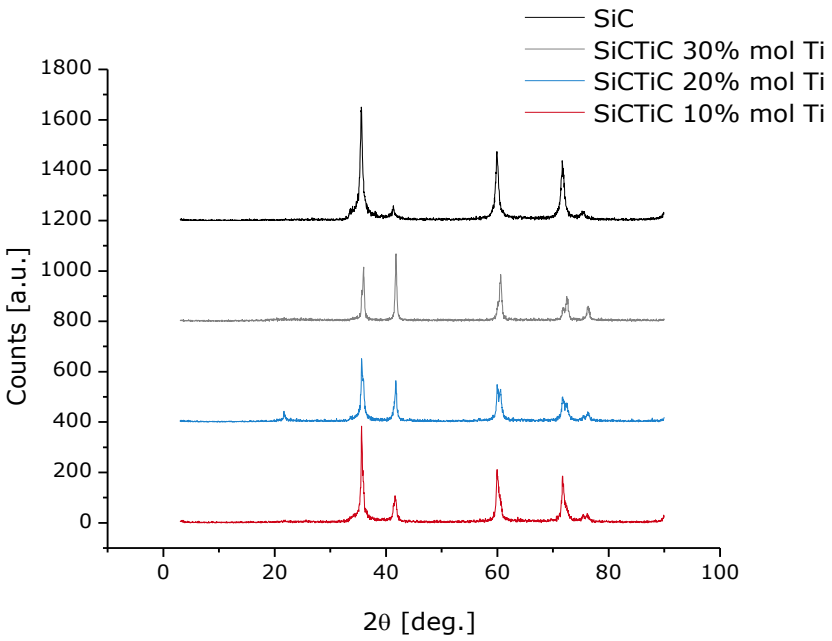

Figure 7.2.XRD patterns of SiC and Si_xTi_yC powders

It can be observed that all materials present similar distance between planes for the peaks studied (0.252 and 0.216 nm, respectively), which means that the addition of TiC has not a clear influence on this parameter. Respect to the crystal size, binary carbides show an increase in the crystal size for the (111) face of the SiC, as compared to pure SiC powder. This size decreases with the Ti content in the binary carbide, as it can be observed in Table 7.1. Opposite, the higher is the Ti content, the larger is the crystal size achieved for main face of TiC.

7.3.2 MPL optimization and characterization

Diffractograms of MPLs prepared with the different SiC based materials are shown in Figure 7.3. Part A shows the XRD patterns of SiC based MPLs with 2.0, 4.0 and 6.0 mg cm^{-2} SiC load, and Part B, the XRD patterns of the $Si_{0.9}Ti_{0.1}C$ based MPLs with 2.0, 4.0 and 6.0 mg cm^{-2} loads. As it can be observed, one high intensity peak appears at 2θ= 26 º and it decreases in size when amount of SiC increases. This peak may be

attributed to carbon [20], and it can be associated with the carbonaceous structure of the gas diffusion layer which supports the microporous layer.

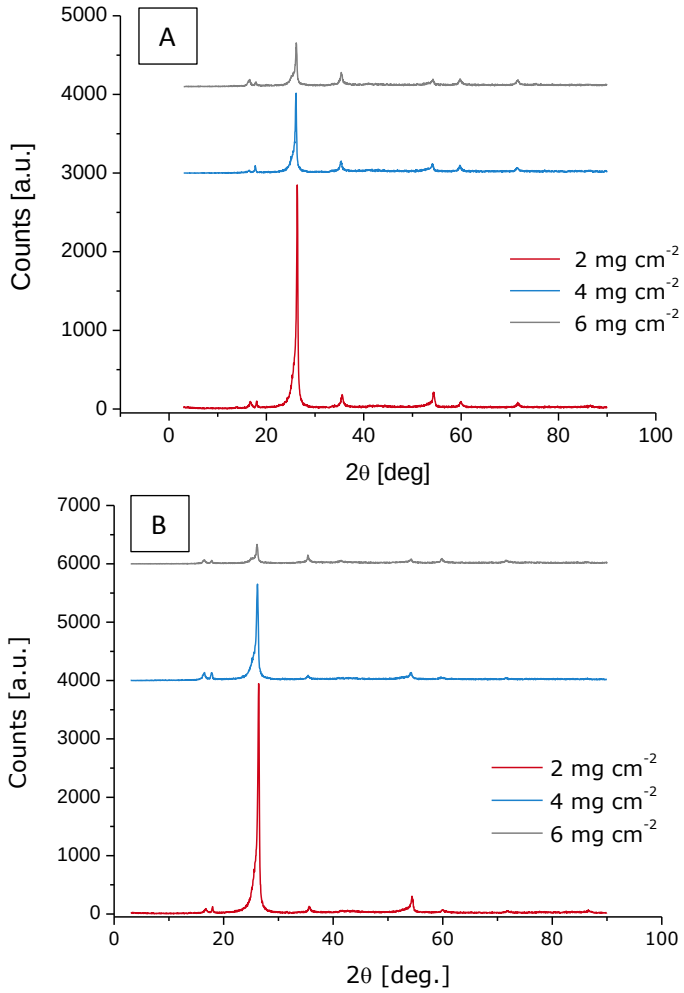

Figure 7.3. XRD measurements obtained for different SiC based materials studied. A) SiC based MPLs with different SiC load; and B) $Si_{0.9}Ti_{0.1}C$ based MPLs with different loads

Hence, the carbon peak indicates that the GDL also affect to the diffractogram and, therefore, values obtained from XRD cannot be taken as real but they will only be used for comparative purposes, when making stability assessments. As it was expected, as the SiC content increases, the MPL thickness increases and hence the carbonaceous layer of the GDL is more coated by the SiC based MPL, which can be confirmed due to the decreasing of the carbonaceous signal in XRD analysis. Tables 7.2 and 7.3 show the L_c and d_{002} values obtained for the different MPLs prepared with SiC-based materials,

before and after thermal and electrochemical tests (which will be discussed later on). In the case of MPLs, L_c and d_{002} values are considered *apparent*, because of the addition of PTFE in the microporous layer, which causes agglomeration, as it was discussed previously in Chapter 5.

Table 7.2. XRD analysis of different SiC based MPLs

Load [mg cm-2]	Peak description	App. d_{002} [nm]	App. Crystal size [nm]	Crystal size change [%]
2	**Initial (2θ =26°)**	**0.338**	**24.1**	
	Post TT	**0.340**	**26.5**	9.9
	Post CV	**0.338**	**27.4**	13.7
	Inicial (2θ=35.5°)	**0.257**	**18.5**	
	Post TT	**0.258**	**17.1**	7.6
	Post CV	**0.257**	**18.0**	2.7
4	**Initial (2θ =26°)**	**0.341**	**21.8**	
	Post TT	**0.342**	**22.7**	4.1
	Post CV	**0.342**	**22.8**	4.6
	Inicial (2θ=35.5°)	**0.255**	**16.4**	
	Post TT	**0.256**	**15.7**	4.3
	Post CV	**0.256**	**16.1**	1.8
6	**Initial (2θ =26°)**	**0.341**	**22.1**	
	Post TT	**0.341**	**22.0**	0,5
	Post CV	**0.341**	**22.2**	0.5
	Inicial (2θ=35.5°)	**0.253**	**14.5**	
	Post TT	**0.255**	**14.1**	2.7
	Post CV	**0.253**	**14.3**	1.4

Table 7.3. XRD analysis of different $Si_{0.9}Ti_{0.1}C$ based MPLs

Load [mg cm^{-2}]	Peak description	App. d_{002} [nm]	App. Crystal size [nm]	Crystal size change [%]
2	**Initial (2θ =26°)**	0.338	24.0	
	Post TT	0.339	24.6	2.5
	Post CV	0.338	24.9	3.7
	Inicial (2θ=35.5°)	0.252	27.5	
	Post TT	0.252	27.2	1.1
	Post CV	0.252	27.0	2.2
4	**Initial (2θ =26°)**	0.340	19.8	
	Post TT	0.340	19.3	2.2
	Post CV	0.340	19.4	1.4
	Inicial (2θ=35.5°)	0.253	25.1	
	Post TT	0.253	24.8	1.3
	Post CV	0.253	24.7	1.6
6	**Initial (2θ =26°)**	0.341	17.6	
	Post TT	0.340	17.3	1.7
	Post CV	0.341	17.5	0.6
	Inicial (2θ=35.5°)	0.253	26.9	
	Post TT	0.253	26.5	1.5
	Post CV	0.253	26.3	2.2

It must be pointed out that since some peaks did not appear properly in the XRD obtained for MPLs (as compared to the peaks obtained from different faces of SiC and TiC in the XRD of the powders), the study and characterization was carried out only for

the main carbon peak (2θ = 26 º approx.) and the main SiC peak (2θ = 35.5 º). Both peaks were used to evaluate the stability of the MPLs and the protection performed over the GDL, in order to determine the optimum SiC-based materials loading required in the MPL.

Respect to d_{002} values, it can be observed that the values are comparable for the powder and the MPL samples of the different material studied. As it was expected with the clear shape of the different peaks of the SiC and Si_xTi_yC diffractograms, the SiC based materials are more crystalline as compared to the Vulcan carbon. This is confirmed by a lower d_{002} value, which means that particles are more ordered.

Figure 7.4 shows the variation of cumulative pore volume for different SiC (Part A) and Si_xTi_yC (Part B) based MPLs, and a GDL with and without Vulcan MPL, added for comparative purposes.

Porosimetry is an important parameter, which may be related to the diffusion coefficient of porous substrates [21], because it is directly related to the gas permeability of the electrode. It must be pointed out that for all porosity analysis, $Si_{0.9}Ti_{0.1}C$ was selected from all Si_xTi_yC materials to perform these studies since this binary carbide exhibited the lowest pore size according to the BET analysis and therefore, which could present the highest gas diffusion limitations. In comparing results shown in Figure 7.4, it can be clearly observed that the higher the SiC and $Si_{0.9}Ti_{0.1}C$ load in the MPL, the lower is the cumulative pore volume. This description is especially accurate on Si_xTi_yC based MPLs, with a high decrease of this parameter when Si_xTi_yC loading in the MPL increases. This behaviour was expected because of the thicker carbides based layer and the change is more pronounced in the highest pore size range, which could be due to the agglomeration of the material. This process has been observed in previous works with

carbonaceous materials [21] and suggests that the highest load of SiC and Si_xTi_yC (6.0 mg cm^{-2}) should be avoided in the manufacturing of the MPL.

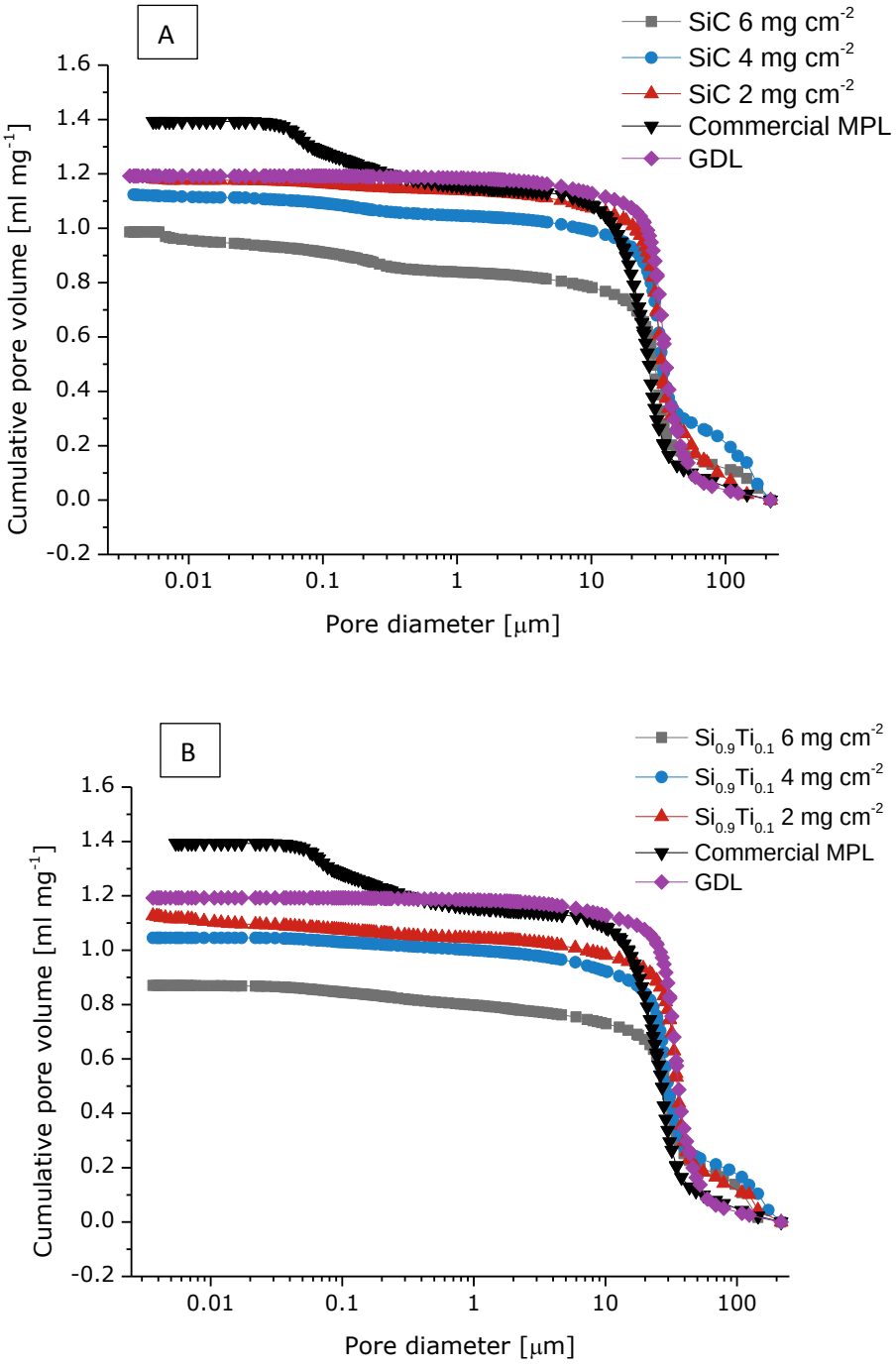

Figure 7.4. Porosity analysis of different SiC based MPLs, comparing the results with commercial GDL and GDL+MPL. A) Cumulative pore volume vs pore diameter of SiC based MPLs with different SiC loads; B) Cumulative pore volume vs pore diameter of $Si_{0.9}Ti_{0.1}C$ based MPLs with different loads.

Figures 7.5 A and 7.5 B compare the porosity and tortuosity of the different MPLs and GDL, respectively.

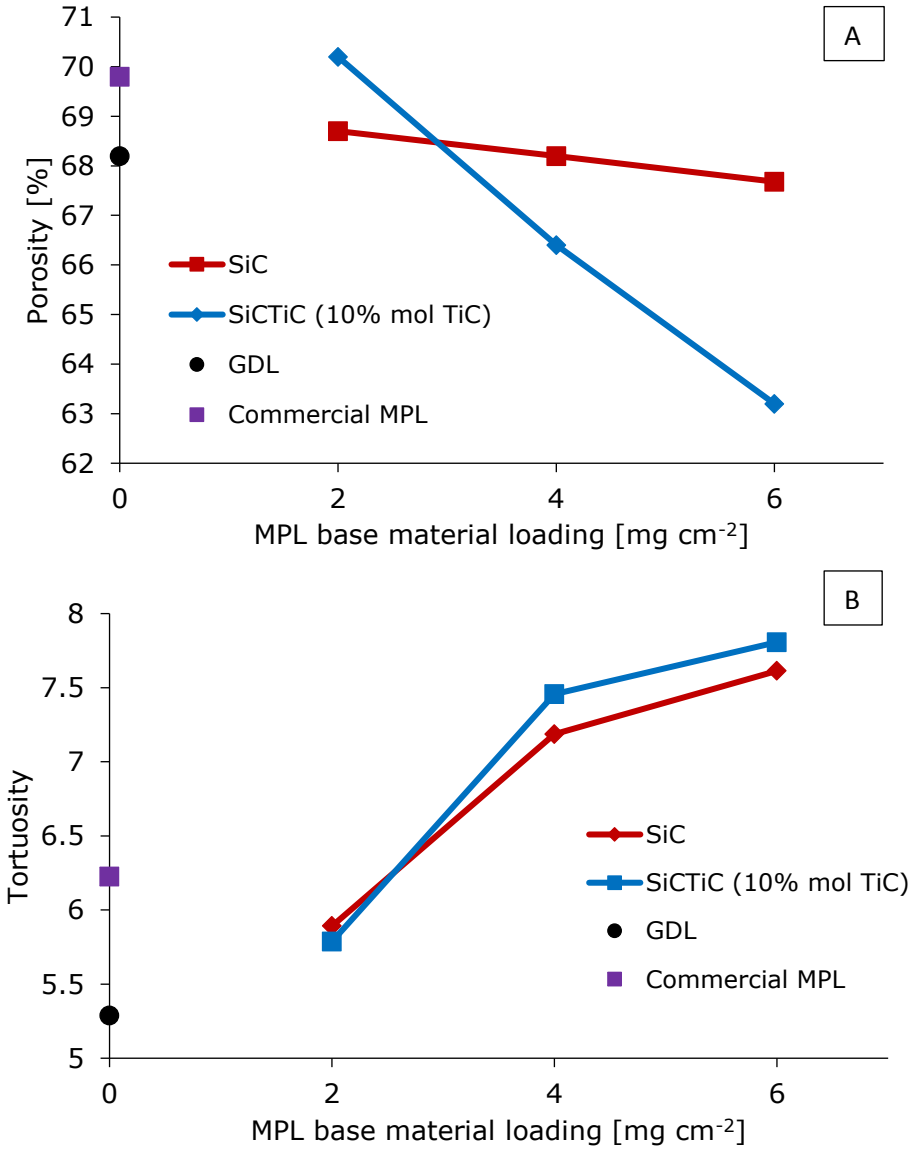

Figure 7.5. Evolution of porosity (A) and tortuosity (B) with the MPL material loading

As it is expected, as the SiC and $Si_{0.9}Ti_{0.1}C$ loads increase, the porosity decreases and the tortuosity increases. This observation can be explained in terms of the MPL intrinsic microporosity, which leads to a decrease in the overall porosity. On the other hand, higher loads mean a thicker MPL layer, which can block part of the macropores of the GDL,

leading to a decrease in the porosity and to an increase in the tortuosity [21]. As it is known, tortuosity can be defined as the ratio between the actual trajectories covered by the fluid when moving through the medium between two points and rectilinear one. As expected, higher amounts of base material lead to greater tortuosity for any fluid when it penetrates into the silicon carbide based electrode, especially in the Si_xTi_yC based MPL, which exhibits slightly higher tortuosity values at higher loadings, as compared to SiC. Nevertheless, the tortuosity values are similar (slightly higher) than others obtained in a previous work, where the influence of carbon load on the MPL was studied for HT-PEMFC[2].

The electrical conductivity was the next studied parameter. Part A of Figure 7.6 shows the electrical conductivities at different temperatures, measured for the electrodes prepared with SiC and Si_xTi_yC based MPLs (prepared with different loadings), and also the values measured for the commercial GDL with MPL Vulcan carbon, included for comparative purposes. In comparing results, it can be observed that the higher the load of SiC or Si_xTi_yC, the lower is the conductivity. It can also be seen that the addition of TiC to SiC has a positive influence in the electrical conductivity. In addition, in the cases of the MPLs with 2.0 mg cm^{-2} and 4.0 mg cm^{-2} of Si_xTi_yC, the electrical conductivities are comparable to the conductivity reached by the standard electrode with the carbon material.

On the other hand, the relative high electrical conductivity achieved by Si_xTi_yC and SiC MPLs prepared with the lowest material loading could be explained by taking into account that the surface of the GDL was not completely coated by the MPL, especially in the case of the SiC based MPL, as it was observed by XRD analysis, where the typical main carbon peak located at 26 º appeared in the non-carbonaceous based MPL. Then, these values could have been influenced by the carbon paper which acts as

GDL. Also, the thickness of these layers is low, which means that the provided electrical resistance is lower than the one of carbonaceous material based MPL, even if the non-carbonaceous materials are less conductive than carbonaceous one. This observation means that the conductivity of SiC based materials with loadings of 2.0 and 4.0 mg cm^{-2} are acceptably enough to be used in a HT-PEMFC. Part B of Figure 7.6 shows the electrical conductivity using higher amounts of TiC in Si_xTi_yC based MPLs. MPLs were prepared with a Si_xTi_yC load content of 4.0 mg cm^{-2}, in order to avoid the effects associates to the high conductivity value of the GDL.

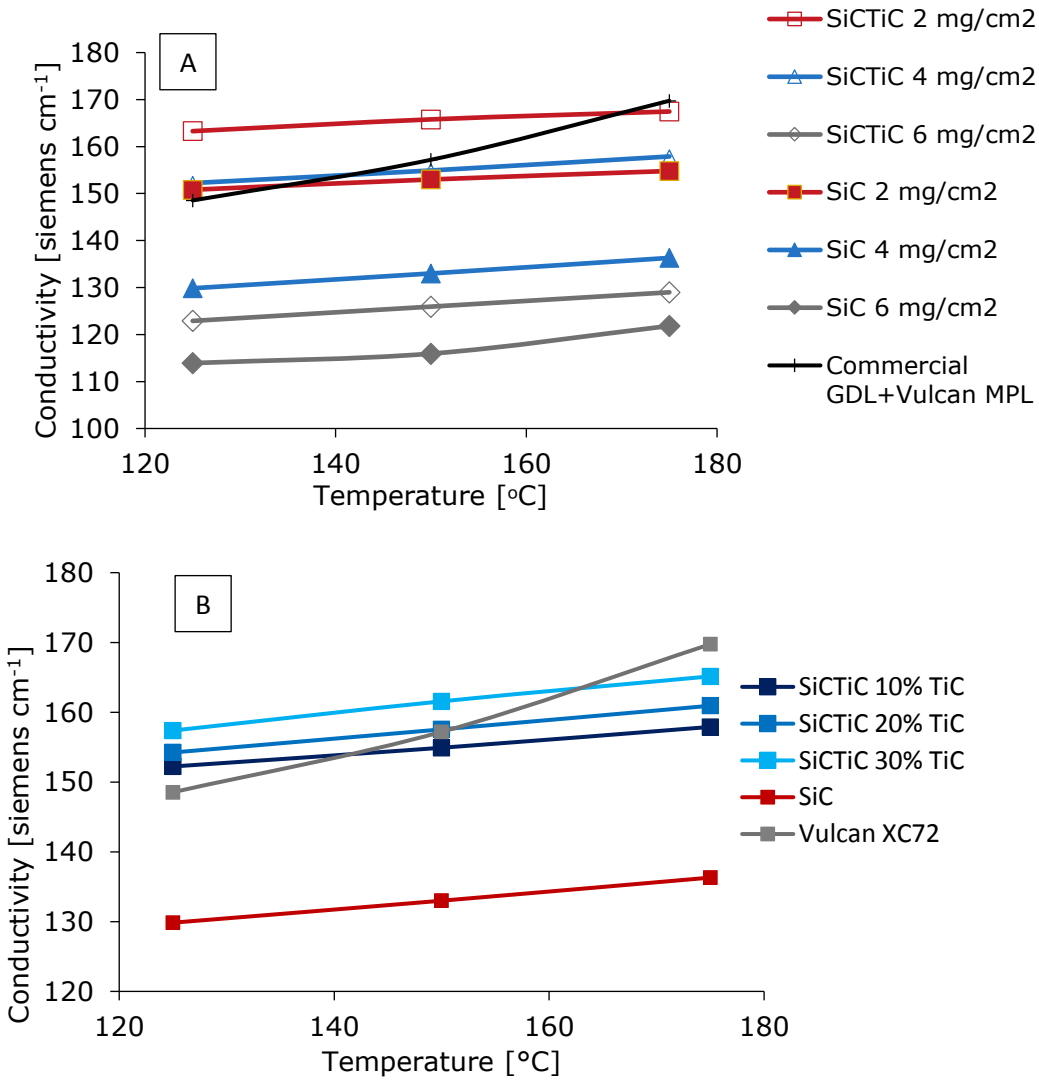

Figure 7.6. Electrical conductivity measured at different temperatures to different SiC and Si_xTi_yC based electrodes. A) Influence of the material loading in the conductivity values; B) influence of the TiC content in the Si_xTi_yC based electrodes

It can be observed that the higher is the TiC content on the binary carbide based MPL, the higher is the electrical conductivity. Thus, the positive influence of the addition of TiC to pure SiC pointed out in Part A is confirmed with the results of Part B of Figure 7.6.

As it has been pointed out previously, high stability of the components of the HT-PEMFC is a challenge, especially if it is taken into account the harsh operation conditions reached during HT-PEMFC performance, which combine acidic environment and high temperature. In order to assess the stability from the viewpoint of the high temperatures that undergo these systems, the MPL studied were subjected to a thermal treatment in hot acidic media. The samples were weighed to determine weight losses associated to the degradation of materials and no changes in the weight were found. XRD were also carried out to the MPLs before and after the thermal treatment. Table 7.2 shows the results of this characterization for SiC based MPLs. In the case of the MPL with standard Vulcan Carbon XC72, studied in Chapter 5 of this document, differences higher than 13% were found in the apparent crystal size before and after the thermal treatment. Conversely, variations lower than 8 % were found in the SiC based MPL with the lowest content of SiC, and lower than 5% for SiC based MPL prepared with higher SiC loadings (4 and 6 mg cm^{-2}). Nevertheless, it is important to take into account that in the case of MLP with 2.0 mg/cm^2, it was observed a higher degradation of the peak associated with GDL (carbon structure) (around 10%), which means that the MPL does not suffer important degradation despite of this lower amount of SiC cannot cover and protect the whole GDL surface. This fact could also explain the higher conductivity reached by SiC MPL prepared with the lowest SiC content, as it was pointed out previously.

On the other hand, Table 7.3 shows the same characterization parameters than Table 7.2, in this case for Si_xTi_yC based MPLs. As it can be observed, all MPLs showed

negligible changes in SiC main peak (between 0.5-2.5%) and in the carbon peak associated to GDL (lower than 4% variations of crystal size for lowest Si_xTi_yC loading). This means that this material, even when the thickness of the MPL is low, exhibits an excellent thermal and chemical stability under hot acidic environments, and it provides a good protection of the electrode.

The influence of the TiC content on this parameter was also studied for Si_xTi_yC based MPLs with 4.0 mg cm^{-2} of Si_xTi_yC. Figure 7.7 shows the XRD patterns of Si_xTi_yC based MPLs prepared with Si_xTi_yC with different TiC content. With comparison purposes, XRDs of standard Vulcan carbon XC72 before and after the thermal treatment are also shown. As it can be observed, all Si_xTi_yC materials exhibit similar evolution of the XRD patterns after the thermal tests. SiC main peak ($2\theta = 35.5^{o}$) suffers small changes in Si_xTi_yC based MPLs with higher TiC content, while the main carbon peak ($2\theta = 26^{o}$) is more appreciable, with high intensities reached also for higher TiC based MPL content. These facts could be explained by taking into account two different possibilities:

- The high density of TiC makes thinner the MPLs prepared with Si_xTi_yC.
- the lower changes suffered in the XRD peaks attributed to SiC or TiC crystallite faces (as compared to the changes observed in the same peaks for Si_xTi_yC with 10% mol TiC content) could be attributed to the lower BET area of SiC and Si_xTi_yC with 20 and 30 % of TiC, which, then, exhibit lower surface to the acid attack.

Furthermore, $Si_{0.7}Ti_{0.3}C$ based electrode exhibits an important change in the intensity of the carbon peak, which suffers a decrease of their apparent crystal size of nearly 8%. This means that this MPL does not provide the same good protection to the GDL than the other two MPL made with Si_xTi_yC materials. Finally, it can be pointed out that all Si_xTi_yC

materials improve the stability in hot acidic media of the electrode as compared to the standard Vulcan XC72 MPL.

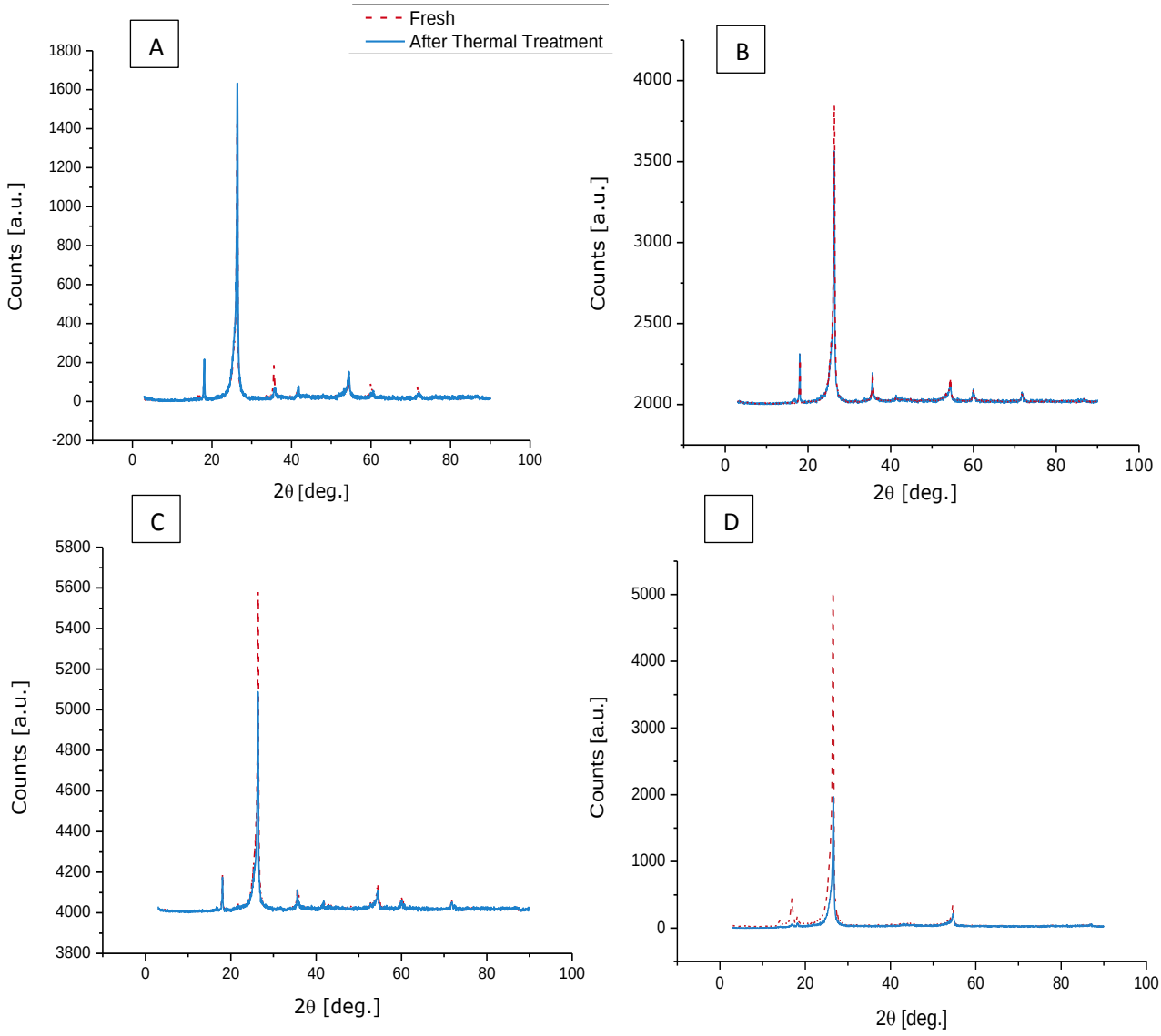

Figure 7.7. XRD patterns before and after the thermal stability study of different MPLs. A) $Si_{0.9}Ti_{0.1}C$ (4.0 mg cm^{-2}; B) $Si_{0.8}Ti_{0.2}C$ (4.0 mg cm^{-2}); C) $Si_{0.7}Ti_{0.3}C$ (4.0 mg cm^{-2}); D) Commercial GDL + Vulcan XC72 MPL (2.0 mg cm^{-2})

Finally, electrochemical resistance of the MPLs was evaluated by sequential cyclic voltammetry tests in PA media. Figure 7.8 shows the changes observed in the voltammograms during the tests carried out for MPLs prepared with 2.0, 4.0 and 6.0 mg cm^{-2} SiC and Si_xTi_yC based materials.

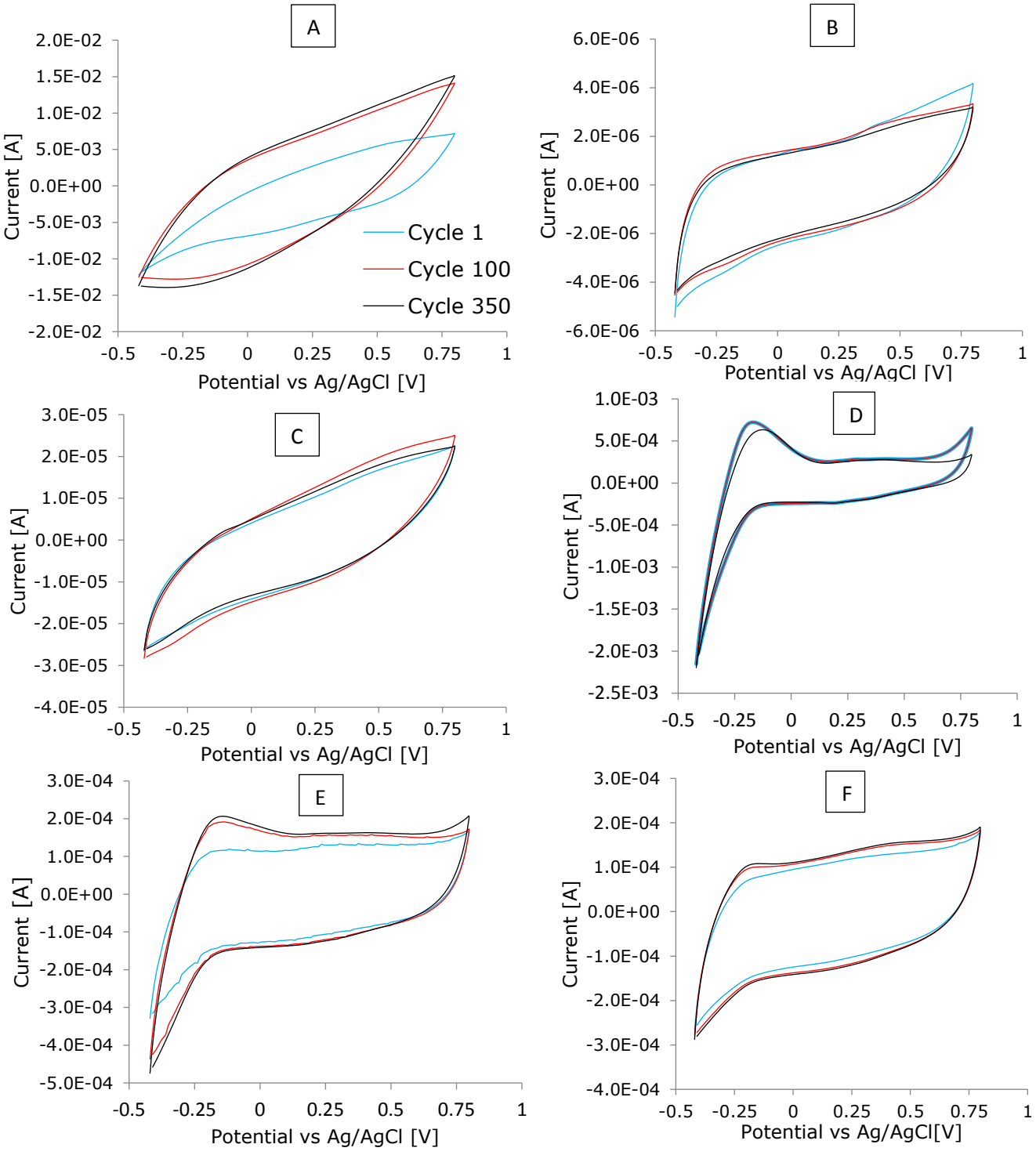

Figure 7.8. Evolution of the voltammetries obtained from the different SiC and SiCTiC MPLs based electrodes: A) SiC (2 mg cm^{-2}); B) SiC (4 mg cm^{-2}); C) SiC (6 mg cm^{-2}); D) $Si_{0.9}Ti_{0.1}C$ (2 mg cm^{-2}); E) $Si_{0.9}Ti_{0.1}C$ (4 mg cm^{-2}); F) $Si_{0.9}Ti_{0.1}C$ (6 mg cm^{-2}).

Changes in the voltammograms are indicative of the degradation of the electrode [6]. However, and opposite to many other studies about degradation of carbonaceous

electrodes, as SiC based materials do not present free carbon in their structure, the changes of the quinone-hydroquinone (Q-HQ) couple does not appear and, hence, they cannot be used as an indicator of the degradation of the surface [6, 22 ,23].

As it can be observed in Part A, the SiC based MPL prepared with the lowest load presents a high change on the shape of the cycle during the first 100 cycles. After that, it presents a very high stability during the rest of the test and changes were very small. This behaviour could be attributed to the presence of impurities on the surface (deposited before the experiment) that are removed with the initial voltammetries, rather than to a low stability. As it was pointed out previously, the formation of the Q-HQ peak, at 0.40 V approx. (vs Ag/AgCl), was not observed in the anodic CV curve (as occurred in the case of the electrodes prepared with different carbonaceous materials, which is indicative of surface oxidation [24]). This means that the carbonaceous GDL is not suffering several damages during the test, which confirms the protection provided by the non-carbonaceous MPLs. However, the higher current and double layer values achieved by SiC based electrode suggests that the GDL probably is located closely to the external surface of the electrode. This fact, in accordance with the electrical conductivity measurements, confirms that the lowest SiC or Si_xTi_yC loading (2 mg cm^{-2}) , especially in the case of SiC, should be avoided in the manufacturing of non-carbonaceous based MPLs for electrodes for HT-PEMFCs, in order to warrant the properly covering and protection of the GDL.

In the case of the MPL prepared with 4.0 and 6.0 mg cm^{-2} of SiC and Si_xTi_yC, the CVs did not change during the tests, which means that these electrodes show a very good electrochemical stability. Furthermore, in the case of Si_xTi_yC based electrodes, in all cases a small peak appears in the region of H_2 desorption, which could mean that this binary

carbide could demonstrate a slight catalytic activity. Nevertheless, this peak was just noticed during the first experiments of Si_xTi_yC voltammetric studies.

It must be pointed out that this particular characteristic decreases with the Si_xTi_yC load, as it can be observed in Figure 7.8 parts D, E and F. The high stability of these non-carbonaceous MPLs under electrochemical corrosion can be confirmed also by the XRD parameters obtained from the samples after the cyclic voltammetries, and shown in Tables 7.2 and 7.3. As it can be observed, the changes of apparent Lc in the case of SiC samples are very low as compared to the Lc variation in the case of Vulcan carbon presented in Chapter 5 (more than 25% of crystal size change). Not new peaks were detected which indicates the absence of oxides or the formation of another substances on the surface of the electrodes did not occur [6, 22, 23].

Figure 7.9 shows the same test performed to different electrodes with MPLs prepared with Si_xTi_yC with 10, 20 and 30% TiC, using a Si_xTi_yC load of 4.0 mg cm^{-2}. This load, according to the previous results, was found to be the optimum for all SiC based MPLs, because of its good balance among protection, electrical conductivity and stability.

Results show that, same in the thermal studies, all Si_xTi_yC materials exhibit similar behaviour under the electrochemical tests, presenting an excellent stability, with negligible changes in the shape of the voltammograms over the tests. It must be pointed that Si_xTi_yC did not show in this second test (or in further tests performed), a peak in the H_2 desorption region. However, the shape, the double layer contribution and the crystal size evolution after the test (around 1.4% for main carbon peak and lower than 1% for SiC main peak) was closely similar to the results achieved during the first test. This confirms the reproducibility of the results in terms of stability.

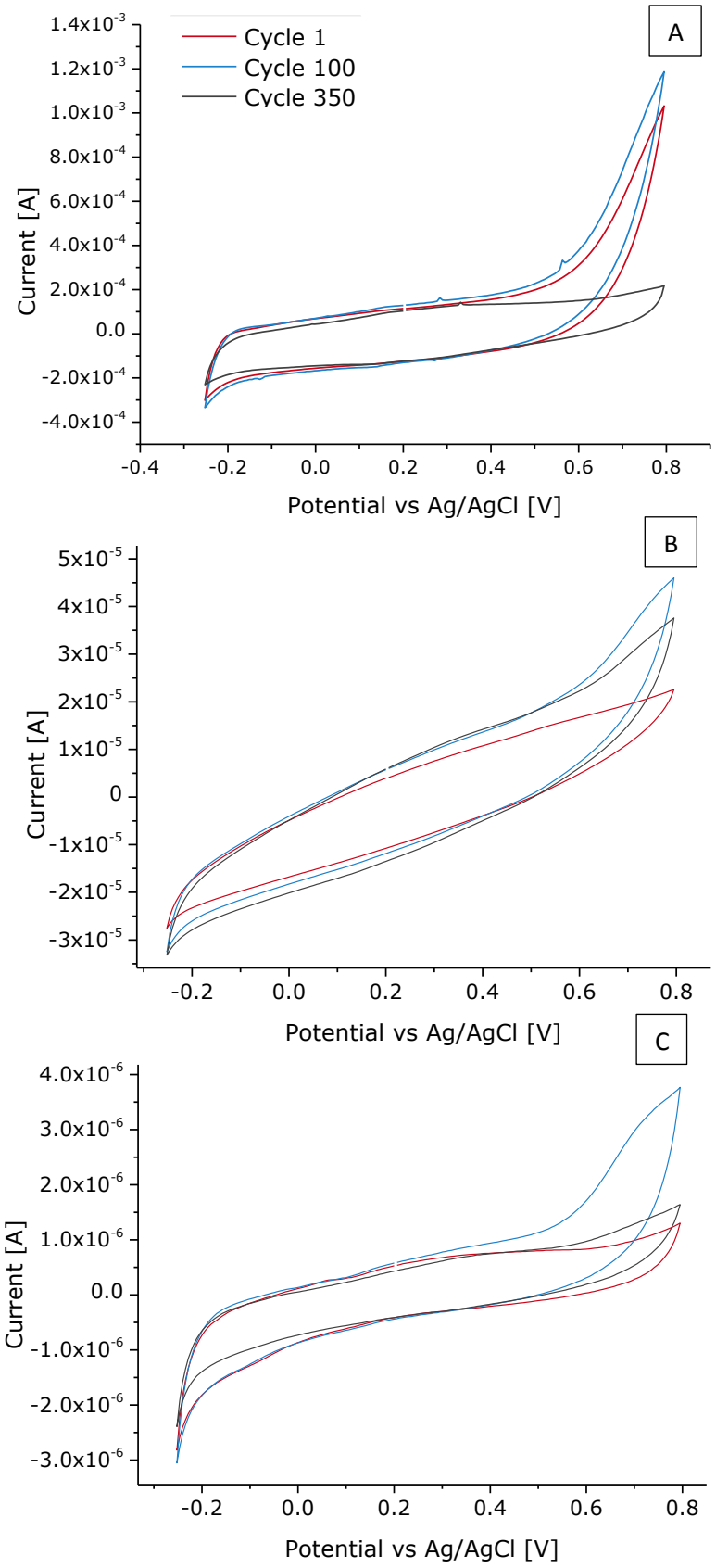

Figure 7.9. Evolution of the cyclic voltammograms during the electrochemical stability test for different Si_xTi_yC based MPLs (load 4.0 mg cm^{-2}): A) $Si_{0.9}Ti_{0.1}C$; B) $Si_{0.8}Ti_{0.2}C$; and C) $Si_{0.7}Ti_{0.3}C$.

$Si_{0.8}Ti_{0.2}C$ and $Si_{0.7}Ti_{0.3}C$ based MPLs presented the same range of crystal size evolution (around 1% of carbon peak changes, lower than 0.7 % in the case of SiC crystal size), which means that the TiC content does not have a significant influence on this parameter. Furthermore, because of the decrease in the BET area, the low double layer contribution of Si_xTi_yC based electrodes containing higher amounts of TiC is very noticeable.

7.3.3 HT-PEMFC results

Once the electrodes were characterized and the thermal and electrochemical degradation characteristics were evaluated, short lifetests with the SiC and Si_xTi_yC based electrodes were performed in a single cell. According to the ex-situ characterization, the base material loading used in the MPLs manufacturing was 4 mg cm^{-2}. At this point, it should be taken into account that it is not an optimized assessment but just a first proof of concept, in which harsh conditions (in terms of monitoring) are going to be applied. It must also be pointed out that $Si_{0.8}Ti_{0.2}C$ and $Si_{0.7}Ti_{0.3}C$ were not considered to be suitable to be used as MPL because of their lower microporosity values observed in BET analysis and because only the electrical conductivity was affected in a positive way by using higher amounts of TiC. Then, it was decided that, no tests were going to be applied to these materials at this time. Taking into account this comment, Figure 7.10 shows the evolution of the cell voltage of the different MEAs tested during the lifetests.

Three characterization protocols were carried out throughout the essay, as detailed in the Section 7.2 of this document. The initial voltage of the fuel cell prepared with SiC based MPL was close to 0.40 V and it decreased continuously during the lifetest. At the end of experiment, the degradation rate of the fuel cell was around 470 μV h^{-1}. When this value is compared with other previously shown in the literature, it can be stated that this

value is excessively high. Thus, for PBI-based membranes, degradation rates measured in previous studies were 14 μV h^{-1} and 250 μV h^{-1} [25], 194.2 μV h^{-1} [26] and 25 μV h^{-1} [27]. However, it must be pointed out that during the essay, different electrochemical characterization tests (polarization curves with air and with oxygen, EIS at different current densities with air and with O_2, CVs and LSVs) were performed, which could have contributed to accelerate the degradation of the performance of the fuel cell.

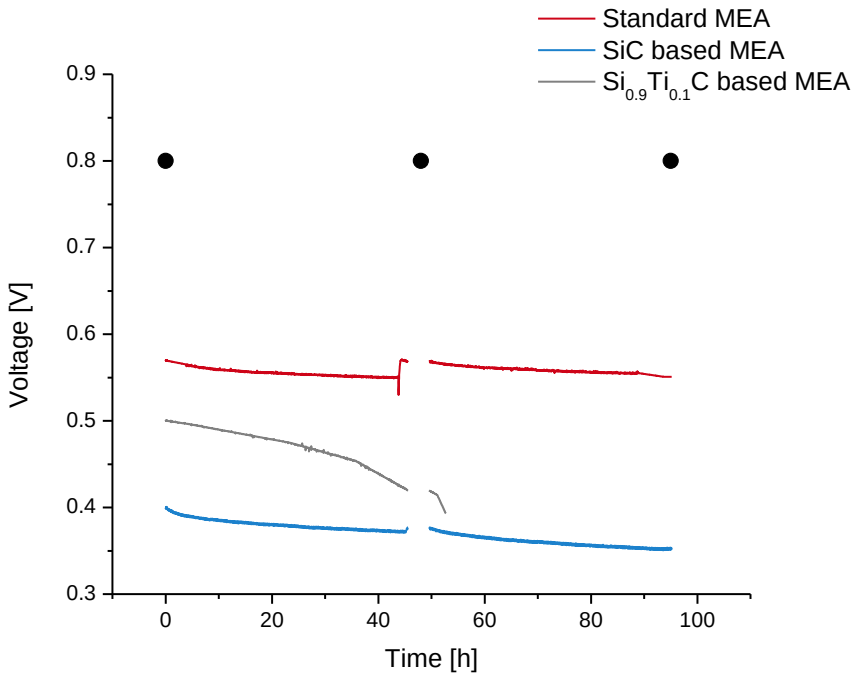

Figure 7.10. Evolution of fuel cell voltage of the different preliminary short-term lifetests. Black dots marks the different characterization tests performed.

Regarding the MEA prepared with $Si_{0.9}Ti_{0.1}C$ based MPL, it exhibited a very high degradation rate during the preliminary lifetest, with a voltage drop close to 2000 μV h^{-1}, with an acceptable starting voltage value around 0.50 V, which after only a few hours decreased down to 0.40 V. Because of this bad performance, it was decided to stop the experiment at this point, because additional data would not be relevant.

Voltage values achieved by non-carbonaceous materials are lower than the voltage achieved at 0.2 A cm^{-2} for the standard Vulcan carbon based MEA (which shows voltages around 0.56 V). However, it must be taken into account that these SiC based materials have not been tested previously in HT-PEMFCs and, hence, the system is not optimized for it. This means that, undoubtedly, it could be possible to increase the voltage values by reducing the PTFE amount, or with a doping process of the Si_xTi_yC, increasing its electrical conductivity.

The high degradation rate observed could be attributed to the low porosity. As it was pointed out in Table 7.1, this material exhibits a microporous character, with small average pore size, which makes difficult the gas diffusion through the electrode. Then, oxygen cannot access easily to the reactive centres of the catalytic layer. In addition, these micropores can be blocked during the test by the H_3PO_4 or by impurities, making even worse the diffusion of oxygen. This explanation could justify the increase of the voltage drops with time in the case of $Si_{0.9}Ti_{0.1}C$ based MEA. In this sense, MEAs prepared with this material probably could work better in the anode side (because of the better transport of hydrogen), or with a lower loading, which could help to the improve diffusion of the reactants, as it was already shown in Figure 7.4, during the ex-situ characterization.
Same conclusions can be drawn for the SiC based MEA, but taking into account the low voltage of this MEA, and the linear behaviour o-f the system during the tests, in this case the low performance can be attributed to the low electrical conductivity of the material rather than to the worse porosity of the system.

Results obtained in the different polarization curves carried out with air and oxygen are shown in Figure 7.11. The maximum power density values were about 100 mW cm^{-2}, when the fuel cell was operated with oxygen, and 79 mW cm^{-2}, when air was used as oxidant, for the case of SiC based MEA. These values are much lower than values

obtained for standard MEA, around 400 mW cm^{-2} with a standard carbonaceous support, as it can be observed in Part C of Figure 7.11. However, this power density values are higher than others reported recently in the literature when new materials for HT-PEMFCs have been tested.

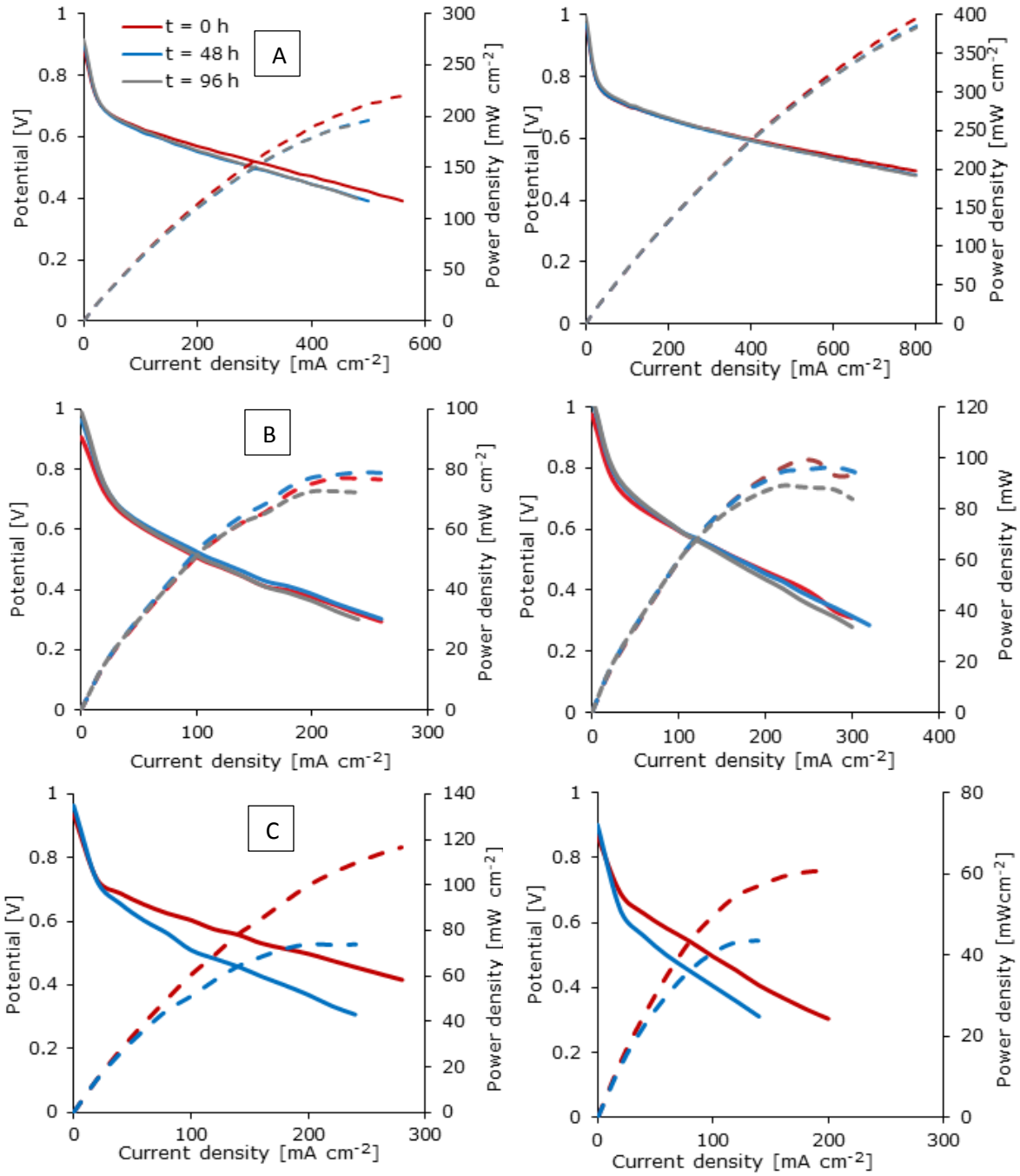

Figure 7.11. Evolution of polarization curves performed to the different MEAs tested. A) Standard Vulcan carbon MEA; B) SiC based MEA; C) $Si_{0.9}Ti_{0.1}C$ based MEA. Discontinuous plots correspond to the power density curves associated to each polarization curve. Left pictures correspond to the curves performed with air; right one, polarization curves performed with oxygen.

Thus, Kurdakova [27] reported power densities around 75 mW cm^{-2} operating with air, at 150 ºC and 0.5 mg Pt cm^{-2} in both electrodes and testing new PBI based membranes in a 5 cm^2 single cell. Ossiander [28] reported only values around 33 mW cm^{-2} operating at 160 ºC and testing new membranes in a 50 cm^2 single cell. No information about the catalyst loading was reported. Regarding to the $Si_{0.9}Ti_{0.1}C$ based MEA, as it was expected due to the high degradation rate achieved during the lifetests, the performance of this MEA experimented a decrease higher than 40% in terms of maximum power density achieved with oxygen.

When air is used as oxidant, the performance of the non-carbonaceous based MEAs is much worse than that achieved with the standard Vulcan carbon MEA. This fact points out again the negative effect of the low porosity of the SiC based materials, which is magnified because of the lower content of oxygen in air. In addition, during the lifetests, the power density decreased 9.7 % when oxygen was used and 5.5 % with air for SiC based MEA. Regarding to the standard MEA, power density drops were 12.4% and 3%, respectively.

Over the lifetests, all MEAs shown very good open-circuit voltage values at 0.0 A/cm^2, indicating that not short circuits, electrical losses or damages in the membrane occurred, which means that the degradation of the material can be attributed only to the electrodes.

As it was pointed out above, during the lifetests, impedance analyses were also carried out at different operation times. Figure 7.12 shows the Nyquist plots of the MEA with SiC based electrodes. For comparison purposes, in Figure 7.12 the Nyquist plots of a MEA with standard Vulcan carbon based electrodes, measured under the same operation conditions and with the same equipment is also shown.

In order to know further, an equivalent circuit R(RQ)(RQ) was used to model the impedance data in this work [29-31]. The parameters obtained after mathematical fitting are shown in the Table 7.4. The high frequency resistance is typically explained in terms of the sum of the ohmic resistances of the electrolyte, membrane and the electrical resistance of the electrodes (GDL + MPL, mainly) and bipolar plates. Since all components are the same except the electrodes, the differences can be attributed only to them.

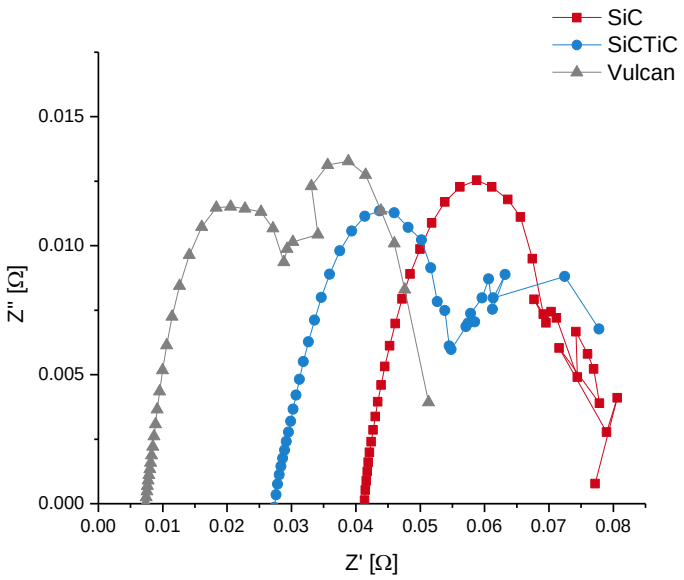

Figure 7.12. Nyquist plots obtained from the impedance data at 0.2 A cm^{-2} performed with air for the different MEAs tested.

It can be observed that this high frequency resistance is higher in the case of the SiC based electrodes than in the standard carbon based electrodes. Ohmic resistance values around 1.0 Ω cm^2 were obtained for the SiC based electrodes, which are five times higher than the values obtained under the same operation conditions with standard Vulcan carbon based electrodes (around 0.2 Ω cm^2). $Si_{0.9}Ti_{0.1}C$ based MEA values are around 650 mΩ cm^2. Thus, it seems that the SiC based materials do not behave in a HT-PEMFC as a good electrical conductor, as it was expected from the results showed in Figure 7.6,

and suggests that probably better results can be attained by using lower SiC materials loadings during the MPL manufacturing. Furthermore, the semicircle observed in the Nyquist plot is explained in terms of the charge transfer resistance (R_{CT}) and can be related to the oxygen reduction reaction (ORR) activation in the cathode catalyst layer. The electrodes prepared with the SiC based MPL show a higher R_{CT} as compared to the carbonaceous supported MPL (0.6 Ω cm^2 vs 0.45 Ω cm^2 for the standard one). These values are higher, although it has to be accounted that the novel SiC based electrodes are not optimized in terms of the overall composition, the ratio ionomer/SiC, the amount of phosphoric acid, etc. $Si_{0.9}Ti_{0.1}C$ based MEA showed a very high increase of this parameter during the first 48 hours, which is a clear indication of problems related with the catalyst. This could mean that, in this case, the Pt/Vulcan catalyst used in this MEA could have undergone damages during the assembling or catalytic layer manufacturing.

Table 7.4. Evolution of the different resistances obtained from the fitting of EIS data to a model R(RQ)(RQ)

		Air			Oxygen		
MPL	Time (h)	Rohm	Rct	Rmt	Rohm	Rct	ECSA
		mΩ cm^2	mΩ cm^2	mΩ cm^2	mΩ cm^2	mΩ cm^2	$m^2\,gPt^{-1}$
SiC	0	1047	790	561	1087	646	15.1
	46	1090	929	620	1175	620	14.2
	100	1192	936	606	1270	678	12.9
Vulcan XC-72	0	184	402	867	182	446	27.9
	46	194	488	707	198	465	22.9
	100	203	514	576	200	458	22.6
$Si_{0.9}Ti_{0.1}C$	0	682	883	1354	626	451	10.3
	46	-	-	-	640	1155	6.8
	100	-	-	-	-	-	-

On the other hand, at low frequency, another arc appears in the EIS that may be related to the mass transport limitations. It can be clearly observed that in the case of the SiC based MEA, this arc is much smaller than that of the Vulcan carbon based electrodes. This could mean that the SiC based MPL improves the mass transfer and it is more beneficial at high current conditions. Nevertheless, despite this good prospect from the mass transfer viewpoint, the worse performance attained with the SiC based MEA can be explained in terms of the low electrical conductivity of the material. The $Si_{0.9}Ti_{0.1}C$ based MEA shows a very high mass transfer resistance, which confirms the bad diffusion of the reactive gas through the MEA, and, in turn, could explain the high voltage drops achieved with this MEA. This fact could be overcome with the usage of $Si_{0.7}Ti_{0.3}C$. This material, as it was pointed out in Table 7.1, exhibited higher average pore size, which could solve the mass transfer problems compared with the $Si_{0.9}Ti_{0.1}C$, but taking into a count that the absence of micro porous could makes less effective the gas distribution through the electrode surface.

Table 7.4 also shows the changes in the ECSA (Electrochemical Surface Area) during the lifetests, obtained from the cyclic voltammetries. Cycles obtained at t = 0 h are shown in Figure 7.13 for comparison purposes, because in this cycle the region used to calculate the ECSA is more clearly seen and, hence, more details can be discussed.

Regarding the SiC based MEA, at the beginning of the lifetest, a value of 15.04 $m^2 g^{-1}$ was obtained. This value is not high but it is fully comparable to others shown in the literature (above 19.4 m^2g^{-1}) [22]. However, there is a significant decrease throughout the test, obtaining a non-negligible percentage of degradation of 14.3%, which cannot only be related to the material but also to the three protocol tests applied during the lifetests. As commented before, they may cause a more pronounced degradation of the performance than that reported by other authors who made a less aggressive

characterization during the lifetests. Nevertheless, this is not a good result, because stability was the main feature looked for in this research and, although off-site tests were promising, lifetest yields less interesting results in terms of feasibility of the application of this novel material.

Regarding the $Si_{0.9}Ti_{0.1}C$ based MEA, Figure 7.13 clearly shows that the observable peak is much lower, which suggests possible problems related to the catalytic layer. As it can be observed in Table 7.2, the starting ECSA value for this material is around 10 $m^2\ g^{-1}$, which is 50% lower than that observed for the standard Vulcan carbon MEA. Since the catalytic layer on the anode side is the same, the low performance achieved during the test could only be related with the degradation of this layer and, hence, it can be stated that performance of this combined $Si_{0.9}Ti_{0.1}C$ material is even worse than that of the SiC, which was not found to be a good replacement for Vulcan Carbon.

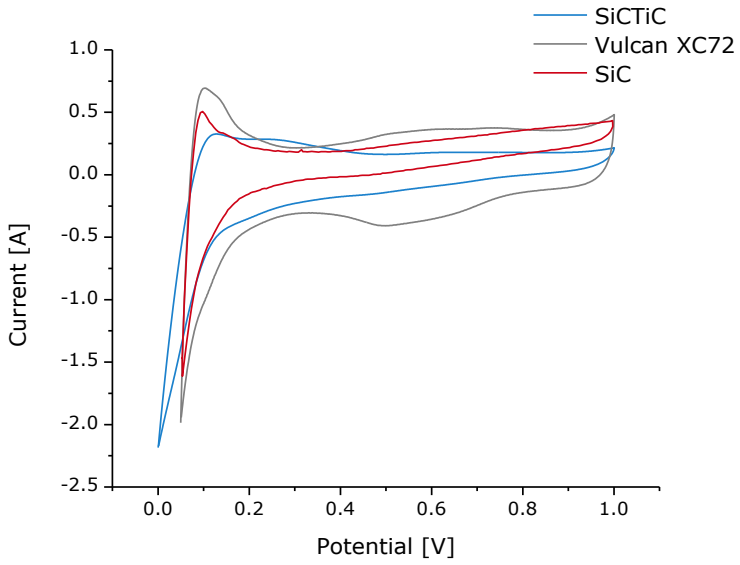

Figure 7.13. Cyclic voltammograms obtained at t = 0 h for the different MEAs tested.

Finally, from the linear sweep voltammetries, evolution of crossover and internal resistance were calculated at E = 0.30 V. Results are shown in Figure 7.14. As it can be

observed, results are in agreement with the high OCV achieved during the polarization curves. All MEAs exhibit high internal resistance values, between 10 and 38 Ω, and no severe changes appeared on this parameter along the tests for all MEAs.

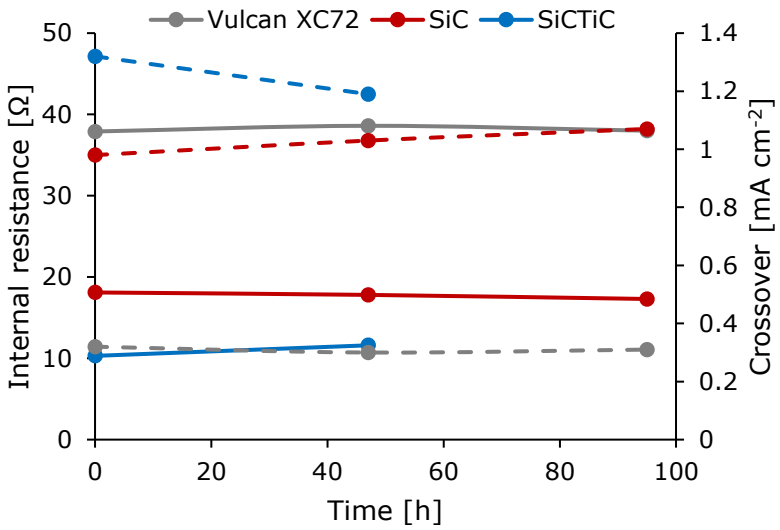

Figure 7.14. Internal resistance and crossover obtained from the different LSV performed to the MEAs during the characterization tests.

This fact suggests that the PBI membranes did not suffer damage during the preliminary short lifetests. This fact can be also confirmed with the very low values of crossover, between 0.3 and 1.2 mA cm^{-2}. This means that the membrane did not allow the electron crossing during the experiments, which is a sign of the good condition of the membranes during the tests.

7.4. Conclusions

Taking into account the results discussed, the following conclusions can be drawn:

- The electrical conductivity decreases with the SiC and Si_xTi_yC content in the MPL. The conductivity for the two lowest contents is comparable to the

conductivities obtained with the carbon based MPL, although this value could be attributed to a bad GDL covering of the non-carbonaceous based MPLs.

- On one hand, the usage of higher amounts of TiC content on the binary carbide increases the electrical conductivity of the material. On the other hand, BET area of the binary carbide decreases, since the microporosity of the Si_xTi_yC goes lower with the increasing of TiC percentage.
- Under the applied experimental conditions, non-carbonaceous based MPLs with 4.0 and 6.0 mg cm^{-2} showed much better thermal and electrochemical stability than carbonaceous based MPLs.
- The electrode prepared with a SiC based MPL shows a very high ohmic resistance which contributes to worse fuel cell performance. The high electrochemical and thermal resistance of these materials does not improve fuel cell performance because it is less important than the low conductivity. This confirms SiC as a promising material that can be used in HT-PEMFCs technology although much work must be carried out in order to improve both the fuel cell performance and durability. Currently, these materials cannot be recommended to substitute Vulcan Carbon in MPLs.
- $Si_{0.9}Ti_{0.1}C$ based MPL exhibit very low gas permeability, which is traduced in a low FC performance. Further investigations, such as testing this materials as MPL on the anode side since with hydrogen these materials could present lower mass transfer limitations, or testing a $Si_{0.7}Ti_{0.3}C$ based MPL since this material presents higher average pore size must be performed in order to optimize a MPL prepared with this material.

7.5. Bibliography

[1] A. Minjeh, C. Yong-Hun, C.Yoon-Hwan, K. Jinho, J. Namgee, S. Yung-Eun, Electrochimica Acta 56 (2011) 2450.

[2] J. Lobato, P. Cañizares, M. A. Rodrigo, D. Úbeda, F. J. Pinar, J. J. Linares, Fuel Cells 10 (2010) 770.

[3] Q. Li, D. Aili, H. A. Hjuler, J. O. Jensen, High Temperature Polymer Electrolyte Membrane Fuel Cells, ISBN 978-3-319-17081-7, Springer (2016).

[4] P. Sehkyu, L. Jong-Won, B. N. Popov, Journal of power sources 163. 2006, 357.

[5] E. Passalacqua, G. Squadrito, F. Lufrano, A. Patti, L. Giorgi, J. Appl. Electrochem. 31 (2001) 449.

[6] B. Avasarala, R. Moore, P. Haldar, Electrochimica Acta 55 (2010) 4765.

[7] Y.Park, K. Kakinumaa, M. Uchidaa, H. Uchidab, M. Watanabea, Electrochimica Acta 123 (2014) 84.

[8] N. Linse, G. G. Scherer, A. Wokaun, L. Gubler, Journal of Power Sources 219 (2012) 240.

[9] J. Park, S. Yima, T. Kima, S. Parka, Y. Yoona, G.Park, T. Yanga, E. Park, Electrochimica Acta 83 (2012) 294.

[10] Y.-C. Park, K. Kakinuma, M. Uchida, H. Uchida, M. Watanabe, Electrochimica Acta 123 (2014) 84.

[11] S. Gianella, D. Gaia, A. Ortona, Advanced Engineering Materials 14 (2012) 1074

[12] Y. Liu, B. de Tymowski, F. Vigneron, I. Florea, O. Ersen, C. Meny, P. Nguyen, C. Pham, F. Luck, C. Pham-Huu, ACS Catalysis, 3 (2013) 393.

[13] A. Walcarius, Chemical Society Reviews, 42 (2013) 4098.

[14] R. Dhiman, E. Johnson, E.M. Skou, P. Morgen, S.M. Andersen, Journal of Materials Chemistry A, 1 (2013) 6030.

[15] Y. Shao, G. Yin and Y. Gao, J. Power Sources, 171 (2007) 558.

[16] B. Avasarala, T.Murray, W.Z.Li, P.Haldar, J. Mater. Chem. 19 (2009) 1803.

[17] S.B. Yin, S.C. Mu, H.F. Lv, N.C. Cheng, M. Pan, Z.Y. Fu, Appl. Catal. B 93 (2010) 233.

[18] S.Y. Huang, P. Ganesan, S. Park, B.N. Popov, J. Am. Chem. Soc. 131 (2009) 13898.

[19] P. Nguyen, C. Pham, Applied Catalysis A: General, 391 (2011) 443.

[20] V. Jiménez, A. Nieto-Márquez, J.A. Díaz, R. Romero, P. Sánchez, J.L. Valverde, A. Romero, Industrial & Engineering Chemistry Research, 48 (2009) 8407.

[21] J. Lobato, P. Cañizares, M. A. Rodrigo, C. Ruíz-López, J. J. Linares, Journal of Applied ElectroChemistry 38 (2008) 793.

[22] K.H. Kangasniemi, D.A. Condit, T.D. Jarvi, J. Electrochem. Soc. 151, 2004, E125.

[23] E. Passalacqua, P.L. Antonucci, M. Vivaldi, A. Patti, V. Antonucci, N. Giordano, K. Kinoshita, Electrochimica Acta 37 (1997) 2725.

[24] M.F. Mathias, R. Makharia, H.A. Gasteiger, J.J. Conley, T.J. Fuller, C.J. Gittleman, S.S. Kocha, D.P. Miller, C.K. Mittelsteadt, T. Xie, S.G. Yan, P.T. Yu Electrochem. Soc. Interface, 14 (2005) 24.

[25] S. Yu, L. Xiao, B.C. Benicewicz, Fuel Cells, 3 (2008) 165.

[26] J. Lobato, P. Cañizares, M. A. Rodrigo, D. Úbeda, J. J. Linares, Journal of Power Sources 196 (2011) 8265.

[27] V. Kurdakova, E. Quarterone, P. Mustarelli, A. Magistris, E, caponetti, M.L. Saladino. J. Power Sources 195 (2010) 7765.

[28] T. Ossiander, C. Heinzl, S. Glech, F. Schönberger, P. Völk, M. Welsch, C. Scheu. J. Membrane Science 454 (2014) 12.

[29] J. Lobato, P. Cañizares, M.A. Rodrigo, J.J. Linares, D. Úbeda, F.J. Pinar, Fuel Cells 10 (2010) 312.

[30] J. Zhang, Y. Tang, C. Song, J. Zhang, Journal of Power Sources 172 (2007) 163.

[31] X. Yuan, H. Wang, J.C. Sun, J. Zhang, International Journal of Hydrogen Energy 32 (2007) 4365.

CHAPTER 8. Evaluation of non-carbonaceous materials as catalyst support for HT-PEMFC

8.1 Introduction and Objectives

As it was pointed out in Chapter 6, Proton Exchange Membrane Fuel Cell (PEMFC) technology has a main drawback related to the reduction of the usage of platinum on the electrocatalyst to become an alternative to combustion engines in the near future. In this sense, two different approaches are being faced to meet this goal. The first consists of reducing of the catalyst usage through increasing platinum utilization in the catalyst layers. This approach can be achieved by alloying Pt with inexpensive metals such as Co, Fe, etc and/or by utilizing durable support materials for Pt nanoparticles deposition, with the aim of protecting the catalyst and maximizing the access of reactants to its surface. The other approach is to develop non-precious metal-based electrocatalysts materials [1], although currently, progresses in this later topic are very scarce, and hence most of the research efforts are focused on the better utilization of platinum, mainly through the improvement of the supporting materials. It is known that supported Pt catalyst improves the Pt utilization. Regarding to the support, surface area, porosity, electrical conductivity, electrochemical stability and surface functional groups are the main desired characteristics for it [2]. It is also well known that the typically used carbon supporting materials may undergo oxidation under the physical, chemical and electrochemical conditions produced at both electrodes in the fuel cell [2-4]. Especially, the higher voltages achieved during the start-up and shut-down processes are known to have a very high impact on the corrosion of the carbonaceous based materials of the electrode [5-6]. Due to the harder environmental and operational conditions of the HT-PEMFCs, the degradation rate attained by the MEA components is more several, which means that the development of new materials with enhanced service lifetime in these aggressive conditions (oxides, carbides…) to increase the durability of the catalyst are a very important target for current research in HT-PEMFC. An interesting overview about them can be found elsewhere [2]. Especially, Si, Ti and W based oxides, carbides or borides have

focused much attention in the recent years for being used as electrocatalyst supports for fuel cell applications, achieving promising results in terms of durability and performance [7-10]

In this Chapter, non-carbonaceous materials based on silicon carbide and binary silicon titanium carbides (SiC, and Si_xTi_yC) are going to be developed and tested as catalyst supports for the cathode layer in HT-PEMFC running with phosphoric acid doped PBI membranes. Several authors have tested previously SiC based materials [4, 11] as catalyst support for electrodes in low temperature PEMFCs (Nafion- based PEMFCs). Although, to the author's knowledge, this has never being the case for PBI based HT-PEMFCs [12].

8.2. Methodology

8.2.1. Catalyst synthesis

All non-carbonaceous catalyst supports used in this work (SiC and the composite Si_xTi_yC with 10, 20 and 30% mol TiC content, represented by molecular formulas $Si_{0.9}Ti_{0.1}C$, $Si_{0.8}Ti_{0.2}C$ and $Si_{0.7}Ti_{0.3}C$, respectively) were provided by SICAT Company (Paris, France). These materials were used as received. More information about these materials was provided in the Chapter 7.

The catalyst synthesis method consists of the deposition of platinum from a precursor salt (chloroplatinic acid hexa-hydrate, Sigma-Aldrich). To prepare a batch of 1.0 g of catalyst, 600 mg of support (SiC, Si_xTi_yC or Vulcan for comparison purposes) were added to a 500 mL of 0.1 M formic acid solution (98 %, Panreac) and the mixture temperature was raised to 80 °C. Then, 21.2 mL of a 50 mg ml^{-1} chloroplatinic acid hexa-hydrate solution were added very slowly, and the mixture was kept under agitation at 80 °C for one hour. Then, the suspension was left to cool at room temperature and the solids were filtered and dried.

After the drying processes, the catalyst powders were weighed and characterized. The target concentrations of platinum in the catalyst were 20 and 40% wt., in order to evaluate

the influence of the Pt amount on the Pt particle size and dispersion of the metallic particles, trying to determine the optimum platinum loading.

8.2.2 Physicochemical characterization

To evaluate the efficiency of the catalyst synthesis, inductively coupled plasma mass spectrometry (ICP-MS) analyses were carried out to calculate the real Pt content deposited on the catalysts.

In order to evaluate the crystallite properties of the Pt particles in the different catalysts synthetized, X-Ray Diffraction (XRD) analyses were performed on a Philips PW-1700 diffractometer with rotating anode, applying Kα corresponding to the transition from copper radiation for different samples. Transmission Electron Microscopy (TEM) analyses were performed to get more information about the dispersion of the Pt particles through the catalyst support. TEM analyses were carried out on a Jeol JEM 2100 TEM operating at 200 kV with an Orius (2x2 MPi) Gatan Digital Camera. Specimens were prepared by dispersing the samples in acetone and depositing a drop onto a C-coated Cu grid. TEM images were analyzed using Digital Micrograph software from Gatan. Temperature Programmed Reduction (TPR) experiments were carried out to different catalysts prepared with the objective to evaluate the presence of Platinum oxides, which indicates the efficiency of the method in terms of metal reduction of the Pt precursor.

8.2.3 Electrochemical characterization

First, a voltammetric study was carried out in a half-cell system, using different electrodes manufactured with these catalysts. The electrodes consisted of a commercial carbon cloth GDL with Vulcan XC72based MPL deposited on it (Freudenberg Vliesstoffe, H23C2) which acts as support, and a catalyst layer onto this support, prepared by the airbrushing of a catalytic ink with the catalyst to be tested.

The voltammetric tests consisted of 400 cycles (-0.20 – +1.00 V vs. Ag/AgCl) at 50 mV s^{-1}, using a 2.0 M phosphoric acid (PA) solution at 50 °C as electrolyte, with a gold sheet as counter-electrode. Before each test, gaseous nitrogen was bubbled for 20 minutes in order to remove the O_2 of the electrolyte and keep it inert. Luggin capillary tube was used to connect reference electrode to the half-cell. More details about the set up can be found elsewhere [13]. After that, degradation of tested catalysts was studied by monitoring the variation of Electrochemical Surface Area (ECSA). The technique for determining the ECSA of fuel cell electrodes by CV analysis involves cycling the electrode of interest over a voltage range where charge transfer reactions are adsorption-limited at the activation sites. As explained in previous Chapters, ECSA values were obtained by the H_2 desorption peak area, using the equation 4.5 [14].

To evaluate the electrochemical behavior of the different catalysts produced, Oxygen Reduction Reaction (ORR) studies were performed on rotating disk electrode (RDE), using an AUTOLAB RDE with a 5 mm Glassy carbon (GC) electrode, and using a gold sheet as counter electrode. Catalyst inks were prepared with 1.0 mg of catalyst powder, solved in 0.75 mL of deionized water and 0.25 mL of isopropanol. Then, the catalyst ink was sonicated for 10 min. To prepare the electrode, the GC head was polished for 5 min in alumina surface, and then, it was cleaned with deionized water and dried. At that point, 10 µL of catalyst ink were placed on the GC surface, drying at room temperature for 30 minutes at 500 rpm. Then, a second deposition was performed following the same procedure, by depositing 8.8 µL of ink in this case.

The RDE studies consisted of:

- Cyclic voltammetries: 25 cycles from -0.25 to 1.20 V (vs Ag/AgCl reference electrode), with a scan rate of 200 mV s^{-1}, using 0.5 M H_2SO_4 solution as electrolyte, in order to polish the electrode. Before the measurements, N_2 was bubbled to remove

the oxygen of the media. Then, 3 cycles were performed at 200, 150, 100 and 50 mV s^{-1}, in order to calculate the ECSA at different scan rates.

- Oxygen reduction reaction: before the tests, O_2 was bubbled for 30 min in order to saturate the electrolyte and then, linear sweep voltammetries were carried out from 0.90 to 0.05 mV (vs Ag/AgCl) at 5 mV s^{-1}, at 400, 900, 1200 and 1600 rpm, in order to analyze the activity of the different catalysts tested. Tafel slopes and number of electrodes transferred were calculated according to the procedure and equations described in Chapter 4.

8.2.4. Preliminary Short lifetest performance

A catalyst layer was deposited by spraying the catalyst ink over the commercial electrodes (Freudenberg Vliesstoffe, H23C2). The catalyst ink for the cathode electrodes consisted of a commercial 40% wt. Pt/C (Fuel Cell Store) (or the lab-made 40 % wt. Pt/SiC or 40 % wt. Pt/Si_xTi_yC catalyst, depending on the study), PBI ionomer (1.5 wt. % PBI in N,N-dimethylacetamide, DMAc, 1-20 PBI/support ratio), and DMAc as a dispersing solvent. The Pt amount of the catalyst powder was fixed according to the results of previous studies carried out by our research group [15] and it is in agreement with the ratios used in other works shown in the literature [16].

For the anode, the commercial catalyst, Pt/C, was used. In all cases, the Pt loading on the two electrodes (anode and cathode) was 0.6 mg Pt cm^{-2}. After the deposition of the catalyst layer, the electrodes were dried at 190 °C for 2 h, with the purpose of removing traces of DMAc. Then, electrodes were wetted with a solution of 10% PA and they were left to adsorb the acid for one day.

For the preparation of the MEA, a PBI membrane was doped in 85 wt. % PA for 5 days, in order to achieve good proton conductivity. The doping level acquired by the membrane was approximately 9 molecules of acid per polymer repeating unit. The thickness

of the doped membrane was 85 μm approx. The superficial acid on the membrane was thoroughly wiped off with filter paper and the membrane was used to prepare the MEA. In order to fabricate the MEA, the doped membrane was sandwiched between a couple of electrodes and the whole system was hot-pressed at 130 °C and 1 MPa for 15 min. The completed MEA was inserted into the cell between end plates of graphite (with a five serpentine channels frame in each plate). The geometrical area of each electrode was 25 cm^2.

MEAs prepared with thermal cured PBI membranes were mounted and characterized in a commercially available Cell Compression Unit (CCU) provided by Baltic fuel cells GmbH (Germany). The break-in procedure consisted of operation at 0.1 A cm^{-2} and $\lambda_{H2\ /\ air}$ excess stoichiometric coefficients of 1.5/2.0 for 48 hours. A preliminary stability test was conducted by increasing the current density to 0.2 A cm^{-2} (160 °C) and working at constant stoichiometric coefficients (λ_{H2} of 1.5 and λ_{air} of 2.0). For further characterization, a protocol test was carried out every 48 h since the final of the break-in procedure as reported elsewhere[12]. This protocol test consists of the following routine:

- Galvanostatic polarization curves. They were performed from the OCV to 0.40 V. First with air at constant $\lambda_{H2/air}$ =1.5/2.0 and then with oxygen at constant $\lambda_{H2/O2}$ =1.5/9.5.
- Electrochemical impedance spectroscopy (EIS) tests. The EIS tests were performed at 0.10 A cm^{-2} with 10 mV AC perturbation amplitude and frequency range from 100 kHz to 100 MHz. This sequence of EIS tests was carried out with air as oxidant and then, the same procedure was repeated with oxygen.
- Cyclic voltammetries (CV). The cathode side was purged with nitrogen and hydrogen flowed through anode side with flows of 0.1/0.1 L min^{-1} N_2/H_2. The CV was carried out from 0.05 V to 1.00 V with a scan rate of 100 mV s^{-1}. Then, the electrochemical surface area (ECSA) of cathode was estimated.

– Linear sweep voltammetry (LSV). This technique was performed to find out any crossover of gas flow through MEA. The same gases of the CV were fed with flows of 0.3/0.3 L min^{-1} N_2/H_2.

Operation conditions change abruptly during this protocol tests and they contribute to an accelerate ageing of the system. This point should be taken into account in the comparison of performance with other results shown in the literature in systems that have not undergone this protocol.

8.3. Results and Discussion

8.3.1. Preparation of the catalysts

After the synthesis process, the Pt content (% wt.) was determined by the ICP method for all catalyst prepared. Results are shown in Table 8.1, together with other results of the characterization that will be discussed later on.

Table 8.1. Pt content, Pt crystallite sizes obtained from XRD analyses, average Pt particle size determined from TEM micrographs and BET values of the supports for the different catalyst evaluated

Catalyst	Real Pt Content [% wt.]	(2 2 0) Pt Crystal size [nm]	Average Pt particle size [nm]	Support BET area [m^2 g^{-1}]
20% Pt/$Si_{0.9}Ti_{0.1}C$	19.7 ± 0.6	7.1	6.5± 0.7	99.54
40% Pt/$Si_{0.9}Ti_{0.1}C$	40.3 ± 0.5	7.4	7.0± 0.6	99.54
40% Pt/$Si_{0.8}Ti_{0.2}C$	39.7 ± 0.4	7.5	7.3± 0.7	54.42
40% Pt/$Si_{0.7}Ti_{0.3}C$	37.5 ± 0.7	7.8	7.7± 0.5	23.25
20% Pt/SiC	21.3 ± 0.5	8.0	7.1± 0.9	35.32
40% Pt/SiC	36.2 ± 1.0	8.7	7.6 ± 0.8	35.32
40 %Pt/Vulcan XC-72 (commercial)	40.2 ±0.3	4.2	3.6± 1.1	220.34

As it can be observed, all synthetized catalysts exhibited similar real Pt content as compared to the nominal one. Only in two cases (with SiC and $Si_{0.7}Ti_{0.3}C$ supports), the Pt content is slightly below. This lower content may mean that probably the low surface area and porosity of these materials prevent the total deposition of all platinum available during the synthesis process although more results are needed to support this conclusion.

Figure 8.1 shows the XRD of the SiC and $Si_{0.9}Ti_{0.1}C$ based catalyst prepared with a 20% wt. Pt, using the synthesis method described in the experimental section, and Figure 8.2 shows the XRD patterns of the Pt/SiC and the different Pt/Si_xTi_yC based material catalysts with a 40% wt. Pt content. The main diffraction peaks are observed at 2θ values of 35.5º, 41.3º, 60º, and 71.7º approx. which correspond to (111), (200), (311) and (222) planes of the SiC, respectively, and confirm the presence of β-SiC (cubic structure), as it can be observed in the SiC powder pattern (also shown in Figure 8.1). For TiC, the main characteristic diffraction peaks are observed at 2θ values of 35.9º , 41.7º , 60.45º, 72.4º , and 76.1º, which correspond to the (111), (200), (220), (311) and (222) planes, respectively. These peaks confirm the faced-centered cubic structure of TiC [17]. The main diffraction peak for SiC is at 35.5º and for TiC is at 41.7º. This would explain the higher intensity of this peak in the Si_xTi_yC sample. This fact can be observed in Figure 8.2, since the higher is the TiC molar content on the Si_xTi_yC sample, the higher is the intensity of the main peak attributed to the TiC. No phase changes, or formation of oxides, were observed for TiC or SiC, indicating that the Si_xTi_yC composite support remained stable during the catalyst deposition process. The other peaks observed at 2θ values of 39.6º, 46.1º, 67.4º correspond to Pt (111), Pt (200) and Pt (220) planes, respectively, and they were observed in all samples. The platinum peaks are assigned according to the International Centre for Diffraction Data PDF 00-004-0802 and show a face-centered-cubic crystal structure for platinum. Moreover, a double type of peak is observed for Pt (111) plane (39.6º), which is most likely due to the SiC (200) plane (41.3º). For this reason, the average platinum crystallite size was calculated from Pt (220) plane (68º)

using the Scherrer formula (Equation 4.2, shown in Chapter 4). This Pt (220) plane is used very often to calculate the crystallite size of Pt based catalysts [18,19]. In comparing catalyst with 20 and 40% wt. Pt, no differences are observed, because the main peaks of the Pt are found in both catalysts. Then, it can be stated that the platinum catalyst at both target loadings were deposited successfully on the different supports.

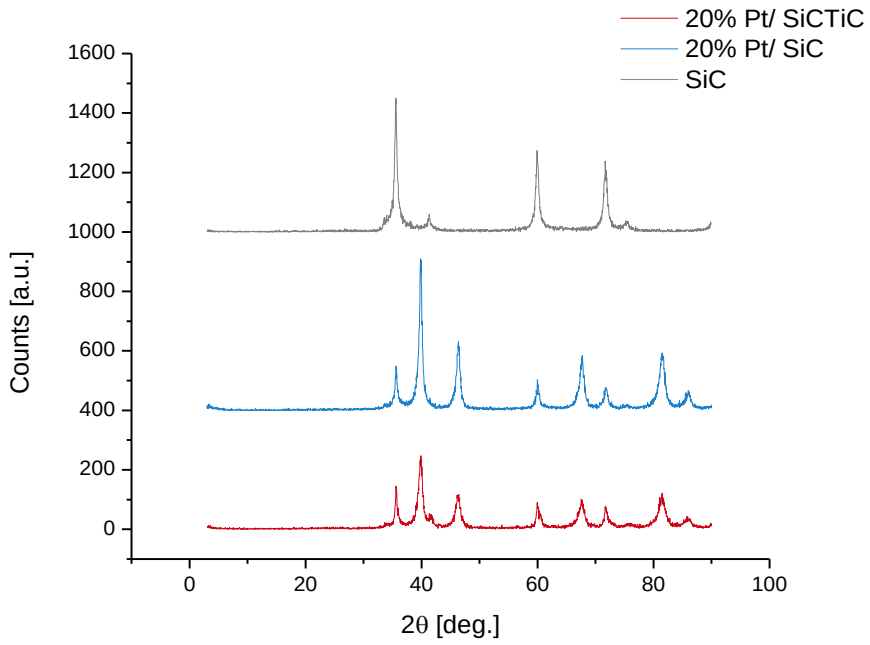

Figure 8.1. XRD patterns obtained for 20% wt. Pt catalysts using SiC and $Si_{0.9}Ti_{0.1}C$ catalysts supports. SiC patterns are also shown with comparative purpose.

Table 8.1 shows the Pt crystallite size on the two supports. All catalysts prepared with non-carbonaceous based materials exhibited larger Pt crystal and particle size than commercial catalyst, as it was expected because of their lower BET area, which prevents the adequate dispersion of the platinum particles through the catalyst support. It can be observed that the highest Pt crystal sizes were reached by SiC and $Si_{0.7}Ti_{0.3}C$, which confirms the influence of the BET area on this parameter, pointed out before. When different Pt loading catalysts are compared, not large differences were found in terms of Pt particle size.

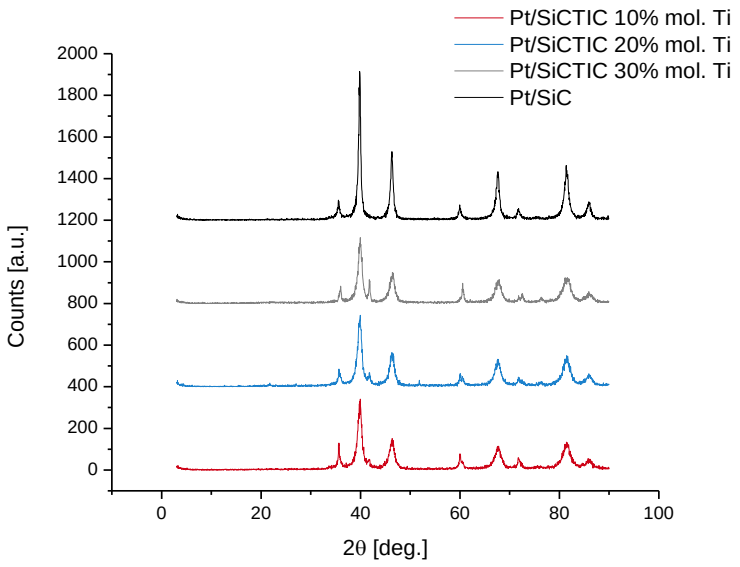

Figure 8.2. XRD patterns obtained for the different 40% wt. Pt SiC based catalysts prepared.

In order to get more information about the platinum dispersion, TEM micrographs were performed to the different catalysts. They are shown in Figure 8.3.

As Figures 8.3G and 8.3H show, no significant differences in the particle size distribution can be observed between the lab-made and the commercial catalyst with the Vulcan carbon support, indicating that the procedure applied in the catalyst manufacturing is robust and that the particle size distribution is only expected to depend on the support.

In comparing the effect of the support on the particle size, a clear influence can be observed, because there is a very significant difference between the catalysts based on Vulcan carbon and binary carbides. Table 8.1 shows the values of the average Pt particle size obtained for each catalyst (obtained by counting 80 particles of each catalyst from the TEM analysys). The carbonaceous commercial catalyst exhibited the smallest particle size, as it was expected because of its larger BET area. Initially, this result indicates that the active surface of the catalyst is expected to be higher in the case of the catalyst with the carbonaceous support material, because of the lower size of the catalyst particles and the more efficient distribution associated with this lower size.

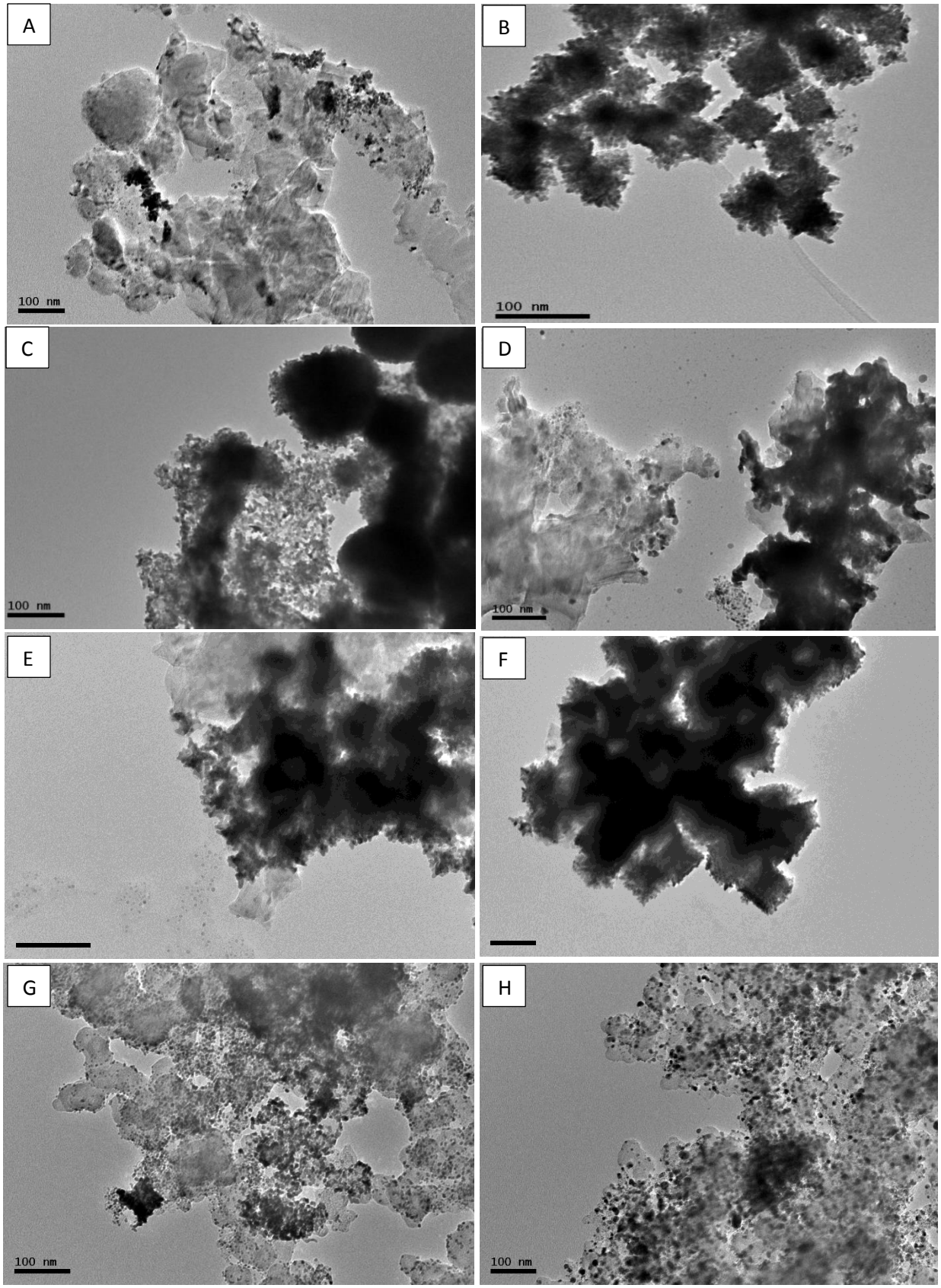

Figure 8.3. TEM micrographs of different catalyst: A) 20% wt. Pt/$Si_{0.9}Ti_{0.1}C$; B), C) and D) 40% Pt supported on Si_xTi_yC with 10, 20 and 30% mol. Ti content, respectively; E) 20% Pt/SiC; F) 40% Pt/SiC; G) Commercial catalyst 40% wt. Pt/Vulcan; and with comparative purpose, H) 40% Pt/Vulcan (homemade)

These results are in agreement with those obtained from the XRD analyses, comparing the crystal size and the particle size results, being sizes calculated by TEM slightly smaller than crystal size values. However, the average platinum particle sizes values are lower than those obtained by XRD. Thus, the Pt particles deposited on the SiC and Si_xTi_yC with 40% Pt loading had a size of around 7.6 and 7.0 nm, respectively, whereas the size of the commercial Pt particles deposited on the Vulcan carbon was around 3.6 nm. Values achieved for catalysts prepared with 20% Pt content exhibited slightly smaller particle sizes, around 6.5 (Si_xTi_yC) and 7.1 nm (SiC). These large Pt particle size values achieved for SiC-based catalyst are similar to those achieved by other authors, with average Pt particle sizes around 5.8 ± 1.9 nm [7]. It must be pointed out that the dispersion for the platinum particles obtained in SiC and Si_xTi_yC materials with higher amounts of TiC was worse than the dispersion achieved by $Si_{0.9}Ti_{0.1}C$. This can also be observed in parts B, C and D of Figure 8.3, and this trend can be explained in terms of the lower BET area of these materials.

It is also remarkable the dispersion of the Pt particles for 20% wt. Pt based catalysts, being more irregular, with Pt agglomeration in some regions and with other regions clear, as it can be observed in part A and E of Figure 8.3. This fact was also observed in 40% $Pt/Si_{0.7}Ti_{0.3}C$. These catalysts should be avoided to be used in a HT-PEMFC, because the irregular dispersion of the platinum particles could have a strong effect on the homogeneity of the electrode, resulting in a bad performance, with zones without catalytic activity. This problem was previously described for the Pt/CNSs in Chapter 5.

From these results, and taking into account that large amounts of non-carbonaceous material on the electrode decreases their porosity and electrical conductivity (as it was pointed out in Chapter 7), it was decided to fix the optimum value of Pt content in 40% wt. for the next experiments. This decision was taken because the Pt particle size achieved was similar for both target Pt loadings catalysts, and the 40% wt. Pt catalysts have a lower support contribution to the catalytic layer.

Taking into account this fact, to get more information about the oxidation state of the platinum particles of the catalysts, Temperature Programmed Reduction (TPR) analyses were carried out to the different 40% wt. Pt catalysts prepared. Figure 8.4 shows the different spectra obtained.

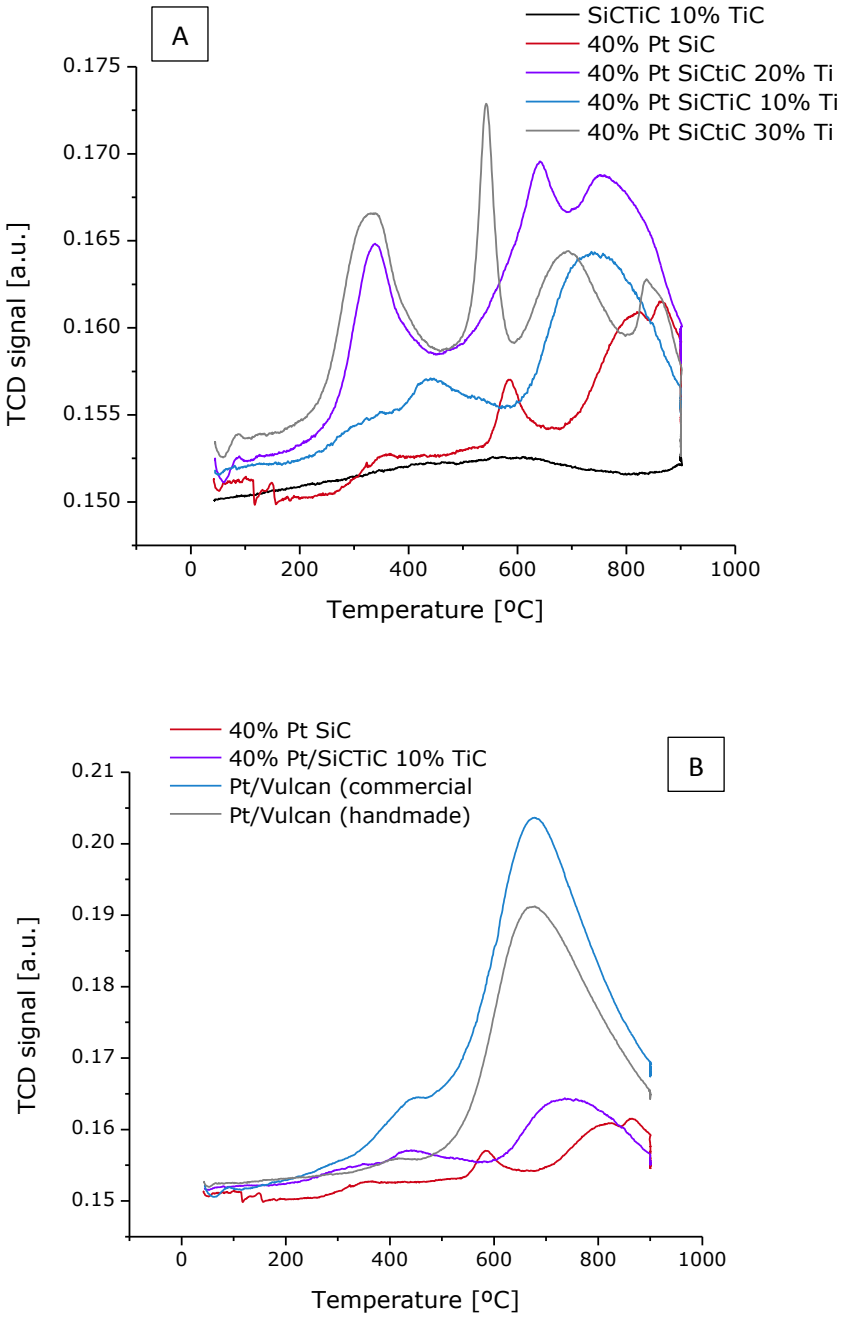

Figure 8.4. TPR spectra for different Pt based catalyst: A) 40% Pt/Si_xTi_yC catalysts with different TiC content; B) commercial, catalyst, 40% Pt/Vulcan (homemade) and 40% Pt supported on SiC and $Si_{0.9}Ti_{0.1}C$

The influence of the TiC content is presented in Part A. As it can be observed, Si_xTi_yC support does not present hydrogen consumption peaks in temperature region studied, just a small and almost negligible peak appears in the 500-800º range, which could be related to small amounts of TiO_2 or negligible hydrogen adsorption process performed by the support [20, 21]. In the next region, between 300 and 550 ºC, another 2 peaks appears at 350 and 450 ºC, which correspond to the reduction of Pt complex and Pt oxides bounded to the surface of the catalyst support, respectively. Also, at temperatures around 400-500 ºC, the reduction of TiO_2 (only in the binary carbide) and SiO_2 species catalyzed by the Pt particles [21], which can be contained in remanent amounts on the Si_xTi_yC and SiC materials [20-22].

This process, and the occupation of the reactive sites formed by the H_2, could explain the peak that appears in this region too [20]. It is very remarkable the high value observed for the peaks produced at 350 ºC in the $Si_{0.8}Ti_{0.2}C$ and $Si_{O.7}Ti_{0.3}C$. They could be justified by the presence of large amounts of Pt oxides or complex bounded to the surface, and also by the presence of higher amounts of TiO_2, which also presents a reduction peak within this region with Pt presence, according to literature [21].

At approximately 600 ºC, a new peak can be observed in the catalysts prepared with SiC, $Si_{0.8}Ti_{0.2}C$ and $Si_{0.7}Ti_{0.3}C$. This peak could be explained in terms of the reduction of PtO with a strong interaction with the support [20-22], since this peak appears only for catalyst prepared with the supports with lowest BET areas. The shift of these peaks in the catalyst could be attributed to the different bounding forces of the Pt particles with the support, being higher for the $Si_{0.8}Ti_{0.2}C$, probably due to their higher surface as compared to the SiC and $Si_{0.7}Ti_{0.3}C$.

Peaks observed at temperatures higher than 600 ºC could be also attributed to the reaction performed by the hydrogen and catalyzed by the Pt particles of reactive sites, formed because of the decomposition of carboxylic acid groups present on the surface of the catalyst supports in the case of the carbonaceous based supports [20]. The peaks which appear in the

same region for the non-carbonaceous based catalysts could be attributed to the catalyst action of the Pt on the carbide support, or related with strong bounded Si or Ti oxides on the support, since these peaks are not located at the same temperature among the different Si based materials. The peak observed at 700 ºC is especially important for the Pt/Vulcan catalysts. This can be clearly seen in Part C of Figure 8.4, which shows the TPR spectra obtained for Pt/Vulcan catalyst. As it was pointed out before, it may be associated to the H_2 consumed during the decomposition of weak acid functional groups of the catalyst, which have a larger presence in the carbon blacks used in the commercial and Pt/Vulcan lab-made catalyst and explain the higher size of the peak. The lower presence of the functional groups or oxides in the non-carbonaceous materials justifies the lower intensity of the peaks in this third region for these type of catalyst. In addition, this observation may also be related to the higher Pt particle size observed in non-carbonaceous based catalysts, since Pt particles do not have a high number of active sites to be bounded to the catalyst support [20, 21].

8.3.2. Electrochemical characterization of the catalysts

To evaluate the electrochemical behavior of the different catalysts studied, a voltammetric test was carried out to electrodes manufactured with them. For comparison purposes, all these electrodes contained the same platinum concentration (nominal content of 40% wt.) and Pt loading (0.3 mg Pt cm^{-2}) and they differ only in the different catalytic supports evaluated. Figure 8.5 shows various cycles of the voltammograms, which compare the performances of the different catalysts prepared.

Within the high voltage region (0.60-1.00V vs. Ag/AgCl electrode), it can be seen an increase in the current, probably associated with the platinum oxides formation [23]. The slope decreases in all cases during the experiment, because of the platinum deactivation processes, caused by the formation of platinum oxide layers that decrease the activity of the

catalyst and also by the migration of the platinum particles to the electrolyte. This fact could also be observed in the platinum reduction region, which appears at 0.70 V vs. Ag/AgCl.

It must be also pointed out that a decrease of the intensity within the highest voltage region (0.90 – 1.00 V vs. Ag/AgCl electrode) appears in the case on non-carbonaceous catalyst. It can be explained in terms of the formation of passive layers containing Si and Ti oxides, which are known to present lower electrical conductivity. Double layer did not undergo changes with the non-carbonaceous materials, which means that these materials do not present important structural or chemical changes during the experiments.

The catalysts made with Vulcan carbon (homemade and commercial one) exhibited a decrease in the width of the double layer region (0.20-0.40 V). This decrease can be explained in terms of a slight decrease of the surface area and could be related to the degradation of the carbonaceous support (because the oxidation of the support decreases the porosity and, in turn, this decreases the surface area of the material) [24, 25].

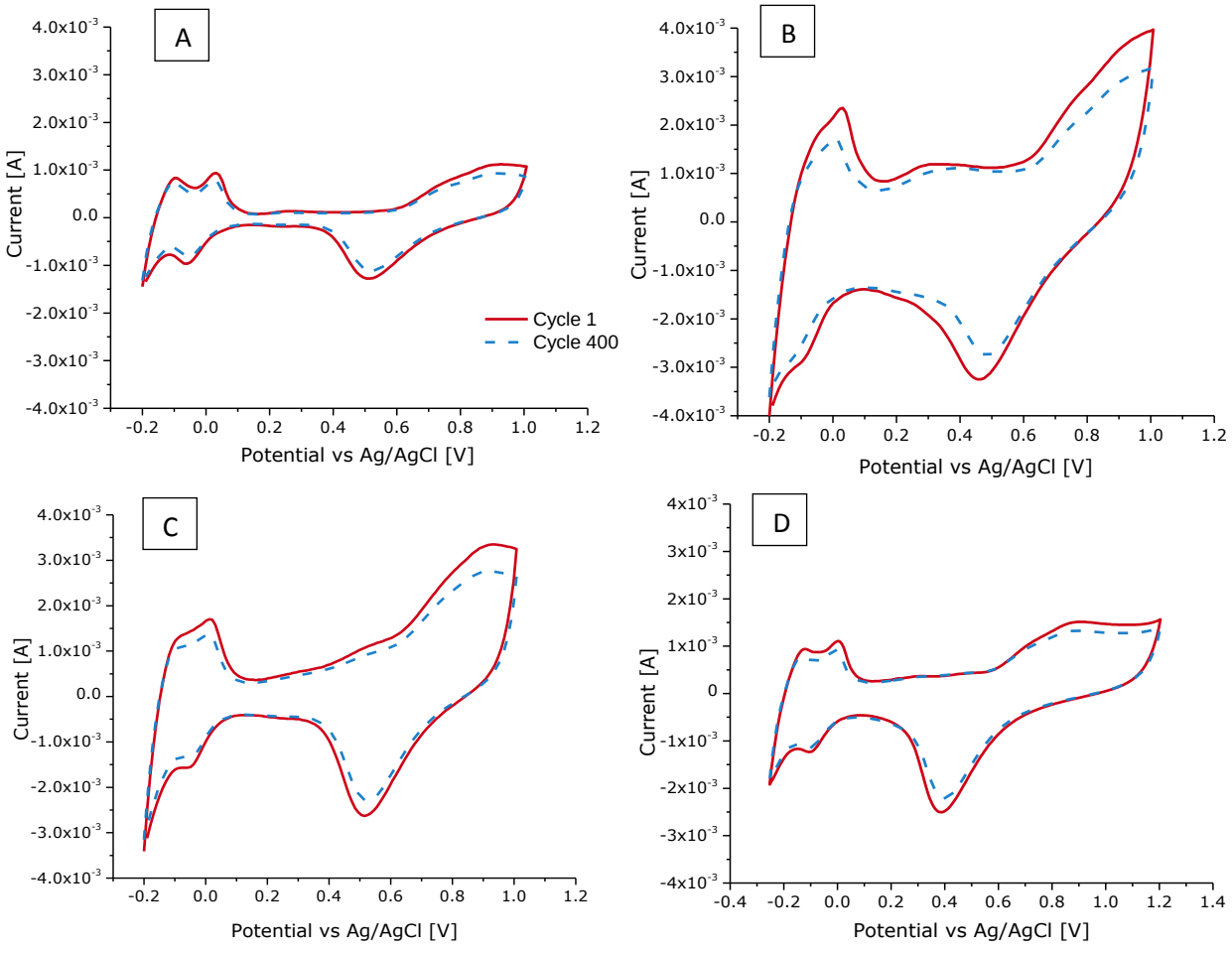

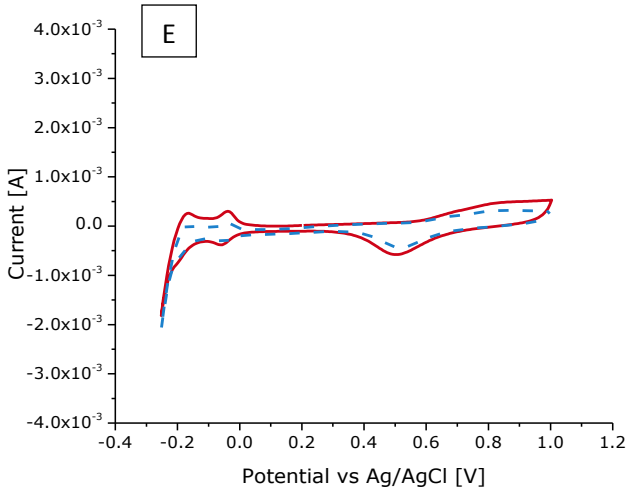

Figure 8.5. Cycle 1 and 400 voltammograms of different catalyst tested: A) 40% wt. Pt/SiC; B) Commercial catalyst, Pt/C; C), D) and E) 40% wt. Pt/Si_xTi_yC 10, 20 and 30% mol. Ti content, respectively.

In all cases, the hydrogen adsorption/desorption peaks appear at same potential region, located between -0.20/0.15 V vs. Ag/AgCl electrode. The BET surface area of the supported catalysts has a clear effect on the double layer contribution in the voltammetries. It can be observed that Pt/Vulcan carbon (184 m^2 g^{-1} BET area) catalyst exhibits the best contribution to the double layer, while Pt/Si_xTi_yC based catalysts (55, 28 and 12 m^2 g^{-1} BET areas for the 10%, 20% and 30% TiC molar content, respectively) and Pt/SiC (18 m^2g^{-1} BET area) present a lower contribution, especially in the voltage region located between 0.10 and 0.30 V vs Ag/AgCl. In addition, these BET area values are lower than BET areas of raw supports. The decrease of surface area is directly related with the Pt loading on the catalysts and it is over 40% in the case of non-carbonaceous materials (44 % for Si_xTi_yC based catalysts and 42% for Pt/SiC), and 34.5% in the case of commercial catalyst, which asseverates the successful Pt deposition in all cases.

Respect to the orientation of the platinum particles, it can be observed that in the case of those supported on the SiC support, this orientation is divided between (1 0 0) and (1 1 1) faces [26, 27], attending to the presence of two H_2 desorption peaks. In the case of Pt

deposited on Si_xTi_yC, the division of the crystalline plane orientation is less evident, with a primary orientation to the (100) face. In the case of the commercial catalyst, Pt/C, (100) orientation is the most importantly observed, presenting only one hydrogen desorption peak. Using the area of these desorption peaks, ECSA values were calculated for each catalyst for cycles 1 and 400, using the equation 4.5 (see Chapter 4), in order to analyze the evolution of the active area of the catalyst during the experiment. The obtained values are shown in Table 8.2, where the degradation of the catalysts, in terms of the variation of ECSA with respect to the initial value, can be also observed.

Table 8.2. ECSA values at different cycles for all catalyst tested in half-cell studies.

Catalyst	ECSA (Cycle 1) [$m^2\ g^{-1}$]	ECSA (Cycle 400) [$m^2\ g^{-1}$]	ECSA degradation [%]
40% Pt/SiC	22.34	16.31	21.66
40% Pt/$Si_{0.9}Ti_{0.1}C$	38.80	31.70	18.30
40% Pt/ $Si_{0.8}Ti_{0.2}C$	23.76	20.08	15.49
40% Pt/ $Si_{0.7}Ti_{0.3}C$	4.37	2.72	37.58
Commercial (40 % Pt/C)	29.35	19.48	33.61
Homemade (40% Pt/C)	31.43	21.66	27.60

It can be seen that Pt/$Si_{0.9}Ti_{0.1}C$ catalyst exhibited higher ECSA values than the commercial Pt/Vulcan one, despite the platinum particles are higher in all Si_xTi_yC catalysts. At this point, it is important to take into account that the higher double layer contribution effect in the case of Vulcan carbon catalyst could mask part of the H_2 adsorption/desorption peak, reducing the active area observed. This means that, probably, the real active surface of the commercial catalyst could be 20 or 30% higher than the calculated result. This fact is also observed in the case of the homemade Pt/C, but in this case, the observable ECSA presents

higher values, which suggests that the synthesis method improves the active area of the homemade Pt/C catalyst as compared to the commercial one, probably due to the formation of lower amount of Pt oxides.

Moreover, Pt/SiC catalyst presents a lower ECSA value, around 50% lower than Pt/Si_xTi_yC, which indicates that, in this case, the low BET area of this material has a strong influence on the electrochemical active surface of the resulting Pt particles deposited on it, as it was expected. It could be pointed out that SiC and Si_xTi_yC catalyst exhibited the lowest ECSA degradation, which could be attributed to the higher electrochemical stability of non-carbonaceous materials as compared to Vulcan carbon [12, 25]. In addition, the higher size of the platinum particles observed in the case of non-carbonaceous catalyst respect to the carbonaceous one could improve the electrochemical resistance of the catalyst, preventing the catalyst agglomeration and migration processes. On the other hand, it can be observed that the catalyst prepared using $Si_{0.7}Ti_{0.3}C$, as it was expected taking into account the physicochemical characterization results, exhibited the lowest ECSA value and the highest degradation rate of all Pt/Si_xTi_yC catalysts tested. The high ECSA losses could be explained in terms of the absence of surface to bound platinum which, in turn, explains that platinum could be easily detached from the catalyst layer during the tests. The low ECSA value could be caused by the high agglomeration of the particles and the irregular distribution of the metallic particles through the surface of the support (as the TEM micrographs indicated in Figure 8.3D).

$Pt/Si_{0.9}Ti_{0.1}C$ and $Pt/Si_{0.8}Ti_{0.2}C$ catalysts showed similar results, being slightly more stable the catalyst prepared with 20% TiC. This suggests that the BET area of this material is enough to provide a good bonding characteristics of the Pt particles to the support. However, because of its slightly better properties, in the next tests only the $Pt/Si_{0.9}Ti_{0.1}C$ is going to be studied as it has demonstrated the best properties to be used as catalyst support,

Finally, rotating disk electrode (RDE) analysis were performed to the selected non-carbonaceous catalysts, in order to pre-evaluate the performance of cathodic reaction (before the lifetest studies). Figure 8.6 shows the voltammograms obtained at different scan rates for the three Pt based catalysts studied.

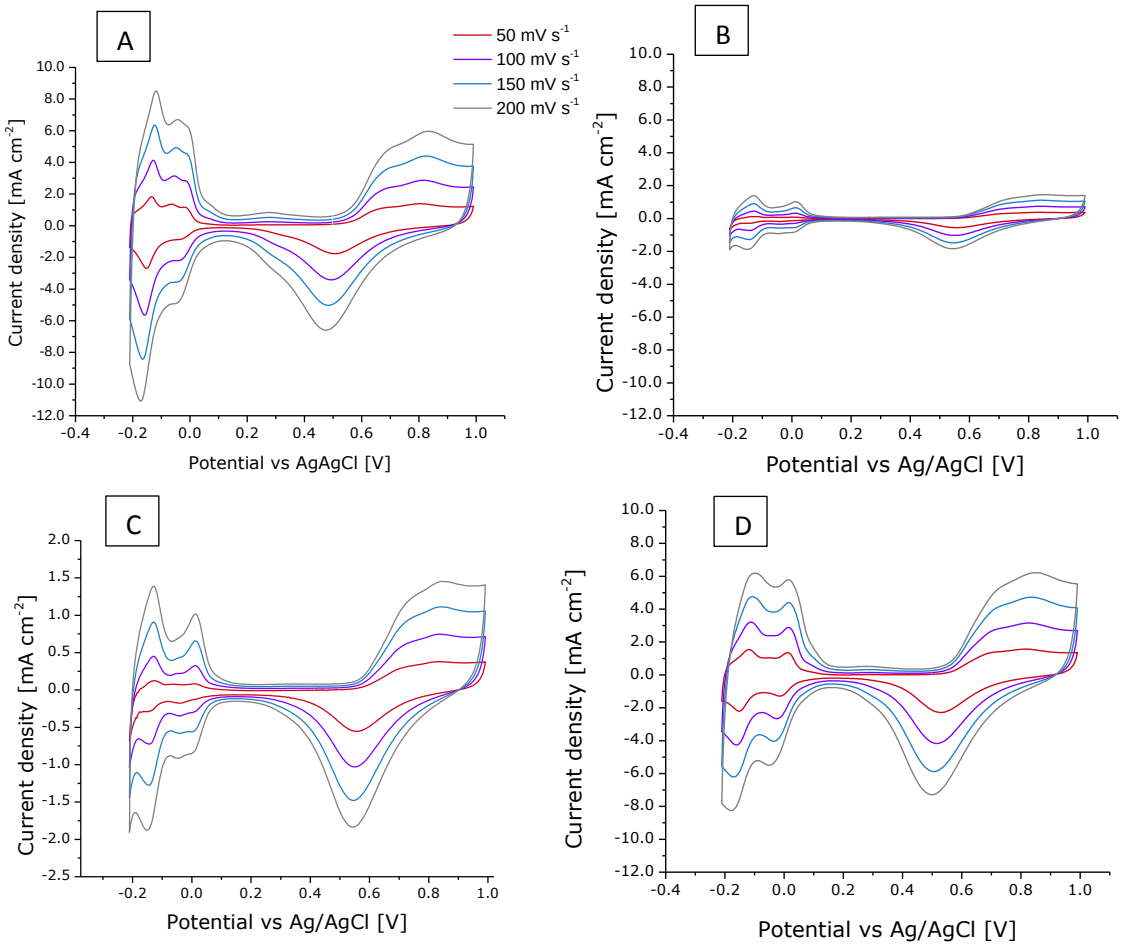

Figure 8.6. Cyclic voltammograms obtained a different scan rates during the RDE measurements for all catalyst tested. A) Pt/Vulcan (commercial); B) Pt/SiC; C) Pt/SiC at higher resolution, and D) Pt/$Si_{0.9}Ti_{0.1}C$

As it can be observed, the shape of the voltammograms obtained in RDE measurements is similar to that of the plots obtained in fixed electrode half-cell experiments. However, in the H_2 adsorption/desorption region, important changes are noticed.

First, it is important to point out that the Pt faces are well defined, especially at low scan rates as compared to the peaks obtained in the test, with the fixed electrodes. This fact was expected since the half-cell experiments used phosphoric acid, while in RDE measurements, electrolyte consisted of H_2SO_4 solutions, which allows the system to achieve

a cleaner signal. Moreover, it can be observed that the preferential face observed in the RDE voltammograms is the (111) instead of the (100) observed in the fixed electrode measurements [26, 27]. This fact could be explained by taking into account that in RDE experiments the amount of sample is quite small, and the agglomeration of the particles on a highly Pt-loaded electrode could make changes on the accessibility of the hydrogen to the active faces of the Pt. Moreover, it can be observed important differences on the shapes of the voltammograms attending to the scan rate. The higher the scan rate, the higher is the current density, which is in agreement to proportionality between current and root square of scan rate given by the Randles-Sevcik equation, as it was pointed out during the study of the Pt supported on advanced carbonaceous materials (Chapter 6) [28]. Using the area of the hydrogen desorption peaks, ECSA values were calculated for each catalyst using Equation 4.5 (see Chapter 4) and they are summarized in Table 8.3.

Table 8.3. ECSA values measured from H_2 desorption peaks of the different voltammograms obtained during the RDE measurements

Catalyst	ECSA (50 mV s^{-1}) [m^2 g^{-1}]	ECSA (100 mV s^{-1}) [m^2 g^{-1}]	ECSA (150 mV s^{-1}) [m^2 g^{-1}]	ECSA (200 mV s^{-1}) [m^2 g^{-1}]
Pt/ $Si_{0.9}Ti_{0.1}C$	37.67	45.83	54.91	60.47
Homemade Pt/Vulcan	68.56	76.46	79.68	84.57
Pt/SiC	11.31	14.32	17.65	19.31

As it can be observed, commercial Pt/Vulcan catalyst (same than in the case of the fixed electrode studies) achieved the highest current density in the peak, but in this case, since the double layer effect has no masking effect, the calculated ECSA is the highest of all catalysts evaluated. This confirms the previous comment on the masking effect of the double layer in the calculation of the ECSA in the electrodes Pt/Vulcan during the cycling voltammetric tests.

Pt/SiC showed the worst ECSA values, around 4 times lower than Pt/CNFp and 6 times lower than Pt/Vulcan. This fact was not observed in the fixed cell tests, in which the Pt/SiC catalysts presented ECSA values only around 35-50% lower. This observation can be explained by taking into account that the Pt/SiC and Pt/Si_xTi_yC powders present large and heavy particles, which make difficult to prepare a perfect homogeneous ink. This means that the difference observed in the calculation of ECSA with the two tests could be related to the concentration of the ink deposited on the GC electrode was not exactly the same (0.4 mg Pt mL^{-1}) than in the case of the commercial Pt/Vulcan XC72 catalyst. Nevertheless, attained values are good enough to propose the further evaluation in a HT-PEMFC preliminary long term testing.

Into the RDE studies, the catalytic activity through the oxygen reduction reaction (ORR) was evaluated, since this is the reaction occurrs in the cathode side [29]. Figure 8.7 shows the ORR curves obtained at different rotating speeds for all catalysts tested.

As it can be observed, non-carbonaceous and commercial Pt/Vulcan showed differences between the limiting current density achieved in the diffusional region [28, 29] (at low potential values). This means that the large Pt particles have a negative effect on the activity of the catalyst, as it was expected. The lowest performance is obtained for the Pt/SiC catalyst, with a maximum current density lower than 4 mA cm^{-2} at 1600 rpm, versus 6 mA cm^{-2} achieved by the Pt/Vulcan catalyst at the same conditions. This observation is in agreement with the lowest ECSA of this material and, as it was pointed out before, it could be related to the fact that real Pt deposited on the surface of the GC electrode could be lower than the theoretical due to the difficulties found in order to obtain a homogeneous dispersion on the catalyst ink. Pt/ $Si_{0.9}Ti_{0.1}C$ presents an intermediate result, with a maximum current density value around 4.6 mA cm^{-2}. Representing the 1/j values versus the inverse of the root square of the rotating speeds, given in rad s^{-1}, real electrons transferred can be obtained from

the slope of the linear plot, according to the previously described (in Chapters 4 and 6) Koutecky-Levitz Equation (Eq. 4.9) [28-30].

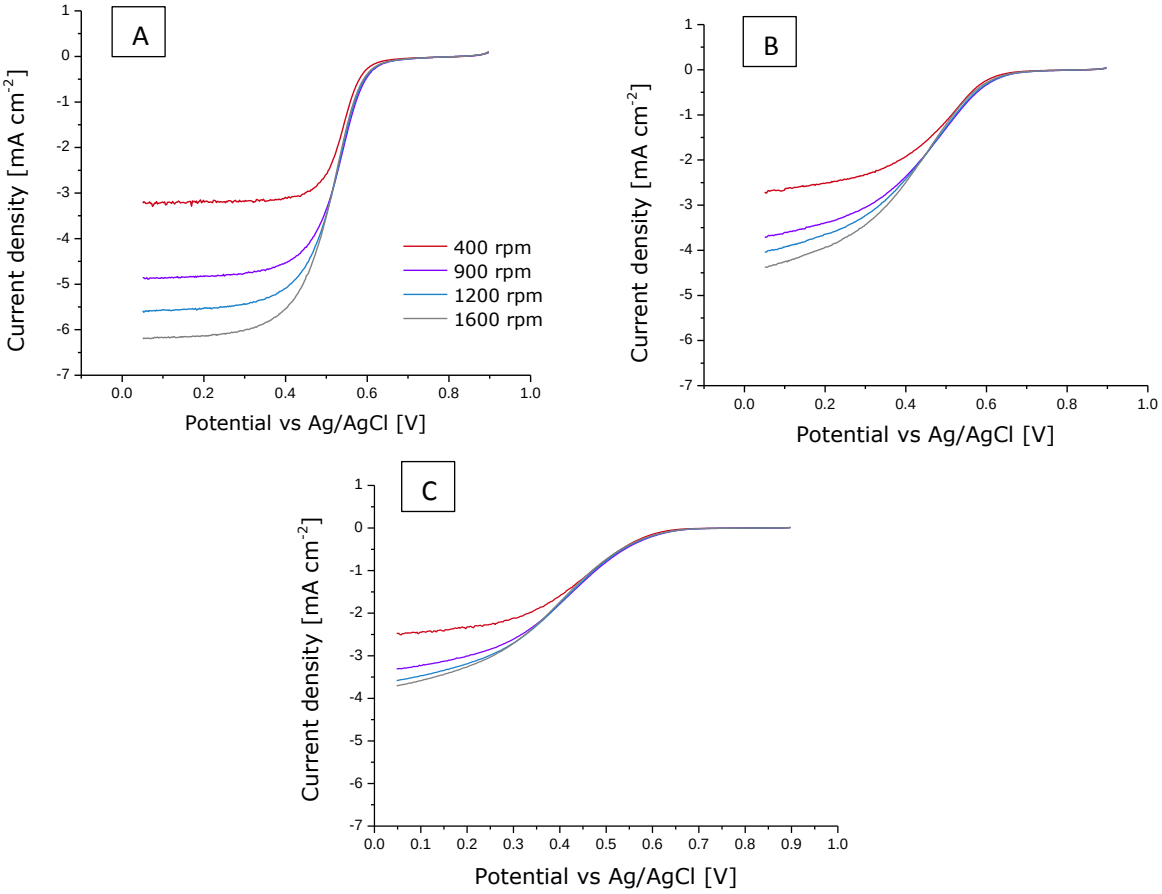

Figure 8.7. ORR performed at different scan rates for the different catalysts tested. A) Commercial Pt/Vulcan; B) $Pt/Si_{0.9}Ti_{0.1}C$; C) Pt/SiC).

In Figure 8.8 can be observed the Koutecky-Levitz plots of the different catalysts tested, and Table 8.4 shows the number of electrons calculated for each catalyst. Since in all cases the catalyst is platinum, all samples showed number of electrons around 4, which means that the complete reduction of the oxygen is performed. Surprisingly, the highest electron transfer was achieved by the non-carbonaceous materials, which means that these catalysts, despite having a lower active surface area, are able to attain the complete reduction of the oxygen, with more efficiency than Pt/Vulcan. Nevertheless, the current density and the performance reached, due to the lower electrochemical active area available, are expected to be lower than that obtained when using carbonaceous catalysts.

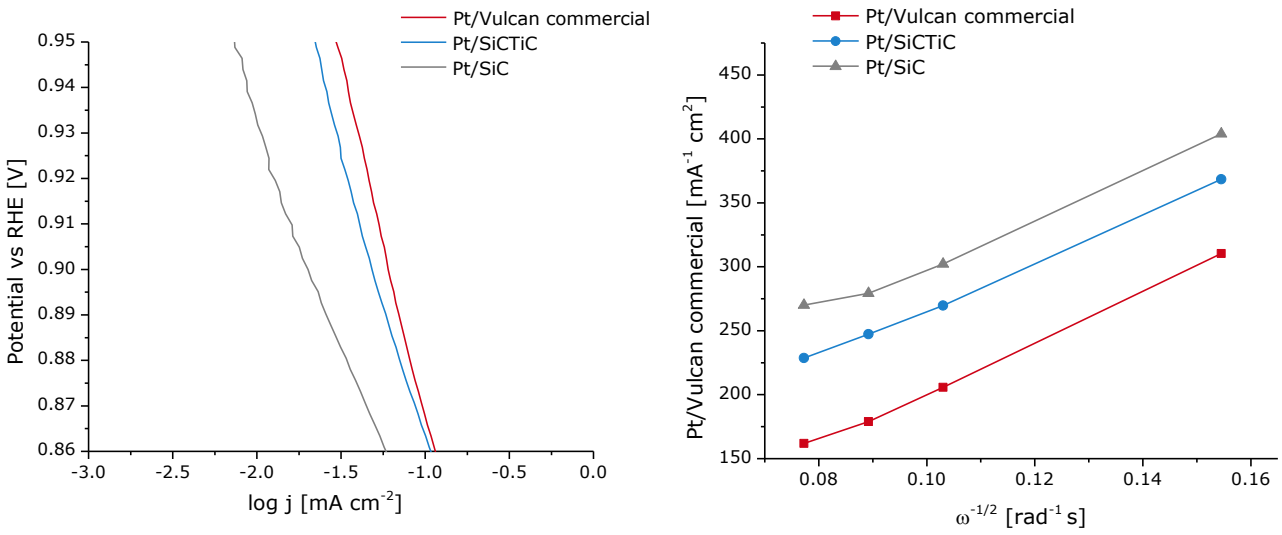

Figure 8.8. A) Comparison of Tafel plots of the different catalysts tested at 1600 rpm. B) Comparison of the Koutecky-Levich plots of the different catalysts tested.

Table 8.3. Additional parameters obtained from the Tafel and Koutecky-Levich plots for the different catalysts tested.

Catalyst	Number of electrons	Tafel slope [mV dec^{-1}]	S A [mA cm^{-2}]	M A [A gPt^{-1}]
Pt/$Si_{0.9}Ti_{0.1}C$	4.27	90.57	4.57E-02	1.19
Pt/Vulcan XC72	4.14	93.2	6.03E-02	1.57
Pt/SiC	4.35	109.8	1.93E-02	0.56

From the current density values presented in logarithm form of the kinetic control region (+120 mV of over potential value) Tafel slopes can be calculated. The comparison of the Tafel plots of the four catalysts at 1600 rpm are shown in Figure 8.8A. Numeric values of the slopes calculated are available in Table 8.3. Values of specific current density (Specific activity) (SA) and Specific Mass Activity (MA), calculated at 0.90 V vs RHE [31] from the LSV of the ORR measurements at 1600 rpm are also presented in Table 8.3.

As it can be observed, values for Pt/Vulcan and Pt/ $Si_{0.9}Ti_{0.1}C$ catalysts are higher than expected (86 mV dec^{-1}) [32], being slightly lower the Tafel slope of Pt/ $Si_{0.9}Ti_{0.1}C$

catalyst, which means that this catalyst is more active than the commercial one. This fact could be related due to the lower Pt oxides amounts detected during the TPR analysis, or the higher resistance towards oxidation of the large Pt particles. MA and SA values confirm that the Pt/ $Si_{0.9}Ti_{0.1}C$ and commercial catalyst reached the best activity.

8.3.3. Tests in a single HT-PEMFC

Taking into account the results obtained in the ex-situ characterization described previously, the 40% Pt/ $Si_{0.9}Ti_{0.1}C$ and the 40% Pt/SiC catalysts were selected to prepare the cathodes to be used in short lifetime tests in HT-PEMFC. These experiments were carried out in order to evaluate if these novel catalysts (prepared with non-carbonaceous material as supports) can overcome the performance and durability of catalyst prepared with the typical Vulcan Carbon. Thus, Figure 8.9 shows the changes in the cell voltage with time during the tests carried out with the three MEAs, prepared each one with one the different catalysts studied in this work (i.e. commercial Pt/C, Pt/SiC and Pt/ $Si_{0.9}Ti_{0.1}C$).

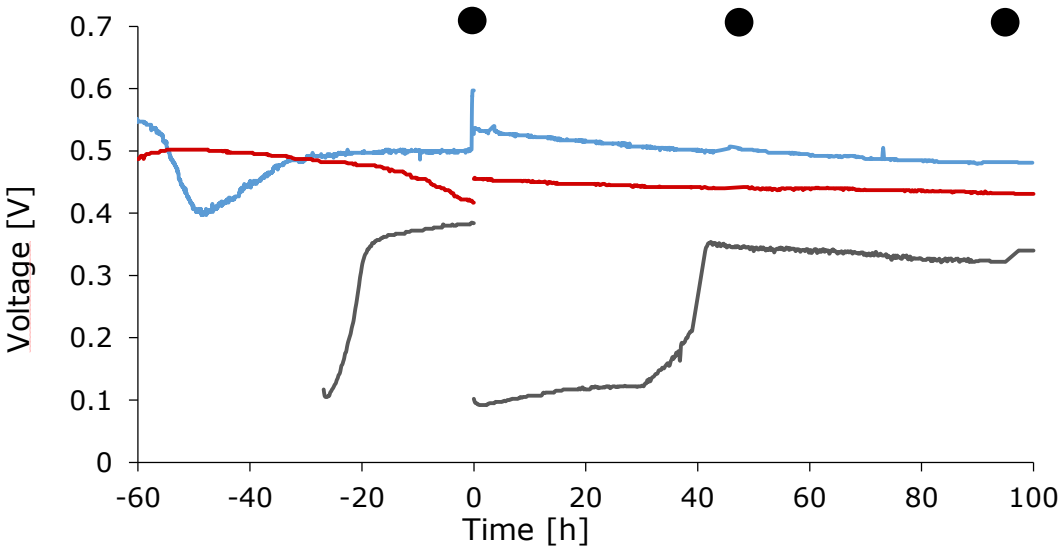

Figure 8.9. Evolution of cell voltage with time of MEAs tested with different catalysts. T= 160 °C; current density 0.2 A cm^{-2}. Break-in period: 60 h at 120 °C and at 0.1 A cm^{-2}. Blue line = Commercial catalysts (Pt/C); Red line = Pt/$Si_{0.9}Ti_{0.1}C$; Grey lane = Pt/SiC; Black dots indicate the timer when different characterization techniques were carried out.

The negative time-values correspond with the break-in period, which lasted approximately 60 h and that was carried out at 120 ºC and 0.1 A cm^{-2}. During this period, the

MEA prepared with the Pt/SiC catalyst showed a strange behavior and, as the performance was very bad keeping a temperature of 120 ºC, it was decided to raise the temperature up to 160 ºC, in order to improve the performance of the system and attain a valid result. In the other two tests ($Si_{0.9}Ti_{0.1}C$ -based catalyst and standard Vulcan catalyst based MEAs), temperature was changed just before the first characterization test, which defined the end of the break-in process. From that moment, the temperature was kept at 160 ºC and current density at 0.2 A cm^{-2} during the remaining 100 hours of duration of the tests.

As already known, the stability is one of the most important limiting factors for the actual application and commercialization of PEMFCs. The weakest point is related to the durability of electrocatalyst, which narrows the service lifetime of this technology. At this point, it is important to take into account that despite 100 hours is not a long period, it can be considered long enough to evaluate preliminarily the stability of new materials, in particular because during these lifetests, three electrochemical characterization tests were carried out at times 0, 48 and 96 h. During these characterization tests, MEAs suffered important changes in the operation conditions, because of the application of polarization curves with oxygen and air, impedance spectroscopy, linear sweep voltammetries, and cyclic voltametries. These changes are known to contribute to accelerate the degradation of the MEAs [33].

Another point to be considered is that, as far the author know, in the literature there are not described any single cell operation results from PBI-based HT- PEMFC systems, where Pt/SiC or Pt/ Si_xTi_yC catalysts are used in the cathode. It means that obtained results cannot be compared with any other previous value and it is the comparison among them, the most valuable result expected, rather than the particular values reached in any parameter. For this reason, special care was taken during the experiments and they were carried out using the same cell and were planned for the same operation conditions in order to have comparable results.

From Figure 8.9, it can be observed that the MEA prepared with Pt/SiC performed in a strange way, not only in the break-in period but over the whole duration of the test. This MEA showed the initial lowest performance and because of the very low voltage reached, after 30 hours, it was decided to fed oxygen to the cathode instead of air (with a stoichiometric coefficient of $\lambda O_2 = 9.5$) in order to evaluate if the observed bad performance was caused by mass transfer limitations. As it can be observed, when air was replaced by oxygen, the voltage started to increase until reaching a steady state value just before the second characterization test. After that, the voltage remained stable until the end of the experiment.

The best performance terms of cell voltage was achieved by the MEA prepared with the commercial catalyst and the lowest one by the MEA prepared with Pt/SiC. To calculate the degradation rate of the three MEAs, only the last 48 hours of operation were used (because during that period the three MEAs performed in a stationary conditions). The MEA prepared with Pt/ $Si_{0.9}Ti_{0.1}C$ showed a degradation value of approximately 191 $\mu V\ h^{-1}$, whereas the MEAs prepared with the commercial catalyst or with Pt/SiC reached a much worse value, close in both cases to 450 $\mu V\ h^{-1}$. If the total duration of the experiment is taken into account, these values are 204 $\mu V\ h^{-1}$ and 555 $\mu V\ h^{-1}$ for the Pt/ $Si_{0.9}Ti_{0.1}C$ and Pt/C, respectively (because of its strange performance, value of the Pt/SiC based MEA was disregard). Thus, the conventional Vulcan carbon based MEA shows a better cell voltage but the Pt/ Si_xTi_yC based MEA outperforms it in terms of a slower degradation rate. In order to know further, results of the characterization tests are of relevance.

Figure 8.10 shows the polarization curves that were carried out at the beginning and at the end of the experiment to the MEAs prepared with the three catalysts with oxygen and air.

The MEA prepared with Pt/SiC based catalyst performed the worst and its performance is particularly bad with air. At the end of the experiment, the differences with the other MEAs becomes smaller, in particular when they were running with oxygen. The

MEA prepared with Pt/ $Si_{0.9}Ti_{0.1}C$ performed worse than the one with the commercial catalyst but the differences diminished at the end of the experiment either when the HT-PEMFC was fed with air or with oxygen. This observation can be explained in terms of the higher stability of the catalyst supported on the $Si_{0.9}Ti_{0.1}C$, that was pointed out before in the half-cell tests.

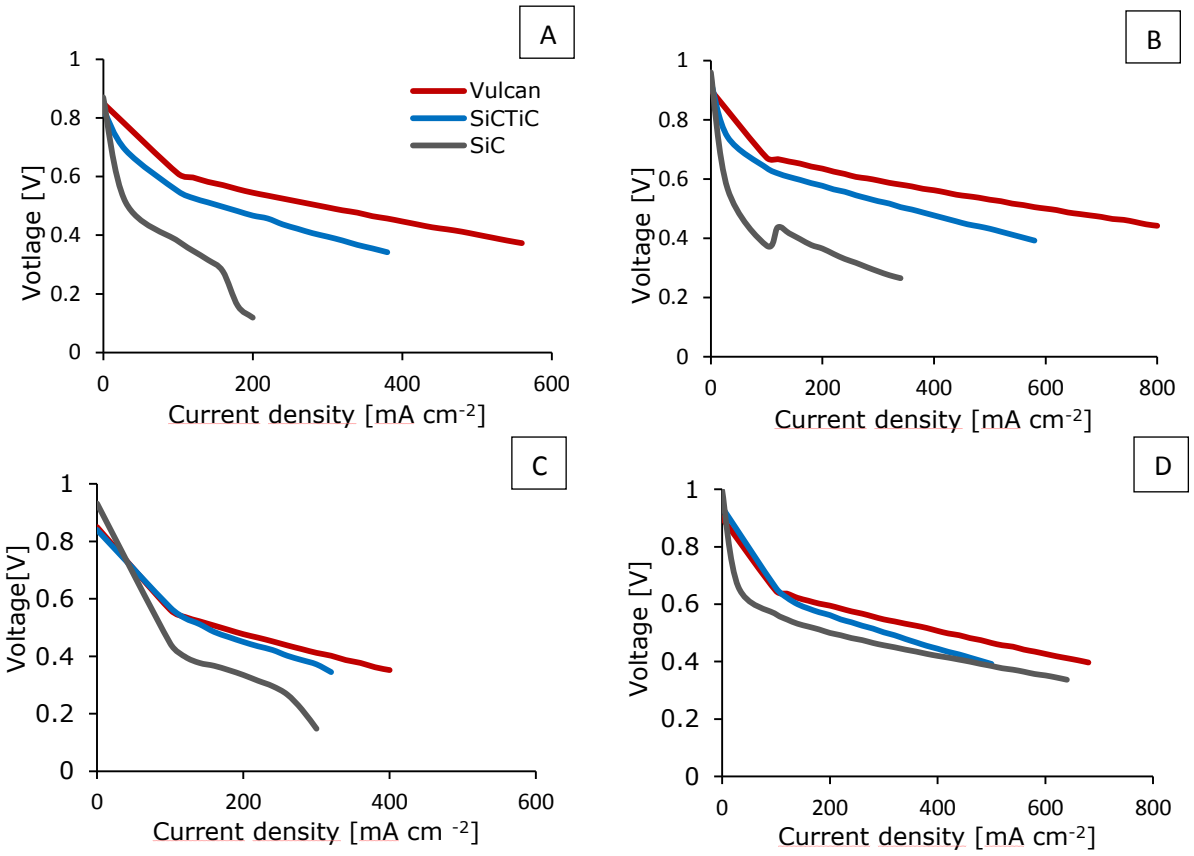

Figure 8.10. Polarization curves carried out at the beginning and at the end with both oxygen and air to the three MEAs (25 cm²) studied in this work at 160 ºC. A) Polarization curves at t= 0 h and with air. B) Polarization curves at t= 0 h and with oxygen. C) Polarization curves at t= 100 h and with air; D) Polarization curves at t= 100 h and with oxygen.

Table 8.3 shows the Open Circuit Voltage (OCV) and maximum power density values obtained from these polarization curves. Thus, the peak power density of the MEA with Pt/ $Si_{0.9}Ti_{0.1}C$ decreased by 17.2 % with oxygen, and by 20.0 % with air, whereas in the case of the MEA with the commercial catalyst, the decrease was 23.7 % and 32.6 % with oxygen and air, respectively.

Table 8.3. Values of OCV and Peak power density at different times, obtained from the polarization curves at 160 °C with oxygen and air.

Catalyst	OCV (O_2) [mV]			OCV (Air) [mV]			Peak Power (O_2) [mW cm^{-2}]			Peak Power (Air) [mW cm^{-2}]		
	0 h	50h	100 h	0 h	50h	100 h	0 h	50h	100 h	0 h	50h	100 h
Pt/SiC	960	980	996	870	895	932	90.1	217.0	215.7	44.32	70.8	71.1
Pt/$Si_{0.9}Ti_{0.1}C$	930	940	940	830	840	840	227.4	196.7	188.2	130	105.6	104.0
Pt/Vulcan XC72	940	940	900	850	840	820	353.6	321.6	269.9	208.9	160.4	140.8

Regarding the OCV, from the values shown in Table 8.3, it can be seen that there were only very slight variations during the test, which means that not important mechanical failures of the phosphoric acid doped PBI membranes occurred and, hence, the degradation should be explained only in terms of the degradation of the electrodes [34].

Table 8.4 shows the ECSA values achieved from the cyclic voltammetries of each MEA tested.

Table 8.4. Evolution of ECSA obtained from H_2 desorption peak of cyclic voltammetries performed during the different protocol tests.

Cathode catalyst	ECSA 1 [m^2g^{-1} Pt]	ECSA 2 [m^2g^{-1} Pt]	Final ECSA [m^2g^{-1} Pt]	Total degradation [%]
Pt/Vulcan XC72	17.05	14.69	13.36	**21.70**
Pt/SiC	13.37	13.29	13.20	**1.27**
Pt/ $Si_{0.9}Ti_{0.1}C$	13.82	13.35	12.98	**6.08**

It can be observed that MEAs prepared with non-carbonaceous based catalyst on the cathode side exhibited lower degradation rates during the tests (1.27 and 6.08 % for the SiC and $Si_{0.9}Ti_{0.1}C$ supports, respectively) than the carbonaceous catalyst (21.70%). The carbonaceous material showed the highest initial value of the ECSA. However, because of its

higher degradation rate, in the end of the experiment the final ECSA values were almost the same for the three materials tested.

In order to get more information about the behavior of these MEAs with Pt on new supports, impedance spectroscopy analyses were carried out at different times (0, 50 and 100 hours). Figures 8.11 and 8.12 show the different resistances obtained by mathematical fitting of the results obtained from the impedance spectroscopy analysis carried out with air and oxygen to a model R (RQ) (RQ). The ohmic resistance (R_{Ohm}) remained almost constant during the lifetest. This means that nor high degradation of the PBI membrane neither loss of conductivity (associated to drainage of phosphoric acid) occurred [34]. With respect to the mass transfer resistance (R_{MT}), it must be pointed out that in the case of the tests operated with oxygen, this resistance did not appear because of the high amount of oxygen available in the cell. Regarding the tests operated with air, the MEA with the Pt/SiC shows the highest values of R_{MT} and also the highest increase of the evolution of this parameter. Both values are in agreement with its worst performance. This observation should be related to the catalyst layer thickness and especially to the porosity. It must be kept in mind that the GDL and the PBI are commercials, so the differences among the different MEAs are only in the cathode catalytic layers. Although, Pt/SiC has been studied recently in literature [5, 13], most of the results shown are in half-cells and not fuel cell results in H_2/Air or O_2 PEMFC have been found by the authors to compare our results with.

Finally, the charge transfer resistance (R_{ct}) indicates the best stability of the MEA manufactured with Pt/ $Si_{0.9}Ti_{0.1}C$ and its lower performance with respect to the MEA manufactured with the commercial catalyst Pt/C. The highest values of mass transfer and charge transfer resistances obtained by the MEA manufactured with Pt/SiC catalyst could explain the lowest performance achieved. However, the polarization curves do not reflect the increase of these resistances when air is used as it can be seen in Table 3, where the same

power density is reached at 50 and 100 h. Hence, Pt/ Vulcan outperforms Pt/ $Si_{0.9}Ti_{0.1}C$ in terms of cell voltage but not in terms of stability.

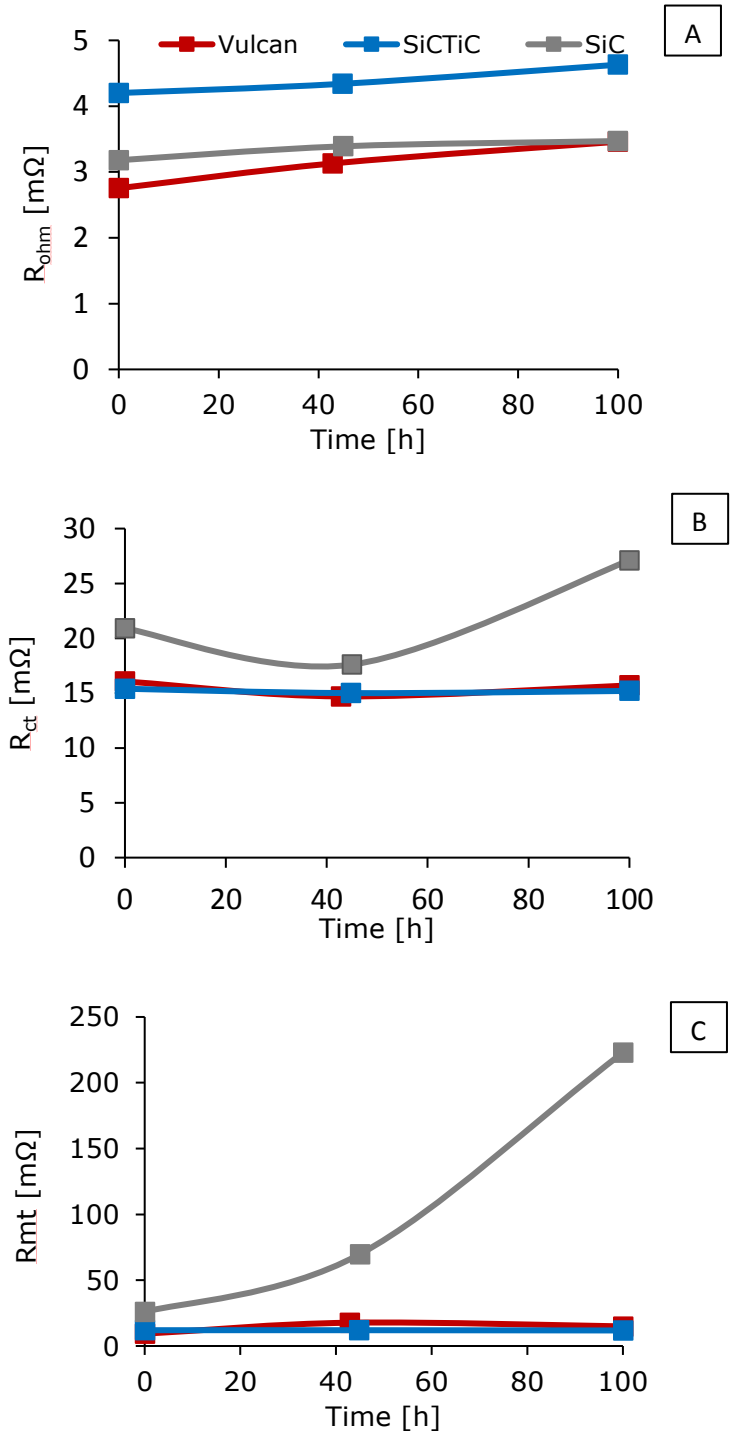

Figure 8.11. Different resistance obtained from the Impedance Spectroscopy analysis carried out at different times to the MEAs with the three catalysts fed with air. j= 0.1 A cm^{-2}. A) Ohmic Resistance; B) Charge transfer Resistance; C) Mass transfer Resistance

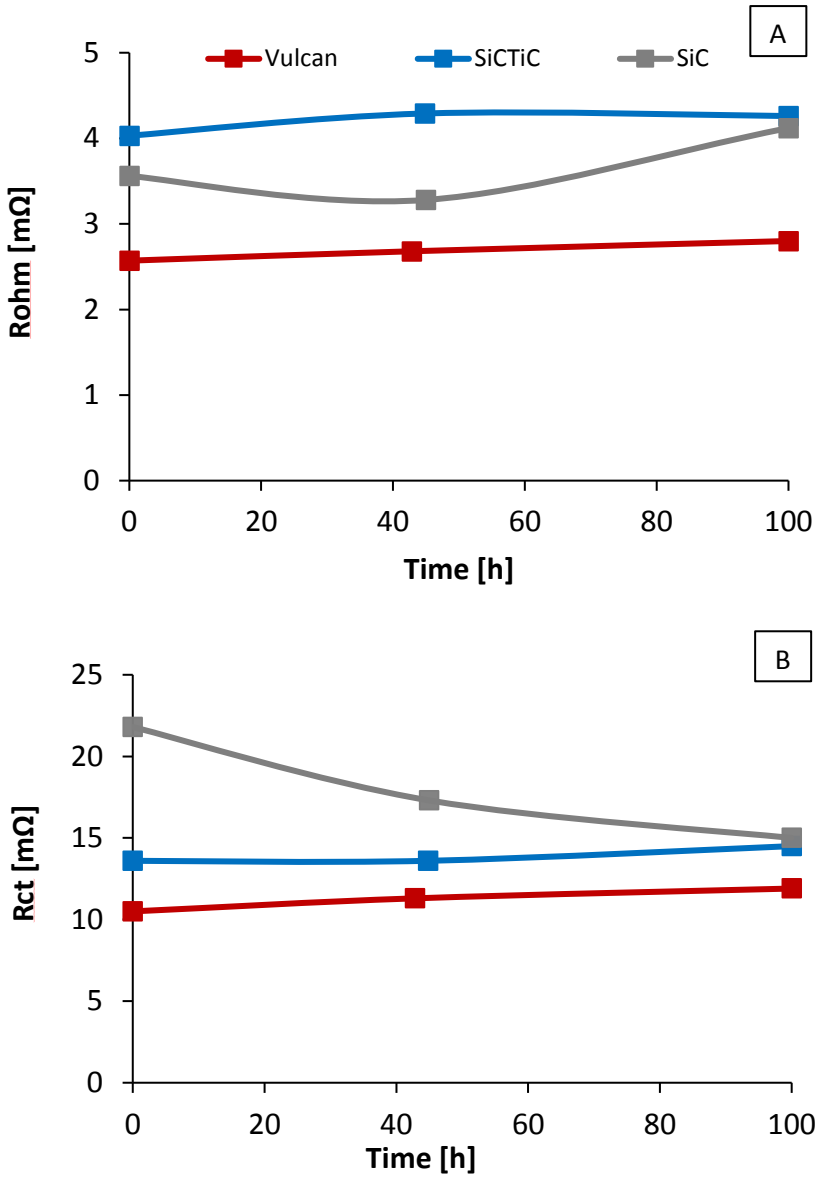

Figure 8.12. Different resistance obtained from the Impedance Spectroscopy analysis carried out at different times to the MEAs with the three catalysts fed with oxygen, j= 0.1 A cm^{-2}. a) Ohmic Resistance; b) Charge transfer Resistance

This highlights the relevance of the Pt/ Si_xTi_yC and indicates that more research should be carried out. Thus, in order to improve the performance of these non-carbonaceous based catalysts, different routes could be faced. An increase of the Pt content in the catalyst reduces the thickness of the layer and the amount of support, which could reduce the problems related to the conductivity and increase the performance of the system, keeping the stability of the layer. Likewise, an improvement of the electrical conductivity of the raw material using doping processes should reduce the resistivity of the material, increasing the voltage

associated to this MEA. Finally, using of bimetallic catalysts could improve the ECSA of the catalyst particles, increasing the performance of the system.

Finally, Figure 8.13 shows the evolution of the different LSV parameters obtained from the linear sweep voltammetry plots carried out during the lifetests. For the Pt/ Si_xTi_yC based MEA, negligible changes are observed in the evolution of the crossover. This fact means that no signs of damage are appreciated in the PBI membrane. The internal resistance of the MEA is very high (over 20 ohms), and its value increases with time, which may be attributed to the hydration of the membrane, which in turns increases the thickness and the proton conductivity of the membrane, and avoids more efficiently the electron crossing.

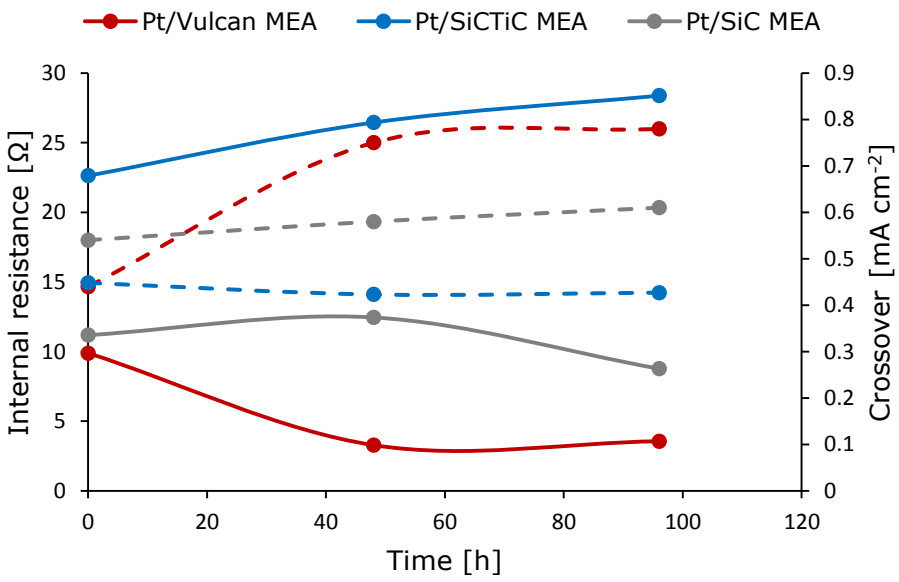

Figure 8.13. Evolution of the LSV parameters for the different MEAs tested during the lifetests. Continuous line: Evolution of internal resistance, expressed in ohms; discontinuous line: Crossover, expressed in mA cm^{-2}, both calculated at V = 0.3 V.

The Pt/Vulcan based MEA presents lower values of internal resistance (around 10 ohms at t=0 hours) and during the experiment it can be observed that after 48 hours the value decreases to 3.5 ohms, value which is high enough to state that the membrane does not suffer important damages during the test. The decrease could be attributed to the possible acid leaching of the membrane, which decreases the thickness and makes easier the charges

crossing, or due to the apparition of microporous or microholes on the PBI membrane, which allow the electron crossing. Nevertheless, crossover values are under 1 mA cm^{-2} during the lifetest and this allows us to consider that during the experiment no severe damages occurred on the membrane, which means the differences between the performances of both MEAs during the tests could only be attributed to the different catalysts used.

The Pt/SiC based MEA presents intermediate values between those of the other two MEAs, with a high internal resistance (more than 10 ohms during all the experiment) and low crossover values (around 0.5 mA cm^{-2} at t = 0 h, and 0.6 mA cm^{-2} at the end of the test). This fact again indicates that the problem of this MEA is located into the catalyst layer, due to the bad active surface of the catalyst and the low porosity and electrical conductivity, which avoid the correct diffusion of the reactive gases to the catalytic centers and the transmission of the electronic charge. This is in agreement with the high OCV values achieved in the different polarization curves during the characterization tests, which is another sign that PBI membrane did not undergo any problems or damages.

8.4. Conclusions

Taking into account the results discussed in this Chapter, the main conclusions that can be drawn are:

- Platinum supported on non-carbonaceous supporting materials (SiC and Si_xTi_yC) can be manufactured successfully by the formic acid method. These non-carbonaceous based catalysts exhibit larger Pt particle size and higher presence of oxides than standard carbonaceous catalysts, due to the lower surface area of the catalytic support.
- TiC content in the binary carbide has a strong effect on the properties of this support, being the $Si_{0.9}Ti_{0.1}C$ formulation the best option for manufacturing catalysts for the cathode of HT-PEMFC.

- 40% Pt/SiC based catalyst does not show adequate results to be used in HT-PEMFC technology, because of the low porosity, surface area, and electrical conductivity of SiC. Much research is required to improve the behavior of this novel material.
- 40% Pt/ Si_xTi_yC exhibit excellent stability in short HT-PEMFC lifetests, although its performance is little bit worse than that obtained with a standard Vulcan carbon based MEA, probably due to the lower electrical conductivity of the material, and the slightly lower ECSA. Results are promising, but an optimization of the catalyst is still required to overcome completely the standard carbonaceous materials currently used.

8.5. Bibliography

[1] Z. Chen, D. Higgins, A. Yu, L. Zhang, J. Zhang, Energy & Environmental Science 4 (2011) 3167.

[2] S. Sharma, B.G. Pollet, Journal of Power Sources 208 (2012) 96.

[3] L.M. Roen, C.H. Paik, T.D. Jarvi, Electrochemical and Solid-State Letters 7 (2004) 19.

[4] R. Dhiman, E. Johnson, E.M. Skou, P. Morgen, S.M. Andersen, Journal of Materials Chemistry A 1 (2013) 6030.

[5] N. Linse, G. G. Scherer, A. Wokaun, L. Gubler, Journal of Power Sources 219 (2012) 240.

[6] J. Park, S. Yima, T. Kima, S. Parka, Y. Yoona, G.Park, T. Yanga, E. Park, Electrochimica Acta 83 (2012) 294.

[7] S.N. Stamarin, J. Speder, R. Dhiman, M. Arenz, E.M. Skou, ACS Appl.Mater. Interfaces 7 (2015) 6153.

[8] S. Yin, S. Mu, H. Lv, N. Cheng, M. Pan, Z. Fu, Applied Catalysis B: Environmental 93 (2010) 233.

[9] Y. C. Kimmel, L. Yang, T. G. Kelly, S. A. Rykov, J. G. Chen, Journal of Catalysis 312 (2014) 216.

[10] D. J. You, X. Jin, J. H. Kim, S. Jin, S. Lee, K. H. Choi, W. J.Baek, C. Pak, J. M. Kim, International Journal of Hydrogen Energy 40 (2015) 12352.

[11] H. Lv, S. Mu, N. Cheng, M. Pan, Applied Catalysis B: Environmental 100 (2010) 190.

[12] J. Lobato, H. Zamora, P. Cañizares, J. Plaza, M.A. Rodrigo, Journal of Power Sources 288 (2015) 288.

[13] J. Lobato, P. Cañizares, M.A. Rodrigo, J.J. Linares, Electrochimica Acta 52 (2007) 3910.

[14] J. Lobato, P. Cañizares, M.A. Rodrigo, D. Úbeda, F.J. Pinar, J.J. Linares, Fuel Cells 10 (2010) 770.

[15] J. Lobato, P. Cañizares, M.A. Rodrigo, J.J. Linares, D. Úbeda, F.J. Pinar, Fuel cells 10 (2010) 312.

[16] A.S. Pushkarev, I.V. Pushkareva, S.A. Grigoriev, V.N. Kalinichenko, M.Yu. Presniakov, V.N. Fateev, International Journal of Hydrogen Energy 40 (2015) 14492.

[17] P. Nguyen, C. Pham, Applied Catalysis A: General 391 (2011) 443.

[18] J. Lobato, P. Cañizares, M.A. Rodrigo, J.J. Linares, Applied Catalysis B: Environmental 91 (2009) 269.

[19] J. Lobato, P. Cañizares, D. Ubeda, F.J. Pinar, M.A. Rodrigo, Applied Catalysis B: Environmental 106 (2011) 174.

[20] S.R de Miguel, O.A. Scelza, M.C. Román-Martínez, C. Salinas-Martínez de Lecea, D. Cazorla-Amorós, A. Linares-Solano, Applied Catalysis A: General 170 (1998) 93.

[21] M.A. Aramendía, J.C. Colmenares, A. Marinas, J.M. Marinas, J.M. Moreno, J.A. Navío, F.J. Urbano, Catalysis Today 128 (2007) 235.

[22] G.C. Torres, E.L. Jablonski, G.T. Baronetti, A.A. Castro, S.R. de Miguel, O.A. Scelza, M.D. Blanco, M.A. Pefia Jim6nez, J.L.G. Fierro, Applied Catalysis A: General 161 (1997) 213.

[23] T. Reier, M. Oezaslan, P. Strasser. ACS Catal. 2 (2012) 1765.

[24] H. Zamora, P. Cañizares, M.A, Rodrigo, J. Lobato, Fuel Cells 15(2) (2015) 375.

[25] F. Büchi, N. Inaba, T.J. Schmidt, Polymer Electrolyte Fuel Cell Durability, Springer Science + Business Media 2009.

[26] Q.He, X. Yang, W. Chen, S. Mukerjee, B. Koel, S. Chen, Phys. Chem. Chem. Phys. 12 (2010) 12544.

[27] K. Kinoshita, J. Electrochem. Soc. 137 (2010) 845.

[28] A.J. Bard, and L. R. Faulkner, Electrochemical Methods: Fundamentals and Applications, 2001, ISBN: 978-0-471-04372-0, Wiley.

[29] L. Zhang, H. Li, J. Zhang, Journal of Power Sources 255 (2014) 242.

[30] R. Vargas, C. Borrás, J. Mostanya, B. R. Scharifker, Electrochimica Acta 80 (2012) 326.

[31] A. Schenk, C. Grimmer, M. Perchthaler, S. Weinberger, B. Pichler , C. Heinzl, C. Scheu, F.A. Mautner, B. Bitschnau, V. Hacker, Journal of Power Sources 266 (2014) 313.

[32] H.A. Gasteiger, S.S. Kocha, B. Sompalli, F.T. Wagner, Appl. Catal. B - Environ.56 (2005) 9.

[33] G-B. Jung, K-Y. Chuang, T-C. Jao, C-C. Yeh, C-Y. Lin. Applied Energy. 100 (2012) 81.

[34] F.J. Pinar, P. Cañizares, M.A. Rodrigo, D. Úbeda, J. Lobato, Journal of Power Sources 274 (2015) 177.

CHAPTER 9. Performance of MEAS equipped with cathodes fully made without Vulcan Carbon

9.1 Introduction and Objectives

In the previous chapters of this Work, some novel carbonaceous and non-carbonaceous materials were tested in order to be used for the improvement of the cathodes of High Temperature Proton Exchange Membrane Fuel Cells (HT-PEMFCs) based on Polibenzimidazole (PBI) membranes. Based on the conclusions of these previous Chapters, the best material for the improvement of the micro porous layer (MPL) of the electrodes was found to be the Carbon Nanospheres (CNSs), since they exhibited excellent stability during the ex-situ and in-situ experiments performed, while the initially promising carbon nanofibers (CNFp) and silicon based materials (SiC and SiCTiC) showed significant operative problems associated to the bad diffusion of reactants through the layers prepared with these materials. Regarding the catalytic support, the conclusions reached were different and the CNFp and the $Si_{0.9}Ti_{0.1}C$ showed the best behavior in terms of performance and stability during the electrochemical characterization.

Then, following the roadmap proposed for this Thesis, these materials have been selected in order to manufacture optimized cathodes (without Vulcan Carbon) and be compared with cathodes made with the standard Vulcan Carbon in a last stability test with a higher duration. Additionally, despite the Si_xTi_yC based MPL exhibited problems related to the gas diffusion, its stability was quite good, and it also exhibited acceptable conductivity values. For this reason, it was decided to include $Si_{0.7}Ti_{0.3}C$ in the final tests carried out in this Chapter, because its porosity was closely similar to that of the CNSs and this material presented the best electrical conductivity properties of all non-carbonaceous materials studied. Thus, two optimized cathodes were manufactured:

- One based on carbonaceous materials, with a CNS based MPL and 40% Pt/CNFp catalytic layer; and
- Other non-carbonaceous based electrode, consisting on a thin $Si_{0.7}Ti_{0.3}C$ based MPL (3 mg SiCTiC cm^{-2} material loading, 10% wt. PTFE content) in order to

cover all electrode surface minimizing the electrical resistance, and 40% Pt/ $Si_{0.9}Ti_{0.1}C$ content as catalyst.

Both MEAs were prepared using standard Vulcan carbon based electrodes as anode, with a thermally treated PBI membrane provided by DPS (Denmark). The standard MEA used for the comparison was prepared using also a thermally treated PBI membrane and two Vulcan carbon based electrodes. These MEAs were evaluated in a single cell preliminary life test of 300 hours at constant loading, using pure hydrogen as fuel and oxygen as oxidant, in order to promote the increase in the degradation of the cathode side [1], performing characterization tests every 48 hours, to evaluate the changes in the critical parameters related to the stability of the cathode side and also to increase the stress of the MEAs, in order to maximize their degradation during the short studies.

9.2. Methodology

In previous chapters, methodology used for the physicochemical and electrochemical characterization of the new materials studied was throughoutly described. Because of that, in this section only the main points related to the lifetest carried out to compare the performance of the three HT-PEMFCs is going to be described.

To manufacture the different MPLs, CNSs or $Si_{0.7}Ti_{0.3}C$ (depending on the electrodes) were deposited onto a gas diffusion media (Toray Carbon Paper -PTFE 10%, Fuel Cells Store, USA) by air-spraying a microporous ink consisting of the carbonaceous material and 10% PTFE (Teflon™ Emulsion Solution, Electrochem Inc.). After the deposition of the MPLs (real support loading of 2.1 mg cm^{-2} and 2.8 mg cm^{-2} respectively), sintering of the PTFE was attained by heating the electrodes at 360 ºC for 30 min. For the anode electrodes, and the cathode electrode used in the standard MEA, a commercial electrode with Vulcan XC72 based MPL (Freudenberg Vliesstoffe, H23C2) was used.

Then, the catalyst layer was deposited by spraying the catalyst ink over the commercial electrodes (Freudenberg Vliesstoffe, H23C2). The catalyst ink for the cathode electrodes consisted of a commercial 40% wt. Pt/C (Fuel Cell Store) (or the lab-made 40 % wt. Pt/CNFp or 40 % wt. Pt/ $Si_{0.9}Ti_{0.1}C$ catalyst), PBI ionomer (1.5 wt. % PBI in N,N-dimethylacetamide, DMAc, 1-20 PBI/support ratio), and DMAc as a dispersing solvent. The Pt amount of the catalyst powder was fixed according to the results of previous studies carried out by our research group [2] and it is in agreement with the ratios used in other works shown in the literature [3]. For the anode, the commercial catalyst, Pt/C, was used. In all cases, the Pt loading on the two electrodes (anode and cathode) was 0.6 mg Pt cm^{-2}. After the deposition of the catalyst layer, the electrodes were dried at 190 °C for 2 h, with the purpose of removing traces of DMAc. Then, electrodes were wetted with a solution of 10% PA and they were left to adsorb the acid for one day.

For the preparation of the MEA, a thermally treated PBI membrane (provided by Danish Power System) was doped in 85 wt. % PA for 5 days, in order to achieve good proton conductivity. The doping level acquired by the membrane was approximately 10 molecules of acid per polymer repeating unit. The thickness of the doped PBI membrane was around 82 μm. The superficial acid on the membrane was thoroughly wiped off with filter paper and the membrane was used to prepare the MEA. In order to fabricate the MEA, the doped membrane was sandwiched between a couple of electrodes and the whole system was hot-pressed at 130 °C and 1 MPa for 15 min. The completed MEA was inserted into the cell between end plates of graphite (with a five serpentine channels frame in each plate). The geometrical area of each electrode was 25 cm^2.

MEAs were mounted and characterized in a commercially available Cell Compression Unit (CCU) provided by Baltic fuel cells GmbH (Germany). The break-in procedure consists of operation at 0.1 A cm^{-2} (160 ºC) and $\lambda_{H2\ /\ O2}$ excess stoichiometric coefficients of 1.5/9.0 for 70 hours. A preliminary stability test was conducted by increasing

the current density to 0.3 A cm^{-2} (160 °C) and working at constant stoichiometric coefficients (λ_{H2} of 1.5 and λ_{O2} of 9.0). For further characterization, a protocol test was carried out every 48 h since the final of the break-in procedure as reported elsewhere[4]. This protocol test consisted of the following routine:

- Galvanostatic polarization curves. They were performed from the OCV to 0.40 V. First with air at constant $\lambda_{H2/air}$=1.5/2.0 and then with oxygen at constant $\lambda_{H2/O2}$ =1.5/9.5.
- Electrochemical impedance spectroscopy (EIS) tests. The EIS tests were performed at 0.10 A cm^{-2} with 10 mV AC perturbation amplitude and frequency range from 100 kHz to 100 MHz. This sequence of EIS tests was carried out with air as oxidant and then, the same procedure was repeated with oxygen.
- Cyclic voltammetries (CV). The cathode side was purged with nitrogen and hydrogen flowed through anode side with flows of 0.1/0.1 L min^{-1} N_2/H_2. The CV was carried out from 0.05 V to 1.00 V with a scan rate of 100 mV s^{-1}. Then, the electrochemical surface area (ECSA) of cathode was estimated.
- Linear sweep voltammetry (LSV). This technique was performed to find out any crossover of gas flow through MEA. The same gases of the CV were fed with flows of 0.3/0.3 L min^{-1} N_2/H_2.

Operation conditions changes abruptly during this protocol tests, and the usage of pure oxygen as oxidant increase the degradation of the system, making more useful the stability data obtained from these short time experiments.

9.3. Results and Discussion

Taking into account the results obtained in the ex-situ characterization described previously, the 40% Pt/ $Si_{0.9}Ti_{0.1}C$ and the 40% Pt/CNFp catalysts were selected to prepare

the cathodes to be used in short lifetime tests in HT-PEMFC. Comparison made in this Chapter aims to determine if HT-PEMFCs equipped with any of these two novel cathodes proposed in this Thesis can overcome the conventional performance and stability of a HT-PEMFC equipped with a Vulcan Carbon Cathode. As far the author knows, in the literature there are not described any single cell operation with PBI-based HT- PEMFC systems, where these new micro porous layer (MPL) and catalysts supports are used in the cathode. It means that results obtained cannot be compared with any other previous value and it is the comparison among them, the most valuable result expected, rather than the particular values reached in any parameter. For this reason, special care was taken during the experiments and they were carried out using the same cell and were planned for the same operation conditions in order to have comparable results.

The stability is one of the most important limiting factors for the actual application and commercialization of PEMFCs. The weakest point in terms of this stability is typically related to the durability of electrocatalyst, which narrows the service lifetime of this technology. At this point, it is important to take into account that 300 hours is not a long period to evaluate properly this parameter. However, this time is around three times higher than that used in the previous studies performed in this Thesis and during this period the systems underwent more aggressive operational conditions, with six electrochemical characterization tests, carried out every 48 h, which are expected to produce a faster degradation, as compared with similar studies of HT-PEMFCs, for which no characterization protocols are performed during the lifetests or they are performed in longer periods of time (f.i. every 200 hours approx.) [4-6]. It is important to take into account that during these characterization tests, MEAs suffered important changes in the operation conditions, because of the application of polarization curves with oxygen and air, impedance spectroscopy, linear sweep voltammetries, and cyclic voltametries. These changes are the real responsibles for the acceleration in the degradation of the MEAs [7].

Figure 9.1 shows the evolution of the cell voltage with time during the tests carried out with the three MEAs. The negative time-values of x-axis correspond with the break-in period, which lasted approximately 70 h and that was carried out at 160 ºC and 0.1 A cm^{-2}

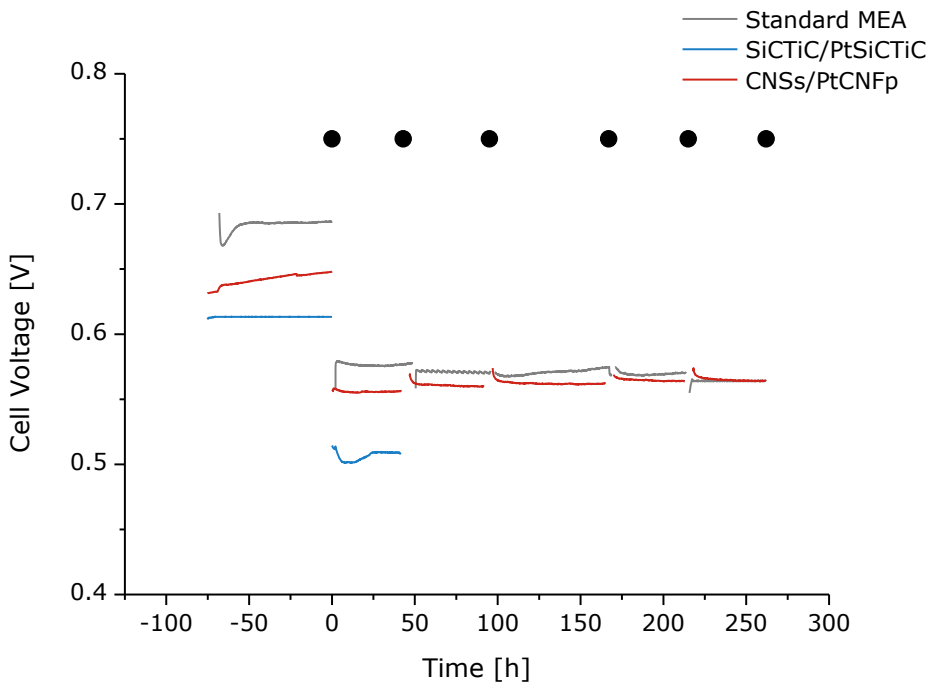

Figure 9.1. Evolution of the cell voltage of the different MEAs tested at constant j = 0.3 A cm^{-2} using pure H_2 (λ = 1.5) and O_2 (λ =9) as fuel and oxidant, respectively. Negative time period corresponds to the break-in process, carried out at j=0.1 A cm^{-2}. Black dots mark the different characterization tests performed to the MEAs during the preliminary lifetests.

As it can be observed, during the break-in procedure, the standard MEA exhibits the best performance, with cell voltages which were around 40 mV over the optimized MEA prepared with CNSs as microporous layer and CNFp as catalyst support (CNSs/PtCNFp based MEA). Opposite, the non-carbonaceous based optimized MEA ($Si_{0.7}Ti_{0.3}C$ in the MPL and 40% Pt/ $Si_{0.9}Ti_{0.1}C$) exhibited the worst performance, with a cell voltage value around 30 mV below the values obtained by the CNSs/PtCNFp MEA. It must be pointed that the standard MEA and the non-carbonaceous one exhibited a very stable break-in process after

the first 10 hours, while the CNSs/PtCNFp MEA showed a continuous activation process, increasing its cell voltage in nearly 20 mV during this conditioning time.

After the first characterization protocol, the current density was increased from 0.1 up to 0.3 A cm^{-2}, and this value was kept constant until the end of the tests. After this change, performance of the non-carbonaceous based MEA remains to be the worse, with cell voltages which were more than 50 mV lower than the exerted by the fuel cell equipped with the CNSs/PtCNFp MEA. For this reason, it was decided to stop this test, since no signs of activation were observed and, hence, this technology was not going to overcome the conventional Vulcan Carbon cathodes.

Regarding the comparison between the other two cells, it must be remarked that the commercial MEA showed a better performance in terms of cell voltage during the first 180 hours of experiment, but then, the cell voltage of the two MEAs evaluated becomes closer and closer, and after 220 hours, the comparison reverses, and the fuel cell equipped with the CNSs/PtCNFp MEA started to overcome the fuel cell equipped with the standard MEA. It must be pointed out that during the different steady states reached, CNSs/PtCNFp MEA did not show any signs of degradation. Thus, after 262 hours, the standard MEA reached an average voltage drop value of -46.5 µV h^{-1}, while the optimized MEA showed an average activation rate of +27 µV h^{-1}. The improvement in the performance of the fuel cell equipped with the novel carbonaceous materials could be explained by a sort of positive effect of the harsh operation conditions which, in turn, produce a slight degradation on the CNFp support, increasing the porosity of this material and improving the gas diffusion through the electrode with time. At the same time, the MPL with CNSs avoids the Pt migration over the catalytic layer, which could explain the enhanced performance observed in this experiment. Thus, despite the conventional Vulcan carbon based MEA shows a better cell voltage during the most time of the life test, the CNSs/PtCNFp based MEA outperforms it in terms of a negligible degradation rate, finally overcoming its performance.

In order to explain this behavior and the worse performance achieved by the $Si_{0.7}Ti_{0.3}C/PtSi_{0.9}Ti_{0.1}C$ based MEA, results of the characterization protocols are going to be further examined. Thus, Figure 9.2 shows the polarization curves measured at the beginning of the tests carried out with the three MEAs, when the fuel cells were fed with oxygen and air.

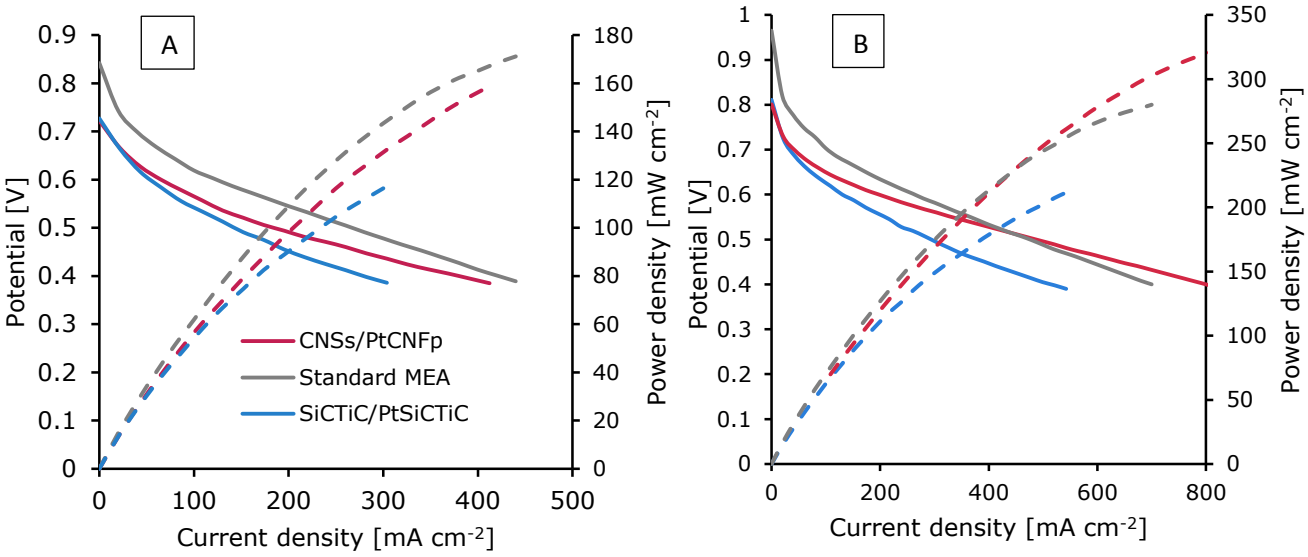

Figure 9.2. Comparison of the polarization curves obtained at t = 0 h for the three MEAs tested. A) Polarization curves performed with air. B) Polarization curves performed with oxygen. Discontinuous lines correspond to the power density curves associated to the polarization curves.

The results obtained are in agreement with the results shown in Figure 9.1. At low current densities (lower than 0.1 A cm^{-2}), both optimized MEAs showed similar OCV values and performances working both with air and oxygen, while the standard MEA exhibited slightly higher performance working with oxygen. At higher current density values than 0.1 A cm^{-2}, the carbonaceous based optimized MEA reached better performance than the non-carbonaceous based MEA. This is in agreement to the cell voltages registered during the break-in and the first 50 hours of the test. It is also very noticeable that the standard MEA showed better performance at low and medium current densities (up to 0.4 A cm^{-2}), but within the high current density region, the optimized CNSs/PtCNFp based MEA overcame the performance of the standard one, achieving higher maximum power densities, around 15% when pure oxygen was used (303.3 mW cm^{-2} for CNS/PtCNFp MEA versus 280 mW cm^{-2}

for the standard MEA at 0.7 A cm^{-2}, and 320.4 mW cm^{-2} for the optimized carbonaceous based MEA at 0.8 A cm^{-2}). When air was used, the standard MEA achieved higher power densities (165 mW cm^{-2} at 0.4 A cm^{-2}), but the values are closer to the CNSs/PtCNFp MEA (around 157 mW cm^{-2} at 0.4 A cm^{-2}). Moreover, the $Si_{0.7}Ti_{0.3}C/PtSi_{0.9}Ti_{0.1}C$ based MEA exhibited maximum power density values around 210 mW cm^{-2} (fed with O_2) and 120 mW cm^{-2} (fed with air). It is very noticeable that the difference (in terms of maximum power density values) with the other MEAs is much lower when air was used, which means that probably the mass transfer problems associated to the $Si_{0.7}Ti_{0.3}C$ based MPL was lower than the CNSs based one, which means that the low performance achieved by this MEA could be not attributed to this layer. Nevertheless, the low performance of the non-carbonaceous based MEA, in addition to the other parameters studied during the characterization protocols (ECSA, crossover and resistances obtained from EIS, which will be discussed later), supports the decision of stopping the evaluation of the $Si_{0.7}Ti_{0.3}C/PtSi_{0.9}Ti_{0.1}C$ based MEA.

Figure 9.3 shows the evolution with time of the polarization curves of the fuel cells equipped with the standard and the CNSs/PtCNFp MEAs. As it can be observed, the evolution of the polarization curves is, again, in agreement to the previous results attained. On one hand, the CNSs/PtCNFp MEA exhibits a progressive and regular activation process during the test, increasing its performance among the different polarization curves performed with air and oxygen. This improvement is especially remarkable at high current densities, for which the maximum power density achieved raised from around 320 mW cm^{-2} at the beginning of the short lifetest until 350 mW cm^{-2} at the end of the experiment. Both values are higher than the maximum values reached by the standard MEA (280 and 217 mW cm^{-2}, respectively). Moreover, it can be observed that at low current densities (up to 0.3 A cm^{-2}) the standard MEA exhibits better performance than the CNSs/PtCNFp MEA, which explains the better cell voltage exhibited during the most part of the short test. However, in the last two

polarization curves, it can be observed a noticeable decrease in the performance of the standard MEA, probably caused by the damage of the membrane.

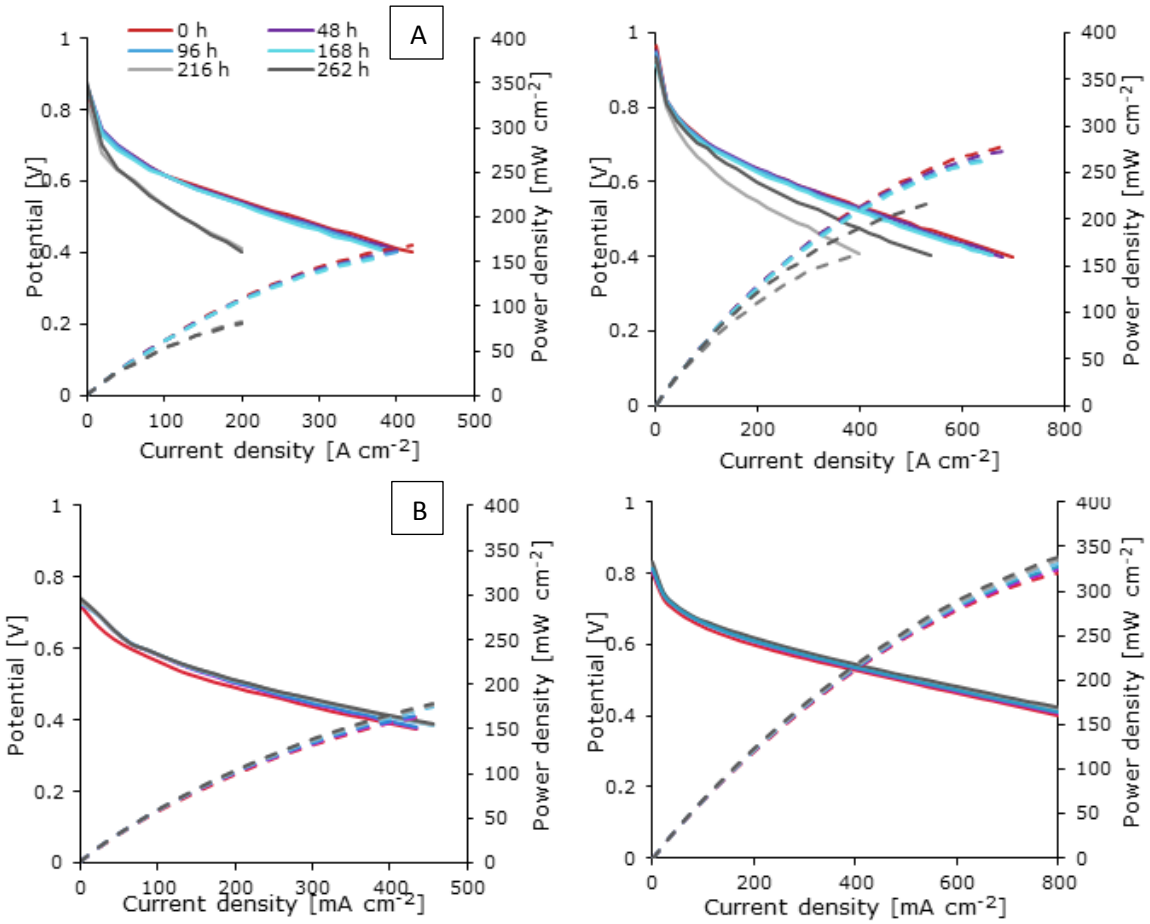

Figure 9.3. Evolution of the polarization curves performed along the different characterization test with air (left) and oxygen (right). A) Standard MEA; B) CNSs/PtCNFp based MEA.

This damage is not reflected in the OCV variation. Thus, open circuit voltages did not suffer noticeable variations during the tests, which means that not important mechanical failures of the phosphoric acid doped PBI membranes occurred and, hence, the behavior of the MEAs should be explained only in terms of the degradation of the electrodes [8].

In order to get more information about the behavior of the MEAs, spectroscopy impedance analysis (EIS) at different current densities were carried out to the MEAs during the characterization protocols. Since the tendency of the evolution of the EIS through the

different current densities was similar, it was decided to focus the study only on the analysis of the data obtained for the steady state current density (0.3 A cm^{-2}). Figure 9.4 shows the comparison between the starting impedance spectra obtained from the three MEAs obtained at 0.3 A cm^{-2} with air and oxygen. Likewise, Figure 9.5 shows the evolution of the impedance spectra at 0.3 A cm^{-2} performed with air and oxygen for the CNSs/PtCNFp based MEA. This Figure illustrates the way in which this spectra changes with time.

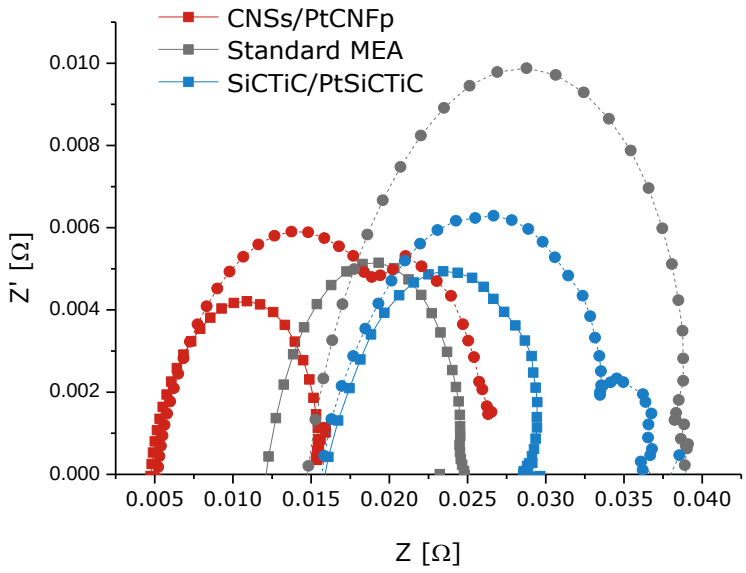

Figure 9.4. Impedance spectra measured at 0.3 A cm^{-2} for the different MEAs tested. Square dots correspond to the data obtained for oxygen; circle dots correspond to air data points.

The spectra data obtained at j = 0.3 A cm^{-2} was fitted to an equivalent electrical circuit model R (RQ) (RQ) [4,8-10]. From this fitting, ohmic resistance (R_Ω), charge transfer resistance (R_{CT}) and for the case of the impedances performed with air, the mass transfer resistance (R_{MT}) were obtained [8-10]. Their values are shown in Table 9.1.

R_Ω remained constant during all life tests, in values around 125 mΩ cm^{-2} for the case of the CNSs/PtCNFp MEA. This means that nor high degradation of the PBI membrane neither loss of conductivity (associated to drainage of phosphoric acid or the electrode degradation) occurred [8].

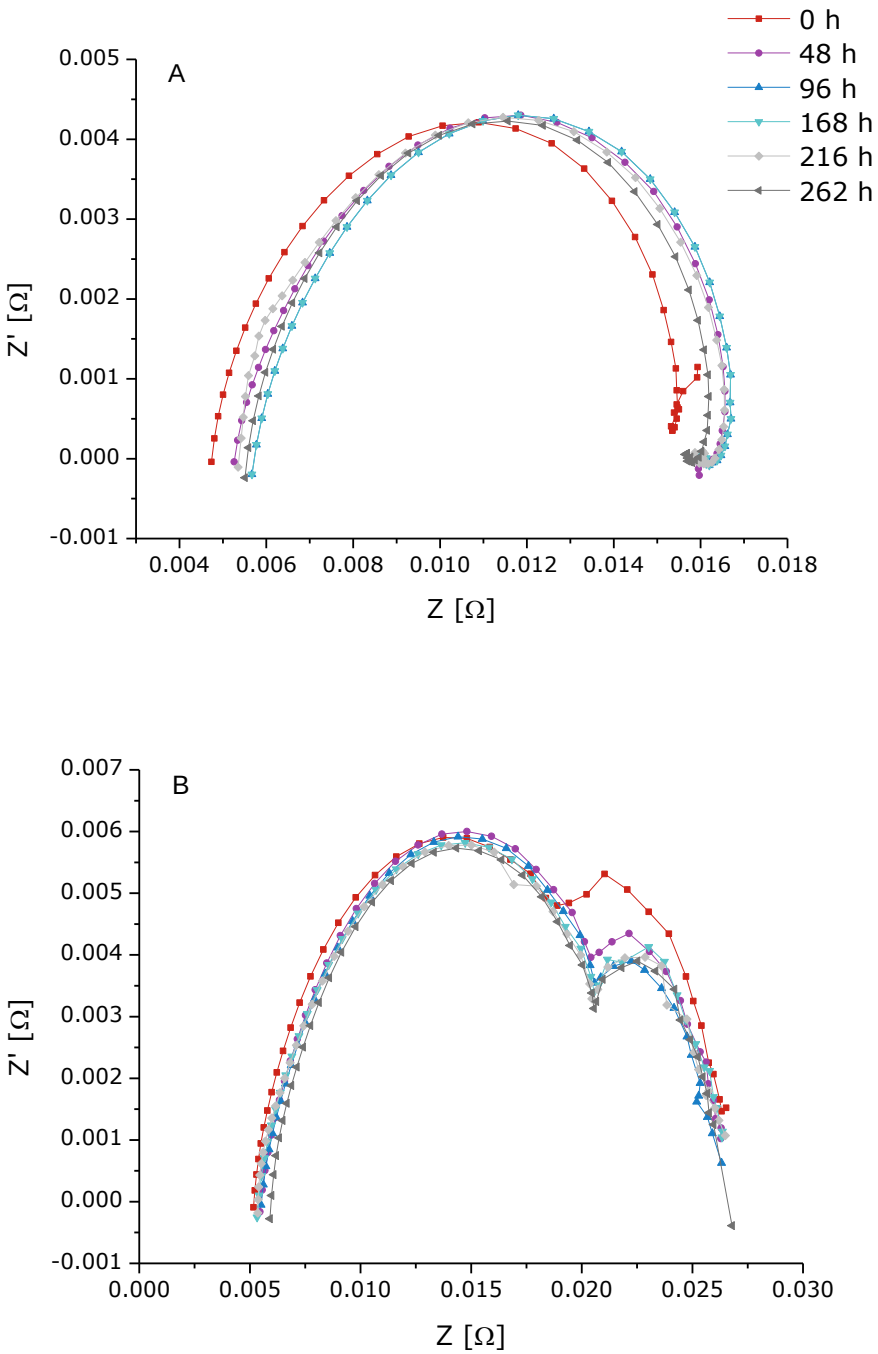

Figure 9.5. Evolution of the impedance spectra of the CNSs/PtCNFp based MEA. A) Evolution of EIS performed with oxygen as oxidant; B) with air as oxydant.

Regarding to the standard MEA, the R_{Ω} value started in a higher value, around 200 mΩ cm^{-2} and after 262 hours, the value was increased until 260 mΩ cm^{-2}, which suggests a degradation process on the electrodes or maybe a phosphoric acid leaching of the PBI membrane occurred during the last 60 hours of testing. Moreover, both optimized MEAs

exhibited closely similar values when comparing their R_Ω values obtained from air and oxygen spectra, respectively, at t = 0 h. This was expected, because this parameter is mainly affected by the ionic conductivity of the membrane, the electrical connection and the electrical resistance of the electrode and plates material [8-10].

Table 9.1. Evolution of the different resistance parameters obtained from the impedance spectra data performed at j = 0.3 A cm^{-2}. All values are given in [mΩ cm^{-2}]

Time		0 h			48 h			96 h		
MEA		**R_Ω**	**R_{CT}**	**R_{MT}**	**R_Ω**	**R_{CT}**	**R_{MT}**	**R_Ω**	**R_{CT}**	**R_{MT}**
CNSs/ PtCNFp	**Air**	120.5	295.6	189.8	127.9	340.3	147.0	128.6	348.8	149.1
	Oxygen	111.1	245.1	0.0	121.2	259.7	0.0	129.7	255.7	0.0
SiCTiC/ PtSiCTiC	**Air**	358.3	413.8	109.0	-	-	-	-	-	-
	Oxygen	360.1	315.2	0.0	-	-	-	-	-	-
Standard MEA	**Air**	278.9	449.8	29.6	216.4	447.9	45.4	210.6	420.5	46.3
	Oxygen	191.0	270.6	0.0	211.9	275.1	0.0	207.1	265.0	0.0
Time		**168 h**			**216 h**			**262 h**		
MEA		**R_Ω**	**R_{CT}**	**R_{MT}**	**R_Ω**	**R_{CT}**	**R_{MT}**	**R_Ω**	**R_{CT}**	**R_{MT}**
CNSs/	**Air**	124.2	347.7	143.1	124.6	350.4	125.6	137.1	337.1	132.5
PtCNFp	**Oxygen**	125.1	251.8	0.0	119.3	256.7	0.0	127.2	244.0	0.0
Standard MEA	**Air**	220.5	455.1	46.5	266.8	552.7	48.2	250.8	552.3	51.7
	Oxygen	221.1	279.0	0.0	262.2	560.8	0.0	247.5	385.9	0.0

However, for the case of the standard MEA, a slight difference between this parameter calculated from the air and oxygen spectra at t = 0 hours can be observed, which could be explained in terms of a bad electrical connection, because for the rest of the protocols, both values are similar. If R_Ω values are compared between the different MEAs, it can be observed that the $Si_{0.7}Ti_{0.3}C/PtSi_{0.9}Ti_{0.1}C$ presents the highest values, which explain the worse performance obtained during the testing of this MEA, as compared to the other two MEAs.

The standard MEA exhibits higher values for this parameter than the values obtained for standard MEAs in the previous chapters of this Thesis, which could be due to an incomplete doping or high acid leaching processes during the operation time of the PBI membrane used in this MEA which, in turn , may also explain the strange behavior observed in the last two polarization curves performed by this MEA, where the activation observed between the 216 and 262 hours could be attributed to the hydration of the membrane after a phosphoric acid leaching during this period of the life test [11].

Regarding to the R_{CT} values, it can be observed that the CNSs/PtCNFp based MEA and the standard one reached similar values during all lifetests, around 250 mΩ cm^{-2} with oxygen for both MEAs, being slightly higher for the standard one. This could help to explain the enhanced performance at high current densities of the CNSs/PtCNFp based MEA. Moreover, the SiCTiC based MEA exhibited higher values, around 315 mΩ cm^{-2}, which also could explain the lower performance achieved, since these high values are related to a lower activation of the catalyst. When air was used as oxidant, the amplitude of the arc increased as compared to the impedances performed with pure oxygen, as it was expected due to the lower oxygen concentration. The lowest differences between the air and oxygen spectra were attained by the non-carbonaceous based MEA, while the highest increase was obtained for the standard MEA, which means that the activation of the commercial Pt/Vulcan catalyst suffers a slower activation process using air than the lab-made CNFp catalyst used in the optimized MEA. Regarding to the evolution of this parameter with time, the CNSs/PtCNFp based MEA showed a slight increasing during the first 48 hours, and then, the value remained constant until the end of the lifetest, with an average value around 350 mΩ cm^{-2}, while the standard MEA exhibits values around 450 mΩ cm^{-2} during the first 200 hours, and then undergoes an increase in the value up to 550 mΩ cm^{-2}. This fact is also observed running with air, which explains the strange decreasing of the performance of the MEA and it could be due

to the degradation of the electrode, in addition to the decrease in the doping level of the PBI membrane during the last 60 hours of the test.

Finally, when air is used as oxidant, it can be observed that another small arc appears in all cases, due to the mass transfer limitations, which may be related to the porosity of the electrode. As it can be observed in Figure 9.4 and Table 9.1, this value is negligible for the standard MEA, which means that the porosity of the MPL and catalytic layer is good, and allows a good dispersion of the gas through all the electrode surface. The highest value is provided by the CNSs/PtCNFp based MEA. As it was shown in the Chapter 5 of this Thesis, the carbon nanofibers provide a highly compact appearance on the layers prepared with them. Thus, the high value of this parameter, as compared with the other MEAs tested, could be attributed to the catalytic layer, and could also explain the lower performance of this MEA during the first hours as compared with the standard one, even if the standard MEA presents worse catalytic activity. It can also help to explain the gradual activation of the optimized MEA, since a small degradation of the CNFp based catalytic layer could increase its porosity, and this increase, in turn, can help to raise the gas diffusion and the performance as well. This fact is in agreement with the evolution of this parameter with time, shown in Table 9.1.

Figure 9.6 shows the evolution of the shape of the voltammograms obtained for the CNSs/PtCNFp and standard based MEAs during the different characterization protocols performed during the short life tests. With comparative purposes, Figure 9.6A compares the voltammograms obtained at t = 0 h from the three different MEAs tested. As it can be observed in Figure 9.6A, the standard MEA exhibits the largest ECSA value at the beginning of the life test, around 40% higher than the CNSs/CNFp based MEA. The non-carbonaceous MEA presents the lowest value, lower than 6 $m^2 g^{-1}$, which also explain the worse results obtained with this MEA. It must be taken into account that in Chapter 8 of this dissertation, the ECSA value of the Pt/SiCTiC based MEA was higher than 13 $m^2 g^{-1}$, and Pt/VulcanXC72 based MEAs achieved ECSA values around 20 $m^2 g^{-1}$, which means that probably the low

ECSA exhibited by this $Si_{0.7}Ti_{0.3}C/PtSi_{0.9}Ti_{0.1}C$ based MEA could be due to other factors different of the catalyst.

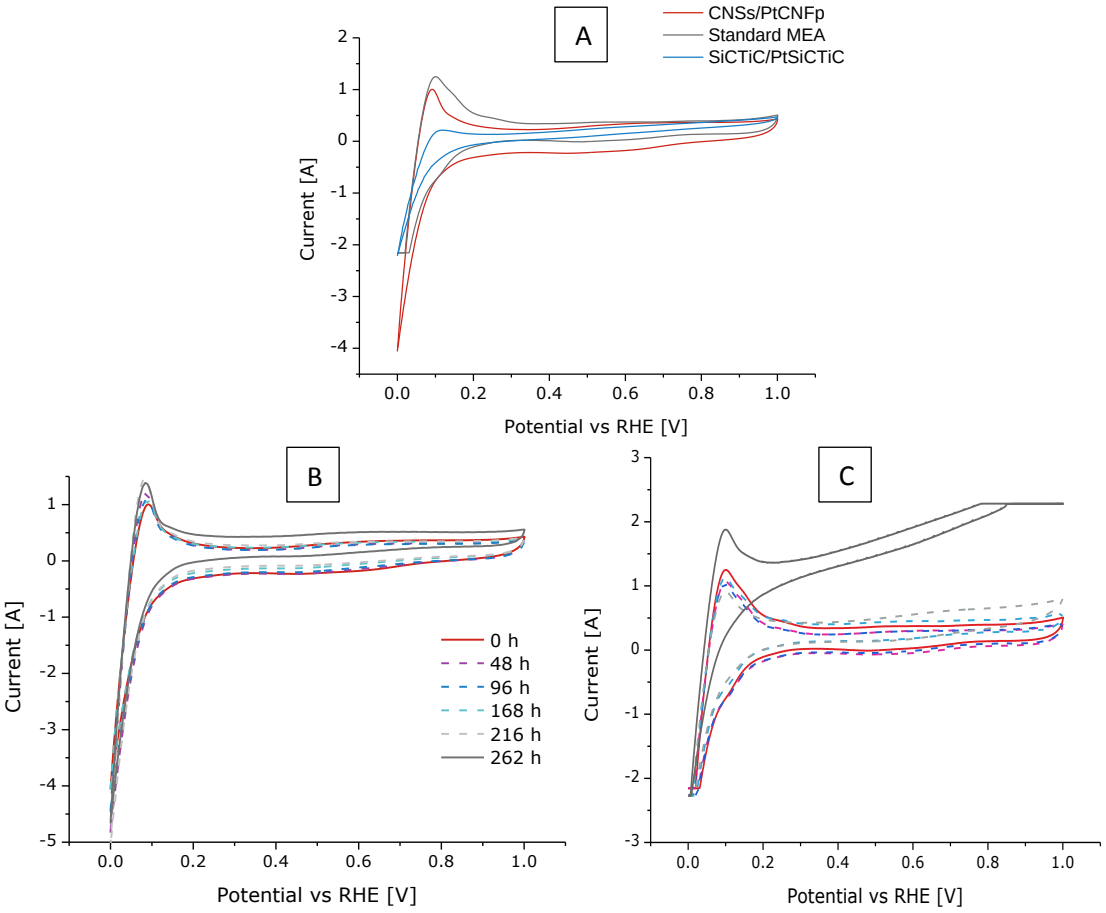

Figure 9.6. A) Comparison of the different voltammograms obtained at t = 0 hours for the different MEAs tested.; B) Evolution of the voltammograms with time for the CNSs/PtCNFp based MEA; C) same, for the standard MEA;

Further studies must be performed to optimize the composition of the non-carbonaceous electrodes, in order to skip out this problem. Additionally, taking into account the very good stability exhibited by this novel material in the previous results of this document, this material probably could be used in a better way on the anode side, since the hydrogen requires lower pore size to achieve a good dispersion and permeability.

Moreover, as it can be observed in Table 9.2, the optimized carbonaceous based MEA undergoes an increase of the ECSA value with time during the first 200 hours. Furthermore, if the starting and ending ECSA values are compared for this MEA, the ECSA degradation

was lower than 7%, much lower than the degradation of the standard MEA, which was around 36%. Furthermore, ECSA values reached by both MEAs after 200 hours of lifetest are closely similar, which means that the starting higher ECSA value exhibited by the standard one does not become a critical advantage respect to the obtained by the CNSs/PtCNFp based MEA.

Regarding to the Figure 9.6C, as it was pointed out previously, it can be observed a strange behavior on the shape of the last voltammogram, compared with the other cycles achieved during the rest of the tests, which could be attributed to damages on the PBI membrane. Fortunately, since this is the last test of the experiment, this fact did not have any influence on the performance of the MEA shown during all life test.

Finally, Figure 9.7 shows the evolution of the linear sweep voltammograms obtained during the different characterization tests performed to the MEAs.

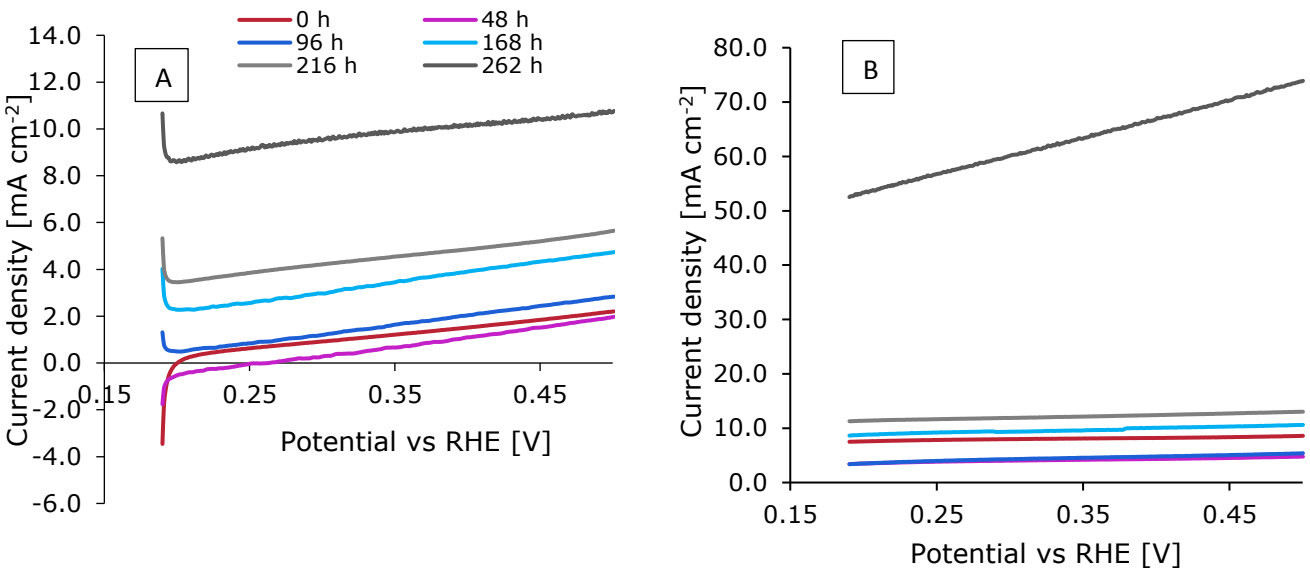

Figure 9.7. Evolution of the linear sweep voltammetries of the two MEAs tested during 262 h. A) CNSs/CNFp based MEA; B) Standard MEA

As it can be observed, the carbonaceous based optimized MEA exhibits similar slope of the linear voltammograms during all the experiment. For the case of the standard MEA, the last LSV exhibits an important increase in the current density and slope of the curve measured, which is related to the crossover of the membrane and the internal resistance of the fuel cell. Table 9.2 shows the evolution of the crossover (calculated at 0.3 V vs RHE) and the

internal resistance values of both MEAs, calculated from the LSV data. Regarding to the internal resistance, R_{int}, the CNSs/PtCNFp based MEA shows a decrease in this value during the first 48 hours, probably caused by changes on the membrane (probably a slight acid leaching process, which could reduce the thickness of the membrane, decreasing the ohmic resistance of the membrane and increasing the crossover, in agreement with the data shown in Table 9.2). Then, the internal resistance started to increase until reaching the starting value after 262 hours, probably due to a hydration process of the membrane, which increases its thickness and in turn, its ohmic resistance. Regarding to the crossover, after 168 hours, the crossover started to increase until the end of the experiment, which suggests that probably the PBI membrane underwent a small damage during the operation time.

Regarding to the standard membrane, it can be observed a similar behavior in terms of the crossover evolution after the first 48 hours operating in steady state conditions, with acceptable crossover values between 4 and 9 mA cm^{-2}. After 216 hours, this value was strongly increased, until reaching 56 mA cm^{-2} at the end of the experiment. This very high value is related to an important mechanical failure of the membrane, probably due to a big hole or the breaking of the membrane, which is in agreement with the severe decreasing of the internal resistance of the cell. Respect to this parameter, the values are slightly higher than others obtained from the previous MEAs tested in this work, which could be due to a deficient electrical contact on the system, or a lower doping level of the membrane at the start of the test, produced by a leaching process of the phosphoric acid of the membrane, which, in turn, could increase the ohmic resistance of the PBI. Since the crossover values are higher than the values obtained with the CNSs/PtCNFp based MEA, it can be considered that the thickness of the membrane was not quite high. Finally, $Si_{0.7}Ti_{0.3}C/PtSi_{0.9}Ti_{0.1}C$ based MEA exhibited acceptable crossover and internal resistance values, which suggest that the low performance achieved by this MEA was not caused by the PBI membrane.

Table 9.2. Evolution of ECSA, Crossover and R_{int} values during the lifetest for the different MEAs tested

ECSA [$m^2 g_{Pt}^{-1}$]						
Time [h]	**0**	**48**	**96**	**168**	**216**	**262**
CNSs/PtCNFp	20.0	23.3	21.8	21.6	25.4	18.6
Standard MEA	33.8	27.4	25.9	24.7	24.6	21.6
SiCTiC/PtSiCTiC	5.6	-	-	-	-	-
Crossover [mA cm^{-2}] at 0.3 V						
Time [h]	**0**	**48**	**96**	**168**	**216**	**262**
CNSs/PtCNFp	0.26	0.62	0.29	1.95	3.51	8.85
Standard MEA	7.75	3.62	3.86	8.81	11.78	56.04
SiCTiC/PtSiCTiC	3.21	-	-	-	-	-
R_{int} [Ohm]						
Time [h]	**0**	**48**	**96**	**168**	**216**	**262**
CNSs/PtCNFp	7.3	5.4	5.2	4.7	6.8	7.3
Standard MEA	19.9	19.7	18.9	17.4	19.5	0.64
SiCTiC/PtSiCTiC	4.2	-	-	-	-	-

9.4. Conclusions

The main conclusions that can be drawn from the results discussed in this Chapter are:

- The MEA prepared with the nanocarbonaceous materials (CNS as MPL and Pt/CNFp as catalyst) exhibited a high stability, which make these materials a very promising candidates to substitute the Vulcan carbon XC72 in HT-PEMFC technology based on PBI membranes. Nevertheless, optimization of the composition of the catalyst layer is required to optimize the performance of the Pt/CNFp as cathodic catalyst for these systems.

- Regarding with the non-carbonaceous materials, further investigations must be performed in order to improve the performance of these materials to be used HT-PEMFC technology. In order to asseverate the bad performance of the non-carbonaceous based MEA, this experiment should be repeated twice.
- Further investigations must be performed mixing the application of the advanced carbonaceous and non-carbonaceous materials in the preparison of optimized cathodic electrodes for HT-PEMCF (CNSs as MPL+Pt/$Si_{0.9}Ti_{0.1}C$ as catalyst, for example).

9.5. Bibliography

[1] F. Büchi, N. Inaba, T.J. Schmidt, Polymer Electrolyte Fuel Cell Durability, Springer Science + Business Media 2009

[2] J. Lobato, P. Canizares, M.A. Rodrigo, J.J. Linares, D. Úbeda, F.J. Pinar, Fuel cells 10 (2010) 312.

[3] A.S. Pushkarev, I.V. Pushkareva, S.A. Grigoriev, V.N. Kalinichenko, M.Yu. Presniakov, V.N. Fateev, International Journal of Hydrogen Energy 40 (2015) 14492.

[4] F.J. Pinar, N. Pilinski, M. Rastedt, P. Wagner, Internation Journal of Hydrogen Energy 40 (2015) 5432.

[5] F.J. Pinar, N. Pilinski, P. Wagner, AlChE Journal, 62, 1 (2015) 217.

[6] R. Kerr, H.R. García, M. Rastedt, P. Wagner, S.M. Alfaro, M.T. Romero, C. Terkelsen, T. Steenberg, H.A. Hjuler, International Journal of Hydrogen Energy 40 (2015) 16860.

[7] G-B. Jung, K-Y. Chuang, T-C. Jao, C-C. Yeh, C-Y. Lin. Applied Energy. 100 (2012) 81.

[8] F.J. Pinar, P. Cañizares, M.A. Rodrigo, D. Úbeda, J. Lobato, Journal of Power Sources 274 (2015) 177.

[9] S. J. Andreasen, J. L. Jespersen, E. Schaltz, and S. K. Kær, Fuel Cells 09 (2009) 463.

[10] J. L. Jespersen, E. Schaltz, and S. K. Kær, Journal of Power Sources 191 (2009), 289.

[11] C. Y. Chen, W. H. Lai, Journal of Power Sources 195 (2010) 7152.

CHAPTER 10. Conclusions / Conclusiones

10.1 Conclusions

In the Chapters of this Thesis, different sets of partial conclusions have been drawn. Because of that, this section only draws the main general conclusions attained in the Thesis and that are:

- It is possible to substitute Vulcan XC72 by nanocarbonaceous materials in the manufacture of the Micro Porous Layer (MPL) of the cathode of High Temperature Proton Exchange Membrane fuel cells (HT-PEMFCs). Among this novel carbonaceous materials, carbon nanospheres (CNSs) were found to be the most interesting materials because the stability of the fuel cell is greatly enhanced as compared with that of a fuel cell equipped with cathodes manufactured with Vulcan carbon based MPL.
- Nanocarbonaceous materials can also be used to manufacture the platinum supported based catalysts contained in the catalytic layer of the cathodes. In this case, the carbon nanospheres are not an adequate catalytic support since their very low surface area avoids the correct dispersion of the platinum particles. Opposite, the carbon nanofibers Platelet (CNFp) achieved exciting results, with an important increase of the performance of the fuel cell during the short term testing, as compared with fuel cells equipped with cathodes made with standard Vulcan Carbon.
- It is possible to use non-carbonaceous silicon based materials (Si_xTi_yC) to substitute Vulcan carbon XC72 in the MPLs of the cathodes of HT-PEMFC. When SiC based materials were used in the MPL, performance was worse than the obtained with the conventional Vulcan carbon, because of their low porosity and average pore size, in addition to the higher electrical resistance. The addition of TiC improves the electrical conductivity of the carbide, but further research must be performed to achieve an adequate usage of these materials. $Si_{0.7}Ti_{0.3}C$ was found to be the more interesting

material to be used in the MPL, because of its suitable pore size and enhanced electrical conductivity, similar to that of the carbon nanospheres.

- SiC based materials can be also used to prepare platinum supported based catalysts for the catalytic layer of the cathodes of HT-PEMFCs. In this case, the $Si_{0.9}Ti_{0.1}C$ achieved the best results, with and acceptable Pt dispersion through the catalyst support surface and an enhancement of the fuel cell stability, as compared with fuel cell equipped with cathodes made with the standard Vulcan Carbon. However, due to the lower electrical conductivity of the carbide material, further research must be carried out in order to improve performance of these cells in the near future.
- Novel nanocarbonaceous materials can be used simultaneously in the MPL and catalytic layer of the cathode of HT-PEMFC. Cathodes made using CNSs as MPL and 40% Pt/CNFp as catalyst get the best results, with a clear enhancement in terms of stability and performance, as compared with cathodes made with the standard Vulcan carbon XC72.

10.2. Recommendations

- Perform longer testing (>1000 hours) with the novel cathodes, in order to confirm and get more information of the benefits associated to the usage of these materials in HT-PEMFC technology.
- Evaluate the effect of a decrease in the Si_xTi_yC loadings in the MPL and catalytic layer of the cathodes (with the optimum Si:Ti ratio in each application). The high stability of these non-carbonaceous materials suggests a good durability of the electrodes with such a lower amount of material used. Also, in order to get a good covering of the electrode surface with these lower loadings, it is interesting to get an improvement of the layer deposition method (especially the microporous layer) in order to increase the porosity and electrical conductivity of the MPL.
- Evaluate the mixture of the novel carbonaceous and non-carbonaceous based materials in the cathode (f.i. $Si_{0.7}Ti_{0.3}C$ as MPL with a Pt/CNFp catalytic layer, or $Pt/Si_{0.9}Ti_{0.1}C$ catalytic layer using CNSs into the MPL).
- Evaluate the behavior of carbon nanofibers with other plane distribution (Ribbon, Fishbone or stacked up), in order to overcome the problems that appear with the porosity of the layer prepared with high amounts of the CNFp.
- Scale up the system to a short stack HT-PEMFC system, using higher electrodes manufactured with these new materials, and evaluate their behavior on long-time stack lifetest.
- The optimization of the MPL and catalyst layers prepared with novel materials, in terms of composition of each layer (catalyst and raw material loadings, PTFE content, PBI content….) must be performed, to improve the fuel cell performance using these advanced electrodes.

- Further studies must be carried out to optimize the material loading using the novel Si_xTi_yC based materials in order to enhance the performance of HT-PEMFCs, since their stability is quite good as compared with that of the conventional carbonaceous materials, especially when they are used as catalyst support, but their low electrical conductivity and porosity decrease the performance of the MEAs in which these novel materials are used.

10.1 Conclusiones

En los distintos apartados de esta tesis se han ido obteniendo conclusiones parciales que respondían a cada uno de los objetivos que se plantearon. Por este motivo, en este capítulo solo se van a plasmar las conclusiones generales de la Tesis, que son:

- Es posible sustituir al carbón Vulcan XC72 por materiales nanocarbonosos novedosos en la preparación de la capa microporosa (MPL) de cátodos de celdas de combustible de membrana de intercambio protónico de alta temperatura. Las nanoesferas de carbono (CNSs) son el material más interesante, ya que la estabilidad de la pila de combustible se mejora en comparación con la que aporta un cátodo estándar preparado con MPL basada en carbón Vulcan XC72.
- Los materiales nanocarbonosos pueden usarse también como soporte de los catalizadores a base de platino contenidos en los cátodos de pilas poliméricas de alta temperatura. En este caso, las nanoesferas de carbono no son un soporte catalítico adecuado puesto que su baja área superficial evita la correcta dispersión de las partículas de platino. Por el contrario, las nanofibras de carbono platelet (CNFp) logran resultados más interesantes, con un aumento significativo del rendimiento de la pila de combustible durante las pruebas a corto plazo, en comparación con el obtenido por una pila equipada con cátodos en los que se utiliza Pt/Vulcan XC72 en el catalizador.
- Se pueden utilizar materiales no carbonosos basados en Silicio (Si_xTi_yC) como sustituyentes del carbón Vulcan XC72 en la MPL de cátodos de pilas de combustible PEM de alta temperatura. Sin embargo, debido a su baja porosidad y mayor resistencia eléctrica comparada con los materiales carbonosos, los materiales basados en SiC obtienen un rendimiento de la celda de combustible más bajo. La adición de TiC mejora la conductividad eléctrica del carburo, pero se deben realizar

investigaciones adicionales para lograr un uso adecuado de estos materiales. El $Si_{0.7}Ti_{0.3}C$ es el material con base no carbonosa más interesante para ser usado en esta capa, debido a su mejor tamaño de poro y conductividad eléctrica, similar a la de las nanoesferas de carbono.

- Los materiales a base de SiC también pueden usarse como soporte de catalizadores a base de platino en los cátodos de celdas de combustible poliméricas de alta temperatura. En este caso, el $Si_{0.9}$ $Ti_{0.1}C$ consigue los mejores resultados, con una dispersión de Pt aceptable en de la superficie de soporte del catalizador y una mejora de la estabilidad de la pila de combustible, en términos de menores caídas de voltaje de la celda durante las pruebas a corto plazo, comparadas con las obtenidas por celdas equipadas con cátodo estándar preparado con carbón Vulcan XC72. Por otro lado, debido a la menor conductividad eléctrica del material de carburo, se deben realizar investigaciones adicionales para superar este desafío, con el fin de implementar este material en la tecnología de pilas de combustible poliméricas de alta temperatura.
- Lo nuevos materiales nanocarbonosos se pueden utilizar simultáneamente en la MPL y capa catalítica de los cátodos de celdas de combustible poliméricas de alta temperatura. La utilización de CNSs como MPL y 40%Pt / CNFp como catalizador, aporta los mejores resultados, con un aumento en términos de estabilidad y rendimiento de la celda de combustible en los ensayos de corta duración realizados en condiciones agresivas para los materiales, en comparación con el rendimiento obtenido por una pila equipada con cátodos fabricados con carbón Vulcan XC72.

10.2. Recomendaciones

- Realizar test de vida de mayor duración (> 1000 horas) utilizando cátodos optimizados, para evaluar el comportamiento de estos nuevos materiales con periodos de funcionamiento más largos y poder obtener más información sobre los beneficios

del uso de estos materiales en tecnología de pilas de combustible poliméricas de alta temperatura y confirmar su aplicación.

- Investigar el efecto de la disminución de las cargas de Si_xTi_yC en la fabricación de MPL y capa catalítica (con la relación óptima Si: Ti en cada aplicación), ya que la alta estabilidad de estos carburos hace fácil obtener una buena durabilidad de los electrodos con menor cantidad de material utilizado. Además, con el fin de obtener una buena cobertura de la superficie del electrodo con cargas inferiores, debería investigarse una mejora del método de deposición de la capa (especialmente la capa microporosa) con el fin de aumentar la porosidad y la conductividad eléctrica de la MPL manteniendo la excelente durabilidad conseguida por los materiales no carbonosos.
- Realizar estudios adicionales mezclando los nuevos materiales basados en carbono y carburos en la fabricación de electrodos catódicos (por ejemplo, $Si_{0.7}Ti_{0.3}C$ como MPL con una capa catalítica Pt / CNFp, o una capa catalítica Pt / $Si_{0.9}Ti_{0.1}C$ usando CNSs como MPL).
- Evaluar el comportamiento de las nanofibras de carbono con otra distribución planar (Ribbon, Fishbone o apiladas) para intentar solucionar los problemas que aparecen relacionados con la porosidad de la capa preparada con altas cantidades de CNFp.
- Evaluar el rendimiento de electrodos optimizados en stacks de pilas de combustible, con objeto de escalar el sistema y evaluar el comportamiento y estabilidad de estos nuevos materiales en test de larga duración.
- Optimizar las MPLs y capas catalíticas de los electrodos preparados con estos materiales, en términos de la composición de cada una de ellas (cantidad de material y catalizador utilizado, % PTFE y PBI, respectivamente…) con objeto de mejorar el rendimiento en celda de combustible de estos electrodos.

- Realizar estudios adicionales para optimizar la carga de material en los electrodos basados en Si_xTi_yC de cara a mejorar el rendimiento de estos materiales en celdas, ya que su estabilidad es bastante buena en comparación con los materiales carbonosos, especialmente cuando se utilizan como soporte de catalizador, pero su baja conductividad eléctrica y porosidad disminuyen el rendimiento de las MEAs en las que se usan estos materiales.

ANNEX. Publications / Conference contributions

Publications

- **Fuel Cells**, 15 (2015) 2, 375-383, *Improving of Micro Porous Layer based on Advanced Carbon Materials for High Temperature Proton Exchange Membrane Fuel Cell Electrodes*, H. Zamora, P. Cañizares, M.A. Rodrigo, J. Lobato
- **Journal of Power Sources**, 288 (2015) 288-295, *Microporous layer based on SiC for high temperature proton exchange membrane fuel cells*, J. Lobato, H. Zamora, P. Canizares, J. Plaza, M.A. Rodrigo
- **ChemCatChem**, 8 (2016) 848-854, *Composite Titanium Silicon Carbide as a Promising Catalyst Support for High-Temperature Proton-Exchange Membrane Fuel Cell Electrodes*, J. Lobato, H. Zamora, J. Plaza, P. Cañizares, M.A. Rodrigo
- **ChemSusChem**, 9 (2016) 1187-1193, *Improved electrodes for High Temperature Proton Exchange Membrane fuel cells using Carbon Nanospheres*, H. Zamora, J. Plaza, J. Lobato, M.A Rodrigo
- **Applied Catalysis B: Environmental**, 198 (2016) 516-524, *Enhancement of high temperature PEMFC stability using catalysts based on Pt supported on SiC based materials*, J. Lobato, H. Zamora, J. Plaza, P. Cañizares, M.A. Rodrigo
- **Applied Catalysis B: Environmental** (Submitted, 2016), *Influence of Ti content of the composite carbide SiCTiC on the properties as catalyst support for HT-PEMFCs,* H. Zamora, J. Plaza, P. Velhac, P. Cañizares, M.A. Rodrigo, J. Lobato.

Conference contributions

- **MRS FALL MEETING,** September 2016 Warsaw (Poland), *A binary carbide, SiCTiC, as a novel support for catalyst in electrodes for HT-PEMFC*, Justo Lobato, Héctor Zamora, María Millán, Pablo Cañizares, Manuel A. Rodrigo (Invited lecture).
- **7th International Conference on Hydrogen Technologies (Hydrogen days 2016),** April 2016, Prague (Czech Republic), *Are SiC based materials good candidates for electrodes in HT-PEMFCs?*, Justo Lobato, Héctor Zamora, Jorge Plaza, Pablo Cañizares, Manuel A. Rodrigo (oral presentation).
- **V Jornadas Doctorales,** October 2015, Ciudad Real (Spain), *Mejora de electrodos para pilas PEM de alta temperatura basadas en membranas de PBI dopadas con ácido fosfórico,* Héctor Zamora (Poster).
- **ECCE10+ECAB3+EPIC5,** September 2015, Nice (France), *Application of carbon nanospheres in electrodes for PBI based HT-PEMFC,* Héctor Zamora, Jorge Plaza, Manuel A. Rodrigo, Pablo Cañizares, Justo Lobato (oral presentation).
- **XI HYPOTHESIS**, September 2015, Toledo (Spain), A preliminary electrochemical assessment of Pt/SiCTiC as catalyst for HT-PEMFC, Héctor Zamora, Jorge Plaza, Manuel A. Rodrigo, Pablo Cañizares, Justo Lobato (poster).
- **XI HYPOTHESIS**, September 2015, Toledo (Spain), *Study of the influence on the titanium content in SiCTiC used in HT-PEMFC*, Héctor Zamora, Jorge Plaza, Manuel A. Rodrigo, Pablo Cañizares, Justo Lobato (oral presentation).
- **Electrochemical Energy Science and Technology (EEST 2015)**, August 2015, Vancouver (Canada), *Electrochemical behavior of Pt supported on SiC based materials in electrodes for high temperature PEMFCs*, Justo Lobato, Héctor Zamora, Jorge Plaza, Pablo Cañizares, Manuel A. Rodrigo (Keynote presentation).
- **V Iberian Symposium on Hydrogen, Fuel Cells and Advanced batteries (HYCELTEC 2015)**, July 2015, Tenerife (Spain), *SiC based materials as catalyst*

support in electrodes for HT-PEMFCs, Justo Lobato, Héctor Zamora, Jorge Plaza, Pablo Cañizares, Manuel A. Rodrigo (oral presentation).

- **CARISMA 2014,** December 2014, Capetown (South Africa), *SiC based Materials for PBI based high temperature PEMFC electrodes*, Justo Lobato, Pablo Cañizares, Manuel A. Rodrigo, Elena Monge, Francisco Ginés, Héctor Zamora (oral presentation).
- **10th European Symposium on Electrochemical Engineering (ESEE)**, October 2014, Sardinia (Italy), *Application of different carbonaceous materials to improve the MPL of High Temperature PEMFC*, Héctor Zamora, Manuel A. Rodrigo, Pablo Cañizares, Justo Lobato (oral presentation).
- **65th Annual Meeting of the International Society of Electrochemistry (ISE)**, August 2014, Lausanne (Switzerland), *Scale up of HT-PEMFC: description of problems to be overcome*, Manuel A. Rodrigo, Justo Lobato, Pablo Cañizares, Francisco J. Pinar, Héctor Zamora, Francisco Jesús Fernandez, Diego Úbeda (oral presentation).
- **Congreso Iberoamericano de Hidrógeno y Pilas de Combustible 2014 (IBERCONNAPICE 2014),** October 2014, Barcelona (Spain), *SiC: a good candidate for MPL of electrodes for HT-PEMFC*, Justo Lobato, Pablo Cañizares, Elena Monge, Manuel Andrés Rodrigo and Héctor Zamora (oral presentation).